awarded 12 9.88

# STUDIES ON MIXING AND MASS TRANSFER ACROSS A SEPARATED SHEAR FLOW

By

MD. MUJIBUR RAHMAN
B.Sc.Eng. (B.U.E.T.), M.Eng.Sc. (Melbourne)

A THESIS PRESENTED FOR THE DEGREE OF
DOCTOR OF PHILOSOPHY

The Department of Civil Engineering
University of Adelaide
Australia

June 1988

To my parents who taught me to read

and

to my teachers who taught me to read with judgement

## STATEMENT OF ORIGINALITY

I solemnly declare that this thesis contains no material which has been accepted for the award of any other degree or diploma in any university and that, to the best of my knowledge and belief, it contains no material previously published or written by another person, except where due reference is made in the text of the thesis. I further declare that I have no objection to the thesis being made available for photocopying and loan, if accepted for the award of the degree.

(Md. Mujibur Rahman)

## ACKNOWLEDGEMENTS

The project was jointly supervised by Mr. Robert Culver and Mr. John Robert Ewers, Reader and Senior Lecturer respectively, in the Department of Civil Engineering. They have been a constant source of unwavering advice, assistance and encouragement. The thesis benefited immensely from their invaluable comments and suggestions. I express my deepest gratitude to these two friends for their help in the preparation of my thesis and for the concern and support towards me during the period of this study.

I am also grateful to other teachers of the Department particularly to Dr. G. Sved, Professor R.F. Warner, Dr. G. Dandy, Dr. J.N. Kay, and Dr. A. Simpson for their valuable comments and friendship.

It is not possible to conduct an experimental programme alone and in this regard I received valuable help from Stan Woithe, Robert Marcussen, Craig Hunter, Gerard DeVries, Bruce Lucas, Tony Zeluk, Brenda Hope and Ivana Rebellato. The fine talents of Stan Woithe and Robert Marcussen turned rough sketches into apparatus which actually worked as intended.

There are several other colleagues who provided friendship, advice and assistance. I would especially like to thank John Botting, Josephine Jolly, Mike Dixon, Kobamelo Kgoboko, Koon Wong and Wen-gang Hua. I am also thankful to Peter Lanspeary of the Mechanical Engineering Department who kindly made available some of his data analysis and plotting programs which saved me hours of programming.

The love and encouragement I received from my wife Mariam, my son Muntasir and my daughter Samia have been a great source of strength to me when

times were tough. The moral support I received from my parents in Bangladesh who had to endure a long painful separation from me for the last six and a half years, provided me with the necessary boost during my hours of depression. I remain indebted to them.

Finally, I would like to thank the University of Adelaide for providing the facilities and the financial support through the University Research Grant which made this study possible. I would also like to thank the Australian International Development Assistance Bureau for sponsoring me to Australia and the Bangladesh University of Engineering and Technology (B.U.E.T.) for granting me leave to carry out the research.

# Contents


Statement of Originality i

Acknowledgements iii

List of Figures xi

List of Tables xvii

Abstract xix

Principal Notations xx

1 Introduction 1

1.1 General . . . . . 1

1.2 Description of the Separated Flow . . . . . 2

1.3 Objectives of the Present Study . . . . . 6

1.4 Scope and Method . . . . . 7

1.5 Organization of the Thesis . . . . . 8

**2 Literature Review** **9**

2.1 General . . . . . 9

2.2 One Dimensional Mixing . . . . . 10

2.3 Mixing with Stagnation Zone Effects . . . . . 14

2.4 The Separated Flow Field . . . . . 21

2.4.1 Flow Pattern in the Recirculating Region . . . . . 21

2.4.2 Measurements in the Flow Field . . . . . 25

2.4.3 Separated Shear Layer vs Plane Mixing Layer . . . . . 29

2.5 Large Coherent Eddy Structures in Free Shear Layers . . . . 36

2.5.1 Formation and Growth . . . . . 40

2.5.2 Effects of Initial Conditions and Free Stream Turbulence 44

2.5.3 Effects of Three Dimensionality . . . . . 47

2.5.4 Entrainment and Mixing . . . . . 49

2.5.5 Coherent Structure Investigations . . . . . 57

2.5.6 Coherent Structures in Reattaching Shear Layer . . . 66

2.6 Mass Transfer in Separated Flow . . . . . 67

**3 Theoretical Considerations** **70**

3.1 General . . . . . 70

3.2 Equations of Motion . . . . . 71

3.3 Eddy Viscosity and Diffusivity Concepts . . . . . 74

3.4 Plane Turbulent Mixing Layers . . . . . 76

3.5 Solutions to the Equations of Motion . . . . . 81

3.6 Taylor's Concept of Turbulent Diffusion . . . . . 85

3.7 Theoretical Basis of Lateral Diffusivity . . . . . 87

3.8 Coherent Structures Analysis . . . . . 89

3.8.1 Decomposition of the Flow Field . . . . . 90

3.9 Mass Transfer Across the Shear Layer . . . . . 96

**4 Experimental Investigations** **101**

4.1 Introduction . . . . . 101

4.2 Experimental Objectives . . . . . 102

4.3 The Separated Flow Model . . . . . 104

4.4 Experimental Parameters . . . . . 104

4.5 Phase I Experiments . . . . . 107

4.5.1 Visualization Techniques . . . . . 107

4.5.2 Experimental Procedure . . . . . 111

4.5.3 Photo Analysis . . . . . 113

4.5.4 Problems and Precautions . . . . . 114

4.6 Phase II Experiments . . . . . 115

4.6.1 The Novar Flowmeter . . . . . 116

4.6.2 Measurements with LDV . . . . . 117

4.6.3 Associated Problems with LDV Measurements . . . . 121

4.7 Phase III Experiments . . . . . 126

4.7.1 The Conductivity Probes . . . . . 126

4.7.2 The Tracer Injection System . . . . . 134

4.7.3 The Digital Data Acquisition System . . . . . 138

4.7.4 Experimental Procedure . . . . . 140

4.7.5 Problems and Precautions . . . . . 145

**5 Presentation and Discussion of Results - Phase I 146**

5.1 Introduction . . . . . 146

5.2 Flow Visualization Results . . . . . 147

5.3 Discussion of Visual Observations . . . . . 167

5.3.1 Shear Layer Development . . . . . 167

5.3.2 Localized Rapid Mixing . . . . . 171

5.3.3 Mass Transfer in Separated Flow . . . . . 174

5.4 Conclusion . . . . . 176

**6 Presentation and Discussion of Results - Phase II 178**

6.1 Introduction . . . . . 178

6.2 Mean Velocity Profiles . . . . . 179

6.2.1 Streamwise Mean Velocity . . . . . 179

6.2.2 Transverse mean velocity . . . . . 187

6.3 Growth of the Separated Shear Layer . . . . . 187

6.4 Similarity in Mean Motion . . . . . 192

6.5 Turbulence Intensity Profiles . . . . . 195

6.5.1 Streamwise Turbulence . . . . . 196

6.5.2 Transverse Turbulence . . . . . 203

6.6 Energy Spectra of Fluctuating velocity . . . . . 204

6.7 Entrainment of Ambient Fluid . . . . . 213

6.8 Discussion and Concluding Remarks . . . . . 217

**7 Presentation and Discussion of Results - Phase III 220**

7.1 Introduction . . . . . 220

7.2 The Concentration Field . . . . . 221

7.2.1 Iso-Concentration Contours . . . . . 221

7.2.2 Short Time Average Concentration Decay . . . . . 228

7.2.3 Spectra of Concentration Fluctuations . . . . . 245

7.2.4 Spatial Average Concentration Decay . . . . . 248

7.3 Mass Transfer Across the Shear Layer . . . . . 253

7.4 Effects of Coherent Structures . . . . . 260

7.4.1 Time Records of Concentration . . . . . 261

7.4.2 Lateral Concentration Distribution . . . . . 266

7.5 Concluding Remarks . . . . . 269

**8 Summary and Conclusions** **271**

8.1 Summary . . . . . 271

8.1.1 Phase I . . . . . 272

8.1.2 Phase II . . . . . 274

8.1.3 Phase III . . . . . 275

8.2 Concluding Remarks . . . . . 277

**Appendices** **279**

**A Laser Doppler Velocimetry** **279**

A.1 Optical Arrangements . . . . . 279

A.2 Basic Principle . . . . . 281

A.3 Frequency Shifting . . . . . 283

A.4 Fiberoptic Probe System . . . . . 285

A.5 Signal Processing . . . . . 286

**B Computer Programs for Data Collection** 290

**C Synchronous Data Collection** 298

C.1 Photo - synchronization System . . . . . 298

C.2 Procedure of Data Collection . . . . . 301

**Bibliography** 305

# List of Figures


1.1 Prandtl's model of flow separation . . . . . 3

1.2 Description of the separated flow . . . . . 4

2.1 Typical concentration distribution curves . . . . . 12

2.2 The general behavior of variance (after Pedersen, 1977) . . . 16

2.3 Mean velocity and Reynolds' stresses in a cavity flow . . . . . 27

2.4 Coherent eddy structures in free shear flow . . . . . 37

2.5 Initial instability of shear layer . . . . . 41

2.6 Subharmonic interaction . . . . . 42

2.7 Streamwise vortexlines . . . . . 49

2.8 Topology of the streamwise vortex structure . . . . . 50

2.9 Entrainment by the large structures . . . . . 54

2.10 Coherent structure cross-section . . . . . 55

2.11 Mixing transition . . . . . 56

4.1 Schematic diagram of the flume model . . . . . 105

4.2 The Novar Streamflow meter . . . . . 117

4.3 Photograph of the laser-Doppler velocimeter assembly . . . . 118

4.4 Photograph of the fiber optic probe . . . . . 118

4.5 Details of the Conductivity Probes . . . . . 128

4.6 Block diagram for conductivity probe circuits . . . . . 130

4.7 Conductivity probe circuit diagram . . . . . 131

4.8 Response characteristics of the conductivity probes . . . . . 135

4.9 Schematic of the tracer injection system . . . . . 137

4.10 Block diagram of digital data collection program . . . . . 139

4.11 Calibration curves for conductivity probes . . . . . 142

5.1 Coherent eddy structures in separated shear layer . . . . . 149

5.2 Pairing interactions of large structures . . . . . 152

5.3 Fluctuating initial layer of vortices . . . . . 153

5.4 Some important features of separated flow; A.R. = 2.0 . . . . 155

5.5 Features of separated flow; A.R. = 4.8 . . . . . 156

5.6 Successive picture frames from high speed cine film . . . . . 162

5.7 Successive frames continued from previous figure . . . . . 164

5.8 Picture frames demonstrating lateral movement . . . . . 166

5.9 Large structures interaction in separated shear layer . . . . . 170

5.10 Interaction between shear layer and recirculating eddy . . . . 173

6.1 Mean velocity profiles; A.R. = 2.0; U = 0.30 m/sec . . . . . 180

6.2 Mean velocity profiles; A.R. = 2.0; U = 0.20 m/sec . . . . . 181

6.3 Streamwise mean velocity profiles; A.R. 4.8; U = 0.30 m/sec 182

6.4 Transverse mean velocity profiles; A.R. 4.8; U = 0.30 m/sec . 183

6.5 Streamwise mean velocity profiles; A.R. 4.8; U = 0.20 m/sec 184

6.6 Transverse mean velocity profiles; A.R. 4.8; U = 0.20 m/sec . 185

6.7 The separated shear layer growth . . . . . 189

6.8 Growth of local momentum thickness . . . . . 191

6.9 Similarity profiles for A.R. = 2.0 . . . . . 193

6.10 Similarity profiles for A.R. = 4.8 . . . . . 194

6.11 Turbulence profiles; A.R. = 2.0; U = 0.30 m/sec . . . . . 197

6.12 Turbulence profiles; A.R. = 2.0; U = 0.20 m/sec . . . . . 198

6.13 Streamwise turbulence; A.R. = 4.8; U = 0.30 m/sec . . . . . 199

6.14 Transverse turbulence; A.R. = 4.8; U = 0.30 m/sec . . . . . 200

6.15 Streamwise turbulence; A.R. = 4.8; U = 0.20 m/sec . . . . . 201

6.16 Transverse turbulence; A.R. = 4.8; U = 0.20 m/sec . . . . . 202

6.17 Time records of instantaneous velocity . . . . . 205

6.18 Power spectra for u fluctuations . . . . . 206

6.19 Spectra of $u'$ at downstream locations; U = 0.30 m/sec . . . . 208

6.20 Spectra of $v'$ within separated region; U = 0.30 m/sec . . . . 209

6.21 Spectra of $v'$ at x = 500 mm . . . . . 210

6.22 Spectra of $u'$ at downstream locations; U = 0.20 m/sec . . . . 211

6.23 Spectra of $v'$ inside separated region; U = 0.20 m/sec . . . . . 212

6.24 Volume flux ratio with downstream distance; A.R. = 2.0 . . . 215

6.25 Volume flux ratio with downstream distance; A.R. = 4.8 . . . 216

7.1 Contours of $C/C_{max}$; A.R. = 2.0; U = 0.30 m/sec. . . . . 222

7.2 Contours of $C/C_{max}$; A.R. = 2.0; U = 0.20 m/sec. . . . . 223

7.3 Contours of $C/C_{max}$; A.R. = 4.8; U = 0.30 m/sec. . . . . 224

7.4 Contours of $C/C_{max}$; A.R. = 4.8; U = 0.20 m/sec. . . . . 225

7.5 Short time av. conc.; A.R. = 2.0; U = 0.30 m/s; y/W = 0.0 . 229

7.6 Short time av. conc.; A.R. = 2.0; U = 0.30 m/s; y/W = - 0.4 230

7.7 Short time av. conc.; A.R. = 2.0; U = 0.30 m/s; y/W = - 0.8 231

7.8 Short time av. conc.; A.R. = 2.0; U = 0.20 m/s; y/W = 0.0 . 233

7.9 Short time av. conc.; A.R. = 2.0; U = 0.20 m/s; y/W = - 0.4 234

7.10 Short time av. conc.; A.R. = 2.0; U = 0.20 m/s; y/W = - 0.8 235

7.11 Short time av. conc.; A.R. = 4.8; U = 0.30 m/s; y/W = 0.0 . 237

7.12 Short time av. conc.; A.R. = 4.8; U = 0.30 m/s; y/W = - 0.4 238

7.13 Short time av. conc.; A.R. = 4.8; U = 0.30 m/s; y/W = - 0.8 239

7.14 Short time av. conc.; A.R. = 4.8; U = 0.20 m/s; y/W = 0.0 . 241

7.15 Short time av. conc.; A.R. = 4.8; U = 0.20 m/s; y/W = - 0.4 242

7.16 Short time av. conc.; A.R. = 4.8; U = 0.20 m/s; y/W = - 0.8 243

7.17 Spectra of $c'$ at different locations. . . . . 246

7.18 Spectra of $c'$ at different locations. . . . . 247

7.19 Spatial average conc. decay; A.R. = 2.0 . . . . . 249

7.20 Spatial average conc. decay; A.R. = 4.8 . . . . . 250

7.21 Diffusivity coefficients; A.R. = 2.0; U = 0.30 m/sec. . . . . 256

7.22 Diffusivity coefficients; A.R. = 2.0; U = 0.20 m/sec. . . . . 257

7.23 Diffusivity coefficients; A.R. = 4.8; U = 0.30 m/sec. . . . . 258

7.24 Diffusivity coefficients; A.R. = 4.8; U = 0.20 m/sec. . . . . 259

7.25 Time records of conc. fluctuations . . . . . 263

7.26 Time records of conc. fluctuations . . . . . 264

7.27 Time records of conc. fluctuations . . . . . 265

7.28 Centroid of lateral conc. distribution . . . . . 267

7.29 Centroid of lateral conc. distribution . . . . . 268

A.1 Basic optical arrangements . . . . . 280

A.2 Basic principle of a dual beam system . . . . . 281

A.3 Frequency shifting arrangements . . . . . 284

A.4 Fiberoptic probe system . . . . . 285

A.5 Typical Doppler burst signals . . . . . 287

A.6 Counter type signal processor . . . . . 288

C.1 Block diagram of the photo-synchronization system . . . . . 299

C.2 The movie camera with synchronization device . . . . . 300

C.3 Computer trigger circuit diagram . . . . . 302

C.4 Trigger circuit time-line diagram . . . . . 303

# List of Tables

4.1 Experimental parameters . . . . . 106

5.1 Regions of rapid mixing . . . . . 158

# Abstract

The study was concerned to examine the mixing and mass transfer processes in a separated shear flow with a free surface. The results of the experimental investigation yielded information regarding the flow field which are of fundamental importance and show effects not previously reported. These will provide a deeper understanding of the basic physical processes involved in mixing and mass transfer across the separated free surface flow field.

The experimental programme was conducted in three separate phases. In phase 1, flow visualization experiments were undertaken to obtain a qualitative understanding of the flow field. The most striking result of this visualization study is the realization of a pulsatile motion in the recirculating eddy in the separated flow region which can cause considerable differences in the mixing and mass transfer rates of such separated shear flows. A localized rapid mixing region in the separated shear layer was identified which is believed to be due to an interaction between the shear layer and the recirculating eddy in the separated region. The development and growth of the separated shear layer structures were found to have similarities and differences from those in other free shear flows, e.g., plane mixing layers.

The second phase of this experimental programme was concerned to the measurements of velocity field in the separated flow using a single channel laser-Doppler velocimeter. The results of this phase of experiments supported the findings of the flow visualization experiments and also provided useful information regarding the behaviour of the mean flow pattern and the turbulent characteristics for the separated shear flow considered. Analysis of the growth rate, similarity behaviour and the entrainment in the separated shear layer showed significant differences from the plane free mixing layer.

In phase III, tracer concentration measurements were undertaken at vari-

ous points of the separated flow region using electrical conductivity probes. The results, showing the temporal and spatial variation of concentration at different locations, provided an insight into the mass transport processes in the separated flow region. Mass transfer analysis and the demonstration of the effects of large coherent eddy structures in the separated shear layer indicated that the calculation of mass transfer rates applying conventional gradient transfer theory could lead to an improper estimate.

# Principal Notations

$a$ = a constant

$b$ = the width of the shear layer

$B_o$ = the width of the main stream cross-section

$c_2$ = a proportionality coefficient

$c$ = the instantaneous tracer concentration

$\bar{c}$ = the time-average tracer concentration

$c'$ = the fluctuating component of tracer concentration

$C_a$ = the spatial average tracer concentration

$C_{max}$ = the maximum value of $C_a$

$d_f$ = fringe spacing (in the LDV system)

$D_t$ = turbulent eddy diffusivity of mass

$f_D$ = doppler frequency (in LDV system)

$k$ = a constant

$l$ = Prandtl's mixing length

$l_c$ = concentration length scale

$l_y$ = mixing length of the transverse velocity component

$L$ = length of the separated region

$L_l$ = Lagrangian length scale

$p$ = the pressure

$ppm$ = parts per million

$Q$ = total volumetric flow rate

$Q_o$ = total volumetric flow rate before separation

$R_{u'}(\tau)$ = Lagrangian correlation coefficient

$t$ = time

$T$ = averaging time period

$T_{lx}$ = Lagrangian integral time scale in x - direction

$U$ = free stream mean velocity

$u$ = streamwise instantaneous velocity

$\bar{u}$ = streamwise mean velocity

$u'$ = streamwise velocity fluctuation

$v$ = transverse instantaneous velocity

$\bar{v}$ = transverse mean velocity

$v'$ = transverse velocity fluctuation

$w$ = vertical instantaneous velocity

$\bar{w}$ = vertical mean velocity

$w'$ = vertical velocity fluctuation

$W$ = the width of the separated region

$x$ = cartesian coordinate in the streamwise direction

$y$ = cartesian coordinate in the transverse direction

$z$ = cartesian coordinate in the vertical direction

$\delta$ = characteristic width of the shear layer

$\epsilon$ = dissipation rate of the turbulent kinetic energy

$\epsilon_m$ = the molecular diffusivity

$\epsilon_{ty}$ = turbulent eddy viscosity in the y - direction

$\epsilon_y$ = transverse diffusivity coefficient

$\epsilon_z$ = vertical diffusivity coefficient

$\theta$ = local momentum thickness

$\lambda$ = velocity ratio in a mixing layer flow

$\lambda_l$ = wavelength of laser light

$\mu$ = dynamic viscosity

$\nu$ = kinematic viscosity

$\nu_t$ = eddy viscosity

$\rho$ = fluid density

$\sigma_x^2(t)$ = variance of tracer concentration

$\tau_{ij}$ = turbulent shear stress

$\phi$ = an empirical constant

$\Phi$ = power spectral estimate in frequency domain

# Chapter 1

# Introduction

## 1.1 General

The impact on the water environment as a result of man's wide variety of activities, needs careful analysis in order to devise effective control strategies and thus preserve nature's ecological balance. Such analysis however, must be founded on the clear understanding of the physical processes of flow of natural water bodies which cause mixing and transport of contaminants or other natural substances. The detailed mixing and transport processes in a turbulent flow field however, are still not very well understood. Part of the reason for this is that they require some knowledge of the behaviour of turbulence in fluids - at best a complicated and inadequately understood problem of fluid mechanics.

The aim of the present investigation is to examine in detail the mixing and

dispersal of a mass of contaminant in a separated flow region in free surface flow, which occurs due to a strong geometrical perturbation of the main stream channel boundary. The ultimate goal is to provide fundamental information on the nature of such flows so that one might have a better understanding of them when approaching engineering problems involving contaminant transport.

It is considered to be of great practical importance in the understanding of contaminant mixing mechanisms along regions in streams caused by groynes and large dead arms of rivers as well as in bays and harbors, in addition to the understanding of the general dispersion phenomena in natural streams.

## 1.2 Description of the Separated Flow

The usual description of the process of flow separation comes directly from Prandtl's boundary-layer concept (see Schlicting, 1975). The separated flow region is characterized as a region of reverse flow (compared to the main flow direction). The point on a surface at which the derivative $(\partial u/\partial y)_{y=0} = 0$ is denoted as the separation point as shown in Figure 1.1.

Inherent in Prandtl's description of separated flow is that the flow is two-dimensional which is only an approximation of the true physical phenomenon of separation. In reality many aspects of reverse flow are three-dimensional, even for two-dimensional geometries, and furthermore, certain properties are time dependant. There are many two-dimensional configurations of importance which contains regions of separated (recirculating) flow. Examples are 'cavity-type' separated flows, sudden expansion or contraction in the flow directions, wake flows behind blunt bodies and so forth.

In the present investigation a rectangular cavity type flow is chosen to pro-

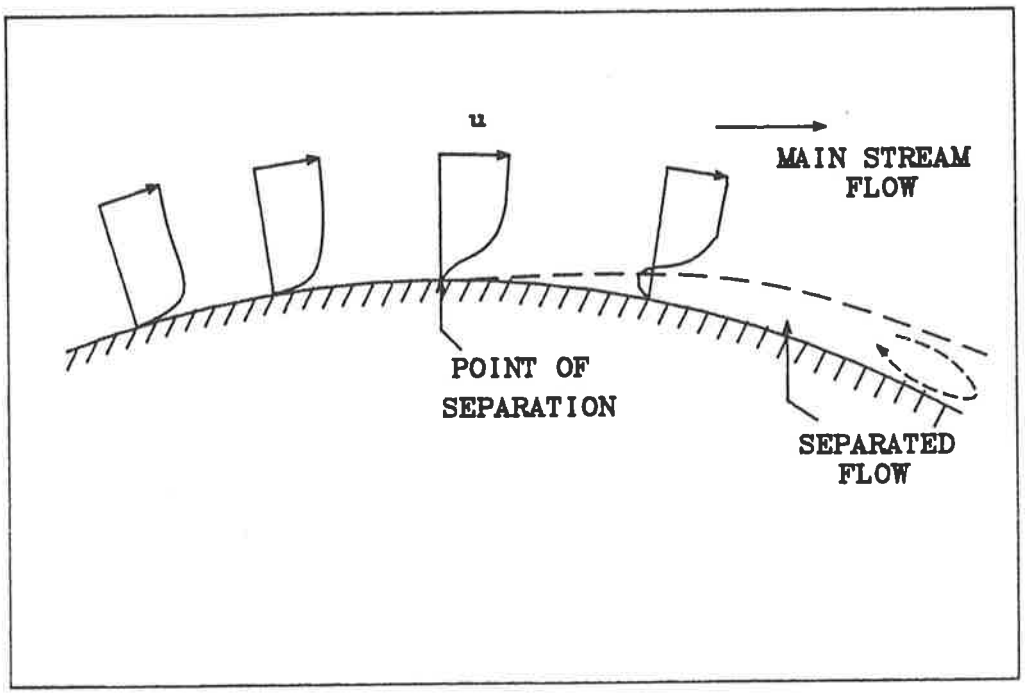


Figure 1.1: Prandtl's model of flow separation, (after Abbot and Kline, 1962)

duce a recirculating flow region. There are two reasons for this -

- firstly, this will provide information directly relevant to the mixing and mass transfer processes associated with groynes and dead arms of rivers as well as bays and harbors; and
- secondly, this will improve the understanding of the general dispersion mechanism in natural channels considering the so-called 'dead-zone' effects.

The separated flow can be considered to be composed of five distinct regions of interest as shown in the Figure 1.2. These are,

(a) the main stream channel flow;

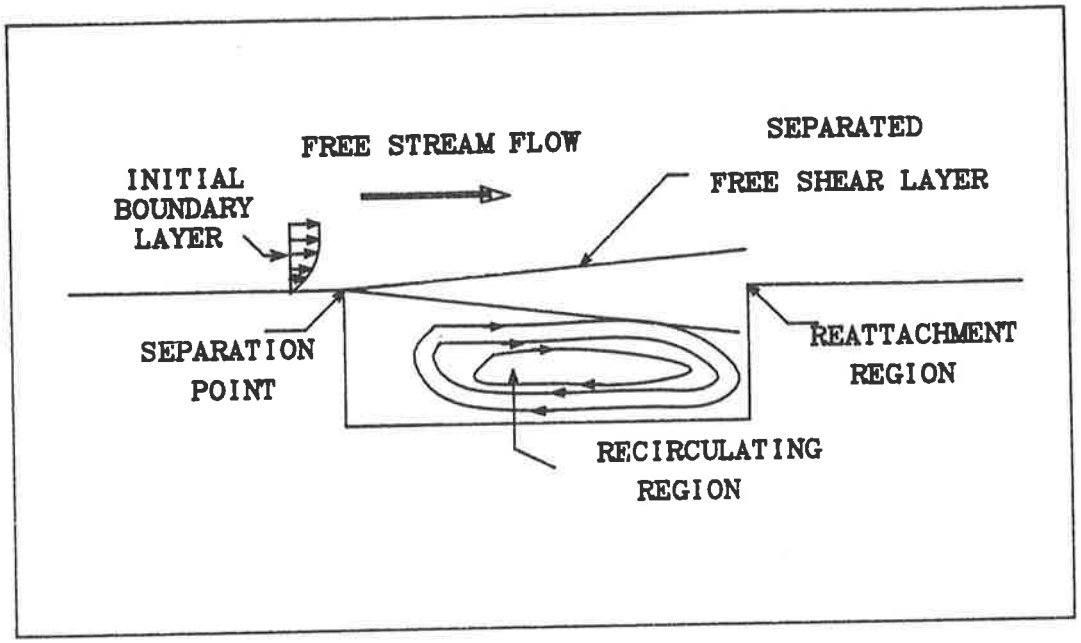


Figure 1.2: Description of the separated flow (after Kistler and Tan, 1967)

(b) the separation point region;

(c) the separated free shear layer;

(d) the reattachment region; and

(e) the recirculating flow region.

The upstream boundary layer separates at the sharp corners forming a free shear layer. The separated shear layer appears to be like an ordinary plane mixing layer. However, as pointed out by Chandrsuda and Bradshaw (1981), the turbulent recirculating flow causes the reattaching region of the shear layer to be substantially different from a plane mixing layer. The separated free shear layer impinges on the wall near the reattachment region. Part of the shear layer fluid is deflected into the recirculating flow by strong adverse

pressure gradient and part moves with the mainstream flow.

Often the separated flow in the recirculating region is designated 'dead' or 'stagnant' (hence 'dead zone' or 'stagnation zone') which does not necessarily mean zero velocity. In fact a complex, unsteady flow prevails in this region. The reverse flow velocity in the recirculating region below the shear layer is usually over 20% of the free stream velocity (Eaton and Johnston, 1981). Usually the properties of separated flows are calculated incorporating only one or two of the above mentioned regions as being of major importance. For example, the heat and mass transfer or drag associated with a separated region is calculated solely on the basis of the properties of the free shear layer considered as having the same properties as the plane mixing layer separating two regions of uniform flow.

However in order to appreciate, in detail, the mechanisms controlling the transport processes between the separated region and the main stream flow, properties of other identifiable parts of the flow should also be incorporated. Particularly their interactions and their effects due to boundary changes may have significant influence on the mass transfer processes. However, it is apparent that the interface i.e., the free shear layer and the recirculating flow region play the major role in the overall transport processes of the separated flow in question.

Earlier studies by other investigators did not explicitly explore the interaction between these two important flow regions although there are numerous studies on plane mixing layer flow. This is not because the problem was not recognized but because of the degree of complexity associated with turbulence phenomena involved in this kind of separated flow problem. The problem has now become even more important with the recent discovery of the large scale coherent eddy structures in free shear flow (Brown and Roshko, 1974) which are now believed to play the dominant role in the mixing and

the mass transfer processes.

## 1.3 Objectives of the Present Study

While the original motivation for the present study came from questions regarding the stagnation zone effects on the dispersion process in natural stream flow, attention was soon turned to even more fundamental questions about the recently revealed large coherent eddy structures in turbulent free shear flows and their role on mixing and mass transfer across the stagnation zone interface with the main stream flow. Literature suggests that these large nearly two-dimensional eddy structures play important role in the growth and mixing in turbulent shear layers. Therefore, in addition to the detail investigation of the separated flow such as mixing and transport of tracer contaminant within the recirculating region and transfer across the free shear layer, investigation of the properties of these large structures in the free shear layer, the dynamics of their growth and decay, and their role in entrainment, mixing and transport, have become equally important objectives of the present study.

More specifically, the main objectives of this study are,

(1) to investigate the origin, growth and decay of large eddy structures in the separated free shear layer;

(2) to study the effects of large structure dynamics on the mixing and mass transfer rates across the shear layer; and

(3) to examine in detail the mixing and transport of contaminant mass within the recirculating region, entrainment and transfer through shear layer, and possible effects due to boundary changes.

## 1.4 Scope and Method

In order to achieve these objectives, emphasis has been given to experimental studies with an intention to provide quantitative information regarding the exact nature of mixing and transport in separated flows of this kind. A considerable amount of theoretical studies was also performed in order to analyse, examine and compare the experimental results.

The experimental programme was conducted at the Robin Hydraulic Research Laboratory of the Department of Civil Engineering in the University of Adelaide. A laboratory scale model of a rectangular separation zone with a main stream flow was developed in a flume. The whole experimental programme was conducted in three phases. In the first phase, flow visualization studies were performed in order to obtain a qualitative understanding of the problem. The second phase concerned the measurements of the separated flow field employing a one dimensional laser Doppler velocimeter and in the third phase tracer concentration measurements were undertaken using a number of electrical conductivity probes designed and constructed during this experimental programme. A novel technique was employed in this phase in which numerical data was collected using the conductivity probes and at the same time a high speed cine camera traversed at the mean speed of the flow was used to photograph the flow structure underneath enabling specific structures to be identified concurrently with the conductivity field.

On line computer data acquisition was possible using the Department's PDP 11/34 computer and software facilities while the subsequent data analyses were performed using the main frame VAX-VMS computer facilities of the University.

## 1.5 Organization of the Thesis

In Chapter 2 an effort is made to present, in brief, a current state of knowledge on various topics closely associated with the present investigation. This is done through an extensive review of previous related works which are grouped under specific headings.

Chapter 3 contains a discussion on earlier theoretical analyses. Also included in the discussion are some new analytical approaches concerning the effects of large coherent eddy structures in free shear flows.

The entire experimental programme was conducted in three distinct phases. The specific objectives and procedure of each phase of experiments are described in Chapter 4. Also included are the descriptions of various apparatus used in different phases. Problems and precautions associated with various measurements are also discussed. (A detailed description of the laser-Doppler velocimeter used in the present study is given in Appendix A)

Chapter 5 contains experimental results and discussion of phase I experiments, i.e., results of flow visualization studies. The results of phase II experiments concerning the velocity field measurements are presented and discussed in Chapter 6. Similarly, Chapter 7 presents the results and their discussion for phase III experiments, i.e., the study of the concentration field measurements.

An overall summary of the entire investigation is outlined in Chapter 8. Also included are the major conclusions drawn from the present study and some recommendations for further future works.

# Chapter 2

# Literature Review

## 2.1 General

The problem of mixing and mass transfer in separated shear flow is complex due to the combination of various processes. The literature available on this subject is very extensive and covers a wide range of topics closely associated with the major thrust of the present investigation. The processes involved are onerous and there have been a large number of studies, both analytical and empirical, made to assess various facets of the associated problems. These studies range over topics such as characteristics of the flow in and adjacent to the separated region, contaminant transfer in natural streams, interfacial problems in the stagnation zone and the structure of turbulence in the flow field. There are a number of 'dead zone' models of varying reliability proposed for the prediction of contaminant mixing and transport in natural streams.

Most recently the importance of the large scale coherent eddy structures in controlling the transfer processes through the shear layer has been more clearly appreciated. This has been the subject of many recent investigations which include the properties of these structures, the dynamics of their growth and decay, the effects of external influences and their role in entrainment, mixing and transport.

This chapter therefore, includes a review of the literature in these fields, particularly which are relevant to the present study. In so doing it is necessary to outline the actual details and the significance of particular studies. These are grouped under specific headings in sections 2.2 to 2.6 of this chapter. The chapter begins with a brief discussion on the one dimensional turbulent mixing processes in natural streams.

## 2.2 One Dimensional Mixing

Most of the early research on the description and prediction of longitudinal mixing properties of stream flow refer to the classic works of Taylor (1922, 1954) who provided formal justifications for representing turbulent mixing processes as an equivalent gradient diffusion process. This is the fundamental and most crucial assumption on which most investigations regarding mixing and transport of contaminants are based. Further details on this topic are covered in the work of Fischer, et al (1979) and Holly (1985) and of course to Taylor's original works mentioned above.

In his first important study of dispersion in turbulent shear flow, Taylor (1954) concluded that the mechanism of turbulent mixing and transport could be described by the one dimensional dispersion equation in terms of the cross-sectional mean concentration,

$$\frac{\partial \bar{c}}{\partial t} + U\frac{\partial \bar{c}}{\partial x} = K_x \frac{\partial^2 \bar{c}}{\partial x^2} \tag{2.1}$$

where, $\bar{c}$ is the cross-sectional average concentration, U is the cross-sectional mean velocity, t is the time, x is the distance in the direction of flow and $K_x$ is the dispersion coefficient. The solution of this equation is a Gaussian distribution of concentration. The distribution is equivalent to the probability density function of the normal probability law with the variance growing linearly with time.

This has been the most widely used model when dealing with mixing and transport of contaminants in natural streams. In many cases however, the results have failed to produce a generally acceptable description of the mixing process and the resulting contaminant concentration distribution. The observed field data of concentration distribution maintain a pronounced and almost constant skewness in contrast to the theoretical prediction of Gaussian distribution.

This is evident in the fifty-one sets of field data on longitudinal dispersion, compiled and published by Nordin and Sabol (1974), where only a few agree with the gradient diffusion theory. Most of the data exhibit a non-Gaussian behaviour with the properties that the variance of concentration distribution increases with time according to the relation,

$$\sigma_t^2 \simeq t^{2H}$$

where, $0.5 \leq H \leq 1.0$ and that the skewed concentration distributions are characterised by an abrupt leading edge and a long tail stretching upstream as shown in the Figure 2.1.

It is also shown (Nordin and Trouttmann, 1980) that even where the Fickian diffusion theory is a good first approximation for predicting longitudinal dispersion processes, the observed data deviate consistently from the theory

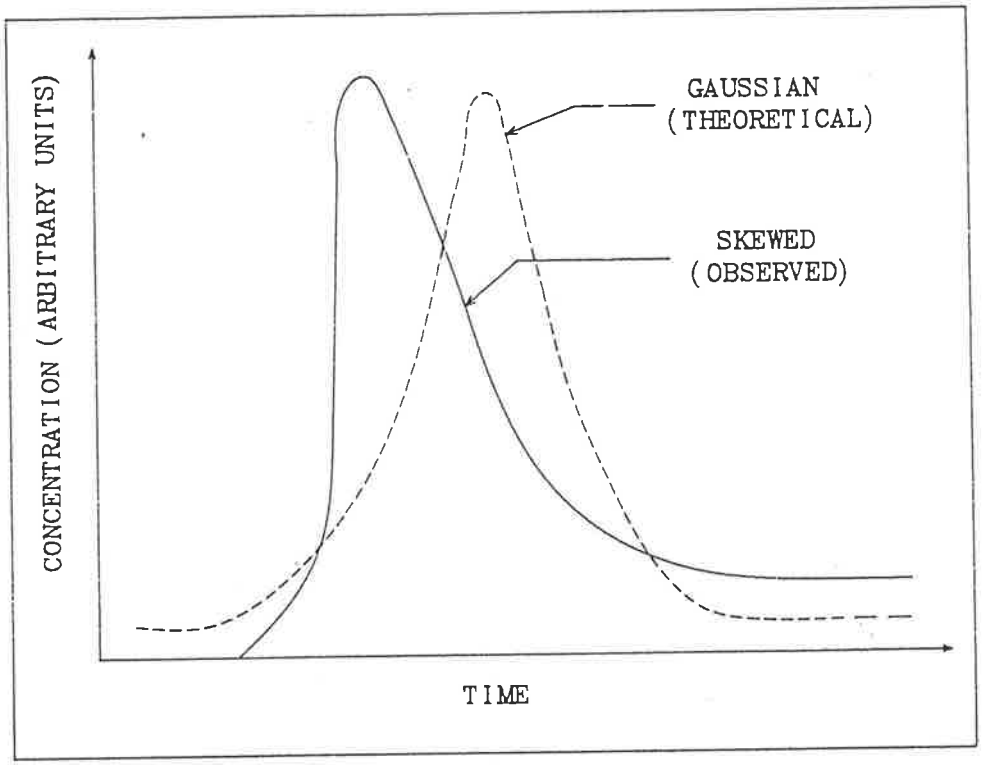


Figure 2.1: Typical concentration distribution curves

in that the skewness of the observed concentration distributions decreases much more slowly than the theory predicts.

Day (1975) has conducted an extensive series of experiments in small natural streams and found that the concentration distribution curves rapidly become skewed in the upstream direction and that this asymmetry is persistently maintained. Day and Wood (1976) stated that there was no evidence to suggest that a Gaussian distribution eventually develops from a flow in a natural open channel. Several researchers have attempted to identify the mechanism involved in this problem.

Taylor (1954) referred the problem to the trapping of tracer material in the viscous sublayer Chatwin (1971) re-examined the experimental data of Taylor (1954) and Fischer (1966) and showed that the inconsistencies between

the theory and the experimental results were due in part to neglecting the effects of viscous sublayer. He also indicated that the storage effects of the viscous sublayer could increase the dispersion rate of the order of 20%. Sullivan (1971) indicated that the skewness is predominantly non-zero because of the contaminant mass in the viscous sub-layer which takes a significently long time to be transferred across the sublayer. However, the presence of a significant viscous sublayer in natural streams has been questioned by Thackston et al (1967).

Hays (1966, in Schnelle et al 1967) included stagnation zone (dead zone) storage terms in his model of mass transport in open channel flow and considered them as integral part of the overall dispersion process. Fischer (1966) explained his view, in preference to the laminar sublayer and the stagnation zone concept, that the skewness develops during the initial advective period when the contaminant cloud adopts the form of the velocity profile. Questioning this view Day (1975) pointed out that the role of the velocity profile in producing asymmetry exists only within the advective period and consequently cannot be an adequate explanation for its persistence throughout.

Cunge et al (1980) after reviewing the two-dimensional model developed by Holly and Preissmann (1977) which predicts the asymmetry without accounting for the dead-zones, concluded that such asymmetry could partly be explained by the fact that once the contaminant cloud has passed a point at the channel there is rediffusion of contaminants from the slower waters near the banks back towards the centre and that only a two-dimensional model can reproduce such two-dimensional phenomena. They also state that the stagnation zone accounting of a one-dimensional model can only partially explain the observed asymmetry.

Valentine and Wood (1977) considering the effects of stagnation zones, demonstrated that the gradient diffusion hypothesis is applicable to the dispersion

of contaminants in natural streams only after considerable distances. Nordin and Trouttmann (1980) showed that the inclusion of a stagnation zone term in the diffusion equation yields a theoretical skewness considerably longer and conforms more closely to the observed values, especially for large distances from the point of injection. However, they also pointed out that even with the stagnation zone model the skewness of the observed concentration distribution does not appear to be decreasing as rapidly as the theory predicts.

The various concepts for explaining the deviations of observed concentration distribution from theoretical predictions have one theme in common - retention of certain amount of contaminant mass or particles of fluid in parts of slower moving waters and their subsequent slow release. However, it appears that the concept of trapping and later release of contaminant or particles of fluid by peripheral stagnation zones is the most important and realistic mechanism present in natural streams. In the following section a review of the existing stagnation zone models is presented in order to identify their principal assumptions and differences.

## 2.3 Mixing with Stagnation Zone Effects

It has been generally agreed that the non-linear growth of variance with time and the production of a long tail on the observed concentration distributions imply the existence of so-called stagnation zones i.e., small-scale bed and bank irregularities in natural streams which trap contaminants and subsequently release them slowly into the flow. This process was incorporated in the model developed by Hays (1966, in Schnelle et al, 1967) in which the main stream is assumed to follow the one-dimensional dispersion equation with a term being added to account for the mass transfer to and from the

stagnation zone.

Hays (1966) considered two types of transport mechanisms - one in which the stagnation zone is assumed to be completely mixed and in the other there is lateral dispersion depending upon the geometry of the stagnation zone. For a stagnation zone with a perfectly mixed cross-section, it was also assumed that the mass transfer is proportioned to the difference between the main stream and stagnation zone concentrations. Hays (1966) obtained solutions to his model equations by Laplace transform methods. Nevertheless it has not been used extensively, firstly because of lack of knowledge of the model parameters and secondly, because no simple analytical solution could be given (Pedersen, 1977).

In an attempt to correlate the parameters of Hays model Thackston and Schnelle (1970) demonstrated the effects of the residence time, and the volume fraction of the stagnation zones, on the time-concentration curves. The residence time in the stagnation zone was found by Thackston and Schnelle to be 0.04 to 0.08 times the time elapsed since the injection. No correlation to the bulk parameters of the stream could be found for the residence time and a mean value of 0.05 is suggested for use in predictive purposes. The stagnation zone volume fraction could however, be correlated to the friction factor, a variable which describes the irregularities of the stream.

Pedersen (1977), in analysing Hay's completely mixed stagnation zone model showed that a model which takes account of the advective period, the uneven lateral distribution of the velocity, and the existence of stagnation zones, can demonstrate the commonly observed non-linear behaviour of dispersion and the skewed concentration distribution. He showed that the advective velocity for the dispersion process is not the same for the main stream and the stagnation zone contribution. The latter being the smallest. Therefore, in the beginning of the dispersion process with stagnation zones present, the vari-

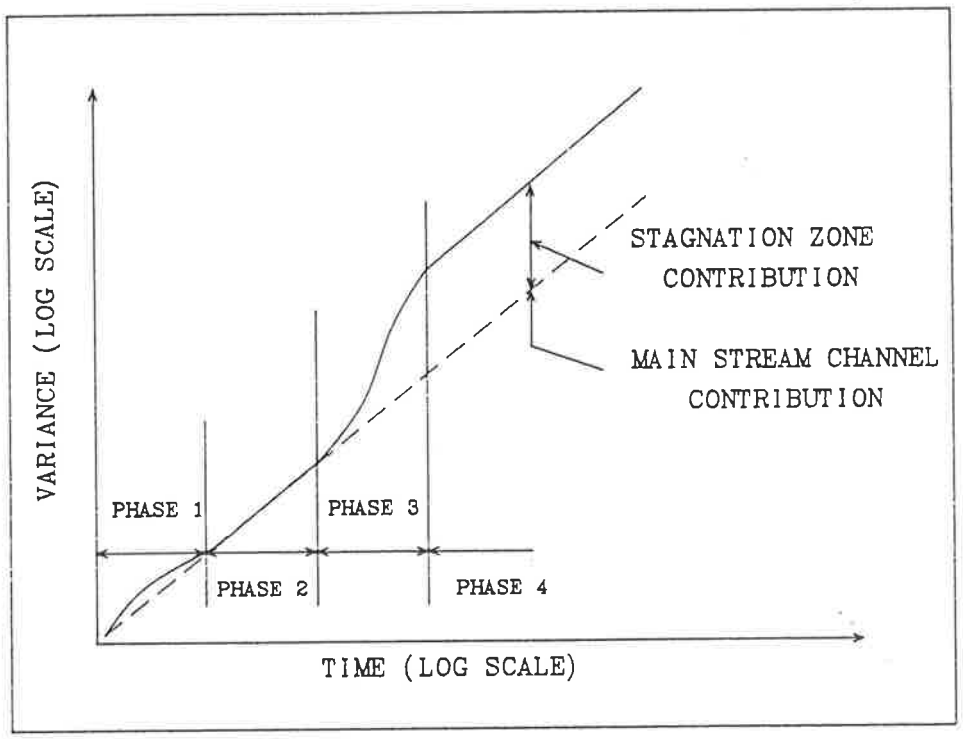


Figure 2.2: The general behavior of variance (after Pedersen, 1977)

ance increases more rapidly with time due to the advective separation. The general behaviour of the variance in natural streams, according to Pedersen (1977), can be shown in four distinct phases as shown in Figure 2.2.

The first phase shows the non-linear behaviour of the variance within the advective period. The second phase, although not always present in the observed data, shows a nearly linear behaviour of the dispersion process. In the third phase the influence of the stagnation zones increases the variance rapidly resulting a region of non-linear behaviour followed by a region where (phase 4) the linear behaviour is re-established in the asymptotic state. Pedersen (1977) using the field data of Nordin and Sabol (1974) also developed prediction formulas for four model parameters namely, the Lagrangian time scale, the normal dispersion coefficient, the volume fraction of stagnation zone and the residence time in the stagnation zone. These parameters have

been correlated to the commonly measured hydraulic parameters.

Valentine and Wood (1977) proposed a model considering the trapping and subsequent release of contaminant particles by peripheral stagnation zones. They considered a two-dimensional form of the basic dispersion equation to describe the dispersion in the main flow zone with a boundary condition at the bed describing the interchange of concentration between stagnation zone and the main stream flow. It was assumed that the mass transfer across the interface is proportional to the concentration difference across it.

Although the mass transfer expression is similar to that developed by Hays (1966, in Schnelle et al 1967), the main difference is that this model considers the dependence of the stagnation zone exchange mechanism upon the mean stream flow velocity. The model was solved numerically to compute the rate of increase of the variance and the co-efficient of skew. The analysis shows that the presence of stagnation zones increases the length of the advective period before the one dimensional dispersion equation is applicable and also greatly increases the rate of dispersion.

From analysis, they (Valentine and Wood, 1977) have identified two independent variables which control the mass exchange between the stagnation zone and the flow cross-section - A, the proportion of the channel bed covered by stagnation zones, and B, the relative depths of the flow section to the stagnation zones. It is also indicated that, whereas increasing the stagnation zone proportion of the bed areas increases the mass which resides in the stagnation zone, it also increases the interface available for mass transfer and therefore has a lesser effect on the time to arrive at equilibrium between advection and the diffusive transfer in the cross-section. However, increasing the depth for a given value of A means that a larger mass residing in the stagnation zone be transferred at the same rate through the same interface areas, thus requiring longer time to reach equilibrium. The transfer rate

represented by a non-dimensional entrainment co-efficient, $K_x$ was evaluated through laboratory experiments and a constant value of 0.02 was obtained which is close to the value obtained by Westrich (1976).

Valentine and Wood (1979a) also describes laboratory experiments in which stagnation zones were produced by placing strips across the bottom of a flume. The depth of cavity produced by the strips was 0.5 cm. The experimental results shows close agreement with the numerical study. Valentine and Wood (1979b) later extended their model to a case wherein they considered both side and bottom irregularities and reached the similar conclusion as for their two-dimensional model.

Westrich (1976), in an attempt to simulate mass exchange in stagnation zones for steady and unsteady flow conditions, presented a spatially one-dimensional mathematical model. The model proposed by Hays (1966, in Schnelle et al. 1967) does not account for some characteristic effects due to the typical flow pattern of such stagnation zones. The improved model of Westrich (1976) includes in particular, the effects of the dependence of the exchange co-efficient on the flow velocity. The advective transport of the tracer material within the stagnation zone, and the influence of unsteady flow conditions. The dependence of the exchange co-efficient on the flow velocity was also considered by Valentine and Wood (1977).

An experimental investigation was also conducted by Westrich (1976) in a 25 cm wide flume with a rectangular stagnation zone in one side wall. Both the experimental and the analytical model yield an exponential decrease of the contaminant concentration with time for steady flow situation. The half-life period of the concentration within the stagnation zone is a characteristic measure of the intensity of mass exchange. It is shown that the half-life period is nearly independent of the exchange length if the length is greater than the depth of the stagnation zone which indicates that the global mass exchange

co-efficient is constant and independent of the length of the interface. The unsteady effect becomes very important for stagnation zones of large volume and small exchange interface.

This model (Westrich, 1976) however, does not address the various turbulence production processes such as in the free mixing layer which stems from the point of separation and are mainly responsible for the mass exchange across the interface of the main channel and the separated region. Further, this model is not capable of predicting the variation of concentration within the separated region and is based on the assumption of constant concentration in the region.

McGuirk and Rodi (1979) developed a two-dimensional model for the calculation of averaged velocity and concentration distribution in open channel flow with depth recirculation in a rectangular cavity. The models which employ the constant eddy viscosity or diffusivity concept, implicitly assume that there is no transport of turbulence quantities in the turbulent flow field i.e., the turbulence is dissipated where it is generated. Such models are inadequate in cases where the state of turbulence at a point is influenced significantly by the turbulence generated somewhere else in the flow.

The model developed by McGuirk and Rodi (1979) accounts for the transport of turbulence which includes transport equations for quantities characterizing the turbulence. The model employs depth-averaged continuity, momentum and concentration equations and solves differential transport equations for turbulence kinetic energy, k and the rate of its dissipation, $\epsilon$. The same model was previously used by McGuirk and Rodi (1978) for calculating the velocity and temperature or concentration distribution induced by a side discharge into an open channel under steady conditions and involving a recirculating region.

The depth-averaged form of the well known $k-\epsilon$ turbulence model (Rastogi

and Rodi, 1978) is used to determine the distribution of the depth-averaged turbulent stresses contained in the momentum equations. When the distributions of the mean velocities, $\bar{u}$, $\bar{v}$ and the eddy viscosity $\nu_t$ are known from the momentum equations and the $k-\epsilon$ turbulence models, the unsteady, depth-averaged concentration equation is solved with the turbulent concentration fluxes being modelled using the relation, eddy diffusivity $= \tilde{\nu_t}/S_c$, where, $S_c$ is the turbulent Schmidt number.

In an experimental investigation, Weiss and Kuo (1982) evaluated the mass transfer co-efficients across the interface of the stagnation zone caused by a sudden expansion in an open channel flow. Both the first order and the second order kinetics assumption were made to find the mass transfer co-efficients for a range of flow conditions. Results show that the non-dimensional mass transfer co-efficients have larger numerical values for the second order assumption than those for the first order Kinetics assumption although the basic trends were similar. However, the values obtained using the first order Kinetics assumption show more significant correlation with Froude number and Reynolds number for both contaminant build-up and release, and the values are of the same range as those reported by Valentine and Wood (1977) for bed stagnation zones and by Westrich (1976) for side stagnation zones.

The existing conceptual models for predicting the effects of stagnation zones on the mixing and transport in natural streams provide a close explanation regarding the non-linear behaviour and the so-called long tail in the concentration distribution curves. Most of these models however are not based on the detailed information of the characteristic effects due to the complex flow patterns of such stagnation zones. The assumption regarding mass transfer to and from stagnation zones are rather arbitrary.

Westrich's (1976) model considers some effects such as those due to changes

in water surface elevation and due to advective transport of tracer material within the stagnation zone. Consideration of the transport of turbulence properties by McGuirk and Rodi (1979) led to a more generalized model. However, this model also involves a number of empirical constants which are subject to experimental verification. Furthermore, the model does not explicitly address the structure of turbulence in the free mixing layer and the recirculating regions, the dynamic influence of which may have immense effect on the transport of mass.

Fischer et al (1979) remarked that the analysis of the stagnation zone models could not be applied directly to natural streams, since the detailed geometry of the stagnation zone and its connection to the main flow which determines the exchange properties, could not be quantified. In the following section the detail flow patterns in the stagnation zone (separated region) and their variations due to goemetry changes are discussed.

## 2.4 The Separated Flow Field

As mentioned earlier, the flow in the stagnation zone is not necessarily 'dead' or stagnant, rather a complex unsteady reverse flow prevails within the region separated by a free shear layer (the interface) from the main stream flow. Hence, it more appropriate to call them separated or recirculating flow regions.

### 2.4.1 Flow Pattern in the Recirculating Region

The flow pattern in the recirculating region has been investigated in the past revealing its complicated nature. Squire (1956) considered the flow region to be consisting of a core region in which viscosity effects are small, although

viscosity is responsible for the development of the motion in the core, and a boundary layer surrounding the core region. It is argued that the vorticity will tend to be constant in the core, because of the residual action of viscosity, since viscosity tends to destroy vorticity gradients.

However, the concept of constant vorticity within the core may not be applicable when the flow in the mixing region (shear layer) is highly turbulent. Due to the high rate of mixing here, some of the streamlines of the core motion may cross into and out of this mixing region. In this case each streamline will have a constant vorticity within the core and the vorticity will not be uniform throughout the core region. Although Squire (1956) did not analyse fully the separated flow he defined, his concept of the flow as consisting of a central core surrounded by a boundary layer has been useful.

Pan and Acrivos (1967) studied the basic features of the steady flow for different Reynolds numbers considering a cavity of square section in the horizontal plane with varying depth. Their experimental results suggest that, within finite cavities (smaller depth to width ratio), the high Reynolds number steady flow should consist essentially of a single inviscid core of uniform vorticity with viscous effects being confined to thin shear layers near the boundaries, while for cavities of infinite depth (large aspect ratio), the viscous and the inertia forces should remain of comparable magnitude throughout the whole domain even in the limit of very large Reynolds number.

The flow in a rectangular cavity with different aspect ratios for a small Reynolds number flow was solved numerically by Mills (1965) and the theoretical results were compared with the photographs of the experimental flow patterns. For aspect ratio of 0.5 (called a shallow cavity) there was a good agreement between theoretical and experimental results. Where the aspect ratio was 1.0 (called a square cavity), the experiments did not show the two corner eddies which he (Mills, 1965) had predicted theoretically. For aspect

ratio of 2.0 (called a deep cavity), a second theoretical vortex did not appear in the low Reynolds number range, although it appeared in large Reynolds number flow.

However, a numerical study by Mehta and Lavan (1969) of the characteristics of flow in a two-dimensional channel with a rectangular cavity concludes that the number of eddies present in the recirculation region depend only on the aspect ratio. Their study also showed that when the Reynolds number was increased, the strength of the vortex increased and then decreased, and the vortex centre moved downstream and upward, creating a thin shear layer.

The study of mass exchange simulation in a rectangular stagnation zone by Westrich (1976) assured a single eddy in the recirculation region for aspect ratio (depth to length of stagnation zone) within the limits of $0.17 < D/L < 3.33$. For aspect ratio greater than 3.33, the primary intensive eddy starts to induce a secondary eddy, which has much less intensity and an opposite sense of circulation.

An experimental investigation by Bogatyrev et al (1976) of the flow of water in a trench of square transverse cross-section used two values of Reynolds number corresponding to laminar and turbulent flow conditions in the external stream. The results demonstrated a core region with constant vorticity in both cases. For the case of the laminar flow a secondary eddy was formed at the downstream bottom corner of the cavity while a stagnant zone was noticed at the upstream lower corner. The areas occupied by the secondary eddy and the stagnant zone made up 6% and 2% respectively of the total area. Similar features were observed for the case of the turbulent flow in the external stream. However the areas of the secondary eddy and the stagnant zone were several times smaller in comparison with laminar flow.

The three-dimensional character of the flow in the recirculation region is reported by Kistler and Tan (1967). In an experimental study of the properties

of approximately two-dimensional flow in a rectangular cavity they encountered several distinct internal flow features as the geometry was changed. A three-dimensional cellular structure of the internal flow was observed for the case of a shallow cavity (aspect ratio less than 2.5), as the pressure measured across the transverse axis at a fixed depth of the cavity showed a periodic variation in the transverse direction. For the deep cavity case (aspect ratio $> 2.5$), the flow appeared to be approximately two-dimensional, the pressure being constant in the central portion of the transverse plane and then fell off near the ends. All the measurements were made for a single Reynolds number flow. Similar cellular structure of the flow was also observed by Maull and East (1963).

Flow visualization studies by Zhak et al, (1981) reports the formation and break-up of cellular structure related to the formation of turbulent spots in the external stream. When the turbulent spots passed through the channel over the cavity, there was an increase in the flow velocity in the cavity and break-up in the cellular structure. After the passage of the turbulent spot, the original velocity was restored together with the cellular structure. No cellular structure was observed at relatively high Reynolds number. Their study (Zhak et al, 1981) also reports the existence of secondary paired vortex structures of Taylor-Goertler type arising in the wall region because of curvature of the flow lines and the effects of centrifugal forces.

The above discussions of the flow pattern in the region of recirculation indicate that the flow is a strong function of the stagnation zone geometry and the external flow conditions. An important fraction of the mass transport in the recirculation region will depend on the flow pattern in that region under particular condition. For instance, the secondary eddy or eddies of even higher order shall have low diffusivity compared to that of the primary eddy. Therefore, the mass exchange process will be strongly reduced if the secondary eddy has a much larger dimension and hence will limit the overall

rate of mass transfer through the separated region.

### 2.4.2 Measurements in the Flow Field

Considerable experimental measurements have been made in the past, of such separated shear flows. However, there is still an incomplete understanding of the flow problem. Eaton and Johnston (1981) have indicated that part of the difficulty lies in the fact that these flows are highly turbulent with frequent flow reversals which limits the reliability of measurements with conventional flow measuring instruments.

Durst and Rastogi (1977) have pointed out that because of the non-linear response characteristics of conventional instruments such as pitot tubes, hot-wire anemometers and hot-film probes, the accuracy of the results is questionable in the presence of high turbulence intensities and changes in flow direction. With the advent of the modern laser Doppler velocimeter (LDV), the situation has improved, since an LDV can be sensitive to flow directions. Earlier measurements, although incomplete and not fully reliable, contributed significantly in the understanding of the flow. Measurements of separated flows usually consist of mean velocity, Reynolds shear stress and Reynolds normal stresses distributions.

Tani et al (1961, in Chang 1970) measured the distribution of turbulent mean velocity as well as turbulent intensity and shear stress in rectangular cavity flow and reduced them to non dimensional quantities by referring them to appropriate free stream conditions. Measurements for two different aspect ratios, as shown in Figure 2.3, indicate that the turbulence intensity and shear stress in the mixing region in the shallow cavity flow are higher than those in the square cavity flow, and that these quantities increase in the downstream direction. The lack of measurements in the reverse flow region

reflects the limitations of the conventional measuring devices.

A more detail measurements of the streamwise and transverse velocities in the reverse flow region were made by Bogatyrev et al (1976) using a laser Doppler velocimeter. The measurements were made employing both laminar and turbulent conditions in the external stream flow. Their measurements showed consistency with theoretical expectations. Secondary recirculation, in the opposite sense, at the bottom corners could be detected clearly by the velocity measurements. However they (Bogatyrev et al, 1976) did not demonstrate the distributions of the turbulence quantities in the separated flow region.

Their (Bogatyrev et al, 1976) velocity measurements also show that the largest value of the dimensionless velocity, $\bar{u}/U$, reaches 0.4 at the downstream wall, 0.27 at the bottom and 0.23 at the upstream wall for the turbulent conditions in the external stream flow. For laminar conditions these values were lower. These values are approximately equal to the values of the maximal velocities in a boundary layer surrounding the core region, obtained by Roshko (1955).

As mentioned earlier, flow separation and reattachment with recirculating flow may occur in many geometrical configurations. Recent measurements have been performed on the relatively simple geometry of single or double rearward facing step flows such as those by Bradshaw and Wong (1972); Chandrsuda and Bradshaw (1981); Stevenson et al (1984); Etheridge and Kemp (1978); and Smith (1979). The flow however, is of similar nature to the cavity type separated flow except that, in the step flows the dividing streamline, reattaching on the side wall, is highly curved thereby adding an extra rate of strain, $\partial v/\partial x$, to the simple shear strain of $\partial u/\partial y$.

Eaton and Johnston (1981) have given a comprehensive review on reattaching

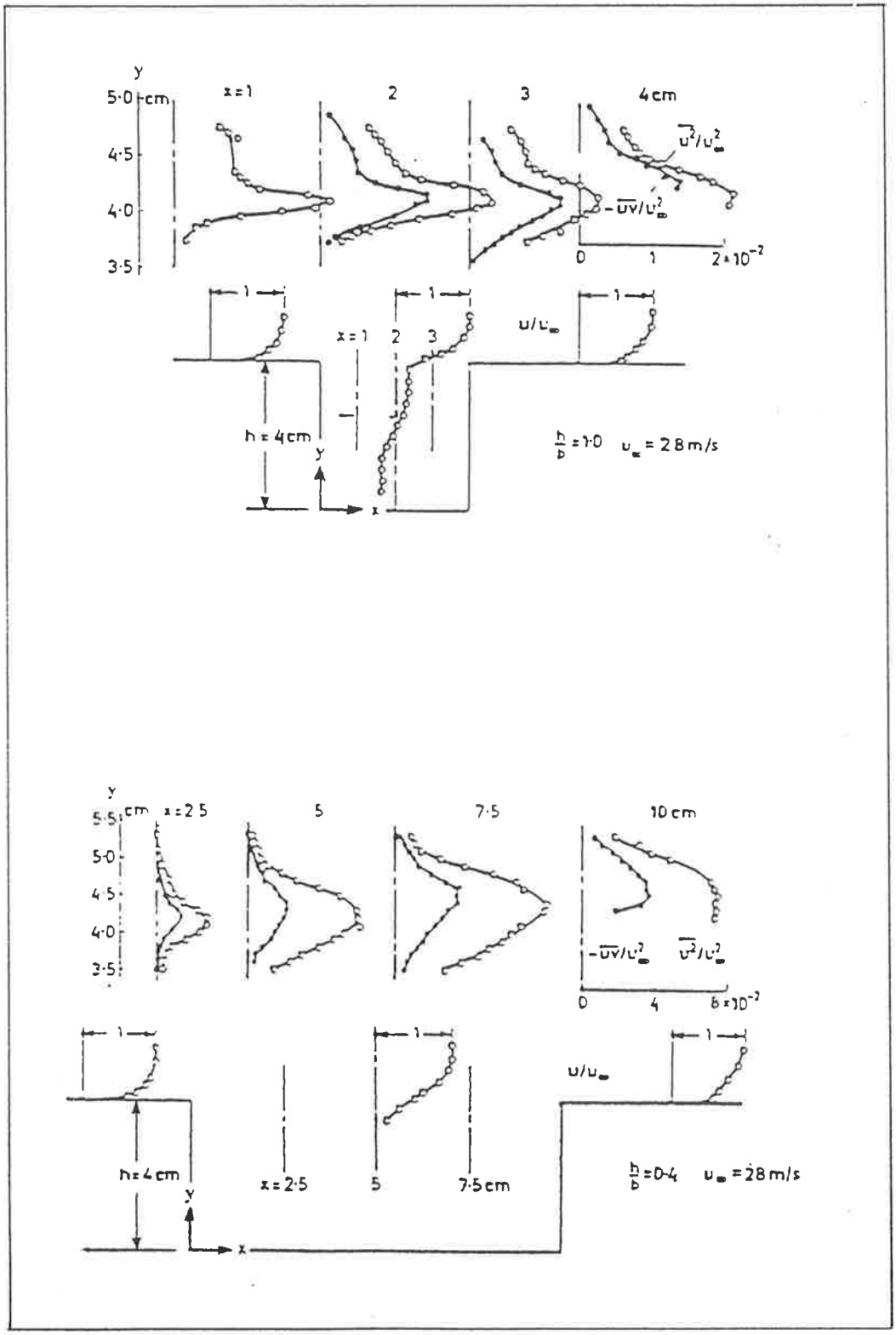


Figure 2.3: Distribution of mean velocity and Reynolds' stresses in a rectangular cavity flow (after Tani et al 1961)

shear flows. The main focus has been on the effect of system parameters on reattachment. The reattachment length of the separated flow varies from 4.9 to 8.2 step heights for various experiments considered. Among others, the initial boundary layer state (laminar/turbulent), streamwise pressure gradient (Kuehn, 1980) free stream turbulence and aspect ratio (channel width/step height) are shown to have significant influence on the reattachment length.

Bradshaw (1966) found that shear layers originating from initially laminar boundary layers grow more rapidly than those originating from turbulent boundary layers. High level of free stream turbulence has the effect of decreasing the reattachment lengths. Measurements of Patel (1978) in plane mixing layer showed that the growth rates increased with increasing free stream turbulence level. The magnitude of the effect of free stream turbulence, as suggested by Eaton and Johnston (1981), is likely to be dependent on,

- The initial conditions of the free shear layer, and
- The spectrum of the free stream turbulence.

The overall pattern of mean velocity profiles measured by various authors (Moss et al, 1977; Stevenson et al 1984; Smyth 1979; and Etheridge and Kemp 1978) in separated flows including the recirculating region measured with LDV and pulsed wire anemometer appears to be similar when one considers the considerable differences in initial and boundary conditions. The turbulence quantities have shown, however, substantial variation between experiments particularly in the peak values of turbulence intensity and shear stress. Eaton and Johnston (1981) attributes such variations to experimental uncertainty rather than to real differences in the flows.

Measurements of Moss et al (1977) show that the maximum values of the Reynolds stresses are found in the regions where the transverse velocity gra-

dient, $\partial v/\partial y$ is close to a maximum. Their results also confirm the observations of Tani et al (1961) that the zone of maximum shear initially lies close to the dividing streamline but deviates outwards from it downstream. In almost every experiment the peak values of the Reynolds stresses increase at first with distance downstream approaching their maxima a little before the region of the reattachment; thereafter decrease rapidly, as observed by Bradshaw and Wong (1972).

The distribution of turbulent kinetic energy as reported by Moss et al (1977), indicates that an appreciable fraction of the peak values in the shear layer remain throughout much of the recirculating region, although the mean velocity locally may be very small. Smyth (1979) shows that the maximum turbulent energy occurs mainly at the edge of the recirculating zone and has a peak value of 6.2% just upstream of reattachment.

### 2.4.3 Separated Shear Layer vs Plane Mixing Layer

The experimental results of many free turbulent boundary layer flows are compared with theoretical expectations by comparing their similarity behaviour. According to Rodi (1975), a flow is considered self-similar when one velocity and one length scale are sufficient to render its time-averaged quantities dimensionless functions of one geometrical variable only.

It is now well known that a plane mixing layer formed by two flows with velocities $u_1$ and $u_2$ approaches self-similarity in the variable y/x at sufficiently high Reynolds numbers based on x. Wygnanski and Fiedler (1970) have shown that, in the self-similar region of the plane mixing layer, mean velocity, Reynolds shear and normal stresses collapse on one curve if they are made dimensionless by the same reference velocity and plotted against the same dimensionless length scale.

Rodi (1975) has reviewed various experimental data for both single and double stream plane mixing layer. Downstream of a certain development region, mixing layers are self-similar for any velocity ratio. This expectation is confirmed by all the experimental data on mean and turbulence quantities. The velocity profiles, however, agree well only when it is non-dimensionalized by a characteristic flow width which Rodi (1975) used as $\delta = (y_{0.1} - y_{0.9})$, where, the subscripts 0.9 and 0.1 represent the transverse locations at which the velocity ratio are 0.9 and 0.1 respectively. When the data on mean and turbulence quantities are plotted against the normalized distance y/x, as is often done in the literature, the agreement is poor; for there is little consensus about the rate of spread, $d\delta/dx$.

A frequently used measure of the spreading rate is the parameter $\sigma$, determined by plotting the velocity profiles onto a standard curve $f(\xi)$ with $\xi = \sigma y/x$ and choosing $\sigma$ for best overall fit. Thus $\sigma$ is actually an inverse measure of the spreading rate. Brown and Roshko (1974) mentioned that the parameter, $\sigma$ is superior to other definitions in that all parts of the profile are involved in the fitting. Shortcomings are that the definition of thickness is tied to a shape function or a computational model, that low speed parts of the profile may not be accurate, that velocity profiles vary in shape and that the fitting procedure is tedious. Simpler measures based on the definition of some characteristic width $\delta$ have therefore, been used by various authors. A useful discussion and compilation of values of $\sigma$ from the literature is given by Birch and Eggers (1972).

The definition of $\delta$ is arbitrary, however. Some investigators use the momentum thickness,

$$\theta = \int_{-\infty}^{\infty} \frac{u - u_1}{u_2 - u_1}(1 - \frac{u - u_1}{u_2 - u_1})dy$$

for a two stream mixing layer where, $u_1$ and $u_2$ are the respective velocities

for the two streams, or,

$$\theta = \int_0^\infty \frac{u}{u_s}(1 - \frac{u}{u_s})dy$$

for a single stream mixing layer where, $u_s$ is the free stream mean velocity. Others use a characteristic width based on the shape of the mean velocity profile,

$$b = y_{0.9} - y_{0.1}$$

and still others prefer a width based on the maximum slope of the mean velocity profile,

$$\delta_w = \frac{u_1 - u_2}{(\partial u/\partial y)_{max}}$$

Birch and Eggers (1972) have shown that the rate of spread can be best represented by the velocity ratio. A recent experimental investigation by Weisbrot et al (1982) however reported that the rate of spread with downstream distance was not uniquely determined by the velocity ratio and indicated that an instability is responsible for this behaviour. The review by Rodi (1975) show rather poor agreement about the rate of spread which is attributed to three reasons.

- Firstly the distance to attain full development of the mixing layer is about a thousand times the momentum thickness of the boundary layer at the separation point according to Bradshaw (1966). The data obtained at low Reynolds number are therefore likely to have effects of initial conditions, even though the velocity profile seems to be developed.

- Secondly, the mixing layer seems to be particularly sensitive to the flow field outside the layer, possibly because of its asymmetry; and

- thirdly, the influence of free stream turbulence appears to be quite significant (Patel 1978).

The effects of various initial conditions on the characteristic measures of a free shear layer were investigated experimentally by Hussain and Zedan (1978). The initial boundary layer state (whether laminar or turbulent), momentum thickness Reynolds number $R_{\theta e}$ and fluctuation intensity $u'_{pe}/u_e$ were considered systematically. It was found that the spreading rate, similarity parameter, and peak turbulent intensity in the self-preserving (self-similar) region are essentially independent of $R_{\theta e}$, but dependent on whether the initial boundary layer is laminar or turbulent. The virtual origin as well as the distance required for attainment of self-preservation depend noticeably on $R_{\theta e}$.

According to Hussain and Zedan (1978) the mean velocity and turbulence intensity profiles appear to reach self-similarity together when the initial boundary layer is laminar but not when it is turbulent. Initially turbulent shear layers manifest two stages of linear growth, the growth rate in the second stage being higher. The reason for this two-stage growth is not explained. However, they (Hussain and Zedan, 1978) speculated that this be controlled by the dynamics of the large scale coherent structures in the shear layer. The effects of initial conditions and large scale coherent structures in the free shear layer will be further discussed in a later section.

While there are considerable differences in measurements in plane mixing layers largely due to the effects of initial and boundary conditions and to some extent due to experimental uncertainty, the measurements in separated shear layers become even more complicated due to reattachment of the shear layer and the reverse flow in the recirculation region. Bradshaw and Wong (1972) mentioned that the differences between the separated shear layer and the plane mixing layer seem to be large even when the influence of the initial boundary layer is negligible.

Eaton and Johnston (1981) reviewing various experiments, showed that the

growth rate of separated shear layers was comparable to the plane mixing layer growth rate. In most cases the mean velocity profiles of separated shear layers upstream of reattachment were nearly identical to plane mixing layer profiles except near the low speed edge as expected. However, they (Eaton and Johnston, 1981) have mentioned the difficulties in comparing the Reynolds stress measurements between the two types of shear layers in plane mixing layers turbulence measurements are usually scaled by the total velocity difference across the shear layer. For separated shear layer however, the velocity difference is not constant.

Bradshaw and Wong (1972) stated that back flow in the separated region increases the effective velocity difference across the shear layer and hence tends to increase the shear stress and intensity. Recirculation and re-entrainment of fluid deflected upstream at reattachment will also tend to increase the shear stress and intensity.

According to measurements of Arie and Rouse (1956) the shear stress in the reversed-flow region is certainly not negligible. Eaton and Johnston (1981) reported that the streamwise turbulence intensity of a separated shear layer is about $10 - 20\%$ higher than typical values measured in plane mixing layers. They attribute this higher intensity level to a very low-frequency vertical motion of the reattaching shear layer (flapping) although there is no general agreement on this point. The peak value of the shear stress in the separated shear layer is however very close to the typical plane mixing layer value.

A separate study by Eaton and Johnston (1982) suggests that low frequency motions (lower than the large eddy passing frequency) occur in the reattaching shear layers. These motions have time scales several times longer than the longest turbulent eddies and make substantial contribution to measured turbulence quantities. The probable cause of such long time scale motions, as indicated by Eaton and Johnston (1982), is the instantaneous imbalance

between shear layer entrainment from the recirculating zone and reinjection of fluid near reattachment. For instance, an unusual event may cause a short term breakdown of the spanwise vortices in the shear layer. The entrainment rate would then be temporarily decreased, while the reinjection rate remained constant. This would cause an increase in the volume of recirculating fluid, thus moving the shear layer away from the wall and increasing the reattachment length.

Rockwell and Naudascher (1979) and Knisely and Rockwell (1980) suggested that the low frequency motions may be the oscillation of the shear layer induced by feedback of disturbances from the impingement point to the separation point. The disturbances would appear as a low frequency modulation of the shear layer downstream of separation which would be amplified by the free shear layer. This is the mechanism responsible for low-frequency motions in cavity flows. However, as mentioned earlier there is no general agreement on the occurrence of such low frequency motion. Chandrsuda (1976, in Chandrsuda and Bradshaw 1981) could not trace such motion. Cherry et al (1984) reported occurrence of similar low-frequency motion the effect of which is significant close to separation, where it leads to a weak flapping of the shear layer.

Although there are large differences in measurements of turbulence quantities in separated shear layers and plane mixing layers, various authors have reported the self-similar behaviour of the separated shear layer. Chandrsuda and Bradshaw (1981) concluded that the separated shear layer in their experiment approaches close to self-similarity before reaching the reattachment region. Thus the effect of initial conditions on the mixing layer should be negligible near reattachment.

Cherry et al (1984) reported that from transition up to some 60% of the separated bubble length, the mixing layer can grow in relative isolation from

the effects of reattachment and the nearly linear growth of characteristic frequencies, shear layer thickness and lateral correlation scales are all similar to values found for the fully developed plane mixing layer and other separated flow experiments. Departures from self-similar development in the separated flow then appear to be associated with the presence of the reattachment surface and shear layer curvature rather than with the relatively low Reynolds number of the tests.

Ruderich and Fernholz (1986) demonstrated that the mean velocity profiles become self-similar further upstream than the fluctuating quantities and remain so for a longer distance, i.e., the self-similar range of turbulence quantities is much shorter than that of the mean velocity profiles. However, they have shown that both the separated and the reattached shear flows show large regions where individual profile families, such as $\overline{u'v'}$ and $\overline{q'^2}$ are similar which they called 'profile similarity'. Eaton and Johnston (1981) concluded that the separated shear layer is indeed very similar to a plane mixing layer upstream of the reattachment zone. The implication is that the effects of many parameters such as free stream turbulence or initial boundary layer state could be predicted using plane mixing layer data.

The reattachment region is however not clearly understood as yet. The rapid decrease of the Reynolds stresses particularly the shear stress still remains a matter of controversy. Bradshaw and Wong (1972) first concluded that a rapid reduction in length scale due to bifurcation of shear layer at reattachment region is responsible for rapid decrease in Reynolds stresses. Castro and Bradshaw (1976) reasoned that sharp curvature at the reattachment region of a rearward step flow could cause rapid decay of shear layer turbulence. Eaton and Johnston (1981) pointed out that a clear understanding of the large eddy structure in the shear layer may have an adequate explanation.

## 2.5 Large Coherent Eddy Structures in Free Shear Layers

Interest in the roles of large eddies in free shear flows intensified following the flow visualization studies by Brown and Roshko (1974) of two-dimensional mixing layers. Clearly visible, vortex-like large 'coherent' eddy structures were observed, which grew in scale with increasing downstream distance as a result of merging interactions among adjacent eddies. Winant and Browand (1974) observed that adjacent vortices tend to roll around each other before merging and generating a larger vortex. They called the process 'vortex pairing'and claimed that it is responsible for the growth of the mixing layer. The pairing process occurs randomly in space and time, resulting in a linear continuous growth of the shear layer with increasing downstream distance. The schematic diagram of Figure 2.4 shows the origin, interaction and growth of large coherent eddy structures in a typical free shear layer flow.

There are however, strong reservations on the part of some researchers regarding the indefinite persistence of such two-dimensional organised structures at very high Reynolds numbers. Chandrsuda et al (1978) suggest that these large vortices can only be seen whenever the free stream turbulence level is very low; in less favourable conditions the flow develops into the classical, chaotic three dimensional turbulence. Dimotakis and Brown (1976) indicated that the mixing layers do develop three- dimensional eddy structures, with substantial smaller scale turbulence, at higher Reynolds numbers, but they concluded that the coherence of the large-scale features was not destroyed by this development.

Some authors (Roshko, 1976, 1981; Cantwell, 1981; Browand and Troutt, 1980, 1985) believe that these structures are more characteristic of all turbulence than were previously thought. Hussain (1981) considers that although

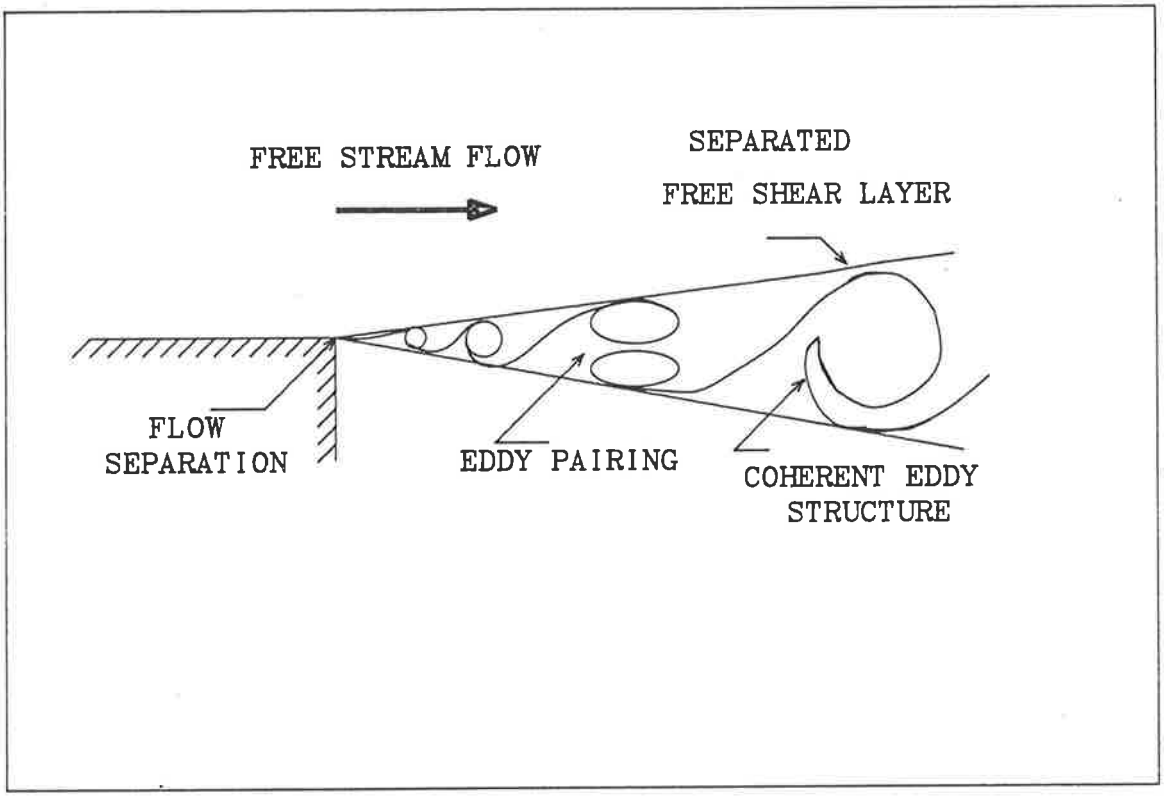


Figure 2.4: Schematic diagram of coherent eddy structures in a typical free shear flow

coherent structures are most probably inherent in all turbulent shear flows, their predominance in fully developed flows may have been exaggerated. The recent work of Wygnanski et al (1979) gives strong support for the persistence of the large scale features by demonstrating high lateral correlation even in the presence of significant levels of free-stream turbulence.

Lumley (1981) indicated that the structures present in the early flow are probably more characteristic of the initial instability, while those present in the fully developed turbulence are probably characteristic of some type of instability of the fully developed flow and are consequently not necessarily the same, unless the initial flow has been set up so that the dominant instability present there, is of the same type as that is present in the fully developed flow. Roshko (1981) points out that these structures are subject to the same type of (Kelvin- Helmholtz) instability at all stages.

Whether these structures originate from the same kind of instability in both developing and developed (self-similar) region or not; whether they are more or less organised (coherence); and whether more or less energetic, it is clear that the presence of such structures in free shear flows (perhaps in all types of turbulent shear flows) is undisputed.

Yule (1981) defined coherent structures as large eddies which, (i) are repetitive in structure, (ii) remain coherent for distances downstream much longer than their length scales, and (iii) contribute greatly to properties of the turbulence; in particular, turbulent energy and shear stress, entrainment and mixing.

Hussain (1983) defined coherent structures as a connected, large scale turbulent fluid mass with a phase - correlated vorticity over its spatial extent. That is, underlying the three-dimensional random vorticity fluctuations characterizing turbulence, there is an organised component of the vorticity which is phase-correlated (i.e., coherent) over the extent of the structure. The largest

spatial extent over which there is coherent vorticity denotes the extent of the coherent structure. Thus, turbulence consists of coherent and phase-random (i.e., incoherent) motions; the latter is superimposed on the former and typically extends beyond the boundary of a coherent structure. Hussain (1983) also indicates that these structures are responsible for transports of significant mass, heat and momentum without necessarily being highly energetic.

In spite of widespread use of the term 'coherent structure', only a few have endeavored to define what is precisely meant by 'coherent structure'. This reflects lack of understanding and agreement, as yet, on various aspects of such structures in different types of flows. Yule (1978) listed specific areas to be resolved when considering flows in terms of coherent structures,

- Growth, decay and interactions.
- Measurements of flow fields of individual structures.
- Local variation of the structures.
- Relationship to the smaller scale turbulence.
- Three dimensional effects.
- Roles in entrainment, mixing etc.
- Dependence upon initial and boundary conditions.
- Incorporation of observed structures in analysis and modelling of turbulent flow.
- Relevance to practical, complex engineering flow.

In order to obtain an unified view of what is precisely meant by coherent structure, it is essential that the above factors be considered in the investigations of coherent structures in different experimental situations.

### 2.5.1 Formation and Growth

The development of coherent structure is initially involved with some kind of instability. As speculated by many authors (Roshko, 1981; Hussain, 1983; Ho and Huerre, 1984), Kelvin-Helmholtz instability is the typical in free shear layers. When the amplitude of a small disturbance (natural or artificial) grows in time, instability results in a free shear layer, as the oscillation amplitude increases, the initially uniformly distributed thin vorticity layer tends to concentrate into two-dimensional lumps. This is the linear instability regime as described by Ho and Huerre (1984) beyond which the instability waves evolve into a periodic array of compact spanwise vortices moving at the average velocity $\bar{u}$ with a wavelength $\lambda_n = \bar{u}/f_n$, which they called the non-linear instability regime. The natural frequency of the layer, $f_n$, corresponds to the most amplified wave calculated according to the linear stability theory. The Schematic diagram of Figure 2.5, due to Winant and Browand (1974), indicates the successive stages of the initial structure development.

The recirculating regions (Fig. 2.5) within the structures contain most of the vorticity and are connected to each other via thin vorticity layers or 'braids'. The main features of the roll up process have been confirmed by many two-dimensional numerical simulations of temporally evolving shear layers (Acton 1976; Patnaik et al. 1976; Aref and Siggia, 1980).

Recent simulation studies (Patnaik et al 1976, Corcos and Sherman, 1984) have also indicated that in a shear layer the presence of an appropriately phased subharmonic is essential to the pairing process and subsequent growth. Observations of the natural or forced transition of a free shear layer (Freymuth, 1966; Browand 1966) indicated that the dominant frequency of passage of disturbances within a shear layer decreases, usually by a factor of 2, as the observation point was moved downstream.

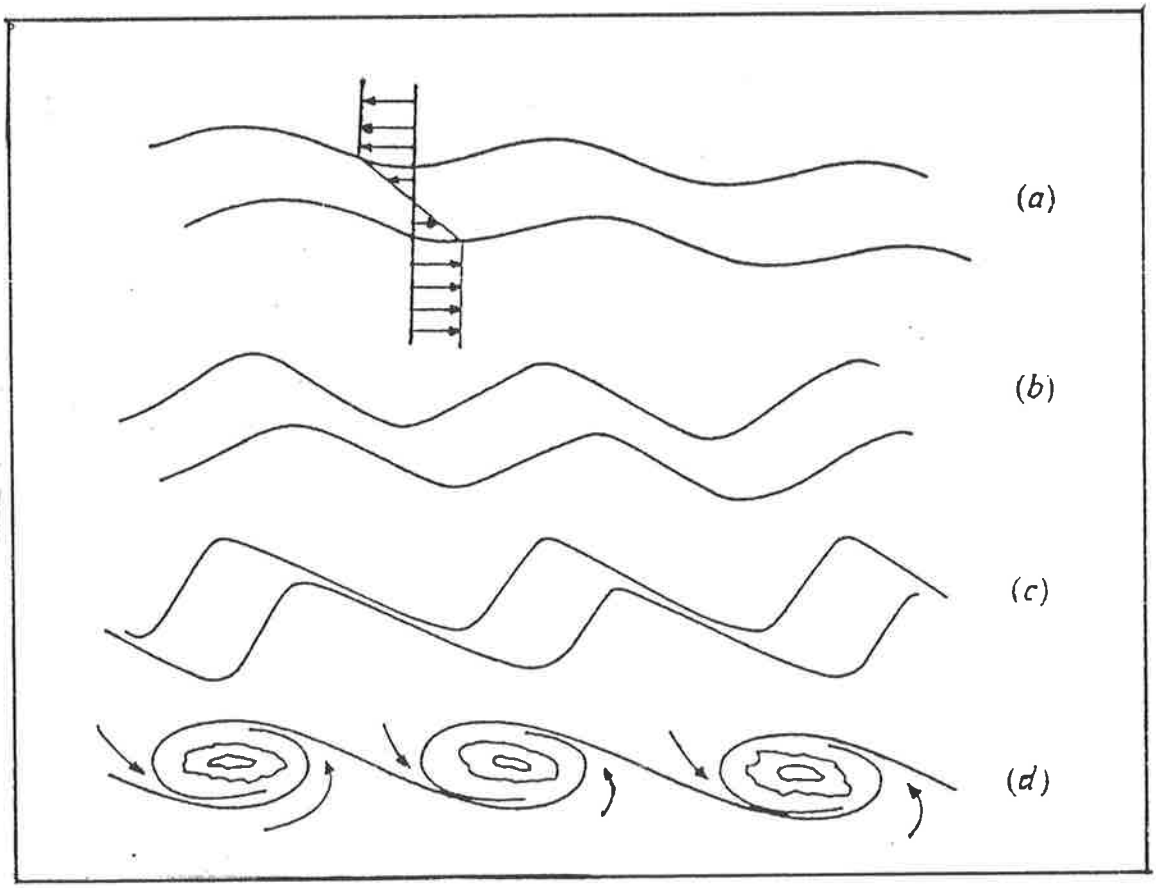


Figure 2.5: Initial instability of shear layer and roll up into discrete vortices (after Winant and Browand, 1974)

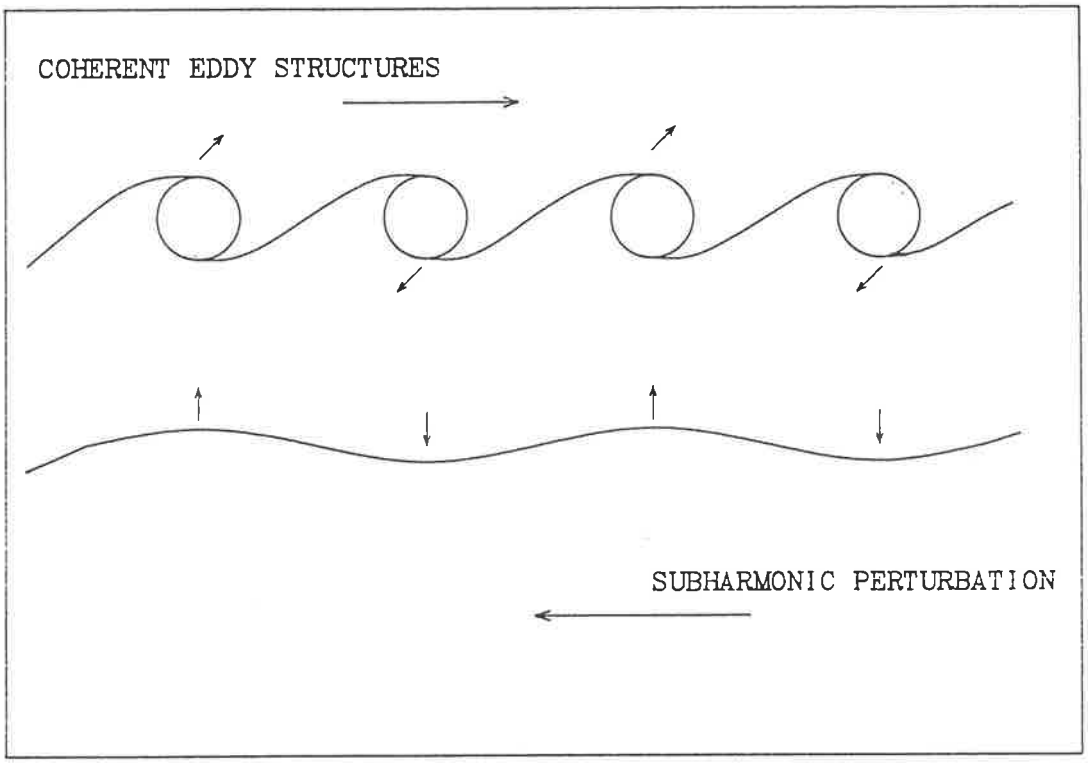


Figure 2.6: Subharmonic interaction (after Laufer, 1980)

Kelly (1967) gave a mathematical analysis in which he added a small subharmonic (perturbation) with wavelength $n\lambda$ and at a particular phase relation to the fundamental. He found that such perturbations could grow rapidly, that their growth rate depended on the amplitude of the primary perturbation and that the growth rate was a maximum when $n = 2$. Pierrehumbert and Widnell (1982) performed a similar analysis and found that a perturbation with a wavelength twice that of the fundamental can grow faster than it would if the latter were absent and that the initial growth rate of that subharmonic increases with the concentration of the vorticity of the fundamental. The primary vortices tend to pair if a subharmonic has the appropriate phase relationship with them as indicated in the Figure 2.6.

Laufer (1981) indicated that in a developing shear layer the subharmonic perturbations could be provided by the induced field of the downstream (al-

ready paired) vortices. Such a feedback mechanism is reported by Ho and Nosseir (1980) in an impinging jet. Even in the absence of an impingement surface it has been speculated by Hussain (1983) and Dimotakis and Brown (1976) that large scale structures produce a feedback upstream. However, such concept is yet to be supported by definitive evidence.

A different dynamical process, referred to as 'tearing', has been suggested by Moore and Saffman (1975) to explain the growth of mixing layers. The flow-visualization study by Hussain and Clark (1981) confirmed that tearing is as dominant as pairing. Large scale structures are continually sheared and typically fragmented due to a segment on the high speed side being torn and swept away from the slower-moving outer portion. They also suggested that the evolution of the large structures occur not primarily through complete pairing as widely believed but quite frequently through 'fractional pairing' between segments which have been torn from different upstream large scale coherent structures or through 'partial pairing' where one structure captures only a part of another.

Pierrehumbert and Widnall (1981) related the tearing mechanism to the energetic properties of a steady arrangement of streamwise periodic vortex structures with uniform vorticity. As explained by Ho and Huerre (1984), the basis for the tearing process relies on the fact that the ratio between the average vortex radius and the streamwise spacing is found to possess a maximum. Thus as the vortex radius increases by turbulent 'entrainment' of irrotational fluids, this ratio reaches its maximum allowable value. Any additional entrainment must then be accommodated by a corresponding increase in spacing through break up of a vortex by the strain of its neighbours.

Tearing process assumes, as noted by Corcos and Sherman (1984), that the dynamical states of the flow are restricted to a particular set of steady configurations, and that the subharmonic instability has been somehow inhibited.

Corcos and Sherman (1984) argued that a shear layer becomes preferentially unstable to a sequence of perturbations of increasing wavelengths and that the relaxation by diffusion of the original roll-up, as suggested by Pierrehumbert and Widnall (1981), is incompatible with the equations of motion.

### 2.5.2 Effects of Initial Conditions and Free Stream Turbulence

The state of the initial boundary layer whether laminar or turbulent, has a profound effect on the free shear layer development. According to the concepts of Reynolds number similarity (i.e. asymptotic invariance) and dynamic equilibrium or self-preservation (i.e. local invariance), all free shear flows should become independent of initial condition in the self-preserving region and thus become universal ( Townsend, 1976). In most of the earlier investigations (Leipmann and Laufer, 1947; Wygnanski and Fiedler, 1970; Patel, 1973), measurements were performed sufficiently downstream so that the flow could be considered to be independent of the initial condition, considerable scatter however, still exist among various measurements even in the self-preserving region. This is evident in reviews by Birch and Eggers (1973) and Rodi (1975) of the free shear layer data (both mean and turbulence quantities).

Hussain and Zedan (1978, 1978a) and Fiedler et al (1981) have also reported similar scatter. Such a scatter could be attributed to the persistence of initial or boundary effects, thus raising the question of the existence of a final universal i.e., initial condition independent state. No reliable criterion however, could be established, as yet, for the development length necessary for the flow to become, if at all, independent of its initial conditions.

Bradshaw (1966) suggested that a distance equivalent to 1000 times the mo-

mentum thickness of the separating boundary layer is necessary for the shear layer to reach self-similarity. Beyond this downstream distance Browand and Latigo (1979) found different spreading rates for turbulent and laminar boundary layer separation. Batt (1975) suggested that approximately 1500 momentum thicknesses may be required in order to achieve self-preserving flow for the turbulent mixing region. Dziomba and Fiedler (1985) have shown that for two stream layers the initial momentum thickness criterion for estimating the development length of the flow is insufficient, where additional parameters , e.g., the trailing edge geometry, have to be taken into account.

Hussain and Zedan (1978, 1978a) have investigated the effects of initial momentum thickness Reynolds number, the initial peak fluctuation intensity and the initial state of the boundary layer (laminar and turbulent). The effect of initial momentum thickness Reynolds number is shown to be insignificant on the various characteristic measures of a free shear layer. This is consistent with the principle of Reynolds number similarity. The other parameters have significant effects as already mentioned in section 2.3. It is, however, difficult to demonstrate practically, the effect of one particular parameter at a time whilst keeping the others unaltered. The influence of the condition of the separating boundary layer (initial condition) on the shear layer structure was also studied by Foss (1977), Batt (1975) and Oster et al (1976, in Fiedler et al 1981). General agreement was found for a stronger spread due to an initially turbulent boundary layer in the one stream shear layer as compared to the case where the initial layer is laminar.

Hussain (1983) indicated that the significant differences between measurements in developed shear flow is perhaps related to the large scale coherent structures. Since the instability and roll-up of a shear layer into structures and the subsequent evolution and interactions depend in some way on the initial condition, it is likely that some influence of initial condition is retained in the downstream large-scale coherent structure. In this sense, the shear

layer, being dominated by large scale coherent structures, may not achieve true self-preservation in a finite flow length even though one can observe self similarity of the average properties. The above speculation is however, regarding the axisymmetric mixing layer of limited region. Relatively large plane mixing layer data (Kleis and Hussain, 1979) suggest that all integral measures of the layer eventually become identical i.e., independent of the initial condition.

As mentioned earlier, the number of vortices produced in the initial stages is determined by the frequency of the most amplified wave predicted by the linear stability theory. However, as mentioned by Laufer (1975), since the vortex pairing process is found to occur randomly both in time and space, the effect of the initial condition is lost after a few pairings. For instance if the initial shear layer thickness is increased (by increasing the initial boundary layer thickness) the frequency of the initially generated vortices is lowered. However, the rate of vortex interaction, being determined by factors other than the initial frequency, will still produce the same spreading rate. This appears consistent with the similarity concept of the mixing layer.

The effects of free stream turbulence on free shear flows have been investigated by Patel (1978). It is shown that the scale of growth of a plane mixing layer was altered by 30% when the stream turbulence intensity was changed from 0.5% to 1.4%. The rate of growth however, is not affected significantly for values of the stream turbulence intensity below 0.6%. It is also shown that the longitudinal turbulence intensity distribution is not affected by the changes in the Reynolds number, but the stream turbulence has significant influence. Chandrsuda et al (1978) suggested that the two-dimensional large coherent structures are formed if the free stream turbulence is low. If the free stream disturbances are significant, three- dimensionality develops at an early stage in transition causing eventual breakdown of the coherent structure. They also suggested that the large coherent structure will not appear

if the initial boundary layer is turbulent.

The experimental investigation by Hussain and Zaman (1985) demonstrates that an initially fully turbulent mixing layer does roll up into organized coherent structures and that these structures could be detected for the entire length of the measurement, i.e., up to x = 3 m or 5000 time exit momentum thickness. The free stream turbulence intensity for their (Hussain and Zaman, 1985) experiment was however, less than 0.2%. There is no general agreement on the issue of the effects of free stream turbulence on large scale coherent structures as experimental evidence on this matter are still insufficient.

### 2.5.3 Effects of Three Dimensionality

In a free shear layer, the primary large coherent structures would, ideally, be two- dimensional, containing the single component of vorticity while secondary and higher modes of instability would introduce three- dimensionality and two other components of vorticity into the flow. There is some evidence which suggests that plane mixing layers contain secondary structures involving the deformation of the primary large scale structures along their span.

Roshko (1981) reported that the development of a mixing layer is largely determined by two sets of organised structures: the primary, spanwise vortices and the secondary streamwise vortices. The Reynolds stress and the growth of the layer are controlled by primary large structures while the secondary streamwise vortices enhance internal mixing. Browand and Troutt (1980) observed skewed structures in their isometric visualization of the velocity field suggestive of three-dimensionality. They however, associated such observations with pairing interactions between vortices.

Roshko (1981) suggests that while the primary structure would be the span-

wise vortex resulting from the Kelvin-Helmholtz instability, the secondary structure evolves due to either a spanwise instability or a secondary, internal instability, the latter being the most likely one. Such internal instability induces secondary motions inside the primary structures and creates pairs of streamwise counter rotating vortices which are embeded in the primary vortices and in the connecting 'braids'.

Such an arrangement had been predicted theoretically by Corcos and Lin (1984). According to their model, a developing and pairing two-dimensional layer fosters the growth of initially small three- dimensional perturbations so that the vorticity whose dominant direction is spanwise acquires a component normal to the span and would be stretched by the straining field produced by the primary eddies into long longitudinal vortices. Jimenez et al (1985) applying digital image processing to laser fluorescence motion pictures, constructed a three-dimensional model which shows that a system of streamwise counter-rotating vortices exists on top of the spanwise large vortices.

More recently, Bernal and Roshko (1986) proposed a model of streamwise vortex structure in the mixing layer. According to their model, the streamwise vortex structure, originating from an internal instability of the primary vortices, are now seen as part of a 'warped - vortex - line' threading its way up and downstream between any two adjacent spanwise vortices as shown in Figure 2.7.

This proposed 'warped-vortex-line' structure was inferred mainly from a frame-by-frame study of high-speed motion pictures. The topology of the streamwise vortex structure and its relation to the spanwise vortices can be visualized from Fig 2.8. They (Bernal and Roshko, 1986) also claimed that their proposed model is consistent with their concentration measurements.

A slightly different model of streamwise vortex structure is proposed by Hus-

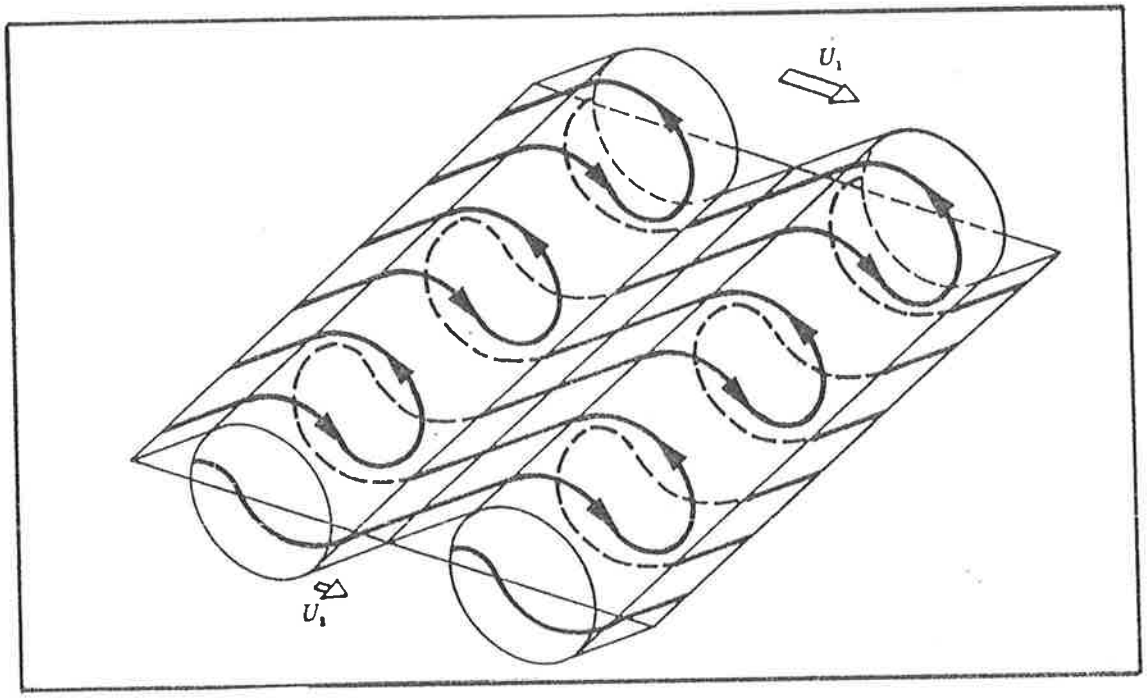


Figure 2.7: Streamwise vortexlines (after Bernal and Roshko, 1986)

sain (1984) which states that the braid connecting two consecutive spanwise vortex rolls is not a continuous sheet but consists of individual strands of vortical 'ribs' and these are stretched continually by the co-rotating spanwise rolls which give rise to transverse motions of external fluid enhancing turbulence production and entrainment. This model is based on his extensive experimental measurements of 'phase-averaged' turbulence production.

### 2.5.4 Entrainment and Mixing

A fundamental property of free shear flow, related to its growth, is the phenomenon of entrainment, that is, the incorporation of ambient irrotational fluid into the turbulent region or the diffusion of the turbulent fluid (vorticity) into the ambient flow. The manner in which entrainment occurs and

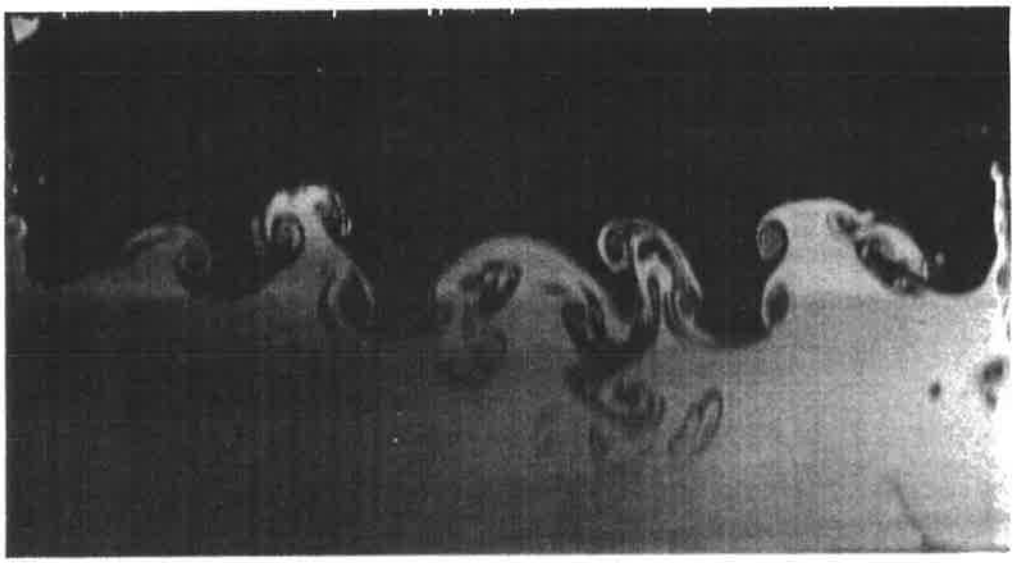

(a) Section across the Braid.

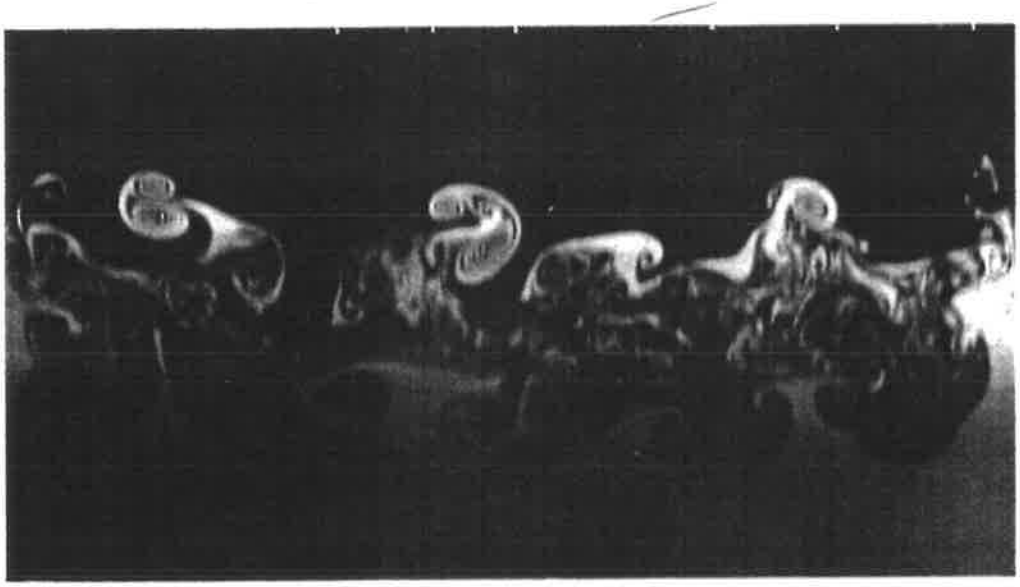

(b) Section across the structure core.

Figure 2.8: Topology of the streamwise vortex structure (after Bernal and Roshko, 1986)

where it takes place is however, a matter of much interest and some debate in recent years, particularly with the revelation of the large scale coherent structures in free shear flows. From various interpretations of the process of entrainment, two basic lines of approach can be mentioned as discussed by Bevilaqua and Lykoudis (1977):

- entrainment is a result of viscous diffusion of vorticity at the smallest scales of the turbulence; or
- it is due to the engulfing action of the large coherent eddies.

It has been known for many years that in free turbulent flows there is a sharp convoluted interface between the region where the flow is turbulent and the external region of irrotational motion. Corrsin and Kistler (1955) pointed out that in a fluid of constant density, vorticity can be acquired by a fluid element outside the turbulent interface only by viscous diffusion of vorticity. They called this interface 'viscous superlayer' which is different from viscous sublayer.

Once a fluid element has been sheared by viscous stresses at the superlayer, its vorticity is rapidly increased by the straining induced by the neighbouring turbulence and becomes comparable to the turbulence itself, and their incorporation into the turbulence is then complete. Since the turbulence in the superlayer exists in a condition of equilibrium between diffusion by viscosity and amplification by turbulent straining, Corrsin and Kistler (1955) considered it as being similar to the turbulence in Kolmogorov's universal equilibrium range of the energy spectrum which is balanced between dissipation at higher wave numbers and amplification at lower wave numbers.

Thus, they concluded, by analogy, that the scale of the turbulence at the boundary and the thickness of superlayer must therefore by small, of the

order of Kolmogorov's microscale (dissipation length),

$$\lambda = (\nu^3/\epsilon)^{1/4}$$

where, $\epsilon$ is the energy dissipation rate in the equilibrium range and $\nu$ is the fluid viscosity. They also suggested that the average rate of advance of the diffusing layer is proportional to Kolmogorov's velocity scale

$$v_s = (\nu\omega)^{1/2} = [\nu(\epsilon/\nu)^{1/2}]^{1/2} = (\nu\epsilon)^{1/4}$$

Phillips (1972) however, argued this view saying that the rate at which the surface advances may be more characteristic of the velocities of the energy containing (large) eddies, although he retained the notion of a small scale entrainment process. Bevilaqua and Lykoudis (1977) raised even a more fundamental question. They reasoned that turbulence in the universal equilibrium range is, by definition, independent of conditions in the mean flow, whereas the speed at which the interface advances must adjust both to the flow geometry and to changes in the spreading rate. They (Bevilaqua and Lykoudis) expressed their view of entrainment process to be controlled by the rotation of the large coherent eddies. This is the second line of approach.

According to this approach, the interface for the turbulent vorticity is kept sharp by the action (rotation) of the large eddy in bringing high intensity turbulence to the surface from the interior of the flow. At the interface, viscosity diffuses the turbulent vorticity, thus retarding the motion of the external flow relative to the surface. The decelerated fluid is then entrained into the turbulent core of the flow by the rotation of the large eddy. The newly entrained fluid is not immediately diffused by the other scales of the turbulence but continues to rotate with the large eddy.

The schematic diagram of Figure 2.9 shows the process of entrainment by the engulfing action of large eddies. This view of entrainment process is supported by the flow visualization studies by Brown and Roshko (1975) and

Dimotakis and Brown (1976). It is also apparent from the study of Dimotakis and Brown (1976) that the processes of entrainment and fine-scale mixing, at high Reynolds numbers, are almost distinct and separate stages.

A recent investigation by Chevray (1984) indicates entrainment of irrotational fluid during roll-up of the cores of the coherent structures and away from the core the entrainment through the interface is very little. He also mentioned entrainment by 'nibbling' as a secondary mode of entrainment in the case of two-dimensional shear layer.

The question of what happens to portions of fluid which have entrained into the mixing region is not very clear. Roshko (1976) suggests measurement of a scale property such as temperature or species concentration could provide necessary information about this. Hussain's (1984) model of coherent structure suggests that mixing is dominant neither at the top or bottom surface of the rolls nor at the saddle but at a point intermediate between these two as shown in Figure 2.10. He argued that mixing implies imparting three-dimensional vorticity. Since vorticity is two-dimensional at the saddle, it is not the likely location of mixing. The point shown in the figure to be the location maximum mixing, imparts three dimensional vorticity due to the interaction between the longitudinal vorticity of ribs and spanwise vorticity of large structures, and hence causes mixing. Such mixing is thus an inviscid mechanism (Hussain, 1984), viscosity being responsible for the final molecular mixing.

Breidenthal (1979) defined the 'mixing transition' as the region through which the 'mixedness' increases from a low value to a high value, by a factor of about more than 10. Roshko (1981) compared this region of mixing transition to the measurements by Bradshaw (1966) of Reynolds shear stress, $-\overline{u'v'}$, in the initial development region of a mixing layer as shown in Figure 2.11. The important point was to show that the end of mixing transition

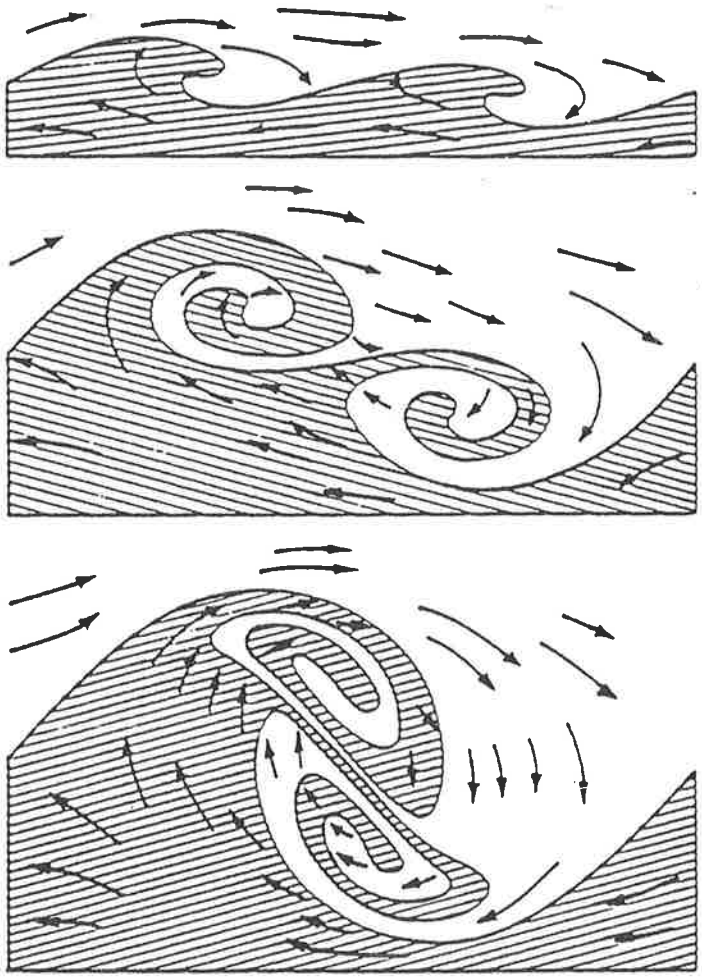

Figure 2.9: Entrainment by the engulfing action of the large structures (after Corcos and Lin, 1984)

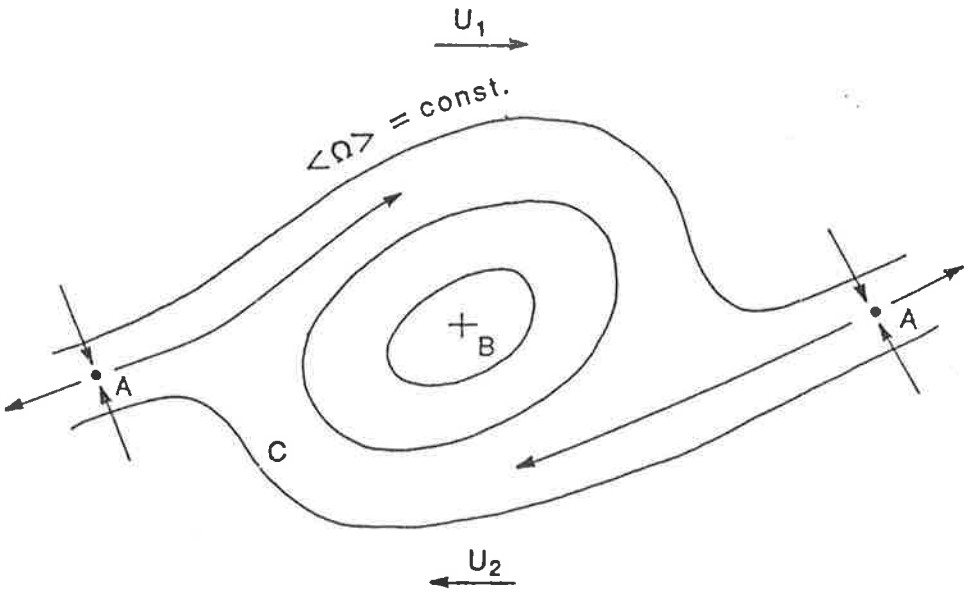


Figure 2.10: Coherent structure cross-section in a mixing layer
(after Hussain,1983)

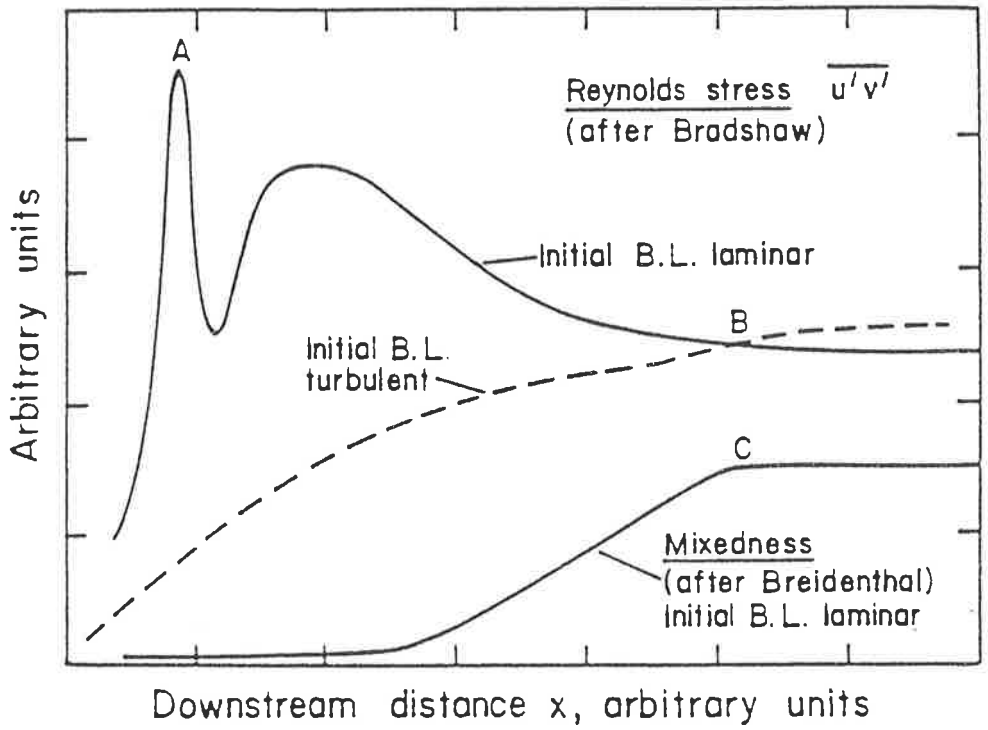


Figure 2.11: Mixing transition (after Breidenthal 1979)

corresponds to the final state of development of a mixing layer.

Bernal and Roshko (1986) demonstrated the relationship between the streamwise vortex structure and the mixing transition. According to their model the streamwise vortices increase the interfacial area in the core of the vortices and thus contribute to mixing. The unmixed core fluid entrained during the initial two-dimensional development is mixed during transition. The streamwise vortices play an indirect role in this process since stretched vorticity along the braids will become part of the spanwise vortex core after amalgamation. This mechanism suggests (Bernal and Roshko, 1986) that the mixing transition should be completed downstream of the three- dimensional instability, after a number of amalgamation.

The above discussion indicates that the dynamic role of the large coherent eddy structures is mainly responsible for the entrainment of the ambient fluid into the turbulent region which appears to be in contrast to the traditionally held concept of vorticity diffusion as the basic process of entrainment. Mixing of the entrained fluid occurs due to an interaction between the spanwise vorticity of the large structures and the small scale streamwise vorticity. This streamwise vorticity is considered to be developed due to an internal instability in the primary large scale structures.

### 2.5.5 Coherent Structure Investigations

As mentioned previously, there are two opposing schools of thought regarding the existence and importance of large coherent structures in turbulent shear flows. One school (eg. Bradshaw, 1966; Chandrsuda et al 1978) feels that

- the well organised coherent structures are present only in the early part of turbulent flows (developing region);
- the degree of coherence decreases as the flows age;
- the earlier investigations were performed in the developed region of the flow thus not revealing the existence of such structures; and
- the coherent structures observed may be attributable in part to the extreme care which is taken to remove adventitious disturbances from the oncoming flow so that the instability of the initial flow will be of a single type, and the transition flow will be dominated by the non-linear evolution of this instability.

The opposing school (eg Roshko, 1976, 1981; Cantwell, 1981; Browand and Troutt, 1980, 1985) appears to consider that

- these structures are characteristic of all turbulent shear flow;
- such structures were overlooked previously because flow visualization was not used;
- previous measurements using conventional statistical approaches smeared out and thus concealed the organisation truly present in the flow, which can be identified using conditional sampling and flow visualization; and
- these structures are responsible for entrainment, mixing and transport of various properties in turbulent flow.

According to Lumley (1981), well organised energetic structures are present only in the flows close to the origin; the structures in fully developed flows contain sufficiently small energy and play a secondary role in transport. There is however, a general agreement on the issue that some form of organised structures are present in turbulent shear flows. Whether such structures are well organised or less; whether they contain more energy or less; or whether they play primary or secondary role in transport are the matters of recent investigations.

## (A) Experimental Measurements

As mentioned above experimental techniques have an important bearing on the analysis and results of coherent structure investigations. Special experimental techniques have to be applied according to the objectives of investigations in order to achieve the necessary information regarding coherent structures in turbulent flows.

### (I) Flow Visualization

Cine photography is an essential first technique to apply for the study of coherent structures in turbulent shear flows. In order to readily observe large patterns of flows, various marking processes have been used in the visualization studies. For air flows, smoke and particle injection can be used;

whilst for water flows dye, particle or hydrogen bubble injections are preferred (Mathieu and Charnay, 1980). Such visualization methods give an excellent description of the generation and development of coherent structures; additionally they give some quantitative data such as eddy passing frequencies, time and length scales, mean advection velocities etc.

Flow visualization has been used by numerous investigators as a basic tool for understanding the fundamental mechanisms of various flows. Brown and Roshko (1974) first pointed out that mixing layer flows are dominated by two-dimensional large coherent structures; Winant and Browand (1974) indicated that pairing of large structures is responsible for growth of mixing layers; Dimotakis and Brown (1976) and Chevray (1984) demonstrated that basic entrainment process is due to the engulfing action of large coherent eddies; Bernal et al (1979) and Bernal and Roshko (1986) observed three-dimensional small scale structures in turbulent mixing layers; Hussain and Clark (1981) postulated that not only pairing but also 'tearing', partial and fractional pairing are the important phenomena involved in mixing layer development and growth, to cite a few flow visualization results. Through digital image processing Jimenez et al (1985) presented quantitative informations e.g., vortex strength, from visualization pictures.

**(II) Conditional Sampling and Averaging**

While flow visualization studies have provided useful qualitative and to some extent quantitative information about coherent structures, most of the quantitative information has been obtained by point measurements using conditional sampling and various averaging techniques. Conditional sampling, as defined by Subramanian et al (1982), is the eduction of information about a coherent structure with respect to the time reference provided by the detection method used to recognise the structure. It can be performed with one or more probes and consists in the observation of a property only when some criterion is satisfied.

However, the major difficulty of conditional sampling is associated with the selection of a sampling criterion as the quantitative results obtained by different criteria on the same flow structure can vary considerably. Hussain and Zaman (1985) for instance, developed optimum conditional sampling criterion by triggering on the peaks of a local reference velocity signal obtained from the high speed edge of the mixing layer.

Average signatures of the coherent structures in a mixing layer have been determined, using conditional sampling, by various investigators (Browand and Weidman 1976; Lau and Fisher, 1975; Brunn, 1977; Yule, 1978). Yule (1980) considered 'phase scrambling' effects on conditionally sampled data and cautioned that conditioning data incorrectly may lead to apparent or 'false' structure. A detail discussion on the various conditional sampling techniques is not included in this review. Van-Atta (1974), Antonia (1981) and Subramanian et al (1982) give further details on this subject.

Some form of averaging of the conditionally sampled data is performed in order to provide meaningful information about the flow. As mentioned by Laufer (1975), the concept of simple 'time averaging' is no longer a useful concept with flows considering large coherent structures with rapid changes in the flow field. One then considers a different type of averaging called 'ensemble averaging' which is obtained over an ensemble of events or structures. In particular, ensemble averages can be obtained relative to a reference point of the structure over a series of time points, each corresponding to a particular phase of that structure. A common form of ensemble average (Antonia, 1981) is

$$\langle f(x,\tau_j)\rangle = \frac{1}{N}\sum_{n=1}^{N} f(x,t_n+\tau_j)$$

where, $t_n$ are the points in time when detection occurs, $\tau_j$ is the time delay and N is the maximum number of events detected.

Another form of averaging, called 'phase averaging' was introduced by Reynolds and Hussain (1972). Similar to the time-average concept, the phase average is the ensemble average of any property at a particular phase of the structure, that is,

$$\langle f(x,y,z,t)\rangle = \lim_{N\to\infty} \frac{1}{N}\sum_{i=1}^{N} f_i(x,y,z,t+t_i)$$

where, t denotes the time corresponding to the reference phase and $t_i$ denotes the random instants of occurrence of successive structures of the selected phase.

### (III) Data Analysis and Results

Correlation analysis of conditionally averaged data provide useful information about coherent structures. Autocorrelation of the velocity measured at a single point, with a time delay, has successfully been used for the characterization of coherent structures. Dimotakis and Brown (1976) computed autocorrelation functions and observed a fundamental periodicity of the large structure in accordance with the expected similarity scaling. The surprisingly long correlation times which they consider associated with large structure dynamics suggest that the large structure phase is not destroyed in the amalgamation process, but remains coupled to the phase of the structures formed subsequently which is in contrast to the similarity behaviour.

A recent measurement by Browand and Troutt (1985) of the conventional correlations in both the streamwise and spanwise directions indicate that the vortex structure becomes independent of the downstream coordinate. Their measurements suggest that the large vortices in the mixing layer undergo a reorganization after initial laminar formation, and rapidly develop a characteristic structure. They consider this observation as a strong experimental evidence for the persistence of such large structures. This is consistent with their earlier (Browand and Troutt, 1980) observations.

Measurements of the spanwise correlations of the longitudinal velocity fluctuations led Chandrsuda et al (1978) to the conclusion that at higher Reynolds number the spanwise scale decreases which is consistent with the conventional development of three-dimensionality. Hussain and Zaman (1985) measured the power spectrum of the streamwise velocity fluctuation on the high speed edge of a single stream mixing layer where $\bar{u}/U = 0.99$, and observed distinct humps in the spectra indicating the presence of large scale structures throughout the entire length of measurement. The hump frequency decreases with increasing downstream distance x, indicating the emergence of continually larger structures through interactions such as pairing. Based on the local momentum thickness $\theta$, they found that the Strouhal number, $S_t = f_m\theta/U$ has a constant value of about 0.024. Browand and Troutt (1985) found average value of Strouhal number based on vorticity thickness, $S_t = \delta_w/(T_p\bar{u})$ of a two-stream mixing layer between 0.26 - 0.27 for the speed ratio of 0.65.

The probability density functions are also used for convenient descriptions of coherent structures. It is well known that in regions affected by coherent structures which introduce internal intermittency, the probability density distribution is not Gaussian (Mathieu and Chennay, 1980). In relation to concentration measurements the probability density functions can provide useful information regarding mixing.

Alongside the statistical information of the coherent structures in free shear layer, another key question is their dynamical significance. Townsend (1956, 1976) hypothesized, in what he called the dynamic equilibrium of large scale structures, that the large scale motion plays a central role in the dynamics of the flow development. According to his hypothesis, the flow dynamics is governed by the balance between the rate of energy extraction by the large structures from the mean flow and the rate of loss of energy by these structures to the small scale turbulence i.e., the rate of turbulent energy production. Laufer (1975) pointed out the fact that the turbulence production

at a fixed point in the flow is not a continuous process.

Browand and Weidman (1976) demonstrated that vortex pairing was associated with Reynolds stress production in a mixing layer. Similar observations were made by Hussain and Zaman (1981) in the mixing layer of an axisymmetric jet. Wygnanski and Oster (1982) have demonstrated that the Reynolds stresses and thus the production of turbulent energy can be manipulated by controlling the interactions between large vortices. When pairing is inhibited, the Reynolds stress changes sign completely, and the turbulence loses energy. Hussain and Zaman (1985), through decomposition of the instantaneous variable into coherent and incoherent components and through 'phase-averaged' measurements show that both coherent and incoherent motions are significant in contributing to the Reynolds stress.

## (B) Theoretical Approach

The realization of coherent large scale motion in free shear flows, through extensive experimental research, has stimulated theoretical and numerical studies along the line which are considerably different from the conventional approach. The conventional theoretical approaches will be discussed in greater detail in the next chapter. One such relatively recent approach is the Large Eddy Simulation (LES) approach, the basic philosophy of which is to explicitly compute the large scale unsteady motions which are directly affected by the boundary conditions (see Cantwell, 1981). The important assumption of this approach is that the small-scale motion (sub-grid-scale fluctuations) which cannot be resolved with the chosen numerical grid are only slightly nonisotropic and can be approximated by an universal model.

Mansour et al (1978) considered the temporally-developing mixing layers using a subgrid scale turbulence model. Both the two-dimensional and the fully three-dimensional cases were treated. In the two-dimensional case, large-scale eddy interaction and pairing was observed. The mean velocity

and turbulence intensity profiles were found to remain self-similar throughout the interaction. The growth rate was observed to be linear although the magnitude was dependent on the choice of the initial condition.

Gatski and Liu (1980) considered the dynamics of growth and decay of a single eddy in the temporally developing mixing layer using the turbulence model of Hanjalic and Launder (1972) for the fine-scale turbulent motion. The initial condition consisted of the mean velocity profile and a small perturbation which represented the most unstable disturbance based on an inviscid stability analysis of the mean velocity profile. A large eddy structure was observed to grow, extracting energy from the mean flow while simultaneously losing energy at a smaller rate to the fine scale turbulence. After a finite time, the growth of the eddy ceased and energy was both transferred back to the mean motion (negative turbulence production) and lost to the fine scale turbulence.

Knight (1979) using the model of Saffman (1977) for fine scale turbulence demonstrated the interaction of large scale coherent structures in the temporally developing two-dimensional mixing layer. Eddy interaction and pairing was observed to occur, with a strong energy transfer from the mean flow to the large scale coherent motion during eddy coalescence and a reverse energy transfer (negative production) to the mean motion following the amalgamation. Two different fine-scale turbulence models, namely a full Reynolds stress equation model and simple eddy viscosity model were used by Knight and Murray (1980). The results using the latter model was compared with experimental results suggesting a significant portion of the total Reynolds shear stress is attributable to the incoherent turbulent fluctuations.

Another approach of numerical simulation of a turbulent mixing layer is by discrete vortex method in which the mixing layers are represented as an assembly of two dimensional, inviscid discrete vortices. This discrete

vortex method can again be divided into two different approaches. In the first approach, the mixing layer is considered to be a time-developing shear layer whose coordinate system is moving with average advection velocity. The major interest is in the time evolution of the distribution of the vortices. Acton's (1976) model based on this concept is consistent with many observed features of the shear layer apart from the situation where the initial layer thickness is large in which case the structures formed after coalescence are only approximately independent of the initial conditions.

The model presented by Aref and Siggia (1980) suggest that the shear layer may be thickened by a scattering of discrete vortices and only partly by vortex amalgamation. The crucial disadvantage of this time-developing approach as pointed out by Inoue (1985) is that the effects of the advection velocity and of the parameter representing speed ratio, can not be incorporated in the computation because the coordinate system is moving with the advection velocity and this makes it difficult to quantitatively compare the calculated and experimental results.

In the second approach, the spatially growing mixing layer is simulated directly. Ashurst's (1979) model is the first along this line who considered both moderate and high Reynolds number flows. With the exception of the normal rms velocity fluctuation in the case of high Reynolds number, all calculations are in agreement with experimental results. Recently, Inoue (1985) simulated a turbulent mixing layer with high Reynolds number adopting this approach. The mixing layer appears to grow through the entrainment of non-turbulent fluid particles induced by clusters of discrete vortices or large eddies. The role of the vortex pairing process appears to increase the strength of vorticity of the clusters of discrete vortices. Thus the self-growth of large eddies found by Hernan and Jimenez (1982) may also play an important role in mixing layer development.

### 2.5.6 Coherent Structures in Reattaching Shear Layer

Very few investigations have been performed of the large eddy structure in reattaching shear layers. McGuinness (1978) observed large-eddy structures in a reattaching shear layer behind an orifice at the entrance of a pipe and tentatively concluded that some of the large eddies were swept upstream with the recirculating flow, while others proceeded downstream. He attributed the rapid decay of turbulent stresses near the reattachment region to this mechanism.

This is in contrast to Bradshaw and Wong's (1972) conjecture that the large eddies are torn roughly into two which is the reason for pronounced decrease in eddy length scale downstream of reattachment. Measurements by Chandrsuda (1976) and Kim et al (1978) supported the view of McGuinness (1978). Flow visualization by Eaton and Johnston (1981) did not show any evidence of large eddies being swept upstream.

A recent investigation by Troutt et al (1984) strongly supports the importance of large scale organised structures in reattaching separated flow fields. Prior to the reattachment region, the organised large structures appear to behave much like the plane mixing layer structures observed in numerous investigations. Pairing interactions between structures occur and spanwise correlation scales are comparable to mixing layer scales. However, pairing interactions appear to be strongly inhibited in the reattachment region, which appears to be the reason for sharp decrease in cross-stream Reynolds stresses and turbulence energy observed near the reattachment region.

## 2.6 Mass Transfer in Separated Flow

The mass transfer between the separated flow field and the main stream flow is due almost entirely to the lateral turbulent fluctuating motion. The mean motion, and particularly the motion in the separated flow zone has, however an effect on the mass transfer in that it governs the advective transport of mass to the mixing zone where the transfer takes place. It has also a determining influence on the concentration distribution within the separated flow region.

The detail understanding of the transfer process and hence theoretical prediction has become complicated due to the complex nature of turbulence in the separated flow field, particularly the turbulence structure in the separated mixing layer. The mathematical models proposed so far attempt only to give a global description of the mass transfer process and are of highly empirical nature (McGuirk and Rodi, 1979). Measurements of scalar quantities such as species concentration, as indicated by Launder (1976), can increase the understanding of the mass transfer process and provide quantitative informations for the development of theoretical models for such flows.

Although the problem of predicting concentration levels in turbulent flows of simple geometry has received considerable attention, such problem in complex separated flows has received very little attention despite their enormous practical importance. Measurements of concentration fluctuations and turbulent fluxes in such flows which could provide the necessary insight to the development of improved prediction methods, have been very few. Moreover, most of the measurements do not explicitly consider the variation of concentration distribution within the separated (recirculating) region.

Westrich (1976) for instance, assumed constant concentration in a rectangular stagnation zone which according to the measurements of Nestmann (1977,

in McGuirk and Rodi, 1979) varies significantly. Measurements at various locations in a small cavity by Valentine and Word (1977) showed that the concentration distribution in the cavity was within 10 percent of the mean. They therefore considered the value at the centre of the cavity to be the representative average value. However, as discussed earlier (section 2.4), depending on the flow of the main stream and the geometry of the separated region secondary or even higher order eddies may develop which will then lead to the concentration variation within the region.

Another important part of separated flows to be considered is the separated shear layer which are now known to be consisted of large scale coherent vortical structures, the dynamics of which apparently dominates the entrainment and mixing processes. Studies on these structures in shear layers (see Sreenivasan, Tavoularis and Corrsin, 1981; and Koochesfahani et al, 1985) have raised a fundamental question of the applicability of the concepts of gradient transports and eddy diffusivity which are the traditionally accepted bases for mixing and mass transfer analyses. A recent model proposed by Broadwell and Briedenthal (1982) attempts to model mixing in chemically reacting shear layer which does not employ the concept of gradient diffusion.

An important result of some quantitative studies (Bernal et al, 1980; Breidenthal, 1981; Roshko, 1981) of entrainment and mixing in shear layers is the mixing transition, which is a consequence of the introduction of small scale, three-dimensional motions into the layer and is associated with a marked increase in the amount of mixed fluid in the turbulent region.

Recently Koochesfahani and Dimotakis (1985) performed an experimental investigation of entrainment and mixing in a non reacting, uniform density, liquid mixing layer using a passive scalar to measure the probability density function (pdf) of the composition field. Their results show that the vortical structures in the mixing layer initially roll up with a large excess of

high-speed fluid in the cores. It is also found that at the beginning of the mixing transition, the fluid is mostly found to be mixed at very high values of concentration and, accordingly, the pdf is considerably asymmetric in favour of the high speed side. The distribution of mixed fluid shifts toward lower concentrations as mixing proceeds.

Direct measurements of the amount of chemical product in their chemically reacting experiments (Koochesfahani and Dimotakis, 1986) show that the product in a liquid layer at high Reynolds number is much less than that in a gaseous mixing layer implying that molecular diffusion plays a role in the turbulent mixing process.

Bernal and Roshko (1986) report spanwise concentration non-uniformities through their concentration measurements (mean and r.m.s. concentration profiles) at various locations in a gaseous mixing layer. They associate this non-uniformities with the secondary streamwise vortex structures which, according to them, contributes not only to mixing of passive scalar but also to all components of the Reynolds stress.

The above important results may lead to a change in the conventional approach to the mass transfer process across a shear layer thereby improving the understanding of mass transfer in separated flows. Particularly an evaluation of the rate of mass transfer to and from the separated region which is often represented by a constant exchange co-efficient, appears necessary in the light of the large structure dynamics along the separated-reattaching shear layer.

# Chapter 3

# Theoretical Considerations

## 3.1 General

In this chapter previous theoretical studies relating to the present study are considered and some new approaches regarding the analysis of coherent eddy structures in free shear flows are discussed. As mentioned in chapter 1, the bulk of this study concerns the experimental investigation of the mixing and mass transfer across the separated free shear layer which divides the separated recirculating flow from the main stream flow. There are two flow regions of major interest which play major role in the overall mixing and transport processes in this type of separated flow. The first and the most dominant one is essentially the two dimensional mixing layer region which controls the transfer rate, and the second is the recirculating flow region which provides fluid for entrainment by the mixing layer.

Of particular interest is the presence of the large scale coherent eddy structures in the nominally two dimensional shear layer and their influences in the mixing and transfer processes. In the later part of this chapter new approaches for the analysis of the coherent eddy structures in the free shear layer are discussed. Based on the suggestions of Hussain and Reynolds (1972) and Hussain (1977), the mass transfer equations are considered and several important quantities are discussed. In the earlier part of the chapter a review of the previous theories on free shear flows are presented. The chapter begins with a brief discussion on the general equations of motion and the equations of the conservation of mass.

## 3.2 Equations of Motion

The starting point for evaluating mixing processes in a turbulent flow field is the well known Navier - Stokes equations. For incompressible flow, the Navier - Stokes equations can be written in the form

$$\frac{\partial u}{\partial t} + u\frac{\partial u}{\partial x} + v\frac{\partial u}{\partial y} + w\frac{\partial u}{\partial z} = -\frac{1}{\rho}\frac{\partial p}{\partial x} + \nu\nabla^2 u \tag{3.1}$$

$$\frac{\partial v}{\partial t} + u\frac{\partial v}{\partial x} + v\frac{\partial v}{\partial y} + w\frac{\partial v}{\partial z} = -\frac{1}{\rho}\frac{\partial p}{\partial y} + \nu\nabla^2 v \tag{3.2}$$

$$\frac{\partial w}{\partial t} + u\frac{\partial w}{\partial x} + v\frac{\partial w}{\partial y} + w\frac{\partial w}{\partial z} = -\frac{1}{\rho}\frac{\partial p}{\partial z} + \nu\nabla^2 w \tag{3.3}$$

where,

$$\nabla^2 = \left(\frac{\partial^2}{\partial x^2} + \frac{\partial^2}{\partial y^2} + \frac{\partial^2}{\partial z^2}\right),$$

u,v and w are the instantaneous velocity components in the cartesian coordinate directions of x,y and z respectively,

$\nu(=\frac{\mu}{\rho})$ denotes the kinematic viscosity,

p denotes pressure, and

t denotes time.

The continuity equation is written as

$$\frac{\partial u}{\partial x}+\frac{\partial v}{\partial y}+\frac{\partial w}{\partial z}=0 \tag{3.4}$$

The above set of equations of motion is general and applies to turbulent as well as non-turbulent cases. However, for the complexity of turbulence, these equations cannot at present be solved for turbulent flows of practical relevance. A statistical approach is therefore, taken and as suggested by Osborne Reynolds, the instantaneous flow properties are decomposed into the mean and fluctuating quantities -

$$u=\bar{u}+u';$$

$$v=\bar{v}+v';$$

$$w=\bar{w}+w';$$

and

$$p=\bar{p}+p'$$

where,

$$\bar{u}\equiv\frac{1}{T}\int_0^T u\,dt$$

and T is the averaging time period which is long compared to the time scale of the turbulent motion. Since the fluctuations are both positive and negative,

the mean of $u'$ is

$$\bar{u'} \equiv \frac{1}{T}\int_0^T u'dt \equiv 0$$

Applying the Reynolds averaging technique to the continuity equation, one obtains,

$$\frac{\partial \bar{u}}{\partial x} + \frac{\partial \bar{v}}{\partial y} + \frac{\partial \bar{w}}{\partial z} = 0$$

and

$$\frac{\partial u'}{\partial x} + \frac{\partial v'}{\partial y} + \frac{\partial w'}{\partial z} = 0$$

Thus both the mean and the turbulent fluctuating components satisfy the continuity condition. Using the continuity equations and applying Reynolds' averaging to the Navier - Stokes equations, the equations of motion for the turbulent incompressible flow are obtained

$$\frac{\partial \bar{u}_i}{\partial t} + \bar{u}_j\frac{\partial \bar{u}_i}{\partial x_j} = -\frac{1}{\rho}\frac{\partial \bar{p}}{\partial x_i} + \frac{\partial}{\partial x_j}(\nu\frac{\partial \bar{u}_i}{\partial x_j} - \overline{u_i'u_j'}) \tag{3.5}$$

where the subscripts i and j denote the usual cartesian tensor notations.

In a similar manner, the transport and diffusion of a scalar quantity in a turbulent flow field can be represented by the mass conservation equation of the form

$$\frac{\partial \bar{c}}{\partial t} + \bar{u}_i\frac{\partial \bar{c}}{\partial x_i} = \frac{\partial}{\partial x_i}(\epsilon_m\frac{\partial \bar{c}}{\partial x_i} - \overline{u_i'c'}) \tag{3.6}$$

where $\epsilon_m$ denotes the molecular diffusivity and $\bar{c}$ denotes the mean concentration of the marked fluid.

Equations (3.4), (3.5) and (3.6) are the equations governing the mean flow quantities $\bar{u}_i, \bar{p}$, and $\bar{c}$. These are exact equations since no simplifying assumptions have been made in deriving them. However, due to the non-linearity

of the Navier-Stokes equations, the averaging procedure has introduced unknown correlations between fluctuating velocities, $\overline{u_i'u_j'}$, and between velocities and concentration fluctuations $\overline{u_i'c'}$. Physically these correlations multiplied by the density $\rho$, represent the transport of momentum and mass due to turbulent fluctuations.

Determination of such correlations is the main problem in calculating turbulent flows. Exact transport equations can be derived for these correlations but again these equations contain turbulence correlations of the next higher order and so on. Realistic turbulence models are, therefore, employed to approximate the correlations of a certain order in terms of lower order correlations and/or mean flow quantities and form a closed set of equations to be solved for turbulent flow quantities.

## 3.3 Eddy Viscosity and Diffusivity Concepts

The eddy viscosity concept is due to Boussinesq's assumption that, in analogy with the viscous stresses in laminar motion, the turbulent stresses are proportional to the mean velocity gradients which, for general flow situations, may be expressed as

$$-\overline{u_i'u_j'} = \nu_t\left(\frac{\partial \overline{u_i}}{\partial x_j} + \frac{\partial \overline{u_j}}{\partial x_i}\right) \quad \text{for} \quad i \neq j \tag{3.7}$$

where $\nu_t$ is the turbulent (eddy) viscosity which, in contrast to the molecular viscosity, is not a fluid property rather it depends strongly on the state of turbulence and may vary significantly within the flow field and also from flow to flow. The total shear stress in a turbulent flow field can be written as

$$\tau_{ij} = \mu(\frac{\partial \overline{u_i}}{\partial x_j} + \frac{\partial \overline{u_j}}{\partial x_i}) + (-\rho \overline{u_i' u_j'}) \tag{3.8}$$

However, in turbulent flow the viscous effect is considered negligible and turbulence modelling is aimed at determining only $-\rho \overline{u_i' u_j'}$.

Equation (3.6) constitutes a framework for constructing such a model and the problem is now shifted to determining the distribution of $\nu_t$, which is often considered proportional to a velocity scale and a length scale characterizing the turbulent motion because the distribution of these scales can be approximated reasonably well in many flows. This is the basis on which Prandtl's well known 'mixing length theory' was developed. This theory and his later modified theory (see Schlichting, 1968) in which the kinematic viscosity is considered proportional to the maximum difference in the time-mean flow velocity and a length scale proportional to the width of the mixing zone, have been applied to different flow conditions and have met with mixed success.

However, the major success of the eddy viscosity concept is in the prediction of two dimensional free shear layers, where the shear stress $\tau = -\rho \overline{u'v'}$ is the turbulent stress of prime importance. In flows of greater complexity, more than one turbulent stress component $\overline{u_i' u_j'}$ is of significance and the assumption of constant eddy viscosity as in eqn (3.6) may not be applicable. In large water bodies $\nu_t$ is often assumed to be different for horizontal and for vertical transport.

By virtue of the famous Reynolds' analogy between the phenomena of momentum and heat or mass transfer, it is assumed that the turbulent mass transport is related to the gradient of the transported quantity. Thus, denoting transfer of material by the term 'concentration', c, in a marked fluid system, one can write expression for mass transfer rate as

$$-\overline{u_i'c'} = D_t \frac{\partial \bar{c}}{\partial x_i} \tag{3.9}$$

where $D_t$ might be called the turbulent eddy diffusivity of mass. A dimensionless ratio which is often used in studies of mass diffusion is the so-called 'Schmidt number', $S_c$, defined as

$$S_c = \frac{\nu_t}{D_t}$$

The turbulent diffusivity, $D_t$, is hardly expected to remain constant in the flow field and is sensitive to the direction of mass flux. However, the Schmidt number, $S_c$, which is the ratio of the momentum and the mass diffusivities, varies very little across any flow and also from flow to flow and therefore, many models make use of constant $S_c$ (see Rodi, 1980) to obtain eddy diffusivity $D_t$ from known eddy viscosity $\nu_t$.

## 3.4 Plane Turbulent Mixing Layers

When a stream of fluid moves over a stagnant mass of the same fluid, a surface of discontinuity in the velocity of flow results. The intense shear at the surface of velocity discontinuity induces turbulence and the stagnant fluid is accelerated whereas a portion of the moving stream loses some momentum. The thickness of the fluid layer affected by this exchange of momentum is known as the mixing layer or a free shear layer and its thickness grows with the direction of mean stream flow.

This type of free turbulent flow is considered to be of boundary layer nature and the following assumptions are usually made in its analysis:

(a) because of the high degree of mixing, the viscous stresses are ignored

compared to the turbulent eddy stresses, throughout the entire flow field;

(b) the pressure remains constant within and outside the mixing zone, hence no pressure gradient;

(c) the velocity gradient in the lateral direction is large compared with the longitudinal direction; and

(d) the lateral dimensions are small compared with the longitudinal directions.

With these assumptions, the pertinent equations of motion for the case of a two dimensional mixing layer reduce to

$$\frac{\partial \bar{u}}{\partial t} + \bar{u}\frac{\partial \bar{u}}{\partial x} + \bar{v}\frac{\partial \bar{u}}{\partial y} = -\frac{\partial}{\partial y}(\overline{u'v'}) \tag{3.10}$$

$$\frac{\partial \bar{u}}{\partial x} + \frac{\partial \bar{v}}{\partial y} = 0 \tag{3.11}$$

As mentioned earlier, a turbulence model is required to describe the shear stress $-\overline{u'v'}$ in order to solve the equations of motion. Phenomenological theories were developed as physical explanations justifying the equation,

$$-\overline{u_i'u_j'} = \nu_t\left(\frac{\partial \overline{u_i}}{\partial x_j} + \frac{\partial \overline{u_j}}{\partial x_i}\right)$$

Among others, Prandtl's 'mixing length' theory has been widely applied in practical situations. For transverse mixing, Prandtl's theory can be summarized as follows.

(i) $-\overline{u'v'} = \epsilon_{ty}\frac{\partial \bar{u}}{\partial y}$

where $\epsilon_{ty}$ is the turbulent eddy viscosity in the y - direction,

(ii) $\epsilon_{ty} \propto l v_*$

where $l$ and $v_*$ are respectively a characteristic length and velocity of the eddies, and

(iii) $v_* \propto l \mid \frac{\partial \bar{u}}{\partial y} \mid$

Thus the model in its final form appears as

$$\tau_{xy} = -\rho\overline{u'v'} = \rho l^2 \mid \frac{\partial \bar{u}}{\partial y} \mid \frac{\partial \bar{u}}{\partial y} \tag{3.12}$$

In free turbulence shear flow, the mixing length is assumed constant in the transverse direction (Abramovich, 1963), so that,

$$l(y) = constant$$

In the longitudinal direction, to account for the similarity of velocity profiles, the mixing length must vary in proportion to a characteristic length, the width of the mixing layer, b, which is again proportional to the distance along the x - axis (mean flow direction). Thus,

$$l = kx$$

where, k is the empirical constant. The equation (3.12) therefore, becomes

$$\tau_{xy} = -\rho\overline{u'v'} = \rho k^2 x^2 \mid \frac{\partial \bar{u}}{\partial y} \mid \frac{\partial \bar{u}}{\partial y} \tag{3.13}$$

Application of the mixing length hypothesis to scalar (species concentration) transport is straight forward as shown by Abramovich (1963). Neglecting molecular diffusion compared to its turbulent counterpart, the two dimensional diffusion equation for the mixing layer can be easily obtained from the general mass conservation equation (3.6)

$$\frac{\partial \bar{c}}{\partial t} + \bar{u}\frac{\partial \bar{c}}{\partial x} + \bar{v}\frac{\partial \bar{c}}{\partial y} = -\frac{\partial}{\partial x}(\overline{u'c'}) - \frac{\partial}{\partial y}(\overline{v'c'}) \tag{3.14}$$

Considering steady flow condition i.e., $\partial \bar{c}/\partial t = 0$, and discarding the second order longitudinal diffusivity term, $-\frac{\partial}{\partial x}(\overline{u'c'})$, one obtains an equation of the form

$$\bar{u}\frac{\partial \bar{c}}{\partial x} + \bar{v}\frac{\partial \bar{c}}{\partial y} = -\frac{\partial}{\partial y}(\overline{v'c'}) \tag{3.15}$$

It appears from the above equation that the turbulent transfer is accomplished by the transport of layers of fluids with different concentration as a consequence of the correlation between fluctuations of velocity and concentration. The fluctuation of concentration is considered as its change of magnitude during transfer of a fluid particle from one layer of fluid to another by a distance of one mixing length, $l$. Hence,

$$c' \approx l\frac{\partial \bar{c}}{\partial y}$$

Also as before,

$$u' \approx v' \approx l \mid \frac{\partial \bar{u}}{\partial y} \mid$$

and

$$l \propto b$$

i.e., since $b \propto x$,

$$l = kx$$

Thus we have mass transfer rate in the transverse direction

$$-\rho\overline{v'c'} = \rho k^2 x^2 \mid \frac{\partial \bar{u}}{\partial y} \mid \frac{\partial \bar{c}}{\partial y} \tag{3.16}$$

One of the major shortcomings of the mixing length model is that the apparent kinematic (eddy) viscosity, $\nu_t$, and the eddy diffusivity, $D_t$, vanishes at points where $\partial\bar{u}/\partial y = 0$, i.e., at points of maximum and minimum velocity. However, in reality, turbulent mixing does not vanish at points of maximum velocity. In order to overcome this difficulty Prandtl proposed his new theory (see Schlichting, 1968) wherein it is assumed that the coefficient of the turbulent viscosity $\nu_t$, and not the mixing length, is constant over a cross-section of the flow zone.

Another objection to the Prandtl's mixing length theory, as pointed out by Stanisic (1985), is based on the fact that in turbulent shear flow simple transport theory is wrong in principle since no account is taken of the effect of pressure fluctuations. He argues that momentum can be transferred by pressure difference alone without a lump of the fluid itself being transported. Because the pressure may fluctuate over the mixing length $l$, the momentum of the fluid lump is not preserved and thus Prandtl's assumption is not satisfied. The most severe shortcoming of Prandtl's theory is its inapplicability close to the wall. Since at the wall, velocity fluctuations are zero, then according to the mixing length theory the shearing stress vanishes. However, experiments (see Abramovich,1963) have shown that in the neighbourhood of wall the shearing stress is a non - zero constant.

Taylor's vorticity transfer theory (Schlichting, 1968) assumes that the vorticity remains constant throughout the process of turbulent mixing and thus instead of momentum, vorticity might be considered as a transferable quantity. Using this fundamental assumption, this theory leads to the derivation of an expression for the turbulent shearing stress in which a new mixing length appears which is larger by a factor $\sqrt{2}$ than that in Prandtl's momentum transfer theory. This theory, however, possesses almost the same phenomenological weaknesses as are found in Prandtl's theory.

## 3.5 Solutions to the Equations of Motion

Prandtl's phenomenological theories have been applied in deriving analytical solutions to the equations of motions for the case of a two dimensional mixing layer. Tollmien (1926, see Rajaratnam, 1976) derived the solution using Prandtl's mixing length theory which predicts the dimensionless velocity profile, $\bar{u}/U_o$, with appropriate boundary conditions,

$$\frac{\bar{u}}{U_o} = F'(\phi) = 0.0176e^{-\phi} + 0.6623e^{\frac{\phi}{2}} \cos\frac{\sqrt{3}\phi}{2} + 0.228e^{\frac{\phi}{2}} \sin\frac{\sqrt{3}\phi}{2} \qquad (3.17)$$

where, $U_o$ is the average free stream velocity,

$\phi = y/ax$, 'a' is an empirical constant, and

$F'(\phi)$ is the derivative of a certain function $F(\phi)$, which is

proportional to the stream function,

$$\Psi = \int u dy = axU_o \int F' d\phi = axU_o F(\phi)$$

Thus the transverse component of velocity can be found by differentiating,

$$\bar{v} = -\frac{\partial \Psi}{\partial x} = aU_o(\phi F' - F)$$

Abramovich (1963) compared Tollmien's theoretical velocity profile with the experimental data of Albertson et al (1950). The comparison shows good agreement between theory and experiment with the value of the empirical constant, $a = 0.09$.

Goertler (1942, in Rajaratnam, 1976) employed Prandtl's constant eddy viscosity model and solved for the two dimensional mixing region which arises at the boundary of two parallel jets having different velocities. Goertler

used the co-ordinate system $(x, \xi)$, in which, $\xi = \sigma\frac{y}{x}$, $\sigma$ being an empirical constant. Then the dimensionless velocity profile is a function of $\xi$,

$$\frac{\bar{u}}{U} = \sigma F'(\xi)$$

where, $U = \frac{1}{2}(U_1 + U_2)$; $U_1$ being greater than $U_2$

the stream function

$$\Psi = \int \bar{u} dy = xUF(\xi)$$

and the transverse velocity profile

$$\frac{\bar{v}}{U} = -\frac{\partial \Psi}{\partial x} = (\xi F' - F)$$

Using the above formulae, and simple transformations, the equation of motion takes the form

$$F''' + 2\sigma F F'' = 0$$

where, $\frac{1}{\sigma} = 2\sqrt{c_2\lambda}$; $c_2 = b/x$; b is the width of the mixing layer; and

$$\lambda = \frac{U_1 - U_2}{U_1 + U_2}$$

With definite values of $\phi$ ($\phi_1 = 0.981$ and $\phi_2 = -2.040$) Tollmien's theory gives a finite layer thickness of the form $b = ax(\phi_1 - \phi_2)$. In Goertler's theory however, the boundary layer is found to be asymptotic, i.e., extending from $\xi = \infty$ to $\xi = -\infty$, and therefore, the layer thickness means a certain finite distance between two points, where the velocity at one point is close to $U_1$ and the other point close to $U_2$, i.e., for instance, $0.90(U_1 - U_2) + U_2$ and $0.10(U_1 - U_2) + U_2$ respectively. The boundary conditions thus, in Goertler's asymptotic solution are,

$$\xi_1 = +\infty, \bar{u} \equiv U_1$$

i.e.,

$$F'(\xi_1) = 1 + \lambda$$

and

$$\xi_2 = -\infty, \bar{u} \equiv U_2$$

i.e.,

$$F'(\xi_2) = 1 - \lambda$$

With these boundary conditions, the solution for the general free shear layer of streams having two different velocities $U_1$ and $U_2$ is

$$\frac{\bar{u}}{U} = 1 + \frac{2\lambda}{\sqrt{\pi}} \int_0^{\xi} e^{-z^2} dz \tag{3.18}$$

For the case of mixing layer with one stream at rest i.e., $U_2 = 0$, say,

$$\lambda = \frac{U_1 - U_2}{U_1 + U_2} = 1$$

and

$$U = \frac{1}{2}(U_1 + U_2) = \frac{U_1}{2} = \frac{U_0}{2}$$

The dimensionless velocity profile is then

$$\frac{\bar{u}}{U_0} = 0.50 + \frac{1}{\sqrt{\pi}} \int_0^{\xi} e^{-z^2} dz \tag{3.19}$$

where, $\xi = \sigma \frac{y}{x}$

Goertler's theoretical solution agrees quite well with the measurements of Reichardts (1951, in Schlichting, 1968) for the case of $U_2 = 0$. However, the empirical constant $\sigma$ has to be adjusted from experimental data. In this case the value of $\sigma = 13.5$.

Liepmann and Laufer (1947) found that the value of $\sigma$ has to be 11.0 for their experimental observations to agree well with the Goertler's solution. In

comparing their measured velocity profiles they found that by an appropriate choice of constant $\sigma$ both the theory based on 'constant mixing length' and the one based on 'constant eddy viscosity' can be made to agree with the velocity distribution obtained by measurement. Liepmann and Laufer (1947) questioned the fundamental concept of these theories. They have shown that neither the measured mixing length nor the measured exchange coefficient is even approximately constant although both the theories could be made to agree with experimental mean velocity distribution.

While dealing with diffusion equation, Abramovich (1963) introduces the term concentration difference, $\triangle\bar{c} = \bar{c} - \bar{c_H}$, where,

$\bar{c}$ = the time mean concentration of a given constituent (tracer) within the shear layer, and

$\bar{c_H}$ = the time-mean concentration in the adjoining fluid medium at rest.

Similarly, $\triangle\bar{c_0} = \bar{c_0} - \bar{c_H}$, where,

$\bar{c_0}$ = the time-mean concentration in the free stream flow.

It is considered convenient to introduce the concentration difference instead of the absolute value because the concentration (similar to temperature) of the adjoining fluid at rest, unlike the velocity, is not equal to zero. Experimental data (Fiedler, 1975) suggest that the edges of the diffusion boundary layer, just like the thermal boundary layer, coincide with the edges of the dynamic boundary layer, and the dimensionless concentration difference profile is universal. Hence as should be expected, according to Prandtl's theory, the dimensionless concentration difference profiles should be similar to the temperature and the velocity profiles, i.e.,

$$\frac{\triangle \bar{c}}{\triangle \bar{c}_0} = \frac{\triangle \bar{T}}{\triangle \bar{T}_0} = \frac{\bar{u}}{U_0} \tag{3.20}$$

However, as pointed out by Abramovich (1963), this is not confirmed by the experimental data, from which it follows that the concentration and the temperature fields are similar, but they differ from the velocity field.

## 3.6 Taylor's Concept of Turbulent Diffusion

The fundamental insight into the process of turbulent diffusion has been given by Taylor (1922) in his classic analysis of diffusion by continuous movements. The framework for the analysis is a homogeneous, stationary, one dimensional turbulent flow, into which a group of particles is instantaneously released at a point. The analysis relates the rate of spread of the particle cloud to the Lagrangian turbulence properties of the flow. Lagrangian turbulence properties are based on the statistical histories of the motion of discrete fluid particles as opposed to Eulerian turbulence properties, which are based on the statistical histories of instantaneous velocities measured at fixed points.

A detailed review of Taylor's (1922) analysis can be found in Fischer et al (1979), Holly (1985) and Sayre (1968). However, the most remarkable result of Taylor's analysis can be mentioned as follows.

$$\sigma_x^2(t) \approx 2\widehat{u'^2} T_{lx} t \tag{3.21}$$

where, $\sigma_x^2(t)$ is the variance of the particle cloud in the x direction; $u'$ is the instantaneous particle velocity with respect to the mean velocity; the overbrace denotes an ensemble average over the particles; and $T_{lx}$ is the Lagrangian integral time scale of turbulence which is defined as

$$T_{lx} \equiv \int_0^\infty R_{u'}(\tau)d\tau \tag{3.22}$$

where, $R_{u'}(\tau)$ is the Lagrangian correlation coefficient.

It states that for very large dispersion time the variance of the particle cloud will increase linearly with time at a rate given by $2\widehat{u'^2}$. Now a characteristic property of a gradient diffusion process is that the variance of a concentration distribution of a marked fluid always grows linearly with time (Fischer et al, 1979). Thus Taylor's diffusion analysis provides a formal justification for representing mixing due to turbulent fluctuations as a gradient diffusion process.

The unknown correlation terms, $\overline{u_i'c'}$, in eqn (3.6) are therefore, modelled using the gradient diffusion hypothesis, by analogy to the Fick's law of molecular diffusion as

$$-\overline{u_i'c'} \propto \frac{\partial \bar{c}}{\partial x_i}$$

This fundamental hypothesis has been applied by Taylor (1953,1954) himself in his dispersion investigations in laminar and turbulent pipe flows and subsequently by numerous researchers (Elder, 1959; Fischer, 1966,1967) in open channel flow.

A requirement of Taylor's theory (1922) is that the eqn (3.21) is valid only for times larger than the Lagrangian time scale. In three dimensional diffusion, the time scale can be generalized (Fischer et al, 1979) by defining

$$T_L = \frac{1}{3}(T_{lx} + T_{ly} + T_{lz})$$

where, $T_{ly}$ and $T_{lz}$ are defined in a similar way to $T_{lx}$, and the requirement for use of constant diffusivity coefficients is that $t > T_L$. To express the requirement spatially a Lagrangian length scale, $L_l$, is defined by the relation

$$L_l^2 = \widehat{u'^2}T_L^2$$

and it has been shown (Fischer et al, 1979) that the requirement for eqn (3.8) to be valid, in terms of the size of the contaminant cloud, $l$, is

$$l^2 > 2L_l^2$$

This means that spatial extent of the contaminant cloud should substantially exceed the distance over which turbulent motions are correlated. In bounded natural water bodies this distance is of the order of the depth of flow (Holly, 1985).

## 3.7 Theoretical Basis of Lateral Diffusivity

The transverse mixing process is represented by the transverse diffusivity coefficient $\epsilon_y$, which can be expressed as

$$\epsilon_y = -\frac{\overline{v'c'}}{\frac{\partial \bar{c}}{\partial y}}$$

This is the consequence of the gradient diffusion hypothesis. The theoretical basis of this equation is through the Reynold's analogy between vertical transport of mass and momentum in a turbulent flow field.

Vertical transport of momentum per unit mass, $-\overline{u'w'}$, can be described as a gradient transport process such that

$$-\overline{u'w'} = \nu_t \frac{\partial \bar{u}}{\partial z} \tag{3.23}$$

Similarly, vertical transport of mass can be described as

$$-\overline{w'c'} = \epsilon_z \frac{\partial \bar{c}}{\partial z} \tag{3.24}$$

where, $\epsilon_z$ is the vertical diffusivity coefficient.

This analogy was further explored by Elder (1959), who assumed that $\nu_t = \epsilon_z$, and noting that $\rho\overline{u'w'}$ is the turbulent shear stress which varies linearly with distance above the bed, obtained

$$\epsilon_z = \frac{(1 - \frac{z}{H})U_*^2}{\frac{\partial \bar{u}}{\partial y}} \tag{3.25}$$

where, $U_*$ is the shear velocity defined as $\sqrt{\frac{\tau_0}{\rho}}$; $\tau_0$ is the bed shear stress, $\rho gRS$; $\rho$ is the fluid density; R is the hydraulic radius; S is the energy slope and H is the average channel depth.

Assuming a logarithmic velocity distribution and integrating eqn (3.25) over the depth of flow, Elder (1959) obtained

$$\epsilon_z = \frac{\kappa}{6} U_* H \tag{3.26}$$

where, $\kappa$ is the von Karman constant approximately equal to 0.4.

The requirement for eqn (3.26) is that the shear stress must vary linearly from a maximum at the bed to zero at the surface. However, no analogous consideration for the transverse shear $\rho\overline{u'v'}$, could be established to achieve a similar transverse eddy diffusivity coefficient. Rather, Elder (1959) proposed a similar expression for the transverse diffusivity $\epsilon_y$, without any firm theoretical background. Thus

$$\epsilon_y = kU_* H \tag{3.27}$$

where, k is a constant requiring experimental determination. The above expression is only qualitatively justified on the basis of the strong correlation between the vertical and the transverse turbulent velocity fluctuations

(Holly, Jr., 1975). However, it is important to note that eqn (3.27) represents transverse diffusion due entirely to bed generated turbulence.

Experimental determinations of $\epsilon_y$ have been usually based on continuous tracer injection into a steady uniform flow of constant velocity U. For these conditions, the concentration distribution is expected to be Gaussian with the variance given by $\sigma_y^2 = 2\epsilon_y t$ which is analogous to Taylor's (1922) diffusion concept (eqn 3.21). Using the transformation, $t = \frac{x}{U}$

$$\epsilon_y = \frac{U}{2}\frac{\partial \sigma_y^2}{\partial x} \tag{3.28}$$

Thus to determine $\epsilon_y$ one need only to estimate the transverse variance of steady state distributions at successive downstream locations.

Similar expression for $\epsilon_y$ can also be derived by taking the second y-moment of the appropriate version of the convective-diffusion equation (Okoye, 1970; Holley, 1971). Implicit in the above analyses is the assumption that the transverse diffusivity is constant within a cross-section, on the ground that transverse variation of velocity is small. However, it should be noted here that in free shear flows the fluctuation in transverse velocity is significant.

## 3.8 Coherent Structures Analysis

As mentioned in chapter 2, the presence of coherent large eddy structures in turbulent shear flows, particularly in predominantly two dimensional shear layers is now evident from numerous recent flow visualization studies. Their dynamical role however, in transporting heat mass and momentum is still unclear. To be dynamically significant, most of the Reynolds stresses and turbulence production should be associated with coherent structures. In measur-

able quantities, as mentioned by Hussain (1983), coherent Reynolds stresses and production must exceed significantly the time-average total Reynolds stress and turbulence production. The analysis of coherent structures must therefore, demonstrate their predominant roles for a theory of shear flow turbulence to be based on the theory of coherent structures.

### 3.8.1 Decomposition of the Flow Field

#### (A) Triple Decomposition

For the purpose of analysis, an instantaneous flow signal, f, could be regarded to consist of the contributions from the time-mean (global) field $\bar{f}$, the periodic coherent field $\tilde{f}$ and the background turbulent (fluctuation) field $f'$, as suggested by Hussain (1983), i.e.,

$$f(x,t) = \bar{f}(x) + \tilde{f}(x,t) + f'(x,t) \tag{3.29}$$

where,

$$\bar{f} = \lim_{T\to\infty} \frac{1}{T} \int_0^T f(t)dt$$

The above decomposition of the instantaneous flow signal into a three component field requires introduction of a new averaging process called 'phase average' the concept of which was put forwarded by Hussain and Reynolds (1970). Phase averaging, similar to the concept of Reynolds' (1877) time averaging, can be defined as the ensemble average of any property at a particular phase of the flow structure. That is,

$$\langle f(x,y,z,t)\rangle = \lim_{N\to\infty} \frac{1}{N} \sum_{i=1}^{N} f_i(x,y,z,t+t_i) \tag{3.30}$$

where, the angular bracket denotes phase-averaged, t denotes the time corresponding to the reference phase and $t_i$ denotes the random instants of occurrence of successive structures of the selected phase. When these structures occur at regular intervals (as in the case of controlled excitation), the periodic phase average is

$$\langle f(x,t)\rangle = \lim_{N\to\infty} \frac{1}{N} \sum_{i=1}^{N} f_i(x, t+iT) \tag{3.31}$$

where, T is the period of occurrence of the structure.

The eqn (3.29) is called 'triple decomposition' (Hussain, 1983), in which the phase-averaged part consists of the time-averaged and the coherent component, i.e.,

$$\langle f\rangle = \bar{f} + \tilde{f} \tag{3.32}$$

That is, the difference between the instantaneous signal and the phase-averaged represents the background random fluctuation, and the difference between the phase-averaged and the time-averaged denotes the periodic coherent component.

Substituting eqn (3.29) for each flow variable into the governing equations for incompressible flow and carrying out first the phase averaging and then the time-averaging (Hussain, 1983; 1977), the corresponding continuity and momentum equations result

$$\frac{\partial \bar{u}_i}{\partial x_i} = \frac{\partial \tilde{u}_i}{\partial x_i} = \frac{\partial u_i'}{\partial x_i} = 0 \tag{3.33}$$

$$\frac{\bar{D}}{Dt}\bar{u}_i = \frac{1}{\rho}\frac{\partial \bar{p}}{\partial x_i} + \nu\frac{\partial}{\partial x_j}(\frac{\partial \bar{u}_i}{\partial x_j}) + \frac{\partial}{\partial x_j}(-\overline{\tilde{u}_i\tilde{u}_j} - \overline{u_i'u_j'}) \tag{3.34}$$

$$\frac{\bar{D}}{Dt}\tilde{u}_i = -\frac{1}{\rho}\frac{\partial \tilde{p}}{\partial x_j} + \nu\frac{\partial}{\partial x_j}(\frac{\partial \tilde{u}_i}{\partial x_j})\frac{\partial}{\partial x_j}(\bar{u}_i\tilde{u}_j) + \frac{\partial}{\partial x_j}(\overline{\tilde{u}_i\tilde{u}_j} - \tilde{u}_i\tilde{u}_j) + \frac{\partial}{\partial x_j}(\overline{u_i'u_j'} - \langle u_i'u_j'\rangle) \tag{3.35}$$

$$\frac{\bar{D}}{Dt}u_i' = -\frac{1}{\rho}\frac{\partial p'}{\partial x_j} + \nu\frac{\partial}{\partial x_j}(\frac{\partial u_i'}{\partial x_j}) - \frac{\partial}{\partial x_j}(\tilde{u}_ju_i' + \bar{u}_iu_j' + \tilde{u}_iu_j') - \frac{\partial}{\partial x_j}(u_i'u_j' - \langle u_i'u_j'\rangle) \tag{3.36}$$

where,

$$\frac{\bar{D}}{Dt} = \frac{\partial}{\partial t} + \bar{u}_j\frac{\partial}{\partial x_j}$$

in the time-mean flow field.

In the above derivations it is assumed that,

(a) the phase average of the time average is just the time average, i.e., $\langle\bar{f}\rangle = \bar{f}$;

(b) the phase and the time averages of the incoherent field have zero values, i.e., $\langle f'\rangle = \bar{f}' = 0$;

(c) the time average of a pulsation-induced quantity is zero, i.e., $\bar{\tilde{f}} = 0$; and

(d) the coherent and incoherent motions are uncorrelated, i.e., $\bar{\tilde{f}g'} = \langle\tilde{f}g'\rangle = 0$.

The terms $-\overline{\tilde{u}_i\tilde{u}_j}$ and $-\overline{u_i'u_j'}$ in eqn (3.34) are the contributions of the coherent and incoherent motions to the mean momentum field. The modulations in these two terms, in eqn (3.35), due to the coherent motion contribute to

the coherent field momentum. The interaction of the incoherent field with the time-average and the coherent fields, in addition to the self interaction, instantaneously contributes to the incoherent field momentum as apparent in the eqn (3.36).

Further insight into the mechanics of interactions among the mean, coherent and turbulence fields can be obtained from energy considerations. In a turbulent flow, the mean flow kinetic energy is transferred to the turbulent field by the work of the Reynolds stress against mean shear, which is again dissipated into thermal energy by the action of viscosity. In the presence of coherent motions the total average energy of the flow field can be considered equal to the sum of the average kinetic energies of the mean, coherent and turbulent fields (Hussain, 1977); thus

$$\begin{aligned} \frac{1}{2}\overline{u_i u_i} &= \frac{1}{2}\overline{\bar{u}_i \bar{u}_i} + \frac{1}{2}\overline{\tilde{u}_i \tilde{u}_i} + \frac{1}{2}\overline{u_i' u_i'} \\ &\simeq E + \xi + e \end{aligned} \tag{3.37}$$

The equations for the average kinetic energies for the three component fields are (considering the production terms only)

$$\frac{\bar{D}}{Dt}E = -(-\overline{\tilde{u}_i \tilde{u}_j})\frac{\partial \bar{u}_i}{\partial x_j} - (-\overline{u_i' u_j'})\frac{\partial \bar{u}_i}{\partial x_j} + \ldots\ldots\ldots\ldots \tag{3.38}$$

$$\frac{\bar{D}}{Dt}\xi = -\overline{\tilde{u}_i \tilde{u}_j}\frac{\partial \bar{u}_i}{\partial x_j} - \overline{(-\langle u_i' u_j' \rangle \frac{\partial \tilde{u}_i}{\partial x_j})} + \ldots\ldots\ldots\ldots \tag{3.39}$$

$$\frac{\bar{D}}{Dt}e = -\overline{u_i' u_j'}\frac{\partial \bar{u}_i}{\partial x_j} - \overline{\langle u_i' u_j' \rangle \frac{\partial \tilde{u}_i}{\partial x_j}} + \ldots\ldots\ldots\ldots \tag{3.40}$$

Detailed derivations and discussion of the momentum equations (eqns 3.34

to 3.36) and energy equations (eqns 3.38 to 3.40) can be found in Reynolds and Hussain (1972) and Hussain (1977).

It can be seen from the energy equations that the mean field provides energy to the coherent and the turbulent fields by the work of the coherent and the turbulent Reynolds stresses ( $-\overline{\tilde{u}_i\tilde{u}_j}$ and $-\overline{u_i'u_j'}$ ) against the mean strain rate, $(\partial\bar{u}_i/\partial x_j)$. These two terms in eqn (3.38) appear as energy source terms in equations (3.39) and (3.40) with opposite signs. The coherent structure also produces random turbulence by the action of the phase-averaged background Reynolds stress $-\langle u_i'u_j'\rangle$ against the coherent motion strain rate, $(\partial\tilde{u}_i/\partial x_j)$. This is represented by the second term in eqn (3.39) which appears as a source term in eqn (3.40).

### (B) Double Decomposition

The triple decomposition provides an understanding of the exchange of kinetic energy between the time-mean, coherent and phase incoherent random motions. However, the decomposition assumes that the coherent structure is a perturbation of the time-mean flow. Hussain (1980, 1983) explained that in a region occupied by a coherent eddy structure, the entire motion (excluding the random part) is due to the coherent structure and hence this can not be a mere perturbation of the mean motion, rather the structure is the flow. In that sense, the double decomposition, introduced by Hussain (1977) appears to be more appropriate. This decomposition considers the entire flow field to consist of coherent and incoherent motions only, i.e.,

$$f(x,t) = \hat{f}(x,t) + f'(x,t) \tag{3.41}$$

Substituting decomposition (3.41) in the governing equations for incompressible flow and taking phase average one obtains the continuity equations

$$\frac{\partial \hat{u}_i}{\partial x_i} = \frac{\partial u_i'}{\partial x_i} = 0 \tag{3.42}$$

the momentum equations for the organized field

$$\frac{\hat{D}}{Dt}\hat{u}_i = -\frac{1}{\rho}\frac{\partial \hat{p}}{\partial x_i} + \nu\frac{\partial}{\partial x_j}(\frac{\partial \hat{u}_i}{\partial x_j}) - \frac{\partial}{\partial x_j}\langle u_i'u_j'\rangle \tag{3.43}$$

and the momentum equation for the turbulent field

$$\frac{\hat{D}}{Dt}u_i' = -\frac{1}{\rho}\frac{\partial p'}{\partial x_i} + \nu\frac{\partial}{\partial x_j}(\frac{\partial u_i'}{\partial x_j}) - u_j'\frac{\partial}{\partial x_j}\hat{u}_i - \frac{\partial}{\partial x_j}(u_i'u_j' - \langle u_i'u_j'\rangle) \tag{3.44}$$

where,

$$\frac{\hat{D}}{Dt} = \frac{\partial}{\partial t} + \hat{u}_j\frac{\partial}{\partial x_j}$$

in the coherent flow field. The term $-\langle u_i'u_j'\rangle$ represents the contribution of the turbulent field to the coherent field and can be termed as coherent Reynolds' stress.

The corresponding kinetic energy equations are

$$\begin{aligned}\frac{\hat{D}}{Dt}\langle\frac{\hat{u}_i\hat{u}_i}{2}\rangle &= -\frac{\partial}{\partial x_j}(\frac{\hat{p}\hat{u}_i}{\rho}) - (-\langle u_i'u_j'\rangle\frac{\partial \hat{u}_i}{\partial x_j}) \\ &\quad -\frac{\partial}{\partial x_j}(\hat{u}_i\langle u_i'u_j'\rangle) + \text{viscous terms}\end{aligned} \tag{3.45}$$

$$\begin{aligned}\frac{\hat{D}}{Dt}\langle\frac{u_i'u_i'}{2}\rangle &= -\frac{\partial}{\partial x_j}\langle u_j'(\frac{p'}{\rho} + \frac{u_i'u_i'}{2})\rangle \\ &\quad +\langle u_i'u_j'\rangle\frac{\partial \hat{u}_i}{\partial x_j} + \text{viscous terms}\end{aligned} \tag{3.46}$$

The second term in eqn (3.45) represents the loss of kinetic energy of the coherent field due to the shear work of the coherent Reynolds' stress $-\langle u_i'u_j'\rangle$

against the coherent flow strain rate $\partial\hat{u}_i/\partial x_j$. This appears as an energy source term in eqn (3.46) with an opposite sign, and is responsible for the production of kinetic energy in the turbulent flow field. The third term in eqn (3.46) represents the kinetic energy transport due to work done by the Reynolds' stresses, $-\langle u_i' u_j' \rangle$.

The double decomposition concept allows analysis of the interaction between coherent and incoherent motions, although this does not address the evolution of coherent structures or extraction of energy by coherent structures from the mean flow field which drives the structures (Hussain, 1983). However, considering the coherent structure properties to be the properties of turbulent shear flow, application of the double decomposition appears more appropriate than that of the triple decomposition in the analysis of turbulent shear flow.

## 3.9 Mass Transfer Across the Shear Layer

Equations for scalar (e.g., species concentration) transport can be derived in a similar fashion as for the momentum equations in the coherent flow field. The general equation for the conservation of mass in a flowing fluid can be written in the form

$$\frac{\partial c}{\partial t} + u\frac{\partial c}{\partial x} + v\frac{\partial c}{\partial y} + w\frac{\partial c}{\partial z} = e_m \nabla^2 c \tag{3.47}$$

where, c is the instantaneous tracer concentration by weight, $e_m$ is the molecular diffusivity and $\nabla^2$ is the Laplace's operator.

The above general equation can now be decomposed into coherent and inco-

herent random field using the double decomposition, i.e.,

$$c = \hat{c} + c';$$

$$u = \hat{u} + u';$$

and so on

Substituting these decompositions into the general equation and assuming two dimensional boundary layer type flow, we have

$$\frac{\partial}{\partial t}(\hat{c}+c') + (\hat{u}+u')\frac{\partial}{\partial x}(\hat{c}+c') + (\hat{v}+v')\frac{\partial}{\partial y}(\hat{c}+c') = e_m(\frac{\partial^2}{\partial x^2} + \frac{\partial^2}{\partial y^2})(\hat{c}+c') \tag{3.48}$$

Applying phase averaging to the above equation and neglecting molecular diffusion terms, the two dimensional diffusion equation in the coherent flow field can be obtained as

$$\frac{\partial \hat{c}}{\partial t} + \hat{u}\frac{\partial \hat{c}}{\partial x} + \hat{v}\frac{\partial \hat{c}}{\partial y} = -\frac{\partial}{\partial x}\langle u'c'\rangle - \frac{\partial}{\partial y}\langle v'c'\rangle \tag{3.49}$$

which is equivalent to the mean flow field equation (3.14).

Considering steady flow condition, i.e., $\frac{\partial \hat{c}}{\partial t} = 0$, and discarding second order longitudinal diffusivity as before, one obtains

$$\hat{u}\frac{\partial \hat{c}}{\partial x} + \hat{v}\frac{\partial \hat{c}}{\partial y} = -\frac{\partial}{\partial y}\langle v'c'\rangle \tag{3.50}$$

The term on the right hand side of eqn (3.50) is the most important one which represents transport due to fluctuating transverse velocity in the coherent flow field and can be termed as the transverse mass transfer due to phase-averaged incoherent (random) motion.

The equation for the fluctuating concentration field can be obtained by subtracting the coherent field equation from the instantaneous equation

$$\frac{\partial c'}{\partial t} + \hat{u}\frac{\partial c'}{\partial x} + u'\frac{\partial \hat{c}}{\partial x} + \frac{\partial}{\partial x}(u'c') + \hat{v}\frac{\partial c'}{\partial y} + v'\frac{\partial \hat{c}}{\partial y} + \frac{\partial}{\partial y}(v'c') = \frac{\partial}{\partial x}\langle u'c'\rangle + \frac{\partial}{\partial y}\langle v'c'\rangle \tag{3.51}$$

or,

$$\frac{\partial c'}{\partial t} + \hat{u}\frac{\partial c'}{\partial x} + \hat{v}\frac{\partial c'}{\partial y} = -u'\frac{\partial \hat{c}}{\partial x} - v'\frac{\partial \hat{c}}{\partial y} - \frac{\partial}{\partial x}(u'c' - \langle u'c'\rangle) - \frac{\partial}{\partial y}(v'c' - \langle v'c'\rangle)$$

Again discarding second order longitudinal fluctuating transport terms one obtains, for steady condition

$$\hat{u}\frac{\partial c'}{\partial x} + \hat{v}\frac{\partial c'}{\partial y} = -v'\frac{\partial c'}{\partial y} - \frac{\partial}{\partial y}(v'c' - \langle v'c'\rangle) \tag{3.52}$$

The first term on the right hand side of eqn (3.52) represents coherent mass transport due to fluctuating motion. The second term is the instantaneous transport term due to the random field. The effect of the coherent field on the turbulence field is apparent in the equation.

The important characteristic properties of coherent structures in a concentration transport field can therefore, be identified as follows,

(a) transverse coherent mass transfer rate : $\langle \hat{v}\hat{c}\rangle$,

(b) longitudinal coherent mass transfer rate : $\langle \hat{u}\hat{c}\rangle$,

(c) transverse phase averaged incoherent mass transfer rate : $\langle v'c' \rangle$,

(d) longitudinal phase averaged incoherent mass transfer rate : $\langle u'c' \rangle$ and

(e) concentration fluctuation intensity : $\sqrt{\langle c'^2 \rangle}$.

As suggested by Hussain (1983; 1981), measurements of these properties will provide an understanding of the size, shape and strength of the structures, these will also indicate where in the cross-section of structure different quantities have their peaks or valleys, which way these are being transported or diffused and also help to determine if these structures are dynamically dominant.

The balance equation for mean square fluctuation of the concentration, i.e., for the variance $\sigma_c^2 = \overline{(c - \bar{c})^2} = \overline{c'^2}$, can be obtained, similarly to the kinetic energy balance equations for the case of momentum transport, using phase averaging for the coherent flow field instead of the time-mean field, for two dimensional case

$$\frac{\partial \langle c'^2 \rangle}{\partial t} + \hat{u}\frac{\partial \langle c'^2 \rangle}{\partial x} + \hat{v}\frac{\partial \langle c'^2 \rangle}{\partial y} = -[2\langle u'c' \rangle \frac{\partial \hat{c}}{\partial x} + 2\langle v'c' \rangle \frac{\partial \hat{c}}{\partial y}] - [\frac{\partial}{\partial x}\langle u'c'^2 \rangle + \frac{\partial}{\partial y}\langle v'c'^2 \rangle] - 2\varepsilon_{c'} \tag{3.53}$$

This is the exact equation governing $\langle c'^2 \rangle$ which determines the concentration scale of the fluctuations and thus is the counterpart to the kinetic energy equations which determine the velocity scale. The first two terms on the right hand side of eqn (3.53) describe the production of $\langle c'^2 \rangle$ by the interaction of turbulent flux of concentration and phase averaged concentration gradient. The third and fourth terms represent diffusion by turbulent velocity fluctuations and the last term, $2\varepsilon_{c'}$, represents dissipation due to molecular diffusion of the fine-scale concentration fluctuations.

The increasing trend towards the use of 'second-order closure modelling' (i.e., modelling of the triple correlation terms) in the calculation of turbulent transport has also led to the derivation of transport equations for the fluxes themselves. The advantage is that the advection and diffusion of the fluxes can be accounted for and thus making the calculation method more general. A transport equation for the lateral flux $\langle v'c' \rangle$ can be derived in the following form

$$\begin{aligned} \frac{\partial}{\partial t}\langle v'c' \rangle + \hat{u}\frac{\partial}{\partial x}\langle v'c' \rangle \;=\; & -[\langle u'v' \rangle \frac{\partial \hat{c}}{\partial x} + \langle v'^2 \rangle \frac{\partial \hat{c}}{\partial y}] \\ & -[\frac{\partial}{\partial x}\langle u'v'c' \rangle + \frac{\partial}{\partial y}\langle v'^2 c' \rangle] \\ & -[\text{pressure-concentration gradient corrl. term}] \\ & -[\text{pressure fluc. terms}] - [\text{dissipation term}] \end{aligned} \tag{3.54}$$

where, the two terms on the left hand side represent the rate of change and the advection of $\langle v'c' \rangle$ due to phase average velocity respectively; the first two terms on the right hand side represent production due to coherent concentration field; and the third and fourth terms represent diffusive transport due to turbulent velocity fluctuations. Further details of the various quantities in eqns (3.53) and (3.54) can be found in Fackrell and Robins (1982), Sykes et al (1984), Rodi (1980) and Monin and Yaglom (1977). Measurements of the quantities in these equations could provide further understanding of the various transport terms in a coherent flow field.

UNIVERSITY OF ... LIBRARY

# Chapter 4

# Experimental Investigations

## 4.1 Introduction

This chapter describes the various phases of experiments undertaken in the present study. The objectives, equipment used and the experimental procedure of each phase are described in some detail. A considerable amount of instrumentation work was involved in the third phase with respect to the conductivity probes and the photo synchronization system. The scope, limitations and associated problems of each phase of experiments are considered and discussed separately.

## 4.2 Experimental Objectives

The primary objective of this investigation was to determine experimentally the mixing and mass transfer rates across a separated shear flow over a range of flow and geometrical conditions. Particular emphasis was given to the behaviour of the large scale coherent eddy structures which are now known to exist in the separated shear flow. Although there has been a large number of experiments on the evolution and role of large coherent structures in two stream and single stream mixing layers, the effects of recirculating flow (which develops due to the finite boundary of the separated flow) on these structures are not clear.

Furthermore because of the apparent importance of the dynamics of the large scale coherent structures in the separated shear layer, it is useful to understand the interaction between these large structures and the recirculating eddy within the separated region. It is therefore evident that detailed measurements are required to shed light on these processes. The experimental program of this study was designed, keeping the above mentioned objectives in mind.

The whole experimental programme can be divided into three distinct phases.

- The first phase of the experimental program concerned flow visualization experiments. Pictures of the flow field were vividly captured both in video tapes and in high speed movie films using respectively a television camera and a high speed cine camera with blue dye used as tracer material. The intention has been to obtain a qualitative understanding of the flow phenomena involved.

- In the second phase, measurements of the velocity field were undertaken. A one dimensional laser Doppler velocimeter (LDV) was used

to measure the separated flow field and the initial boundary layer conditions at the separation point. The main purpose of this phase of the experiments has been to determine the mean and the turbulence properties of the flow field.

- Measurements of concentration of a passive tracer (salt solution) using electrical conductivity probes were undertaken in the third phase. The major aim was to determine the mass transfer rate across the shear layer and to provide quantitative information about the entrainment, mixing and transport of the tracer mass by the large coherent structures in the separated shear layer and by the recirculating eddy within the separated region. To substantiate the flow visualization results in a more meaningful way simultaneous dye photography was undertaken along with the fixed point measurements through synchronization of the cine camera with the computer data collection from the conductivity probes. This enabled the analysis of the large scale structure properties more explicitly thus demonstrating their role on the overall process.

Useful information could certainly be gained if it were possible to measure concentration in a Lagrangian frame of reference by following the evolution of a structure in its passage downstream. Such an experiment would be difficult to undertake in practice and one must be content with measurements made at fixed points. However a qualitative understanding of the evolution of the structure was made possible by motorizing the cine camera mounted which could be moved with the average speed of the large structure in the separated shear layer. Use of a total number of sixteen conductivity probes arranged laterally at three different downstream positions also provided useful quantitative information about structure evolution. All the above experiments were conducted in a separated flow model constructed in a laboratory flume, the description of which follows.

## 4.3 The Separated Flow Model

All the experiments were conducted in a 15.8 metres long flume situated in the Robin Hydraulic Laboratory. The flume has a cross-section of 0.915 metre wide and 0.60 metre deep. The detailed dimensions of the flume are shown in Figure 4.1. The overhead tank supplied the water through a 300 mm diameter outlet pipe and a constant level was maintained in the overhead tank by pumping water into it from a sump, with the overflow being returned to the sump. At the end of the flume a tailgate could control the depth of the flow in the flume. The water from the flume outlet was allowed to fall into a concrete chamber from where it was returned to the sump through an underdrain. The fall of water from the flume outlet could be diverted into a measuring tank thus enabling direct measurement of the discharge rate.

A separated flow region was created in the flume as shown in the Figure 4.1(b). The width of the separated region was 0.5 metre and was constant, thus leaving 0.415 metre wide free stream channel flow. The length of the separated region could be varied up to 2.4 metres. The separated flow region was built at a level 0.305 metre higher than the flume bed in order to avoid any three dimensional boundary layer effects on the quasi two dimensional large eddy structures which were expected to develop in the separated free shear layer.

## 4.4 Experimental Parameters

In the present study all the experiments were conducted in two geometrical configurations of the separated flow model. Two aspect ratios (A.R., defined as the ratio of the length, L to the width, W of the separated region) of 2.0 and 4.8 were used in all phases of experiments. For each geometrical

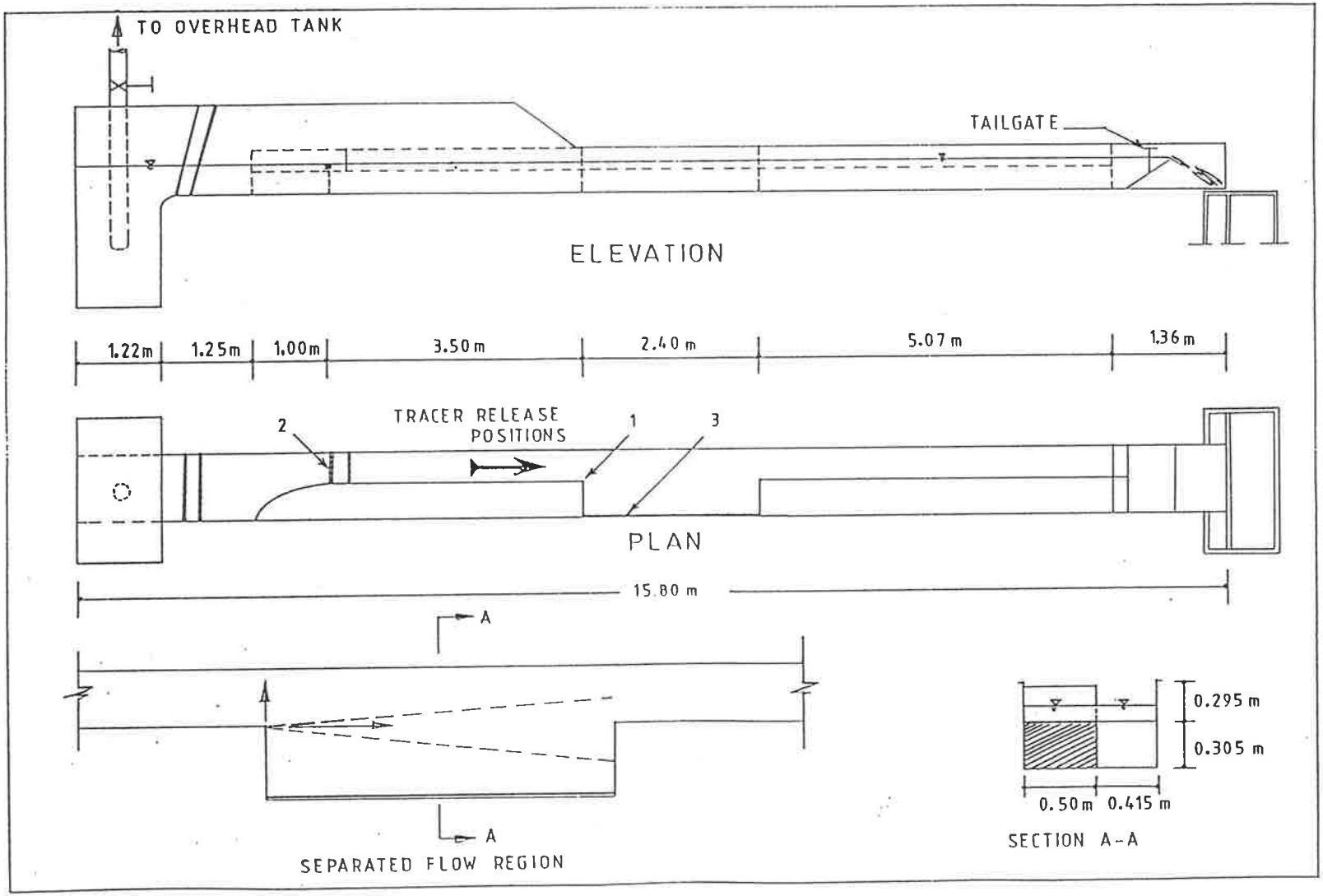


Figure 4.1: Schematic diagram of the flume model

configuration, two different flow conditions, which were defined by the free stream (main channel) mean velocity, were considered. These flow conditions can be designated as the faster free stream flow case and the slower free stream flow case. The following table clearly shows all the experimental conditions used in the present investigation.

Table 4.1: Experimental parameters

| Geometrical conditions | Flow conditions |
|---|---|
| A.R. = 2.0 | U = 0.30 m/sec. |
| | U = 0.20 m/sec. |
| A.R. = 4.8 | U = 0.30 m/sec. |
| | U = 0.20 m/sec. |

The flow conditions mentioned in the above table were chosen to suit the dimensions of the present experimental set up. For instance, a higher free stream mean velocity of 0.40 m/sec was tried which resulted an unsteady flow condition in the main stream channel as well as in the separated flow region. It was also found difficult to photograph using strobe light, because of the reflection from the rippled water surface at higher velocity. On the other hand, velocity lower than 0.20 m/sec was not used because some of the interesting flow features in the separated region were found to be too slow to be captured by the present data collection program, particularly during concentration measurements in the third phase of the experiments, at a desired faster sampling rate.

However, the above experimental parameters are not meant to be the extreme cases. Rather they were chosen to demonstrate the effects of flow and boundary change on various flow processes.

## 4.5 Phase I Experiments

As mentioned earlier, flow visualization was the subject of this phase of experiments. It was more than a century ago when Osborne Reynolds (1883) injected a thin thread of liquid dye into a flow of water through a glass tube to demonstrate the transition from laminar to turbulent flow. Since then flow visualization has flourished as an important tool in experimental flow mechanics. In the present time, flow visualization has assumed a prominent place, particularly in turbulent flow research.

### 4.5.1 Visualization Techniques

The methods of flow visualization can be broadly classified into two major categories,

- Visualization by direct injection of a foreign material; and
- Visualization by optical methods.

The first category comprises all techniques by which a foreign substance is added to the flowing fluid either gaseous or liquid. The most commonly used techniques in this category are the use of dye and hydrogen bubbles in a water medium, and smoke and helium bubbles in an air medium.

The injection of dye has long since been a popular method of visualizing streak lines in water flow. The dye is released either from a small ejector tube placed at a desired position in the flow field or from small orifices which are provided in the wall of a certain model under investigation (Merzkirch, 1974). In both cases the main flow is, to a certain degree, disturbed by the presence of the ejecting devices. There is a wide variety of dye materials for use in flow visualization experiments to suit particular experimental

conditions. Fluorescent rhodamine, methylene blue, writing ink, food colouring, crystal violet are a few among many others used for flow visualization. The important considerations in choosing a particular dye are however, its visibility and good reflective properties for a high photographic contrast.

Crow and Champagne (1971) used fluorescent dye to observe large structures in jet turbulence; Csanady (1963) used similar dye mixture to study turbulent diffusion in an open lake; Dimotakis and Brown (1976) observed large eddy structures dominating in entrainment and mixing in a free shear layer. These are only a few examples of numerous visualization studies by direct dye injection technique. The main disadvantage of dye injection method is however, the quick decay and mixing of the dye filaments in relatively highly turbulent conditions.

The hydrogen bubble technique is relatively recent method of flow visualization. If the flowing fluid is an electrolytic conductor, bubbles can be generated by the electrolysis of this fluid. This technique of flow visualization is attractive since the bubbles can be produced at a controlled rate and at any desired location of the flow. However, unlike other solid tracer materials, a gas bubble can change its shape during its motion with the fluid flow, thus making the analysis of the bubble motion in the fluid complicated.

An estimation of the error sources and uncertainties associated to the hydrogen bubble technique has been given by Schraub et al (1965). Roos and Willmarth (1969) used this technique to study low Reynolds number flow; Kim et al (1971) and Grass (1971) applied in the investigation of flow instabilities and turbulent fluctuation characteristics; Rockwell (1972) and Maxworthy (1972) used the technique for velocity measurements in plane jet flows and vortex rings respectively.

Small solid particles are also used as tracer materials in flow visualization studies. Aluminium powder and the beads of polystyrene are the most fre-

quently used tracer particles in water flow. The particles must be small enough so that one can assume the motion of the particles is the same as that of the fluid. The visualization using such particles can be considered as an indirect method, since one observes the motion of the particles instead of the fluid itself. However, the difference between the movement of the fluid and the particles can be minimized, although not totally avoided, by making the density of the particles almost coinciding with that of the fluid. Further information on the use of particles as tracer material can be found in Cox and Mason (1971) and Merzkirch (1974).

In the second category of the flow visualization methods, various optical techniques are employed to visualize the flow field. These are particularly applied in compressible flows which display variation of the fluid density with time and space. Since the fluid density is a function of the refractive index of the flowing medium, compressible fluids can be made visible by means of certain optical methods which are sensitive to changes of the index of refraction in the field under investigation.

The commonly used optical visualization methods are - the shadowgraph method, the schlieren method, and the Mach-Zehnder interferometer method. An important application of the shadograph method of visualization is the discovery of the large coherent eddy structures by Brown and Roshko (1974) in their helium-nitrogen mixing layer. A detailed description of each of these methods is given by Merzkirch (1974) and is not included here as they are not directly relevant to the present study.

A third category of flow visualization method is mentioned by Merzkirch (1974) which is rather a combination of the first two categories. In this case, the tracer material introduced into the flowing fluid is energy, i.e., in the form of heat or electric discharge. The fluid elements thus marked by their increased energy level need a suitable optical visualization method so

that they can be discriminated from the rest of the fluid. This is not a very frequently used method of visualization and is usually applied to low density gas flows.

A flow pattern visualized with one of the methods or techniques discussed above can be observed by eye or recorded by photographic means. In case of photography, one may either expose single photographic pictures or record the visualized flow with a movie camera if the flow pattern changes with time. In rapidly changing flow fields however, the key to the visualization of flow is the high speed photographic technique. The requirements to be fulfilled in a high speed photographic system are, according to Merzkirch (1974),

- short exposure time of each single image in order to avoid blurring in the image of the moving object;
- intense illumination system because of the short exposure times;
- image frequency high enough to resolve the fast motion of the flow under study; and
- synchronization of the exposure with the high speed event.

Ordinary or high speed cine camera or a television camera can be used for high speed photography depending upon the requirements for the flow condition under study. The separation of the individual exposures can be achieved either by stroboscopic illumination of the object or with continuous illumination by a system of rotating mirrors.

The digital image processing technique and the computer generated colour graphics have brought about a revolution in the recent history of flow visualization. It is now possible to automatically analyze flow visualization film by means of digital image processing and thus extract qualitative information about flow behaviour which may not be readily available from conventional

measurements. Computer generated colour graphics display flow solutions and flow field data in addition to directly assisting conventional flow visualization techniques for speedy and quantitative information. A wealth of further detailed information about these two recent developments can be found in Yang (1985).

After a careful consideration of each of the above relevant visualization techniques, and within the scope and limitations of the present study, the conventional direct dye injection technique and high speed photography were employed for the present phase I investigation the description of which follows.

### 4.5.2 Experimental Procedure

Passive blue dye ('Permicol Blue - 19.2640') dissolved in flume water was used as tracer material for visualizing the large scale coherent eddy structures and the separated zone flow field. Tracer could be released from three different release points from a constant head tracer tank designed for the purpose. The locations of these three release points were,

- Vertical line source injection at the separation point;
- Plane source injection at 4.4 metres upstream of the separation point in the main stream channel; and
- Plane source injection at the deep end of the separation region along its length.

The details of these injection systems will be further discussed in Phase III experiments in a later section.

The technique of cine photography was employed to picture the flow field, in this phase of experiments. The 16 mm 'Paillard Bolex' movie camera was equipped with an electronic triggering device which led the camera pulses into a LED display unit to show the frames per second and also supplied the drive pulses for the strobolume flush unit used as the light source. Photoflood lights could have been used, but the advantage of the strobe light is that it could effectively 'freeze' the movement of the flowing water to the time period of the flash strobe (in this case 50 microseconds). The result is that the pictures were of much sharper definition than those which could be obtained using photoflood lights.

The camera was mounted on a frame structure built on the top of the flume covering the separated flow region. From a single camera position, pictures could be taken over a flow area of approximately 1.44 $m^2$. The position of the camera could be varied from upstream to downstream along the guide rail upon which it was mounted.

A few films were used at the initial stage to adjust the aperture and camera speed suitable for the flow conditions considered. It was found that the camera speed of 32 frames per second at an aperture of F2.8-4.0 were the optimum conditions for good quality pictures. The films used were 'Kodak high speed daylight film 7251 (ASA 400/27 DIN)' and were each 30.5 metres long. At 32 frames per second, one film would last approximately 125 seconds and each run was approximately 15 to 20 seconds long. Longer runs could be taken, but the speed variation of the camera was found to be a limiting factor. It was found that the speed of the camera dropped down to about 25 frames per second for runs longer than 20 seconds.

Although a 20 seconds long run was found to furnish adequate information about the flow pattern, particularly when used synchronously with concentration measurements (Phase III experiments), longer photography was nec-

essary to obtain useful information regarding the 'random' behaviour of the large coherent eddy structures in the separated shear layer. A high resolution video camera and a recorder was therefore, used to capture the flow field for much longer period of time. Typical runs were about 10 to 15 minutes long. Various types of quantitative information were obtained from these longer runs, in particular, the structure passage frequency at suitable downstream locations, the (random) pairing events and the lateral movements of the shear layer were the important information.

### 4.5.3 Photo Analysis

A 'Super Slim Slot Load' (224-S-MK-VIII) data analyzer, manufactured by the EIKI International Inc., was used to analyze the developed positive from the Cine film. A remote control box was connected to this 16 mm projector via a control cable. The advantage of this slot load projector is that the film can be analyzed at any desired frame without going through the entire film. Using the remote control box, the projector could be operated at various frame speeds and also at a single frame advance. The film was analyzed by projecting the picture onto a screen. The time could be read either from the electronic frame counter set in the remote control box or from the LED display which showed the number of frames during photography and appeared in each frame.

Information from the video tape was obtained using a television monitor. The LED display unit was converted into a timer counter in this case which showed the elapsed time in one-tenth of a second i.e., the number appeared on the display divided by ten was the actual time in seconds. This facilitated obtaining direct information regarding structure passage frequency, approximate structure advection velocity, occurrence of pairing and lateral movement of the shear layer.

### 4.5.4 Problems and Precautions

Two major problems were encountered during the flow visualization experiments,

- disturbances in the flow due to the presence of the injecting devices; and
- quick decay and mixing of the dye filaments with the surrounding fluid.

The first one is a very common problem in any flow visualization method employing direct injection of foreign tracer particles. However, precautionary measures were taken to avoid any significant influence of the presence of these injecting devices on the flow. Among the three locations of tracer release, as described earlier, the first one i.e., the vertical line source injecting device was the most critical one as it was located very close to the separation point. Extreme care was therefore taken when using this device. The holes were faced towards the wall so that the tracer jets do not disturb in any way the separation and the large eddy evolution phenomena. No problem associated with the wake generation behind the injecting tube was encountered as it was placed just within the separated region. The second injecting device was placed sufficiently upstream (4.4 metres) from the separation point in order to minimize any effect on the separated flow of interest.

The third tracer injection device was located along the side wall of the separated region and the ejection holes were again faced to the wall so that the impact of the tracer jets do not interfere with the relatively weak recirculating jet flow near the wall. Although the disturbances due to the presence of these injection devices could not be completely eleminated, the precautionary measures taken minimized the effects on the flow.

There is no immediate solution to the problem of quick decay and mixing of the dye filaments with the surrounding fluid. Merzkirch (1974) reports the use of milk with dye solution with the assumption that the fattiness of the milk retards diffusion of the dyed solution. However, the role of milk in a dye solution has not been investigated quantitatively and is not yet a well established practice. In this study effort was made to overcome this problem by releasing dye from different injection points and photographying from different camera positions to get the desired flow pictures. Among other problems, the densities of the tracer solution and the flume water were checked before each experiments to avoid any density difference and contamination of the flume water by the dye solution was found insignificant over the period of experiments.

## 4.6 Phase II Experiments

Velocity measurements in the flow field were undertaken in this phase of the experimental program. At the earlier stages of the experiments, in the absence of a laser Doppler velocimeter, a 'Novar - streamflo' digital propeller type flowmeter was used to measure the velocity profiles in the free stream channel upstream of the separated flow region. At a later stage when the laser Doppler velocimeter was procured by the department, a detailed measurements of the velocity field in the separated flow region was undertaken by reproducing the original flow conditions as closely as was possible. Point gages were used to measure the depth of water in the flume and to determine the slope of the water surface. A description of the digital flowmeter and the laser Doppler velocimetry follows.

### 4.6.1 The Novar Flowmeter

The flowmeter shown in Fig 4.2, is particularly designed for measuring accurately the velocities in hydraulic models and has the ability to measure velocities as low as 2.5 cm/sec. The propeller probe,originally designed by the British Department of Scientific and Industrial Research, has a measuring head comprised of a five bladed PVC rotor mounted on a hard stainless steel spindle terminating in fine burnished conical pivots which run in jewels mounted in a shrouded frame. This ensures minimum frictional resistance. An insulated gold wire contained within the tube terminates 0.1 mm from the rotor blade tips. The measuring head is joined by a slim tube to the plug and socket which connects to the measuring instrument.

When the rotor is revolved by the flow of water, the passage of the rotor blades past the gold wire tip causes a variation of impedance between the tip and the tube. This variation modulates a 15 kHz carrier signal, generated within the indicating instrument which in turn is applied to the electronic detector circuits, producing a square wave signal after amplification and filtering. The resulting pulses are then counted by a digital counter and averaged over a set time interval to obtain a digital reading related to blade passing frequency.

In the present study the resulting pulses were fed into a HP5326B timer counter where the period was displayed. These counter values were then transferred to the PDP 11/34 computer for subsequent calculations of instantaneous (averaged over one second) and mean velocities. The probe was calibrated over a range of flow speeds and the calibration obtained was used in a computer calibration correction program for velocity calculations.

The major limitations of this flowmeter were its inability to predict flow reversal (recirculating flow), thus prohibiting measurements in the separated

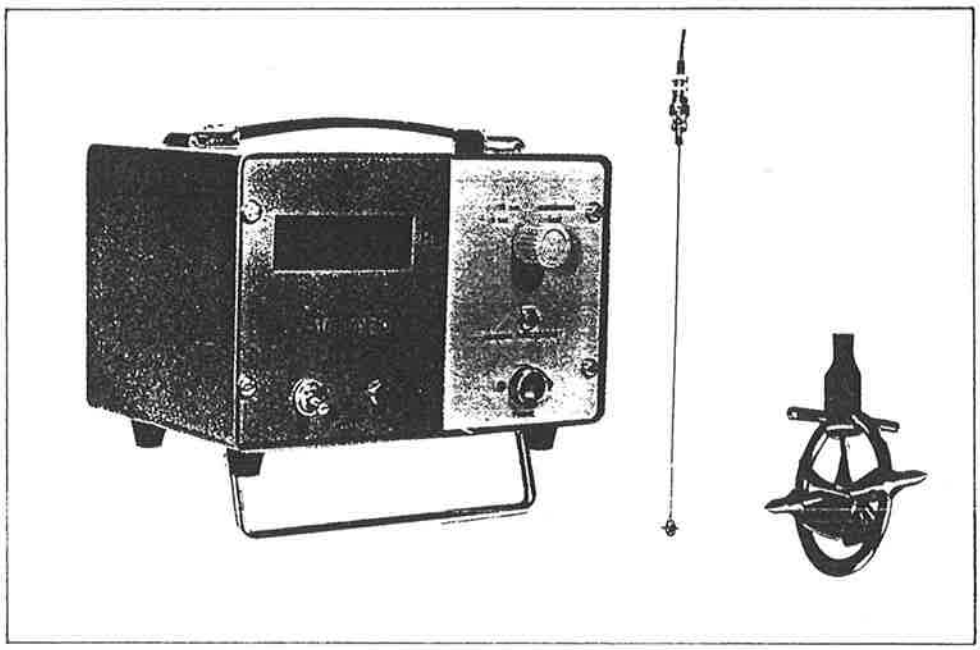

Figure 4.2: The Novar Streamflow meter

flow region of the present study and its interference with the velocity field.

### 4.6.2 Measurements with LDV

A single channel laser-Doppler fibre optic velocimeter (LDV) was employed in the present study in order to measure the velocity field of the separated flow region. A dual beam method with back-scatter mode of light collection is employed in the present measurements. In this section only the procedure of measurements will be described followed by a discussion on the associated problems and precautions in the next section. The photographs of Figures 4.3 and 4.4 show the necessary arrangements of the LDV used in the experiments. A detailed description of the laser-Doppler velocimeter used in the study is included in Appendix A.

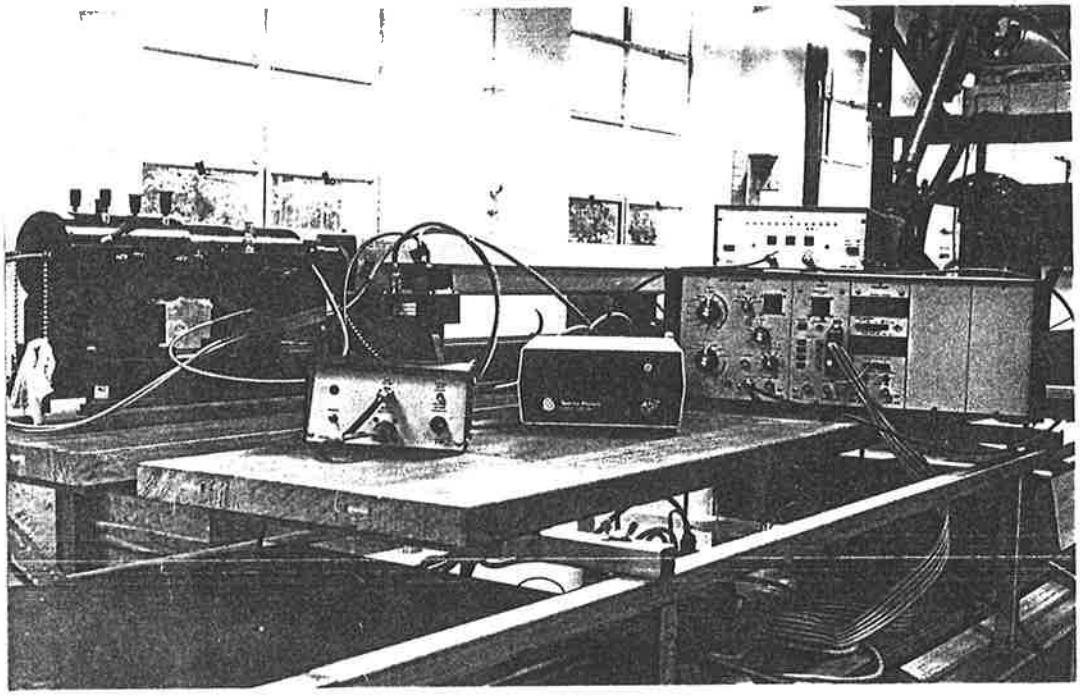

Figure 4.3: Photographs showing the arrangements of the LDV system.

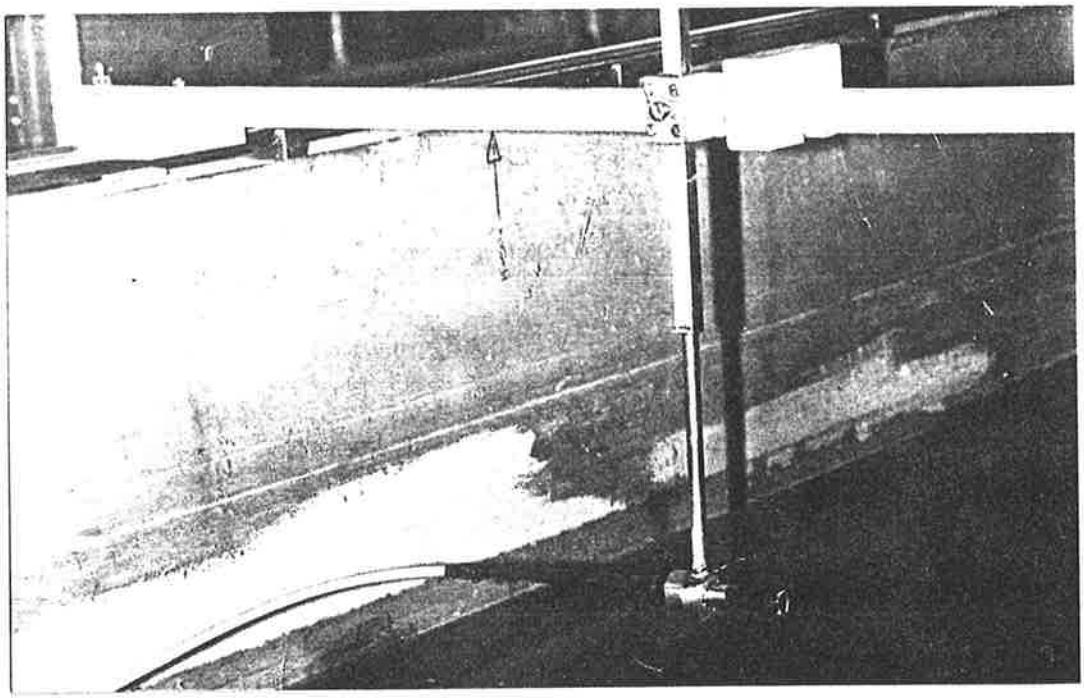

Figure 4.4: Photograph showing the fiber optic probe system.

There were two major areas of interest in the measurements of the flow field using the laser Doppler velocimeter. Firstly, the measurements of the mean and the turbulence quantities across the entire separated flow region to obtain the general flow pattern, and secondly, measurements at various important locations within the separated shear layer to obtain an understanding of the large structure dynamics and their interactions with the recirculating eddies. Similar measurements were carried out for all the geometrical and the flow conditions considered.

Prior to the commencement of the measurements the laser Doppler velocimeter using the fibre-optics option was calibrated in a separate large flume of 1.2 metres wide and 30.48 metres long. Water in the flume was kept stagnant and the entire set of equipment including the fibre-optics probe was attached to a motorized trolley placed just over the flume. The probe was propelled underwater along the flume length at a constant speed. The speed of the trolley was measured by using metal wheels to successively trigger two electrical contacts, the time between the triggers being measured with an HP frequency counter in interval timing mode. While the contact spacing and the recorded time interval yielded the trolley speed, the LDV data were displayed on an small computer using TSI's 'realtime' program. A number of runs were performed to check whether the computed LDV velocity and the trolley speed were in reasonable agreement. It was found that the mean LDV velocity agreed quite closely with trolley speed, the error limit being within $\pm 1\%$.

The angle of intersection between the laser beams was obtained by projecting the diverging beams onto a flat surface and measuring the geometry. Thus the half angle 'k', was found to be $3.347^0$. Following the fringe model of the dual beam LDV system (Adrian, 1983), the fringe spacing, $d_f$, was calculated

as,

$$d_f = \frac{\lambda}{2\sin k} = \frac{632.8\text{nm}}{2\sin 3.347^0} = 5.419\mu m$$

where, $\lambda$ = the wavelength of the laser light.

The fluid velocity then could be calculated using the following equation (see Appendix A),

$$f_D = \frac{2\sin k}{\lambda} u_i$$

or,

$$u_i = f_D . d_f$$

where, $f_D$ is the frequency of the burst signal obtained from the timer module of the counter processor.

With a frequency shift of 0.5 MHz for the velocity range within $\pm$ 1.0 m/sec, the low-limit and the high-limit filters on the timer module was set to 100 kHz and 1 MHz respectively. The choice of the up-shift or the down-shift on the electronics module of the frequency shift system was dependent on the orientation of the probe corresponding to positive or negative values.

In optimizing the data rate and the output signal, it is best to obtain the maximum data rate (samples/second) without allowing the occurrence of scattering or invalid data points due to noise. This procedure is best accomplished by observing the output signal directly on the oscilloscope. In most flows with reasonably high data rates, erroneous or invalid data can be spotted immediately on an oscilloscope as they appear randomly scattered on the display. This problem was effectively controlled by setting the Gain on the counter timer to its optimum level.

Setting the Gain to its optimum level could easily be performed by observing the histogram of velocity values vs. percentage of occurrence produced by the 'realtime' program and adjusting the Gain to the highest level which does

not produce any false data points. In circumstances where a high rate of data points were of interest such as measurements in the shear layer a few points due to noise were accepted which were then removed during data processing. However, this Gain setting had to be checked before each experimental run as the threshold level appeared to be changing fairly rapidly with time.

It is important to note that the data from a laser Doppler velocimeter are not continuous, rather it is a record of values obtained at discrete intervals. The period of measurement varied both in time and in space depending on the availability of scattering particles through the measurement volume, thus varying data rate. Typical data rate was in the neighborhood of 100 measurements per second in the main channel and within the high speed side of the separated shear layer.

The rate fell well below this level in the low speed side of the shear layer and in the separated region as expected. Even in a single run at a particular point the data rate was not uniform due to velocity biasing, an inherent problem of LDV measurements which will be further discussed in the next section. This non-uniformity of the data rate was particularly observed in the shear layer where the quasi-periodic large structures played the role. However, continuous seeding of scattering particles slightly improved the situation.

Data from each experimental runs were stored on floppy disks using a small computer which were later transferred to the main VAX computer for subsequent processing and analysis. The following subsection discusses some important problems associated with LDV measurements.

### 4.6.3 Associated Problems with LDV Measurements

#### (A) Velocity Bias

The problem of velocity bias arises because, in a flow which is uniformly

seeded with scattering particles, more particles per unit time will be carried through the measurement volume when the velocity is high than when it is low compared to the actual mean flow velocity. If the signal processor validates all of the Doppler signals it receives, the average of this data set would be higher than the true mean velocity. This error occurs in the computation of statistical quantities such as mean, r.m.s velocity and spectra from ensembles of individual data points and generally increases with increasing level of turbulence (McLaughlin and Tiederman, 1973).

This problem has been the subject of a number of investigations and several 'bias correction' methods have been proposed. McLaughlin and Tiederman (1973) have suggested the application of bias correction to averaged properties by assuming a linear dependence between the particle arrival rate and a measured velocity component. Durao et al (1980) indicated that such 'one-dimensional' correction can lead to even larger errors. Stevenson et al (1984) suggested that if velocity samples can be taken at equal time intervals a correct mean velocity can be obtained assuming velocity fluctuations are random. Equal time interval sampling can be approached if the seeding density is very high and the processor is controlled so that it will accept a signal only when a fixed waiting time has passed after the previous signal has been read. Provided this waiting time is long compared to the average time between particle arrivals in the measurement volume, a data set consisting of velocities acquired at essentially equal time intervals can be obtained.

In cases where high seeding density can not be attained a 'time-weighting' approach of correction based on the time interval between successive velocity samples as proposed by Hoesel and Rodi (1977) can be used. George (1975) and Dimotakis (1976, in Durst et al, 1981) have also suggested similar correction technique. The details of this correction method is given by Durst et al (1981).

The total burst mode of the counter counter processor is designed to correct for velocity bias at low data rates. The proper value of the mean velocity is expressed as,

$$\bar{u} = \frac{\sum u_i \, t_{Bi}}{\sum t_{Bi}} \tag{4.1}$$

where, $u_i$ is the measured velocity and $t_{Bi}$ is the time for particle to traverse the measurement volume (i.e., the time for total burst) which is used as the weighting factor. If $n_i$ is the number of fringes crossed during the time $t_{Bi}$ and $f_{Di}$ is the frequency of the input signal being measured, then

$$u_i \sim f_{Di} = \frac{n_i}{t_{Bi}} \tag{4.2}$$

Substituting into the equation for $\bar{u}$, one obtains,

$$\bar{u} \sim \bar{f}_D = \frac{\sum n_i}{\sum t_{Bi}} \tag{4.3}$$

Both $n_i$ and $t_{Bi}$ can be measured digitally with the model 1980B counter processor used in this study. Similar procedure is applied to calculate r.m.s. fluctuations, and higher order moments with $t_{Bi}$ being used as the weighting function.

**(B) Fringe Biasing**

The problem of fringe biasing occurs when the signal processor requires a minimum number of cycles to make a measurement, and certain particle trajectories fail to provide this number. Thus the data rate is greatest when the velocity vector is perpendicular to the fringes, and it decreases as the angle between the velocity and the fringes approaches zero. The resulting data are biased toward samples from perpendicular velocities.

As indicated by Adrian (1983), there is no satisfactory method of correcting for fringe bias analytically. However, it can be reduced to negligible levels in most cases by frequency shifting. Frequency shifting effectively adds cycles to a Doppler burst by moving the fringes with respect to the fluid. Then, if the fringe velocity is large compared to the flow velocities, particles travelling

even parallel to the fringes will produce an adequate number of cycles as the fringes move over them. Fringe biasing is also minimized by using the total burst mode of the counter, because this mode requires the least number of cycles for a measurement. Fringe biasing is only important for low-burst-density signals, because the signal is almost always present in high-burst-density signals.

### (C) SNR effects

In general, the maximum amount of flow information can be achieved when the signal-to-noise (SNR) ratio is high, and therefore it is desirable that an adequate level of SNR can be obtained within the constraints of the experiment. High SNR can be obtained by minimizing the extraneous light the major sources of which are the laser flare and reflections of background light. If the background is brighter than the light scattered by the particles, extraneous light will contribute appreciably to the shot noise. In the present study effort was made to keep the background light to a minimum possible level.

Another problem arised when measurements were made very close to the separation point. The flare from the wall produced a large amount of noise in the signal. This was eliminated by painting the near wall with black paint to provide high absorption and low flare thus reducing the noise level.

### (D) Scattering Particles

The scattering particles are the basic source of the Doppler signal and have more influence on the quality of the signal than any other component of the LDV system. In some cases the natural particles occurring in the fluid are adequate seed. However, in most applications, the data can be improved by adding appropriate seed particles to the flow.

There are three basic requirements for good quality seeding particles which are,

- the seed must be able to follow the flow;
- the seed must scatter sufficient light to produce measurable signals; and
- the seed must be present in desirable numbers.

At present, no absolute rules can be found regarding the light scattering properties as well as the size and concentration of various seeding particles. Melling and Whitelaw (1975) discussed some of the particle characteristics and their implications for practical laser velocimetry application. Durst et al (1981) addressed the topic in more detail. Recently Durst and Ruck (1987) stressed the optimum particle size distribution to achieve better quality signals.

Haghgoogie et al (1986) experimentally investigated the performance of several seeding techniques. They have used phenolic microballoons and alumina as two different seeding particles. From their analysis it appears that the microballoons with an average size range of about 40 to 50 microns accurately reflects the amplitude of the velocity fluctuations for frequencies less than about 0.1 kHz. For frequencies larger than this smaller particles are preferred. On the other hand larger particles scatter more and yield better signals than the smaller particles (Adrian, 1983). The smaller particles add more noise than signal and hence are undesirable. However, very large particles are also undesirable because they are not likely to follow the flow.

In the present study phenolic microballoons produced by Union Carbide were used as seeding particles. In dry condition they are lighter than water and of size ranging from 20 to 40 microns. They can absorb water and was found that when they were soaked in water for about 24 hours the density was almost equal to that of water. Since there was no established rule regarding their number concentration, a trial and error method was adopted to achieve

a better signal at a desired data rate. Particle seeding with the phenolic microballoons improved the data rate reaching to about 200 samples per second. This was particularly important for measurements in the separated shear layer.

## 4.7 Phase III Experiments

This part of the experiments was concerned with the measurements of concentration of a passive tracer (salt solution) at various locations of the separated flow region. An important aspect of this phase of the experiments was the synchronous photography of the flow field at the time of numerical data collection. The major apparatus used in this phase were the electrical conductivity probes, the tracer injection equipment, the cine camera and the PDP 11/34 computer for data collection. A significant amount of electronics and instrumentational works were involved with the computer data collection from the conductivity probes which are discussed in the following subsections. A detail description of the photo synchronization system is given in Appendix C and is not included here for brevity.

### 4.7.1 The Conductivity Probes

#### (A) Design Considerations

Measurements of concentration variations in a turbulent flow field by using electrical conductivity probes is based on the principle that the electrical conductivity of a solution is a function of its composition. Hence, such measurements provides an understanding of the transport of mass concentration due to turbulent velocity fluctuations.

A number of researchers have used electrical conductivity probes to mea-

sure the concentration fluctuations in various flow conditions. Different sizes and types of probes have been used to suit experimental conditions and requirements. For instance, Prausnitz and Wilhelm (1956) developed a two electrode probe with 1.2 mm long platinum wires spaced 1.00 mm apart. They used this probe to measure salt concentration fluctuations in a packed bed.

Lamb et al (1960, in Gibson and Schwarz, 1963) used a two-electrode probe but reduced the cell volume of the probe considerably by making one electrode much shorter than the other so that the resistance of the fluid between the electrodes would be dominated by the resistivity of the solution very close to the smallest electrode. One disadvantage of such arrangement was that some of the current might be lost to stray grounds in the system. Also this design restricted the circuit's use to large conductivity fluctuations. Gibson and Schwartz (1963) used a single electrode probe. This encountered a problem of signal attenuation associated with the spatial resolution of the probe.

Fischer (1966), Okoye (1970) and Daniell (1974) used three-electrode probes for measuring the concentration fluctuations in turbulent flow field. The motivation behind using three-electrode probes was that the generated electric field was confined to a comparatively smaller region within the outer electrodes of the probe thus offering greater sensitivity and better response to the concentration variations at a point. However, the larger size and the shape of their probes may have had a deleterious effect on the turbulence flow field in an unknown way which should be minimized by a more suitable design of the probe.

In the present study a two-electrode probe system is employed. It is considered that if a two-electrode probe can achieve the desired greater sensitivity and better response to concentration fluctuations at a point through proper

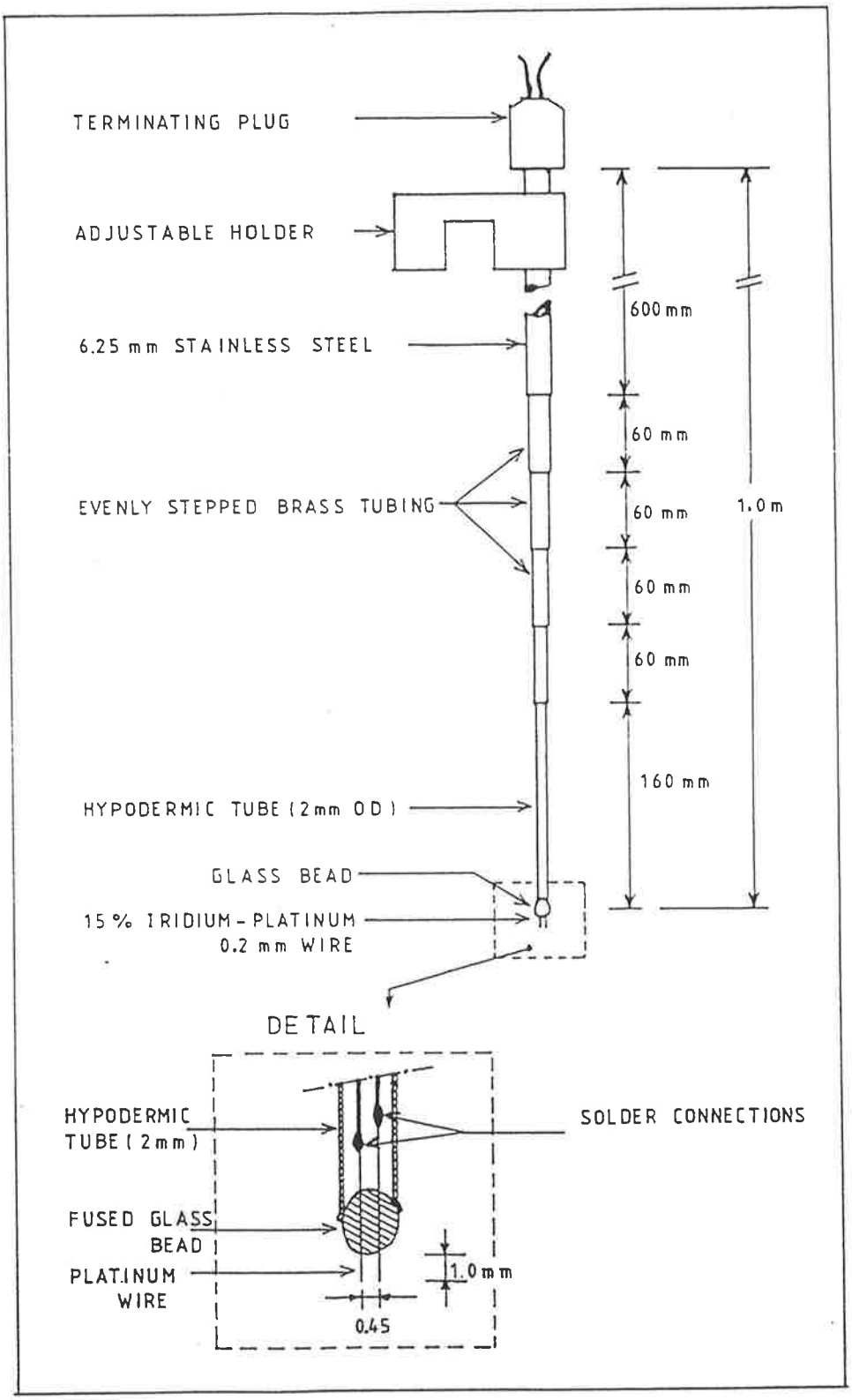


Figure 4.5: Details of the Conductivity Probe

design, it is much simpler and economic to construct a two-electrode probe rather than a three-electrode one. The design of the probe is a slight modification of the probe reported by Alonso (1970). Figure 4.5, shows the construction details of the probe. The body of the lower 160 mm part of the probe is built from stainless steel hypodermic tubing of 2.00 mm outer diameter. The diameter of the upper part of the probe is increased in steps as shown in the figure, in order to minimize the lateral vibration when subjected to turbulent flow field. It was expected that only the lower 160 mm will be immersed within the flow.

Two 0.2 mm thick platinum wires are spaced at 0.45 mm apart and secured by melting glass on them and thus making a glass bead of desired shape which fits at one end of the 2.0 mm hypodermic tube bored out to obtain an inside bevel. Electrically insulated leads are then soldered to each platinum wire and both connections are coated properly before covering by a piece of heat shrink tube. The platinum wires are left projecting 1.0 mm beyond the fused glass bead to form the electrodes. A total of twenty probes were constructed among which sixteen were used in the experiments thus leaving four of them available as standby units.

### (B) Circuit Description

The block diagram of Figure 4.6, shows the various component parts of the electronic circuitry used in conjunction with the conductivity probes. The power supply section produces $\pm 15$ volts power for the entire unit and a 10 kHz carrier frequency signal for the probes. Both the $\pm 15$ volts power and the 10 kHz carrier frequency are used by the probe section to produce an output voltage proportional to the conductance of the liquid in which the probes were inserted. The unit has a total of 16 separate probe circuits which have separate level set controls. This means that the flume water conductance value for each probe could be adjusted to the same reference value, and thus minimizing the initial set up time.

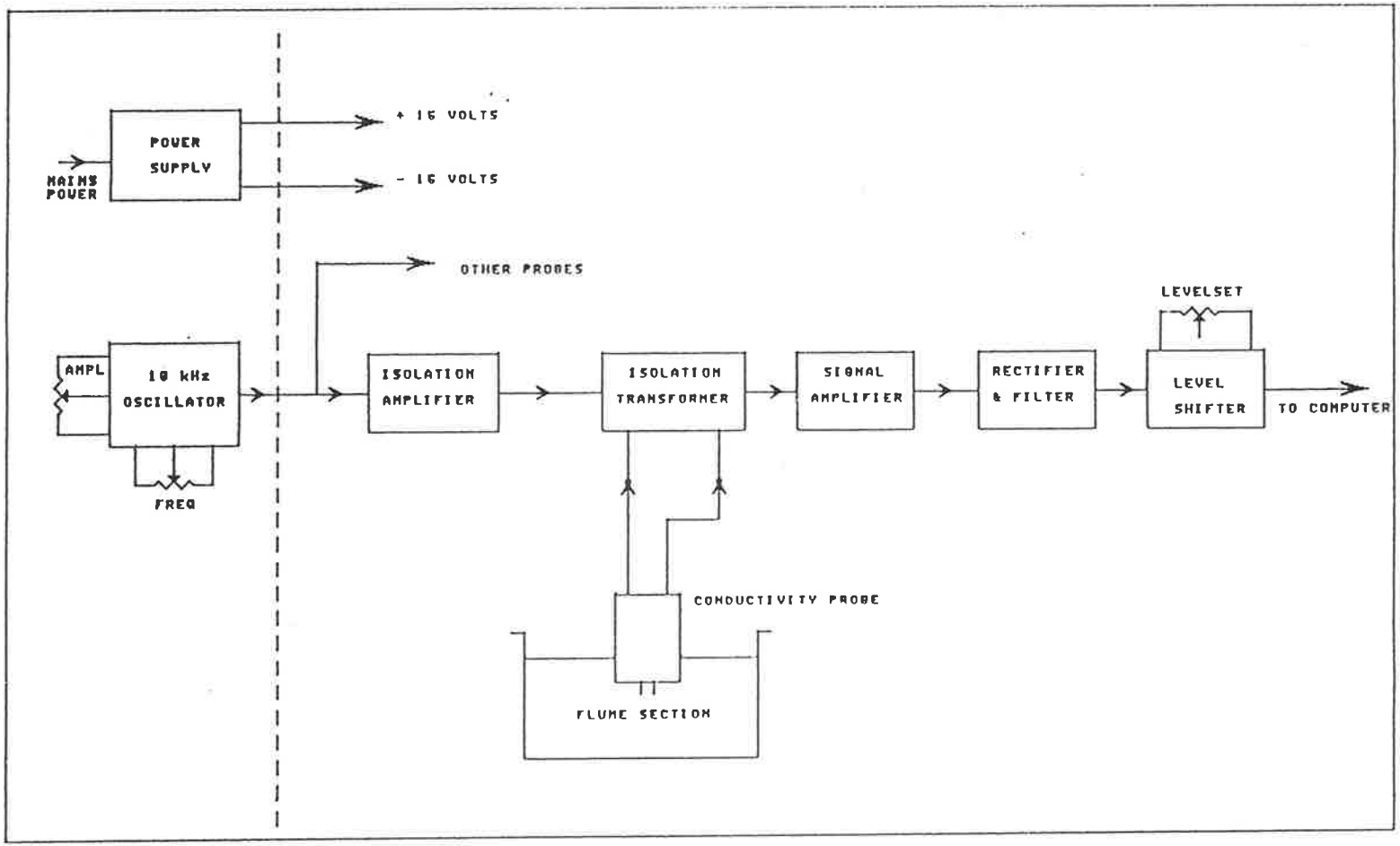


Figure 4.6: Block diagram of the electronic circuitry for conductivity probe

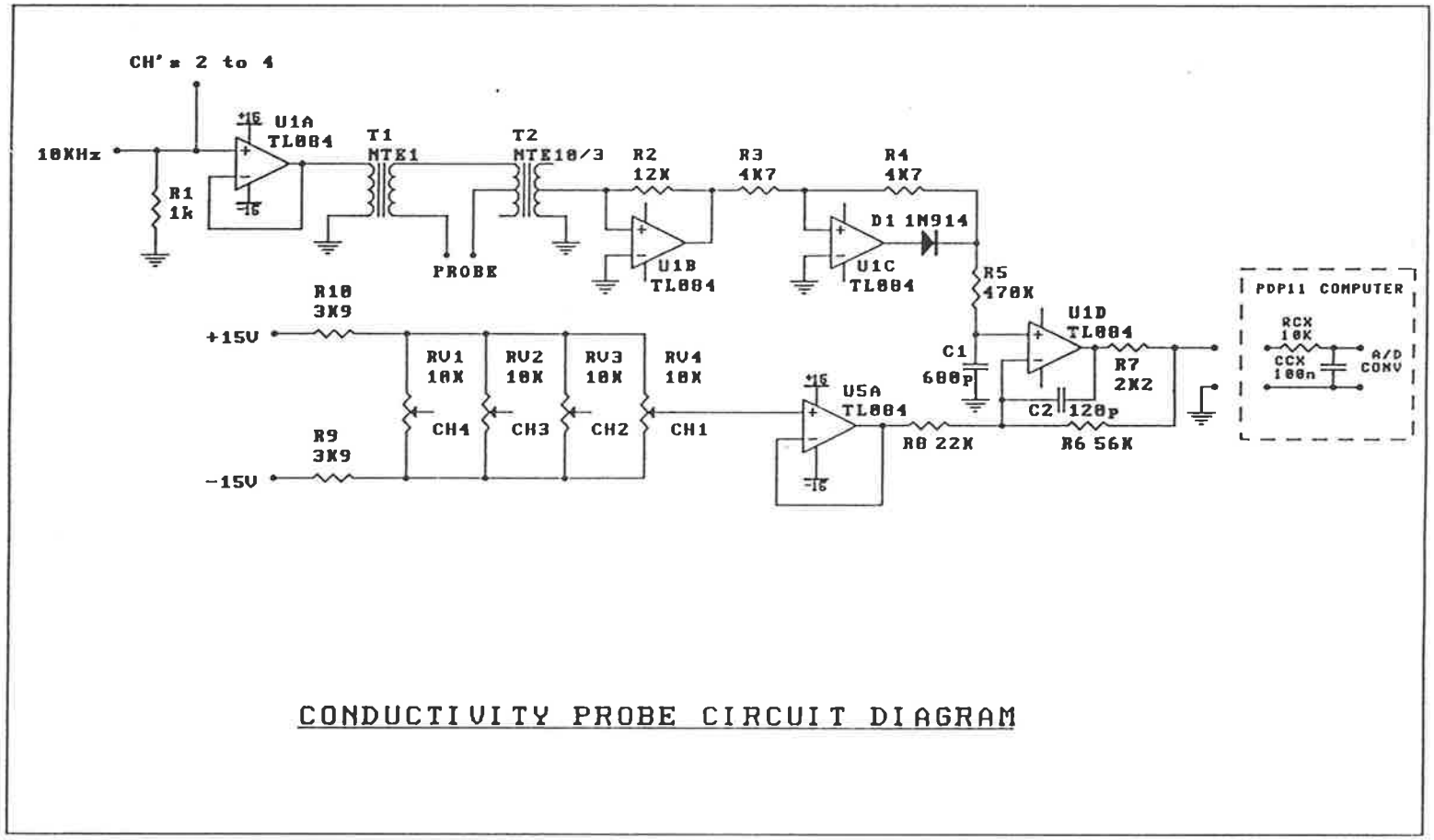


Figure 4.7: Conductivity probe circuit diagram

In order to eliminate the interference between probes in water, a two transformer isolation technique was adopted. During operation, each of the probes has an alternating voltage applied across the two platinum wire tips, where a current will flow in proportion to the conductance of the water in between them. However, if there is any common point in the probe circuit with another probe in the same water, an interference current will flow between the probes and will change the conductivity readings of both the probes. This is prevented by employing the transformer isolation circuit. The detail circuit diagram is shown in Figure 4.7.

The 10 kHz carrier signal generated on the power supply board is applied to the input buffers of each probe circuit. This consists of a non - inverting unity gain amplifier, whose output is applied to the input side of the input isolation transformer. The input isolation transformer has a 1:1 input to output ratio and this effectively isolates the input buffer from the probe circuit. One side of the secondary of this transformer is connected to one of the probe tips, while the other tip goes to the primary of the output isolating transformer. Hence there is no other path for the signal on the probe to go, except across the probe tips and to the other side of the output isolating transformer. Coupling from one probe circuit to another will not occur under normal conditions, because the only common point for all the probes is the fluid medium itself.

The current which passes through the conducting fluid also passes through the primary of the output isolating transformer. Since the secondary of this transformer is connected to the summing junction of the following amplifier, a very low impedance is reflected back to the primary. This has the effect of producing a linear transfer function between the conductance of the liquid and the output signal. In practice however, there is a non-linearity of the order of 5% at the maximum output signal which is of little consequence.

The signal rectifier in the circuit produces a full wave rectified version of the input signal coming from the amplifier. The full wave rectified signal is then applied across a single pole RC filter network before going to the input of the level shifter. This gets rid of most of the high frequency components of the rectified signal and produces a DC voltage proportional to the conductance of the liquid surrounding the probe, at the level shifter input. The amplitude of this signal can range from 0 to about +5 volts.

Since the range of the A/D converter on the PDP 11/34 computer is set at ±5 volts, the task of the level shifter is to match the range of the conductance probes to these values. This is achieved by amplifying the signal by a factor of about 3.5 and shifting the zero conductance level (i.e., the value when the probe tips are out of the water) to negative 5 volts. However, the level shift control may be used to adjust this point anywhere within the output voltage range of ±5 volts to match the A/D converter input level.

**(C) Interference Test**

To check for the interactions between probes, one probe was immersed into a beaker of salt water solution and the voltage deflection was recorded on the oscilloscope. A second probe was then immersed in the same beaker and was traversed in the vicinity of the first probe (as close as 5 mm apart) and no change in the oscilloscope deflection was noticed thus indicating elimination of the interference problem between probes by the isolation transformer.

**(D) Response Characteristics**

To measure the concentration fluctuations in a turbulent flow field it is imperative to determine the probe response to a rapidly changing load. The response of the conductivity probe depends on the transducer used and the cell volume surrounding the electrodes, the response being slower for larger electrodes of a given transducer (Okoye, 1970). The response time is generally evaluated by the ability of the instrument to reproduce an abrupt change

in the input load. The rate at which the output rises when a step function is applied is commonly expressed in terms of the time it takes the output to rise from 10 to 90% of its full amplitude. This is called the 'rise time'.

In the present study the probe response was determined by subjecting the probe to a nearly instantaneous load. This was done by dropping the probe at a certain speed across an air - liquid interface. The speed of submergence was determined by adjusting the height of the free fall and two different electrode lengths (1.0 mm and 2.2 mm) were used to observe the variation in response time with electrode size. The results are shown in the oscilloscope photographs of Figure 4.8.

The results clearly indicate that the rise time varies with electrode size, being longer for larger electrodes, i.e., the response is slower. It is also evident from the test results that changes in rise time with liquid concentration is insignificant. The submergence speed has also some effect on the rise time, the time being shorter for higher speed.

### 4.7.2 The Tracer Injection System

The schematic diagram of Figure 4.9 shows the various components of the tracer injection system employed in the concentration measurement experiments. The system was designed and built for the purpose of releasing the tracer from different release points to suit various measurement conditions which are explained in an earlier section. The tracer was a sodium chloride solution coloured blue with dye primarily for visual effects. The tracer solution was stored in a large 30 litre tank placed on a wooden base about 1.5 metres above the flume bed. A small 5 litre jar was placed inside the large tank and the tracer solution was constantly pumped from the large tank into the jar to make a constant head discharge through the bottom of the jar

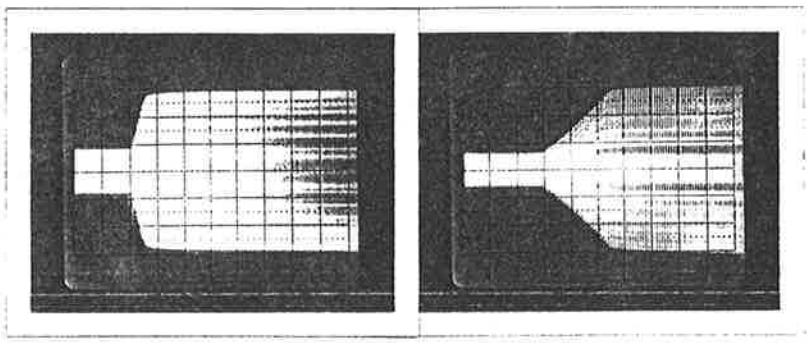

(a)

Electrode size = 1.0 mm
Liquid conc. = 300 ppm
Submergence speed = 1.1 mm/ms
Estimated rise time = 1 ms

(b)

Electrode size = 2.2 mm
Liquid conc. = 300 ppm
Submergence speed = 1.1 mm/ms
Estimated rise time = 2.5 ms

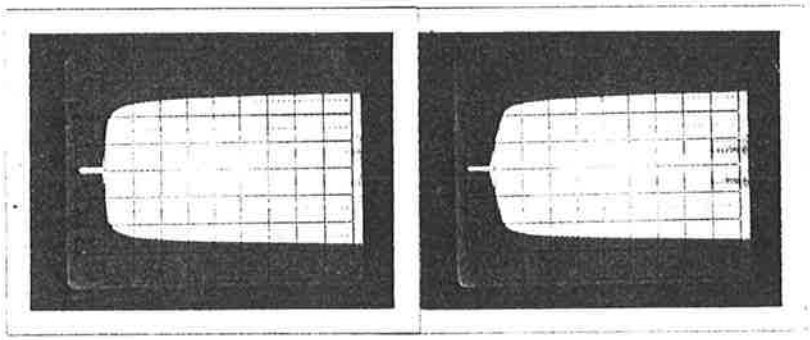

(c)

Electrode size = 1.00 mm
Liquid conc. = 20000 ppm
Submergence speed = 1.1 mm/ms
Estimated rise time = 1.3 ms

(d)

Electrode size = 2.2 mm
Liquid conc. = 20000 ppm
Submergence speed = 1.1 mm/ms
Estimated rise time = 2.7 ms

Figure 4.8: Response characteristics of the conductivity probes

with the overflow back into the large tank. The tracer flow rate was measured and controlled by a precision flowmeter which used a floating cylinder as a flowrate indicator. Three control valves were used to control the tracer flow from three different release positions.

At position 1 (i.e., at the separation point), as mentioned earlier, the release can be assumed to be a line source where the tracer is approximately uniformly distributed over the depth of flow immediately after release. The tracer was injected through a 6 mm diameter aluminium pipe with 2 mm diameter holes at 5 mm spacings. The holes are located at the bottom part of the pipe covering 75 mm of its length which was expected to be within the flow depth. The pipe was placed at the separation point just inside the separated region in order to avoid any disturbances to the boundary layer separation phenomena. The flow around the pipe was almost stagnant and the holes in the pipe were faced towards the wall so that the tracer jets do not interfere with the actual flow pattern at the separation point.

At position 2 (i.e., at an upstream point in the main channel), the system was designed to achieve approximately a plane source of tracer injection. The system consisted of a total of eighteen 2.5 mm diameter nozzles discharging tracer into the flow. The nozzles were attached to 2 mm thick flat bars placed horizontally with the flow in two layers along the flow depth, each layer having nine nozzles placed 40 mm apart.

All the nozzles were connected to a 15 mm diameter PVC distribution pipe through separate plastic pipes in order to achieve an uniform, instantaneous discharge through all the nozzles thus approximating a plane source of injection within a few millimeters from the exit point. The system was designed considering the maximum flow velocity and the anticipated flow depth. During an experimental run, special care was taken to ensure that the tracer discharge velocity was closely equal to the local water flow velocity. This

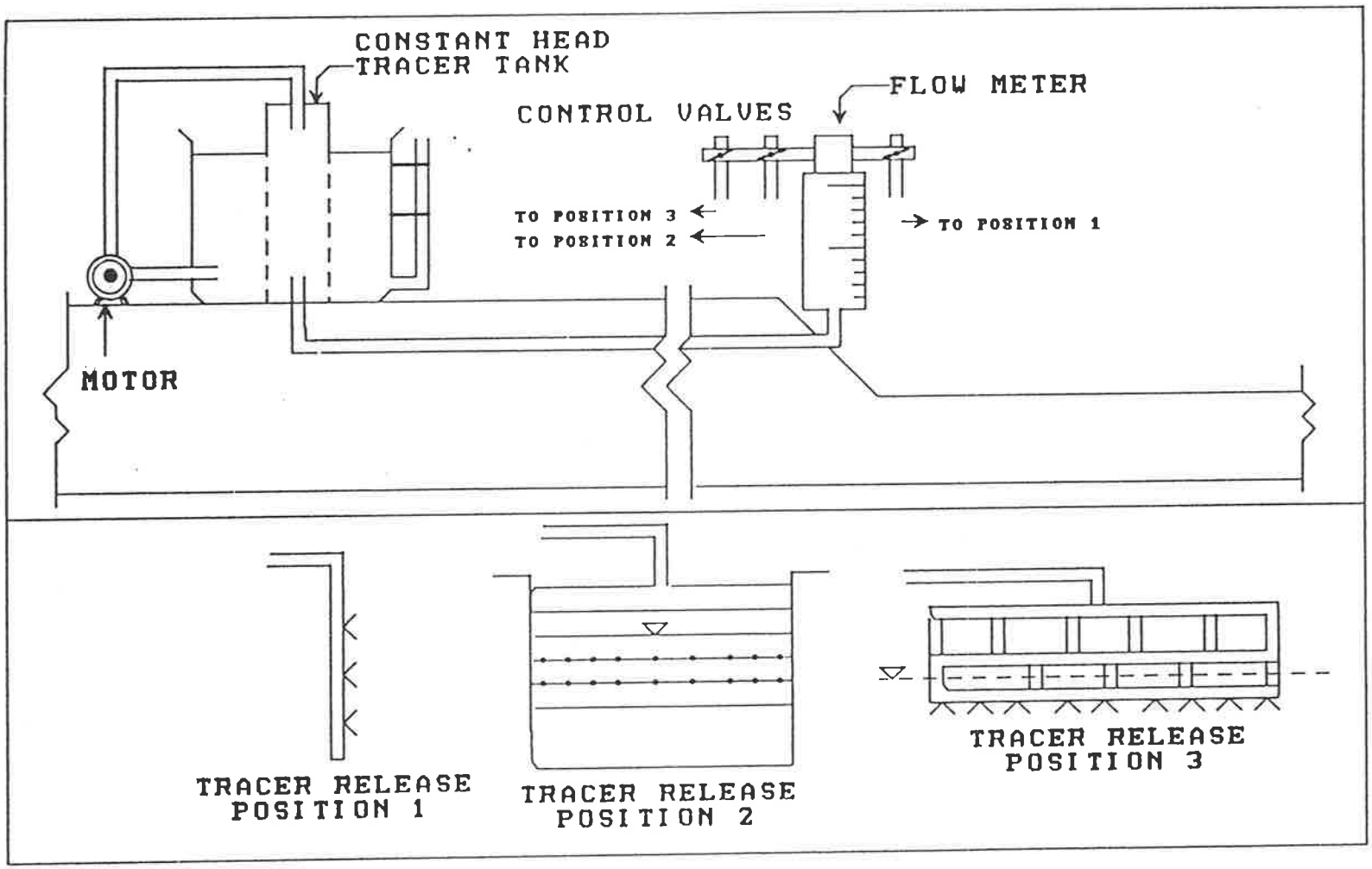


Figure 4.9: Schematic diagram of the tracer injection system

could be achieved by using the corresponding control valve and setting the flowmeter at a certain flowrate consistent with the water flow velocity.

The third tracer injection system was built attached to the side wall of the separated region throughout its entire length. The system consisted of a network of PVC pipes with 2 mm holes in the bottom pipe placed at the mid-depth of the flow. In this case also, attention was given to the simultaneous uniform discharge of the tracer solution throughout the entire length of the region and to achieve as closely as possible a plane source of tracer injection. Since the flow in this separated region was much slower than the flow in the main stream channel, a single layer of release facing the wall was sufficient to achieve a uniform distribution across the depth within about 50 mm from the wall.

### 4.7.3 The Digital Data Acquisition System

The digital data acquisition was undertaken by utilizing the department's Peripheral Data Processor (PDP 11/34) which is interfaced with a K-series data acquisition option. This involves calling up various internal subroutines necessary for collecting and storing raw data values onto a computer disc. The main data collection program 'REDAT' and the subroutines used in conjunction with the main program are listed and explained in Appendix B. The block diagram of Figure 4.10 shows the various components of the overall data collection program.

The details of the probe conditioning circuit (see Figure 4.7) are discussed in a previous sub-section. A low pass filter is connected to each of the probe lines at the input of the K-series analog to digital (A/D) convertor. The reasons for using the filter were as follows.

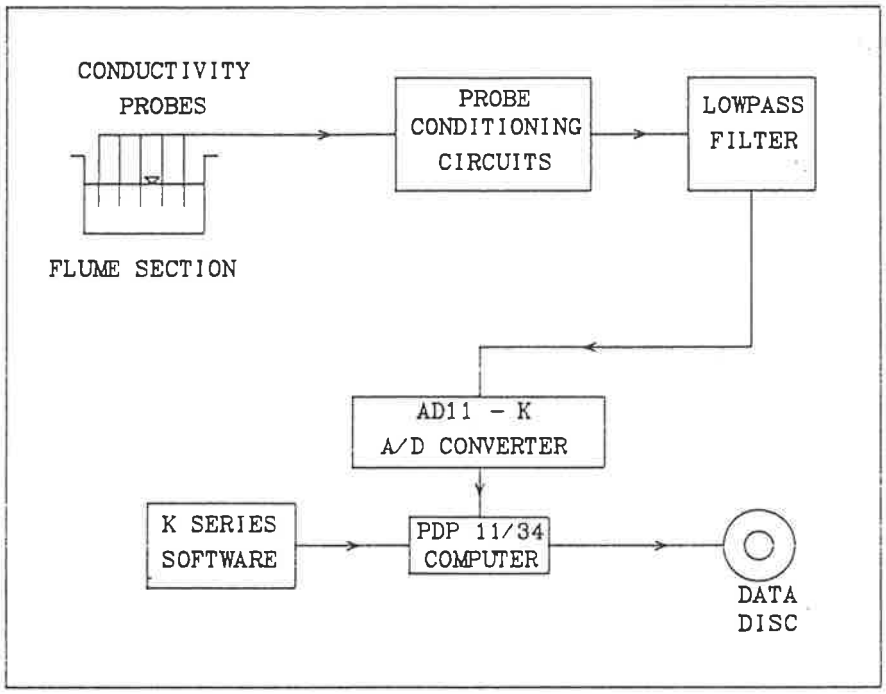


Figure 4.10: Block diagram of digital data collection program

(a) to suppress the noise picked up by the cable between the probe conditioning circuits which were located near the experimental set up in the laboratory and the PDP 11/34 computer in the computer room (approximately 50 metres long cable); and

(b) to further suppress the remaining 20 kHz frequency component on the line originating in the probe conditioning circuit as a result of rectification of the 10 kHz raw probe signal.

The component values for this filter were selected, through trial and error, to attenuate all the noise voltages at the input of the A/D convertor to a value lower than the least significant digit value of the A/D convertor. For this computer the least significant digit value is 2.5 millivolts. The final filter chosen was a single pole passive type with a cut-off frequency of about 160

Hz.

Consideration was also given to the maximum sampling rate of digital data when selecting the filter. The maximum sampling rate chosen for the present experimental program was 100 samples per second which means that, according to the Nyquest sampling theory, the maximum frequency could be sampled is 50 Hz. With the low pass filter of cut-off frequency of about 160 Hz however, it would have been possible to sample the data at a much higher rate. A fast fourier transform (FFT) analysis was therefore, performed by feeding the unfiltered signal to a HP analyzer in order to determine a suitable sampling rate. It was found from the analysis that no significant frequency component beyond 50 Hz was present in the signal. Therefore, sampling at a rate of 100 samples per second was accepted as a reasonable rate for accurate result. This sampling rate was considered representative of the actual variation of the tracer concentration. A comparison of an analog record with respective digitized record sampled at 60 samples/sec by Okoye (1970) showed accurate representation of the concentration variation.

### 4.7.4 Experimental Procedure

There were two different geometrical set-ups of the separated region for which experiments were performed and in each set up there were two different flow conditions considered. Under each flow condition there were several series of experiments considering various tracer release conditions and probe positions. The first few series of runs were considered preliminary as they encountered various problems of releasing the tracer from different positions and at various flow depths, locating the probe positions for useful results and some associated problems of synchronous photography. Although these runs were not included in the analysis, they were invaluable in gaining a physical insight into the behaviour of the turbulent fluid flow.

The various experimental runs were coded with some alpha-numeric numbers to represent different flow, geometrical and tracer release conditions. For instance, the code 'RUN CS2F105' denotes run number 5 of the series 100, which represents the tracer release condition, of the flow condition F varying in the main stream mean velocity, S2 represents geometrical set up 2 (aspect ratio = 2.0), and C denotes concentration measurements. Similarly, 'RUN CS1E315' denotes run number 15 of series 300, flow condition E and of set up 1 (aspect ratio = 4.8). There were several runs in series 100 in which the camera was moved at a speed consistent with the average speed of the large eddy structure in the separated shear layer to obtain a qualitative understanding of the structures evolution.

In this sub-section, the procedure for a typical experimental run is described. There are several steps to be performed before the beginning of an experimental run. These are preparation of the tracer material, establishment of uniform flow in the flume, calibration of the conductivity probes, placing the probes at various suitable locations, loading the camera and resetting the frame counter. A tracer batch was prepared by dissolving salt (NaCl), methylated spirits and some blue dye in flume water. The concentration of the tracer batch was determined using a conductance meter and the density was checked with a density meter to achieve a desired neutrally buoyant solution of about 5000 ppm. Several batches of salt solution were prepared and stored in the tracer tank and left overnight so that, during an experiment, tracer and flume water temperatures were approximately equal.

At the commencement of each group of runs, mean velocity measurements in the main channel flow upstream of the separated region were made and the water depth was set at a desired value by adjusting the discharge and the height of the tail gate. Uniform flow conditions were assumed to prevail when flow depths at various locations were constant within $\pm$ 2 mm.

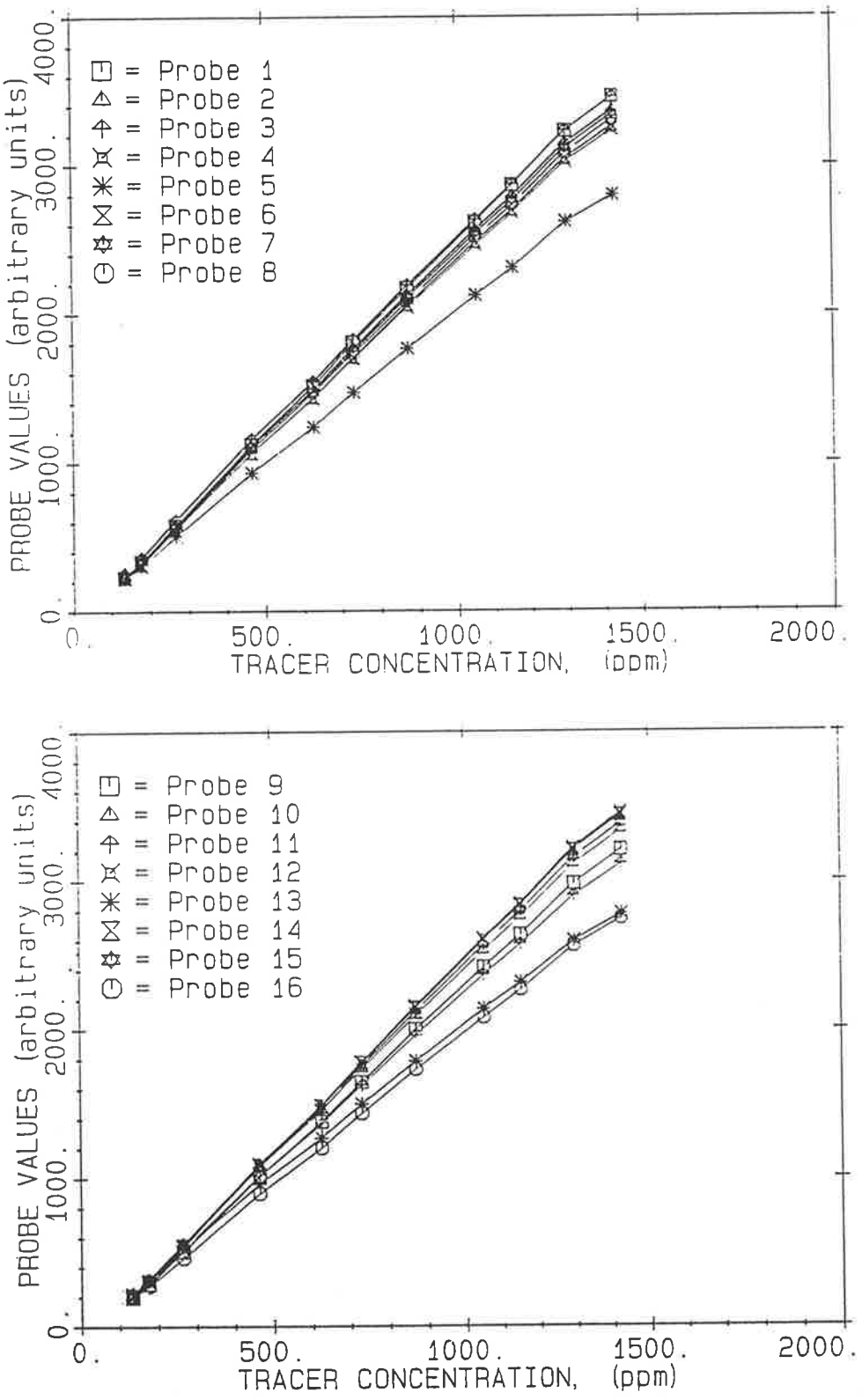


Figure 4.11: Typical calibration curves for conductivity probes

The calibration of the conductivity probes was necessary before each test to develop a relationship between the tracer concentration and the conductivity, i.e., the resultant output voltage for each probe. A computer program (see listing in Appendix B) was developed for the purpose of calibrating all the 16 probes simultaneously before each group of experiments. The probes were immersed separately into a glass beaker of salt solution of known concentration and the computer which was connected to the probes through each individual channel and probe circuit, recorded the voltage information along with the corresponding salt solution concentration. Figure 4.11 shows typical plots of calibration for each probes before a group of experimental runs.

The calibration curves for the various probes were linear within the range of salt solution concentration values considered. These calibration curves were subsequently used to convert the voltage information of various experiments into concentration values for further processing.

A typical run which involved collection of raw data from the conductivity probes synchronously with the high speed photography is outlined here. It should be mentioned here, that data could also be collected without being synchronized with photography when it was not necessary. The outline of the procedure of a run is set out below.

- The tracer solution was prepared and stored in the constant head tracer tank. The tracer injectors were stationed at three different locations as mentioned earlier. It was therefore, just a matter of selecting the desired injector suitable for the run. Injector 1 at the separation point was used, for instance, when the large eddy structure characteristics were of interest.

- The probes were calibrated and placed in the flume at important locations consistent with the objectives of the experimental run. For instance, when the properties of the large coherent eddy structures

in the mixing layer were sought, most of the probes were located in the separated shear layer positioned laterally at different downstream stations.

- The mean flow velocity in the main stream channel was measured and the depth of flow adjusted to the required level.
- The background concentration level of the flume water was recorded by using all the probes for about 10 seconds and were stored in the computer.
- The photo synchronization system was then switched on and the camera was loaded and set at desired speed and aperture.
- The data collection program 'REDAT' was run and the trigger channel switched on. This started monitoring the voltage value in the trigger channel and waited for the pulses from the camera to be superimposed on these values for the data collection to be commenced.
- Tracer was released at this stage from the desired location. The injection velocity was adjusted using the control valve of the flowmeter.
- Finally, the camera was switched on after allowing an initial period of process establishment and the data collection by the conductivity probes commenced from the preselected sixteenth frame of the film. The duration of each experimental run varied from about 20 to 30 seconds. The camera was then stopped and the trigger channel switched to stop position for the data collection to cease. This completed one experimental run.

The data obtained from each experimental run were actually the voltage information from individual probes. A computer program (listing in Appendix B) was written to convert these voltage values to concentration values using the calibration record obtained earlier. The background concentration

of the flume water was also deducted from the actual concentration values. The data files containing the concentration information were then transferred from the PDP 11/34 computer to the main frame VAX/VMS computer for further processing and analysis.

### 4.7.5 Problems and Precautions

The disturbance in the flow field due to the presence of the conductivity probes was an important problem considered in this phase of experiments. Within the separated region the problem was minimal and was of little concern. In the main channel flow particularly in the separated shear layer this problem was of some concern.

However, from visual observations it appeared that the wakes generated behind the probes in the form of small vortices did not affect the large eddy structures significantly. It may be that these small scale vortices were of similar strength to the naturally occurring small vortices contained within the large eddy structures and were far less energetic than the large structures. No particular distortion of the coherence of the large structures could be noticed as they passed through the probes. Although there may have been some effect in mixing within the structures which were unavoidable, they were considered to be of secondary effect.

# Chapter 5

# Presentation and Discussion of Results - Phase I

## 5.1 Introduction

The inherently complex characteristics of unsteady separated flows can not be readily envisaged through conventional measurements. Attempts at resolving the three dimensional, temporally and spatially dependent, unsteady separated flows have therefore resulted in a notable absence of comprehensive investigations (Martin et al, 1973). Standard single point velocity measurement techniques require extensive grid mapping of the entire flow field and prohibit simple parametric studies across independent variables (Adler et al, 1985). The recent interest in 'quasi-steady' or repeatable large scale structures which co-exist with small scale turbulent phenomena has further intensified the complication of the problem. Adler et al (1985) pointed out

that the separation of these unsteady structures in resolving the relative contribution of each can be a very difficult task.

Historically, the flow visualization method has been used to help alleviate many such complex phenomena in fluid flow. As mentioned previously in chapter 2, much useful information was obtained regarding the large scale coherent eddy structures in turbulent shear flows by employing direct flow visualization techniques of one kind or another.

The present investigation has been carried out to study in a more fundamental way the effect of large scale vortices in a separated shear layer on the recirculating flow confined by the separated region. Flow visualization experiments were considered a necessary part of the investigation in order to better appreciate the flow phenomena involved. A simple technique of dye tracing was employed the procedure of which has been described in chapter 4.

The visualization experiments provided a tremendous amount of valuable information regarding the flow field, particularly the interactions between the recirculating eddy and the shear layer vortices. Although the fundamental information is qualitative, this enabled not only a correct network to be set up for further quantitative measurements in the second and the third phases of the experimental programme, but also a better understanding of the physics involved. The results of the visualization experiments are presented and discussed in this chapter.

## 5.2 Flow Visualization Results

The results of the flow visualization experiments, as mentioned in the previous chapter, are recorded on video tape and high speed 16 mm movie films.

The important features of the flow could be best appreciated by directly observing the flow visualization experiments or by viewing the recorded motion pictures. Dimotakis and Brown (1976); and Hussain and Clark (1981) have expressed similar opinions in presenting their flow visualization results. An attempt is made here to present some pictures from the video tapes in the printed form representative of observations of various important aspects of the flow. However, the kinematic details of the flow may not be clearly observed in such a presentation. A second approach is therefore, taken in which pictures from the cine film is presented in a sequential order at very short time interval so that the kinematic behavior of the important flow events can be perceived.

The existence of the large scale coherent eddy structures in the separated shear layer is documented in Figure 5.1. The first two pictures, i.e., (a) and (b) of Figure 5.1 show coherent structures in the separated shear layer in two different flow conditions, (b) being for the faster free stream flow, for the aspect ratio of 2.0. Pictures (c) and (d) of Figure 5.1 show the development of large eddy structures in similar flow conditions for a different geometrical set-up (aspect ratio = 4.8). The dimension of each side of the square divisions shown in the pictures, is 100 mm, and the line marked with numbers increasing at 100 mm is the dividing line between the main channel flow and the separated region. The upper part of each picture shows partial width of the main channel, the flow in the main channel being from left to right. The lower portion is part of the separated region, the point of separation being located at the zero mark. The tracer was released from the point of separation (just within the separated region) throughout the entire depth of flow thus assuming a line source of injection. All four cases of different flow and geometrical conditions, as shown in Figure 5.1, demonstrate that the large scale coherent eddy structures do develop in the separated shear layer as in the cases of other free shear flows and, as will be seen later,

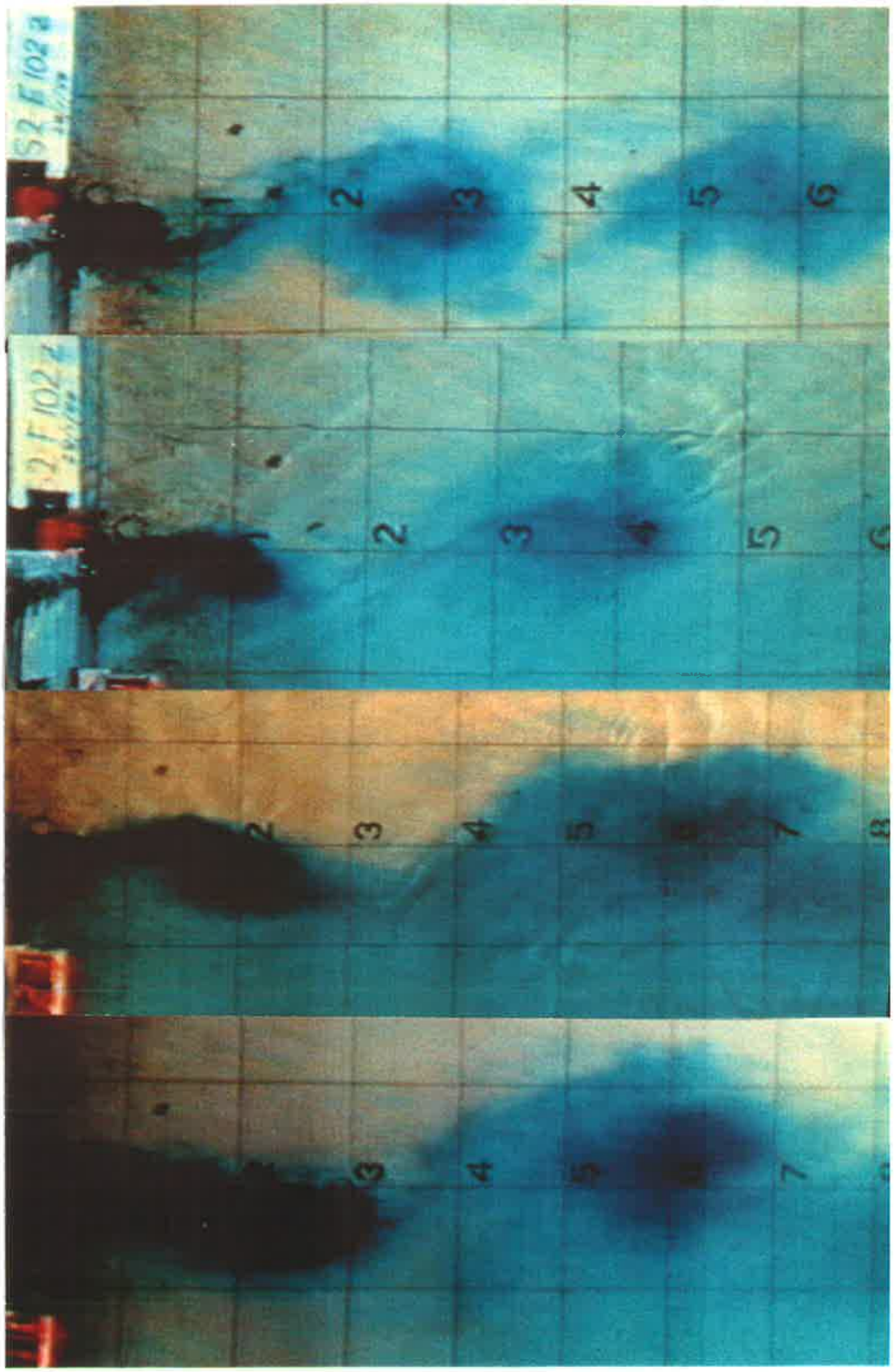


Figure 5.1: Coherent large eddy structures in the separated shear layer;
(a) U = 20 cm/sec, A.R. = 2.0; (b) U = 30 cm/sec, A.R. = 2.0;
(c) U = 20 cm/sec, A.R. = 4.8; (d) U = 30 cm/sec, A.R. = 4.8

persist throughout the entire length of the separated region considered in this study.

Having established the presence of large coherent eddy structures in the separated shear layer, it was then intended to look into the interactions of these large structures and the mechanism of growth of the shear layer. Figure 5.2 shows three independent events where the large eddy structures interact with each other; a condition which is widely known as eddy pairing. As a result of this interaction two or more structures amalgamate together to form a larger structure downstream of the interaction. This process is believed to be the mechanism of growth of free shear flows (Winant and Browand, 1974) along the streamwise direction. The pictures of Figure 5.2 show three different stages of pairing action. They are captured at different instants of time and although they involve different eddies in an experimental run, they serve to explain sequentially the generally observed stages of pairing - their longitudinal position has no significance in these selected pictures.

The first picture (Figure 5.2a) shows the beginning of a pairing event when one large structure falls in the low-speed side of the layer, stagnates for a while and then advects downstream very slowly. A second structure approaches from the high-speed side of the layer and as it rolls over the structure on the low-speed side, it attains a position when the second structure is exactly on top of the first structure which can be referred to as full pairing phase (see Figure 5.2b). It can be noticed in picture (a) that at the beginning phase both the structure retain some form of coherence, while as they rotate and advect downstream they become elongated due to the shearing action across the layer. Figure 5.2c shows the final stage of pairing when the structure in the low-speed side is in much more elongated shape. The structure in the high-speed side then engulfs the low-speed side structure during its rotation across the layer as it advects downstream and thus completes the pairing action. A new larger structure thus develops and advects downstream to

encounter another pairing interaction after travelling a distance of the order of the size of the structure itself. The above processes of pairing interactions are much more clearly explained later in this section through a sequential frame by frame analysis of the high speed cine films.

A different type of pairing action is also observed in this separated shear flow. As a large structure rotates across the layer and advects downstream, it is elongated due to the shearing action of the layer and part of the elongated structure, as was observed occasionally, is torn and swept away into the high-speed side of the layer while the other part of the torn structure is available for pairing by the subsequent structure. This process is termed 'partial' or 'fractional' pairing and is also observed by Hussain and Clark (1981) in their visualization study of axisymmetric jet mixing layer. An important observation of the present case of separated shear flow is that during a pairing event the structure on the low speed side breaks before being paired with a subsequent structure. This was observed during every pairing action at any downstream position, but the upstream events were more prominent.

It was observed that the pairing interaction among structures is not a regular process rather it occurs randomly in time and in space. An oscillatory motion was however noticed in the initial layer of vortices at the separation point which was also found to be irregular. As a result of this irregular oscillatory motion at the separation point, large vortices were ejected into the high-speed side or the low-speed side of the layer in a random manner. It is considered that this random motion at the separation point is the cause of various eddy pairing actions occurring randomly in time and space.

Demonstrating such oscillatory motion by still pictures is a difficult task. However, an attempt is made in Figure 5.3 to show various positions of the initial layer of vortices at the separation point region thus indicating a fluctuating motion in that area.

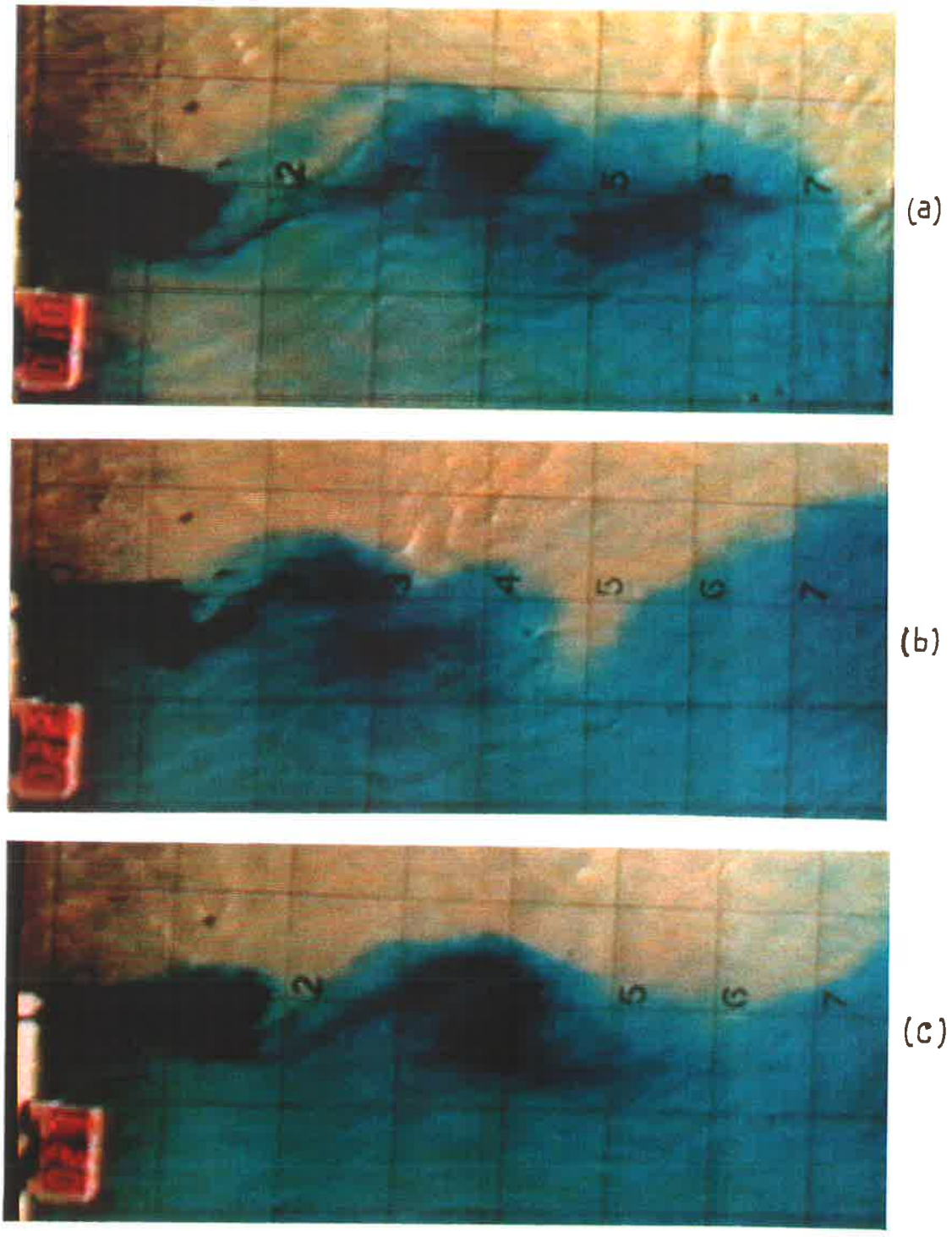


Figure 5.2: Pairing interactions of large structures in the separated shear layer

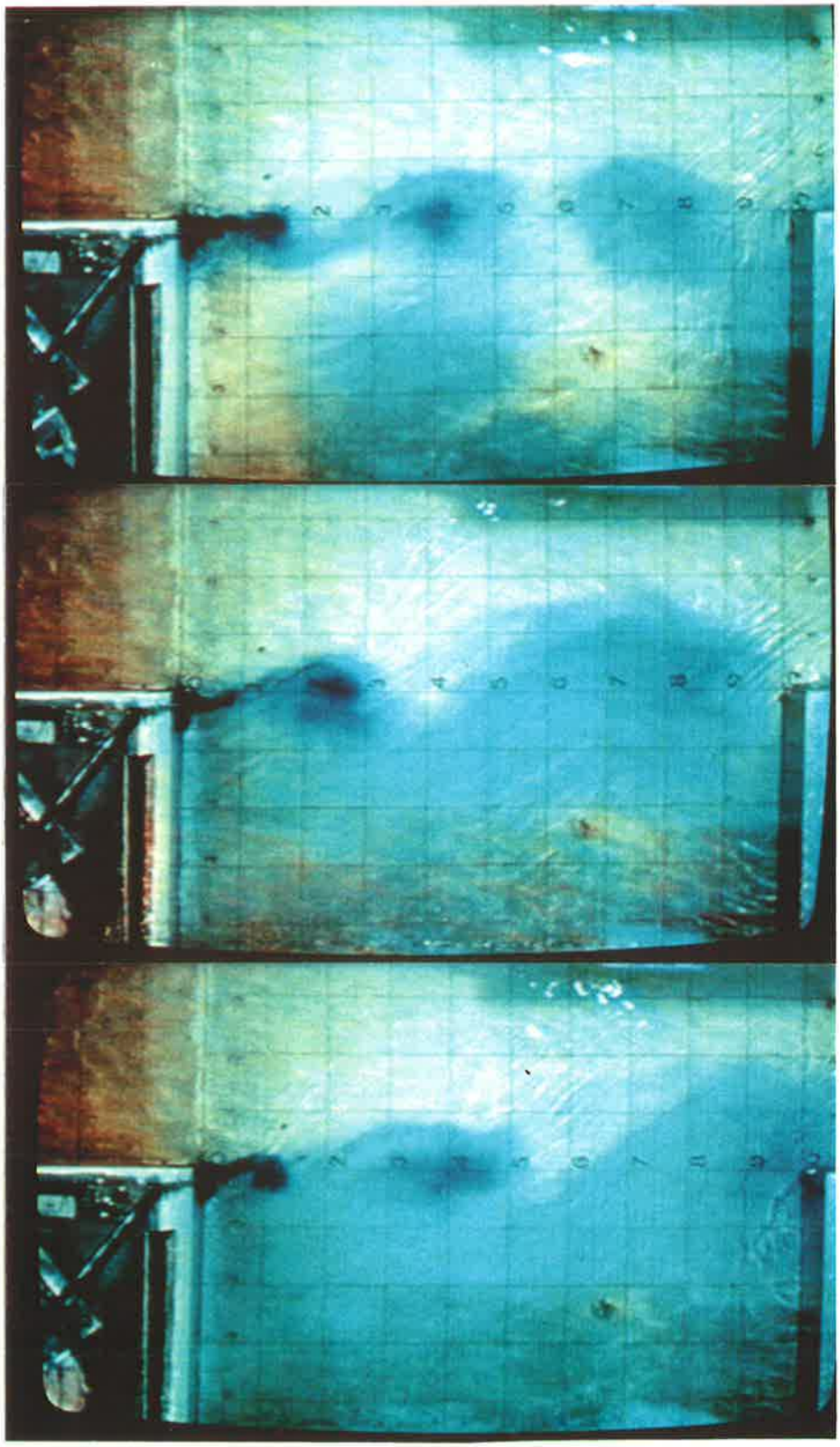


Figure 5.3: Fluctuating initial layer of vortices

Figure 5.3(a) shows a straight array of large structures at the separation point without much oscillation at that instant of time. Pictures (b) and (c) of Figure 5.3 show the downward and upward concave shape of the initial layer of vortices indicating the oscillatory motion. When the motion is downward, i.e., structures are ejected into the low-speed side of separation, immediate pairing was observed by a subsequent structure in the vicinity of about 50 mm from the separation point. Outward ejection of structures into the high-speed side due to outward oscillatory motion was observed to delay such pairing events.

More structures were found to be ejected into the high-speed side than into the low-speed side thus involving more structures in the interaction process such as 'tripling' which occurs when a third structure immediately behind the two interacting structures gets involved in the amalgamation process.

Figures 5.4 and 5.5 show the transport of tracer within the separated recirculating region for two different geometrical conditions. Tracer was released in these cases from the lower end of the separated region along its entire length. Pictures (a) and (b) of Figure 5.4 are taken from the faster main channel flow (U = 30 cm/sec) and those of (c) and (d) from slower flow (U = 20 cm/sec) of the same aspect ratio, A.R. = 2.0. Pictures of Figure 5.5 represent the similar flow conditions for the other geometrical configuration (A.R. = 4.8) of the separated flow model.

Several important features of the separated recirculating flow can be noticed. The recirculating eddy fronts, their interactions with the shear layer eddy structures and the process of entrainment of ambient fluid by the shear layer structures are the most important observations. Referring back to Figure 5.3a, a primary eddy in the separated region is clearly visible with a relatively stronger eddy front approaching towards the shear layer at about 200 to 400 mm position. Similar eddy fronts were found to be present in all cases shown

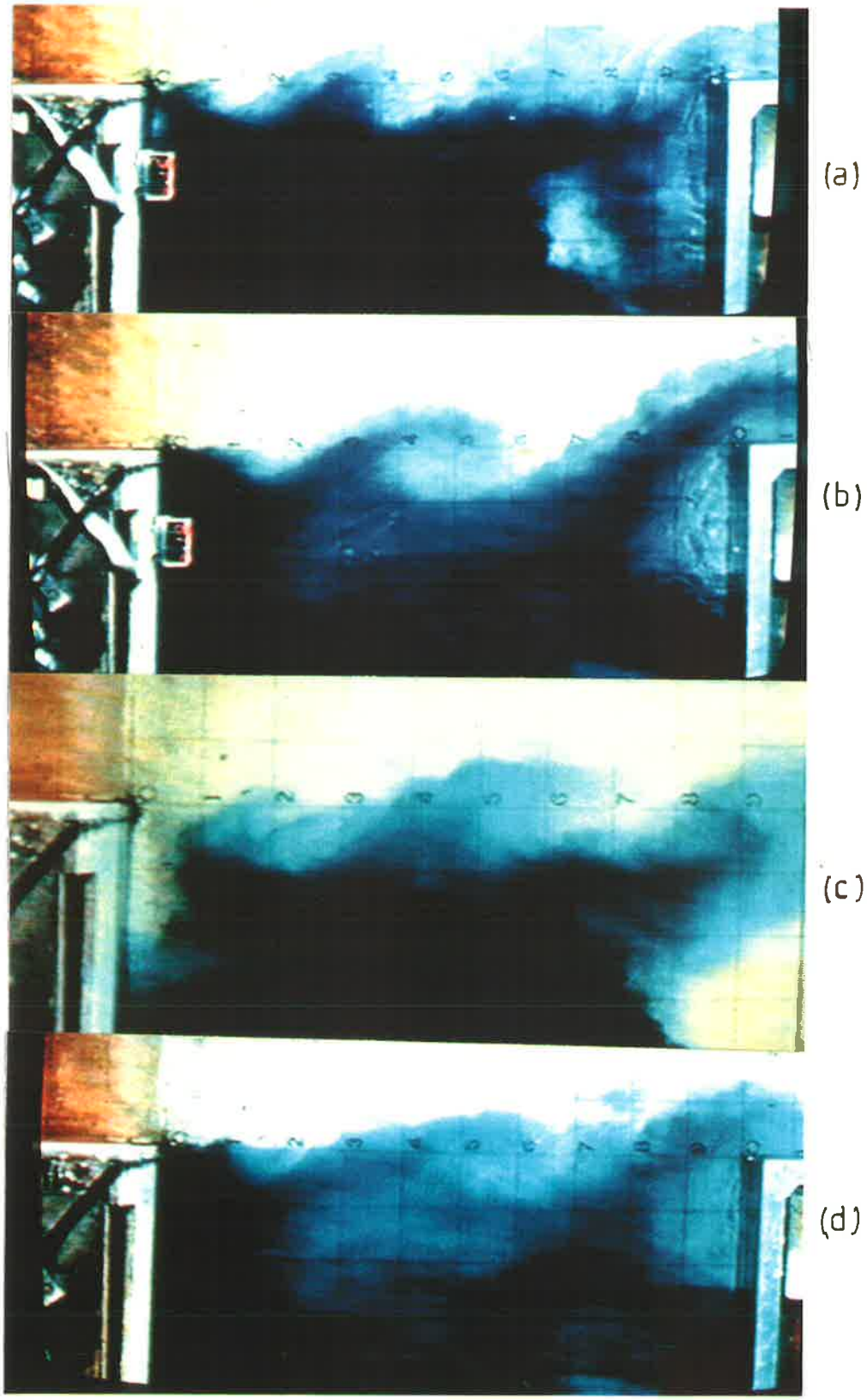


Figure 5.4: Important features of the separated flow region; A.R. = 2.0; (a) and (b) U = 30 cm/sec; (c) and (d) U = 20.0 cm/sec

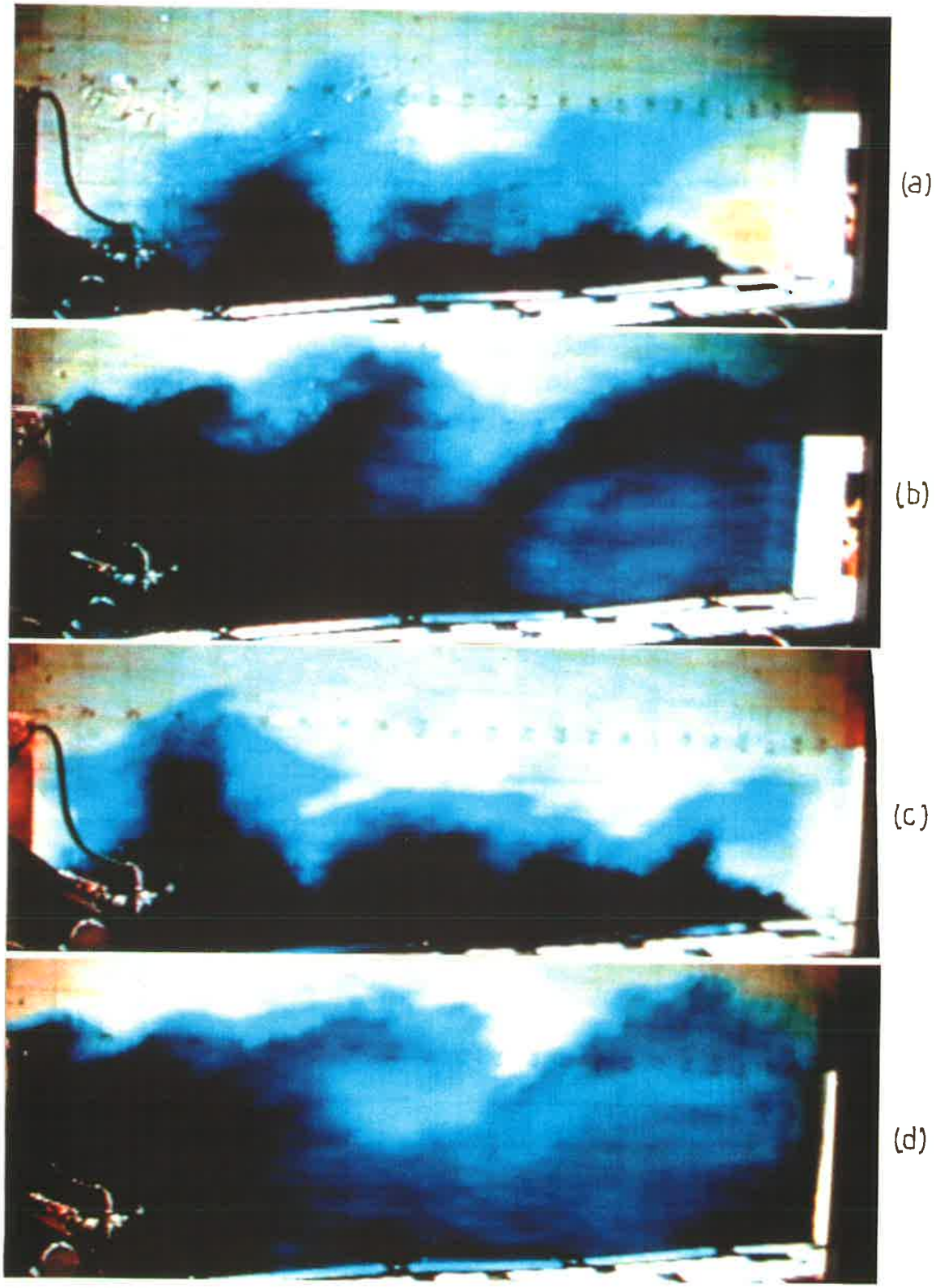


Figure 5.5: Important features of the separated flow region; A.R. = 4.8;
(a) and (b) U = 30 cm/sec; (c) and (d) U = 20.0 cm/sec

in Figures 5.4 and 5.5, varying in position depending on flow and geometrical conditions. The pictures (a) and (c) of Figure 5.4 were taken at some later stage when the recirculating eddy front has just begun its interaction with the shear layer structures. As the interaction begins, the recirculating eddy front is observed to be divided into two, each divided front going in opposite directions induced by the rotating, as well as the advecting, motions of the large structures in the separated shear layer. The position of such interaction was also found to vary with the orientation of the structures and their pairing actions.

Other recirculating fronts were also observed at the downstream end of the separated region in a much weaker form and were easily engulfed by the shear layer structures without much interaction. One such front can be seen in Figure 5.4a which is deflected back in the recirculating region by the large structure in the shear layer as it was not in the correct mode of entrainment.

Pictures (b) and (d) of Figure 5.4 were taken at a much later stage when the entire separated region was filled up by the tracer cloud. These pictures clearly show the process of entrainment by the large eddy structures in the separated shear layer from both side of the layer and indicate the transfer of tracer mass from the separated region into the main stream flow.

Figures 5.5(a) and 5.5(c) show the recirculating eddy fronts for the faster and the slower flows respectively, approaching towards the shear layer at about 300 to 600 mm positions of the downstream distance. It can also be noticed from these pictures that the recirculating eddy front is relatively stronger and closer to the separation point for the faster flow than for the slower flow. Pictures (b) and (d) of Figure 5.5 were again taken at some later stage when the tracer cloud was approximately uniformly spread over the entire separated flow region showing entrainment and transport of tracer material from the separated region into the main stream flow. These pictures

also provide evidence for the persistence of large coherent eddy structures throughout the entire length of the separated region, which was a maximum of 2.4 metres in the present study, for both the faster and the slower flows considered.

Another important observation of the present visualization study is the location of a 'rapid mixing region', where the tracer concentration changed abruptly and approached uniformity over the entire structure dimension. Referring back to Figure 5.1, such abrupt change in concentration can be noticed in all four cases. The region where this change in concentration takes place varies from about 200 mm to 800 mm, depending on the flow and the geometrical conditions. Rapid mixing was delayed when the flow in the main stream channel was slower and also when the aspect ratio of the separated region was higher. This variation of the point at which uniformity of concentration occurs within the structure dimension can also be seen in the four different pictures of Figure 5.1 representing four different flow and geometrical conditions. Based on the visual observations, approximate locations where rapid mixing takes place for various flow and geometrical cases are shown in Table 5.1.

Table 5.1: Regions of rapid mixing

| Main channel flow velocity | Region of rapid mixing | |
|---|---|---|
| | A.R. = 2.0 | A.R. = 4.8 |
| 30.0 cm/sec | 100 to 500 mm; 200 to 400 mm being the frequent spot. | 300 to 700 mm; 400 to 600 mm being the frequent spot. |
| 20.0 cm/sec | 200 to 600 mm; 300 to 500 mm being the frequent spot. | between 400 to 800 mm; 500 to 700 mm being the frequent spot. |

It can be noticed from the table that even for a single flow and geometric condition the rapid mixing region changes considerably. This was observed to be associated with the position of the structures and their pairing interactions within the respective ranges. The reason for rapid mixing at these particular regions is considered to be due to the interaction between the shear layer structures and the relatively stronger recirculating eddy front. As shown earlier, this eddy front approaches the shear layer at about the same regions as indicated for the rapid mixing (see Figures 5.4a, 5.4c, 5.5a and 5.5c). However, this result could be better appreciated by directly measuring the concentration of the tracer mass at places of interest which has been done in the third phase of the experimental program and will be presented in Chapter 7.

Among other important results, it was observed that most of the entrainment by the shear layer occurs upstream of the rapid mixing region which is made available by the relatively weaker (almost stagnant) secondary recirculating eddy at the upstream corner of the separated region. Figures 5.4b and 5.5b show that region containing highly concentrated tracer cloud relative to the other parts of the separated region.

Transfer of tracer material from the main stream flow into the separated region was found to be mainly due to the deflection of the shear layer at the reattachment region, as is evident in Figure 5.3a. A small amount of tracer mass was also observed to be diffused from the structures as they advected downstream. Transfer of tracer through the braid region could not be clearly observed.

Transfer from the separated region into the main stream flow is clearly observed as shown in Figures 5.4 and 5.5, major transfer being occurred at the reattachment region through entrainment by the large structure (see pictures (b) and (d) of Figures 5.4 and 5.5). The quantity of transfer varies depend-

ing upon the orientation of the large structure at reattachment. As shown in Figure 5.4a, the recirculating eddy front is deflected back into the separated region as the large structure was not in a right phase to entrain that front.

Another important phenomenon was observed to be associated with the variation of the transfer of the tracer material from the separated region into the main stream flow and vice versa. A lateral movement of the entire shear layer was observed and it appeared to be a quasi steady oscillation occurring with an approximately constant frequency. The initiation of such movement of the shear layer was noticed at the rapid mixing region when a large structure was pushed into the main stream flow after every few structures passed that region. This indicates that the recirculating eddy front intermittently becomes stronger and pushes the shear layer into the main stream flow. As a result, the major part of the shear layer was found to be deflected into the main channel at reattachment and deflecting only a small part into the recirculating region.

Figure 5.6 shows the sequences of picture frames taken from the high speed cine film captured during one of the experimental runs. As mentioned before, in most cases, cine photography was performed at the rate of 32 frames per second. However, after a careful examination of the individual frames, pictures are taken for presentation at every 10 frames interval, as it was found that pictures closer than this do not show significant differences. The pictures in this figure are shown for the smaller geometrical set up (aspect ratio = 2.0) so that the entire separated flow length can be indicated in the pictures. The flow was the faster one (U = 30 cm/sec) and the direction of the flow in the pictures is from left to right. The time increases with increasing frame number as marked on the figure and the increment between successive frames is 0.3125 second. The tracer was released, in this case, from the separation point region which can be seen in the pictures (dark black corner region on the left). The upper part of each picture shows partial width of the

main stream channel and the lower part shows partial width of the separated region.

Several frequently occurring features of the separated shear layer flow can be observed in the picture sequences of Figure 5.6. The evolution of large structures at the separation point region; their pairing interactions and growth; and tearing at the reattachment region are the important events. Beginning with frame 1, three separate large structures can be seen in three different downstream positions, the third structure still being in its final stage of evolution. By frame 3, this evolutionary stage is complete and it turns into a larger coherent form when the second structure becomes elongated due to local shearing action. In frame 4, the third structure appears to be pushed slightly into the high speed side of the layer while it advects downstream and the second structure becomes more elongated with a narrow front being available for interaction. As the third structure advects downstream and rotates across the shear layer it captures the low speed side elongated structure and the growth of a larger coherent eddy structure due to this interaction is complete by frame 7. Afterwards this large structure becomes slightly elongated (frames 8 to 10) but does not lose its coherence very much and advects downstream when it reaches the reattachment region (frame 18) without any further interaction with other structures. In frame 20, it can be noticed that the structure is torn into two with the major part being deflected back into the separated region and only a smaller part swept away into the main stream channel.

Looking back at frame 12, it can be seen that the formation of another two structures are complete by this period. The larger one breaks on the low speed side (frame 13) between 200 and 300 mm downstream which can be seen elongated by frame 16. The next structure at about 200 mm downstream position also becomes slightly elongated and partly broken in the low speed side. This structure is again followed by another newly formed structure. By

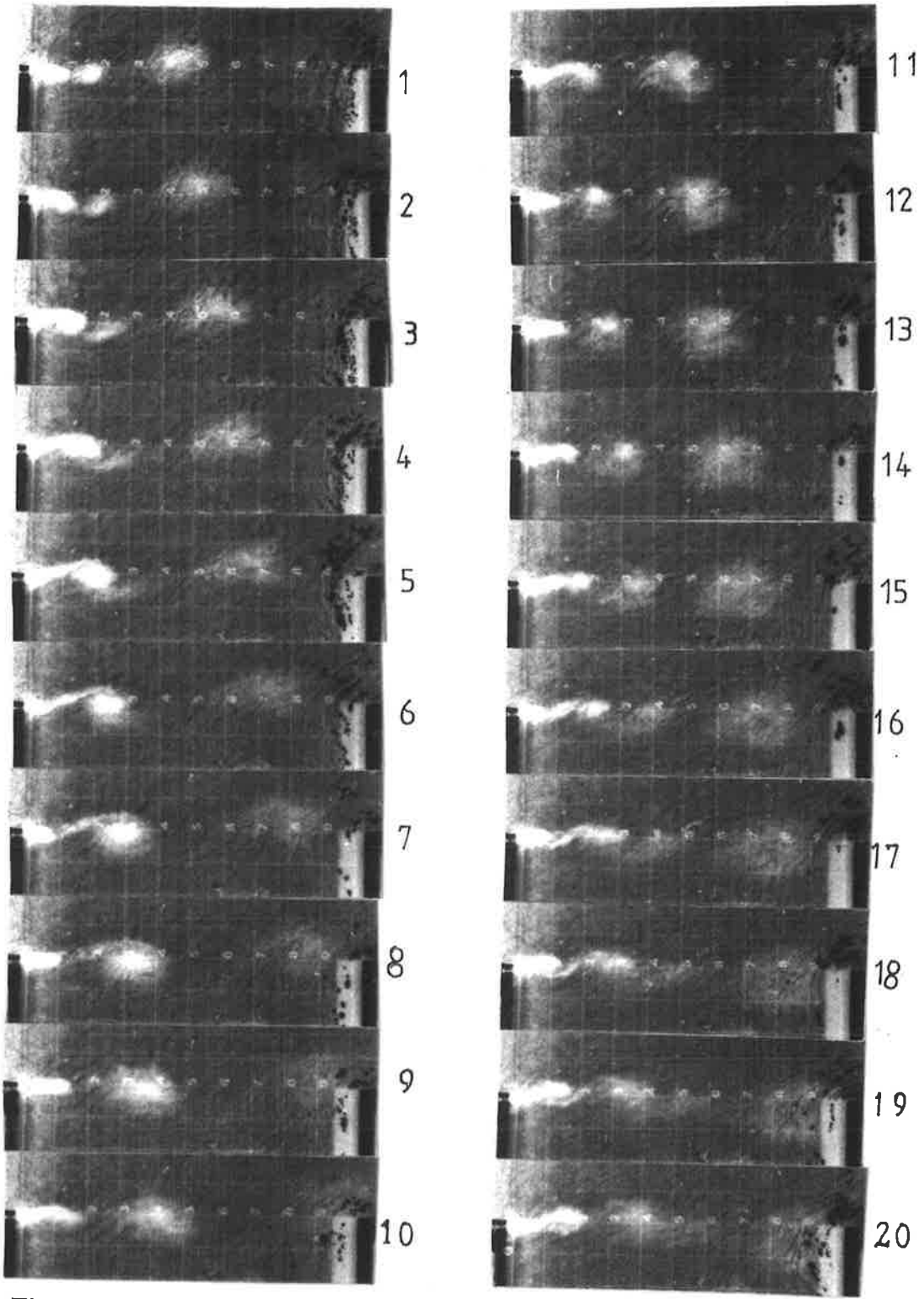


Figure 5.6: Successive picture frames taken from high speed cine film (A.R. = 2.0; U = 30.0 cm/sec)

frame 18, these three structures are in a mode of pairing with each other and by frame 20, interactions among these structures are almost complete and grow into a larger 'cats-eye' shaped structure as can be seen at about 400 mm position.

Figure 5.7 contains an ensemble of picture frames which are the continuation of the frames in the previous figure and are taken from the same experimental run at 10 frame intervals. Two interesting but less frequently occurring features are explained in this figure. Firstly, starting with frame 1, two large structures can be noticed at about 250 and 500 mm downstream from the separation point. It is interesting to note that both the structures are mainly in the high speed side of the layer and advect downstream one after another until they reach the reattachment region by frame 7. There was no interaction between these two structures during the period of their travel because the downstream structure could not attain a position of correct pairing mode. By about frame 11 both the structures are torn at reattachment, the major part being swept away into the main stream channel.

The second feature can be observed from these pictures starting with frame 5. Two large structures are being paired at about 200 mm downstream of separation and by frame 7 become a larger rounded structure. This large structure is then elongated by the action of local shear (see frames 8 to 11) and in frame 11 the elongated structure appears to be torn apart. During this period (frames 7 to 11) new structures evolving from the separation region travel in an almost straight array of vortices behind the elongated structure. Thus there was no interaction until in frame 12 when the initial array of vortices is slightly deflected upward to get into a pairing mode. By frame 14 a clear pairing interaction can be seen and in the next frame interaction with the torn structure can be noticed. The interaction is complete by frame 19. This is not a very regularly occurring feature in the shear layer, even less frequent in the slower flow, and during this event the shear layer becomes

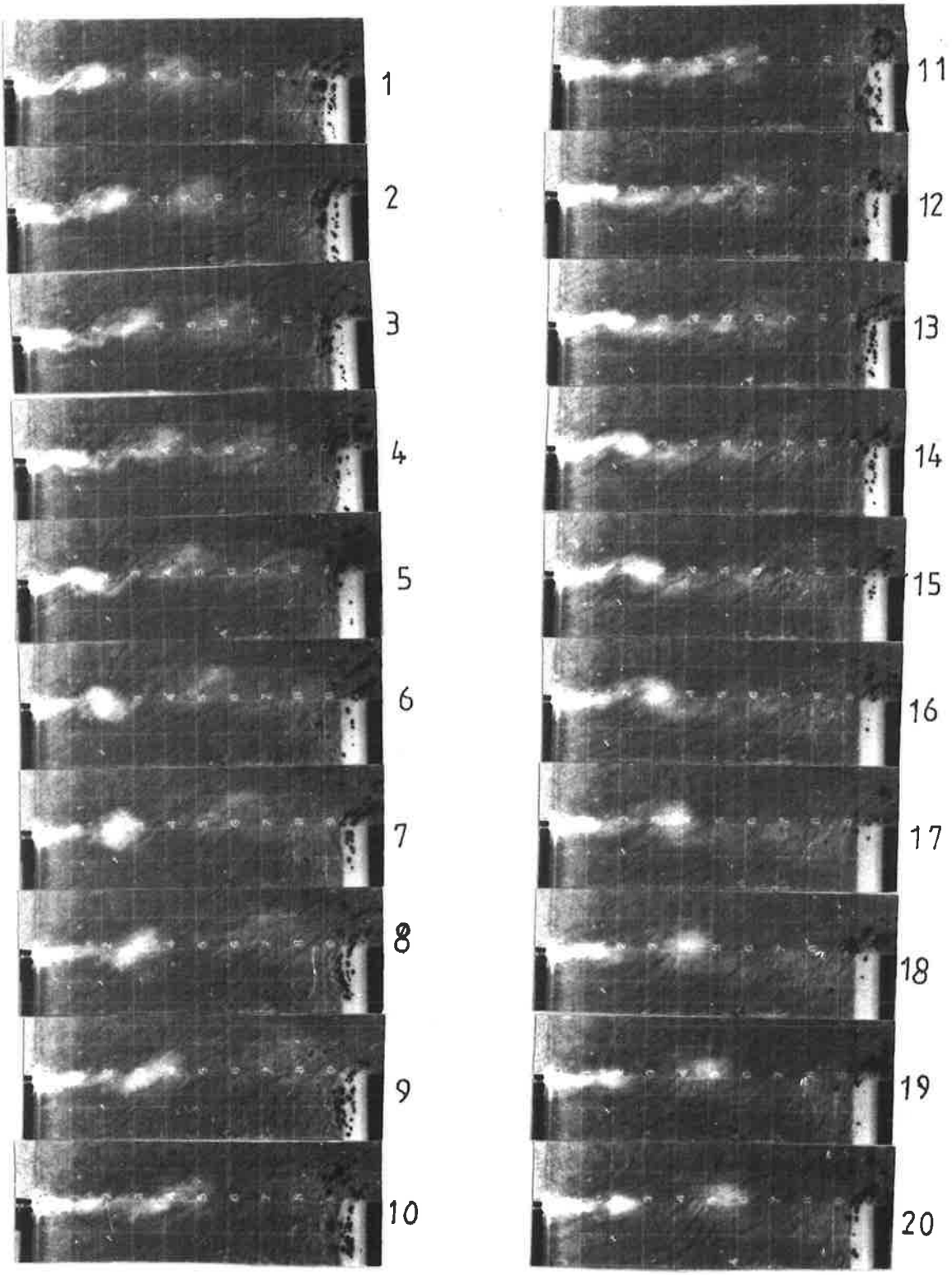


Figure 5.7: Successive picture frames continued from the previous figure

thinner and remains in a disorganized form for some time as can be seen in the pictures.

In Figure 5.8 an attempt is made to demonstrate the low frequency fluctuation (lower than the large structure passage frequency) of the separated shear layer, although it is difficult to demonstrate such slow movement (lateral) even with sequences of picture frames. These pictures are taken from a different experimental run again at 10 frame intervals thus making the time increment between the successive frames to be 0.3125 second.

Starting with frame 2, it can be seen that the initial layer is slightly deflected into the high speed side relative to the other structure in the front (at about 200 mm from the separation). By frame 5, pairing between the two structures is clearly visible and is almost complete by frame 7 the location being at about 300 mm downstream of separation. During this interaction both the structures are deflected further into the high speed side (further than is needed for an interaction to begin). This deflection is most probably due to a thrust by the recirculating eddy front available at about the same location as discussed previously. As a result of this deflection the large structure (paired at about 300 mm in frame 7) is seen to be mostly in the high speed side of the layer. It should be noted here that the normal position of the shear layer would be inclined into the separated region because of its asymmetry, i.e., major part of the layer would be below the dividing line shown in the pictures. It can be noticed that the structure at about 400 mm position in frame 11 stays in the high speed side throughout (frames 11 to 20) and is swept away mostly into the main stream after frame 20.

For comparison one can see the preceding structure (between 400 and 500 mm in frame 1) stays mostly in the low speed side throughout the entire length of travel until it reaches the reattachment region by frame 14 when the major part of it is deflected back into the separated region. Whilst having

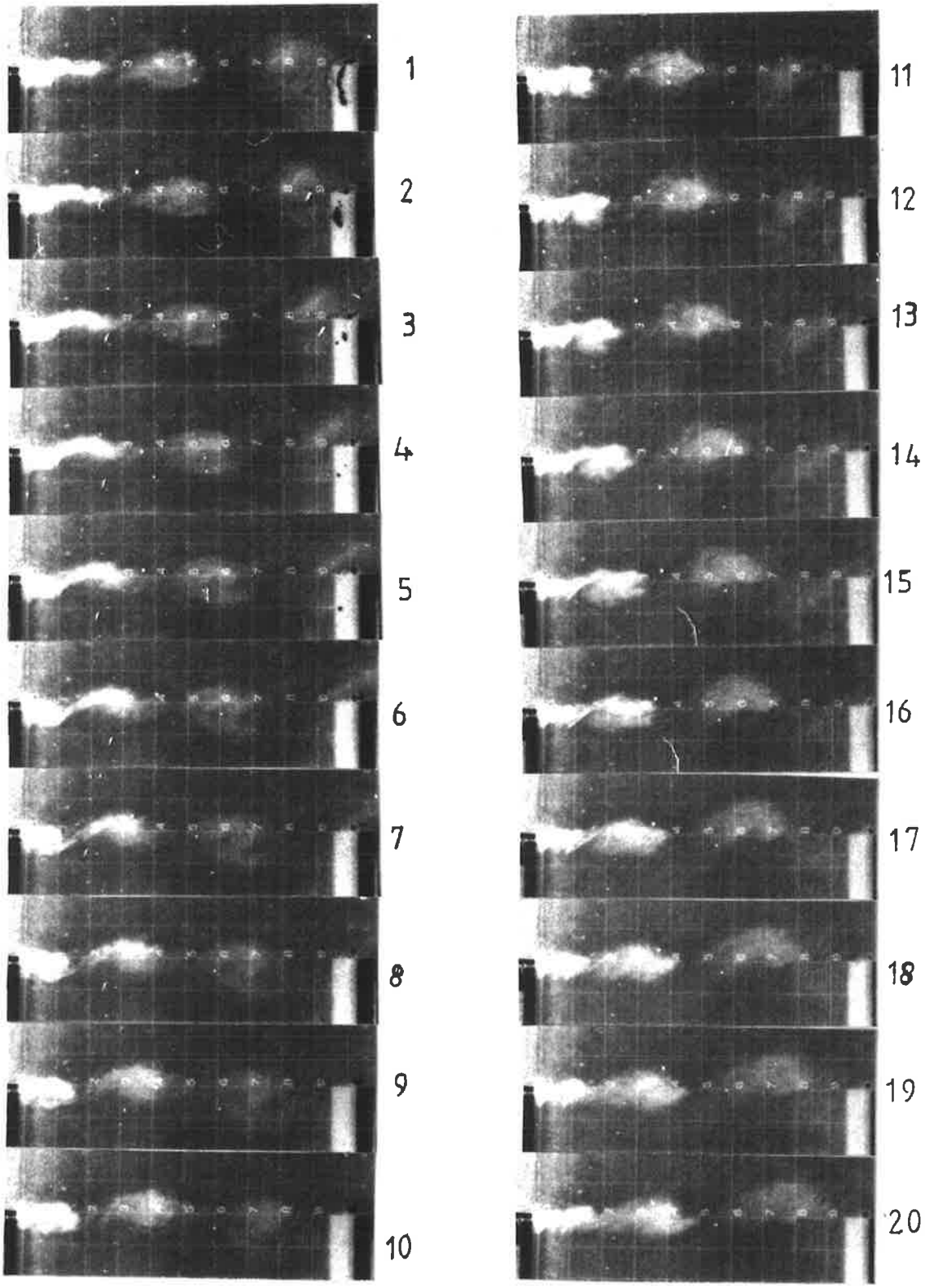


Figure 5.8: Picture frames from cine film demonstrating lateral movement (A.R. = 2.0; U = 20 cm/sec)

a closer look at the phenomenon through viewing of the video tape, it was observed that such deflection of the shear layer was a quasi-steady oscillatory process. At a particular location downstream of the interacting region, it was observed that on the average, every fourth structure was deflected into the main stream flow. The apparent reason of this lateral movement of the separated shear layer will be further discussed in the following section.

## 5.3 Discussion of Visual Observations

The flow visualization pictures presented in the previous section provide some interesting details of the separated flow problem. The various flow events in individual single shot pictures and the sequences of picture frames from high speed cine film confirm that, as in plane and axisymmetric jet mixing layers, large scale coherent eddy structures develop in the separated shear layer which is confined by a rectangular separated region. There are however, similarities but also significant differences in the details of these flow structures observed in the present study. These will be discussed in the following subsections concerning the development of a separated and reattaching shear layer; localized rapid mixing in the shear layer; and the transfer of tracer mass to and from the separated region.

### 5.3.1 Shear Layer Development

It was indicated in Chapter 2 (pp. 30-31), that the development of shear layers downstream of the separation point is initially dominated by a linear instability mechanism. Although this initial instability region could not be clearly seen, the roll-up of an initially unstable vorticity layer into larger two-dimensional vortexlike structures, was clearly observed in the close proximity

of the separation point region. For the faster flow case this roll-up was observed as close as $0 \leq x/W \leq 0.1$ whereas for the slower flow this was shifted to $0 \leq x/W \leq 0.2$. No significant variation of the initial roll-up process could be observed with geometry changes of the separated flow model, indicating independence of the size of the separated region.

Beyond the initial roll-up phase, the development of the shear layer is dominated by the large vortexlike eddy structures and their interactions. It was also indicated previously, that an appropriately phased subharmonic is essential in a shear layer for pairing interactions to occur and the location of such interaction depends on the growth of such a subharmonic. Ho and Huang (1982) suggest that the interaction occurs at a downstream station where the subharmonic reaches a maximum. Kelly (1967) demonstrated that the growth of a subharmonic reaches a maximum when the frequency is twice that of the fundamental. Controversy, however, still remains about the source of such subharmonic perturbation.

In the present study the separated shear layer impinges on the downstream boundary of the separated region and it appears reasonable to assume a feedback mechanism from the impingement surface as the source of subharmonic perturbation propagating upstream through the pressure field. Ho and Nosseir (1979) considered such a feedback mechanism as the source of perturbation responsible for the so called 'collective interaction' among the large structures in the shear layer of an impinging jet flow. However, the present flow visualization study leads to an understanding that the induced upstream motion produced by a downstream large (already paired) structure, as it advects downstream and rotates across the layer, provides the necessary subharmonic perturbation. Such an induced field can be noticed (although direct observation gives much clear perception) in Figures 5.4(a) and 5.4(c). This observation is consistent with the speculation by Laufer (1980) and Hussain (1983).

The oscillatory motion observed in the initial part of the shear layer close to the separation point as explained in the pictures of Figure 5.3 is most probably the effect of such induced motion. This oscillation in the initial layer is observed to be associated with the so called collective interactions (interactions involving several structures) and the random nature of such interactions. However, the feedback effect of impingement can not be totally ignored which may have some indirect influence on the shear layer development. It is most likely that this impingement effect prohibits the subharmonic to be in the correct phase thus prohibiting any interactions in the downstream part of the layer near reattachment region.

The interaction mechanism in the separated shear layer appears to be different from what is widely known as eddy pairing between two large coherent structures in case of other free shear layer flows. The scenario of events which take place during an interaction in the separated shear layer are as follows. The large eddy structure after the initial roll-up, collapses on the low speed side of the layer after travelling a distance of the order of its size and stagnates for a while. It is then elongated due to shearing action, when a following structure (or structures) captures the collapsed elongated structure as it passes over, in a fashion similar to the engulfing action of large structures during rotation across the layer (see for example picture frames 1 to 7 of Figure 5.6).

As a result of this interaction the structure grows and regains its coherence when it breaks again on the low speed side of the layer and is available for another similar interaction downstream. This process continues and appears to constitute the growth mechanism for the shear layer associated with the present problem of separated flow. The process involved in such interaction is thus not the pairing of two coherent structures as is established to be the mechanism of shear layer growth, but rather the process is entrainment (through engulfing action) by the large structures which leads to the growth

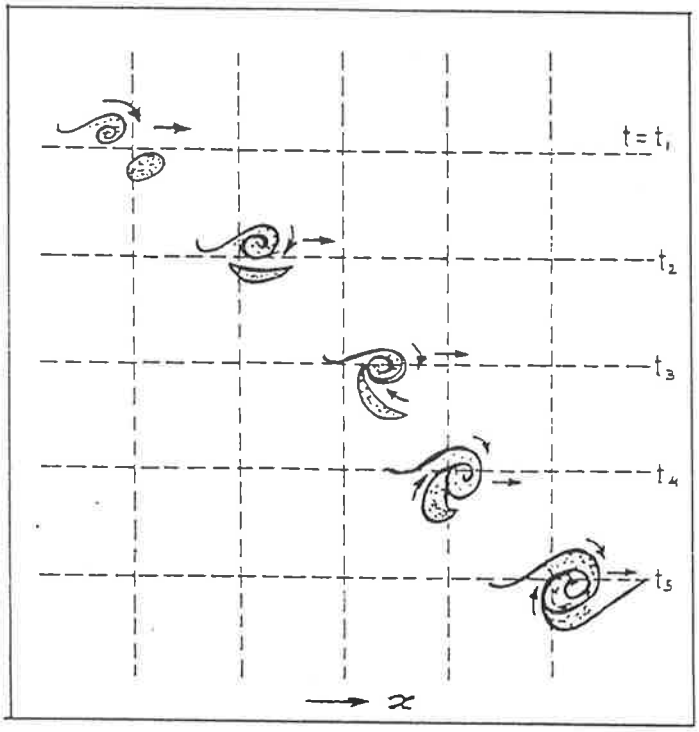


Figure 5.9: Schematic of large structures interaction in the separated shear layer

of the layer with streamwise distance. In fact the complete pairing of two coherent structures was not observed during the present visualization study. The following schematic diagram of Figure 5.9 explains more clearly the process of interaction between structures in the separated shear layer.

In most cases there were three or more structures involved in an interaction process which is related to the oscillatory motion observed in the initial vorticity layer at separation. When the intial layer was deflected into the high speed side, several structures were observed to be ejected into the high speed side in quick succession more than when the layer was deflected into the low speed side. Thus more structures were available on the high speed side during an interaction, with a collapsed elongated structure on the low

speed side. In some cases the collapsed elongated structure was found to be torn apart probably due to high shearing action and swept away into the high speed side while the other part was involved in the interaction, a process which is referred to as 'partial pairing'. Hussain and Clark (1981) also noticed such a partial pairing interaction in their axisymmetric mixing layer visualization study. However, this was an infrequently occurring event and is explained in Figure 5.7.

The reason for the collapse of structures on the low speed side is not clearly perceived. It is however, conjectured that the process is typical of this separated flow and is associated with the interaction of a small scale vorticity layer in the recirculating eddy with the streamwise vorticity of the shear layer.

### 5.3.2 Localized Rapid Mixing

It is now well established that alongside the large scale primary eddy structures which are responsible for the growth and development (through the redistribution of Reynolds stresses by eddy interactions) of the free shear layer, there exist small scale streamwise counter-rotating vortex structures which are responsible for internal mixing. The experimental evidence obtained by Konrad (1976) in gas mixing layers, Breidenthal (1978) in experiments in water and subsequent studies by Bernal et al (1981), Jimenez et al (1979) and Bernal and Roshko (1986) confirm the existence of such secondary streamwise structures superimposed on the spanwise pattern of primary structures. What is not quite clearly understood as yet, is the origin of these structures and the location of the so-called 'mixing transition' where rapid mixing takes place with the development of these small scale three dimensional motion.

A secondary internal instability within the primary structure, in preference

to the spanwise instability, is however, believed to be the origin of such secondary motion (Roshko, 1981). Various criteria have also been introduced to characterize the location of small-scale mixing transition. Bradshaw (1966) for instance, selected the location where the peak Reynolds stress reaches a maximum. In chemically reacting flows, Konrad (1976) and Breidenthal (1981) considered the streamwise station where the 'mixedness' sharply increases. This mixedness is a measure of the amount of product formed in a shear layer initially carrying two distinct chemicals.

The context of the present study however, is slightly different from that which has been discussed above. The present visualization study reveals that the interaction between the recirculating eddy front and the shear layer structures also cause rapid mixing in regions shown in Table 5.1. This interaction became obvious when it was noticed that the 'rapid mixing region' shifted upstream with the shift of the recirculating eddy front when the geometry of the separated region was reduced from A.R. = 4.8 to A.R. = 2.0. Since the evolution of large structures and their subsequent interactions were independent of the aspect ratio, shifting of the rapid mixing region with the change of aspect ratio indicates such interaction between the shear layer structures and the recirculating eddy front. However, mixing due to this interaction is perhaps in addition to the mixing due to the interaction between the streamwise small structures and the spanwise large structures within the shear layer.

The question now arises as to how this interaction between the shear layer structures and the recirculating eddy front occurs and causes rapid mixing. It is speculated that secondary Taylor-Goertler type vorticity layers develop along the recirculating eddy due to the curvature of the flow lines and the effects of centrifugal forces as was also observed by Zhak et al (1981). As the recirculating eddy front approaches the shear layer near the rapid mixing region, it is divided into two parts which go in opposite directions. One part moves upstream and forms a much weaker (almost stagnant) secondary

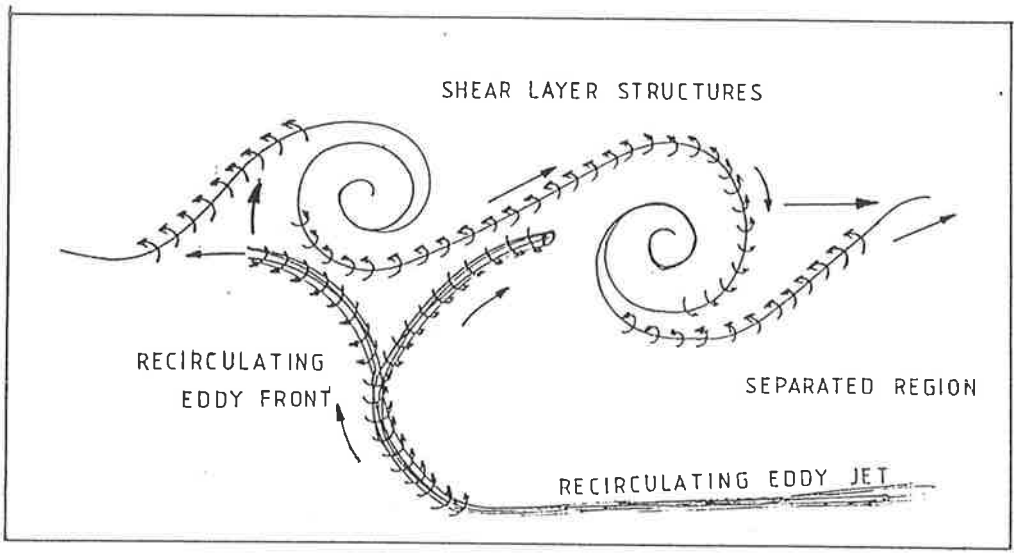


Figure 5.10: Mechanism of interaction between the shear layer and the recirculating eddy.

recirculating region. The other part moves downstream to complete the primary recirculating eddy. Now when this division takes place the secondary Taylor-Goertler type vorticity layer (which is extended throughout the depth) along the recirculating eddy front interacts with the secondary streamwise vorticity layer in the braid region between two large coherent eddy structures (also superimposed on the edges of these large structures) and triggers a vigorous mixing in that region. The schematic diagram of Figure 5.10 is an attempt to explain the process of interaction more clearly.

This however, implies that the small-scale streamwise vortex structures are already developed prior to the interaction at the rapid mixing region peculiar to the present separated flow case. That means the internal mixing within

the spanwise structure due to the development of the streamwise structures begins much earlier than the occurrence of rapid mixing. In fact the visual observation of the present study suggests that the development of the secondary streamwise vorticity begins with the initial roll-up into large structures. Thus in the absence of a recirculating eddy front, i.e., in case of a plane mixing layer, mixing begins with the development of streamwise vorticity and continues through the stretching of this vorticity layer in the braid region by the co-rotating large structures and interacting with them (large structures) as their size increases with downstream distance until mixing reaches uniformity after several interaction events. This is compatible with what has been proposed by Hussain (1984) regarding mixing in coherent structures. The theoretical analysis of Lin and Corcos (1983) also suggests that the mixing transition is related to the dynamics of the three dimensional structures in the braid region.

It, therefore, appears that the mixing transition in the case of a plane mixing layer is a gradual process compared to the vigorous mixing observed in the present case due to the interaction of the shear layer structures with the recirculating eddy front. The variation of the rapid mixing region along the streamwise distance even in a single flow and geometrical condition, as indicated in Table 5.1, is due to the movement of the recirculating eddy front associated with uneven entrainment of fluid in the separated region which will be discussed in the next subsection.

### 5.3.3 Mass Transfer in Separated Flow

It is clearly observed from Figures 5.3, 5.4 and 5.5 that the transfer of tracer mass to and from the separated flow region is mainly controlled by the large coherent eddy structures in the separated shear layer. The transfer is mostly through the deflection of large structures at the reattachment region as can

be seen in those figures. This is coupled with another interesting phenomenon of shear layer movement in the lateral direction which occurs because of the interaction between the shear layer structures and the pulsating recirculating eddy motion.

This lateral movement of the separated shear layer, as mentioned in Chapter 2, has been reported previously by some authors. The reason for such movement however, was not very clear. Eaton and Johnston (1982) observed low frequency motions (lower than large eddy passing frequency) in the reattaching shear layer. The instantaneous imbalance between the shear layer entrainment from the recirculating region and the reinjection of fluid near reattachment was indicated to be the probable cause of such long time scale motions. Rockwell and Naudascher (1979) and Knisely and Rockwell (1980) suggested that the oscillation of the shear layer was caused due to the feedback of disturbances from the impingement point to the separation point.

The present visual observations however, suggests a different explanation for the lateral movement of the shear layer. As the large eddy structures in the shear layer impinge on the reattaching surface, part of the structures are deflected back into the separated region giving rise to a quasi-periodic pulsatile motion in the recirculating eddy. This pulsatile recirculating eddy motion coupled with the uneven entrainment process, as described below, produces the lateral movement of the shear layer.

Normally, the shear layer would be deflected into the separated region due to its asymmetric nature. More fluid, therefore, is entrained into the separated region during this time which must be accommodated for in the region and then re-entrained in the upstream shear layer. The recirculating jet which is now stronger and at the same time pulsatile, interacts with the shear layer near the rapid mixing region and pushes the shear layer outward into the main stream flow. Consequently, near the reattachment region the major

part of the shear layer structure is deflected into the main stream and only a small part of the structure fluid is transferred back into the separated region. The fluid available for entrainment by the shear layer is now less than before and the recirculating eddy becomes relatively slower. The shear layer is then deflected back into the separated region without being pushed by the recirculating eddy front. The process appears to be a continuous pulsating one and it takes some time for the recirculating eddy jet to gather momentum to be able to push the shear layer again. That is why the deflection of large structures into the main stream flow near the rapid mixing region was observed to occur, on the average, after every three structures in case of the faster free stream flow. For the case of the slower flow, the lateral movement of the shear layer was also observed to be slower.

A small amount of diffusive transfer by the large structures was also noticed which can be considered to be of secondary nature. Transfer through the braid region as suggested by Hussain (1984) and Hussain and Zaman (1985) could not be clearly observed.

The visualization pictures however, clearly indicate the major role of large structures in the separated shear layer on the mass transfer processes. Thus the application of gradient diffusion hypothesis in this case of separated shear flow becomes questionable.

## 5.4 Conclusion

The most striking result of this visualization study is the realization of the important role of the recirculating eddy which previously was believed to be of secondary importance. The interaction of this recirculating eddy with the shear layer structures can cause considerable differences in the mixing and mass transfer rates of such separated shear flows. Although qualitative,

the result of this flow visualization study has certainly instigated further quantitative measurements along this line.

# Chapter 6

# Presentation and Discussion of Results - Phase II

## 6.1 Introduction

The experimental results of the second phase of this study are presented and discussed in this chapter. The stimulating results of the flow visualization experiments have led to the measurements of the flow field employing a laser Doppler velocimeter at various points of interest in order to provide supportive quantitative information.

Measurements were made for different conditions by varying the experimental parameters as explained in Chapter 4. The results consist of mean velocities, streamwise and transverse turbulence intensities in the separated shear layer and the recirculating region. Spectral analysis was also performed on records

of instantaneous fluctuating velocities at different important locations of the shear layer to demonstrate large structure development, interactions and shear layer movement.

## 6.2 Mean Velocity Profiles

Figures 6.1 to 6.6 show measurements of the mean velocity distributions at various locations of the separated flow downstream of the point of separation. Both streamwise and transverse velocity measurements are presented for two different geometrical configurations and two different flow conditions for each configuration. In all cases the velocity is normalized by U, the free stream mean velocity which is equivalent to the maximum mean velocity measured at each streamwise location. The streamwise and the transverse ordinates, x and y respectively are normalized by the width of the separated flow region, W which was kept constant (0.5 metre) in all cases. The positive and the negative values of the mean velocities are in accordance to the co-ordinate system shown in (a) of each figure. In the case of transverse velocity, for instance, the positive values indicate motion towards the main stream flow and the negative values indicate motion towards the separated recirculating region.

### 6.2.1 Streamwise Mean Velocity

From the streamwise velocity profiles in Figures 6.1b, 6.2b, 6.3b, 6.3c, 6.5b and 6.5c linear growth of the shear layer is apparent except near the reattachment region (see for instance, at x/W = 1.8 and 1.9 of Figure 6.1b) where the growth rate decreases due to the impact of the shear layer on the reattaching wall. After the impact, reverse flow is developed and a recirculating

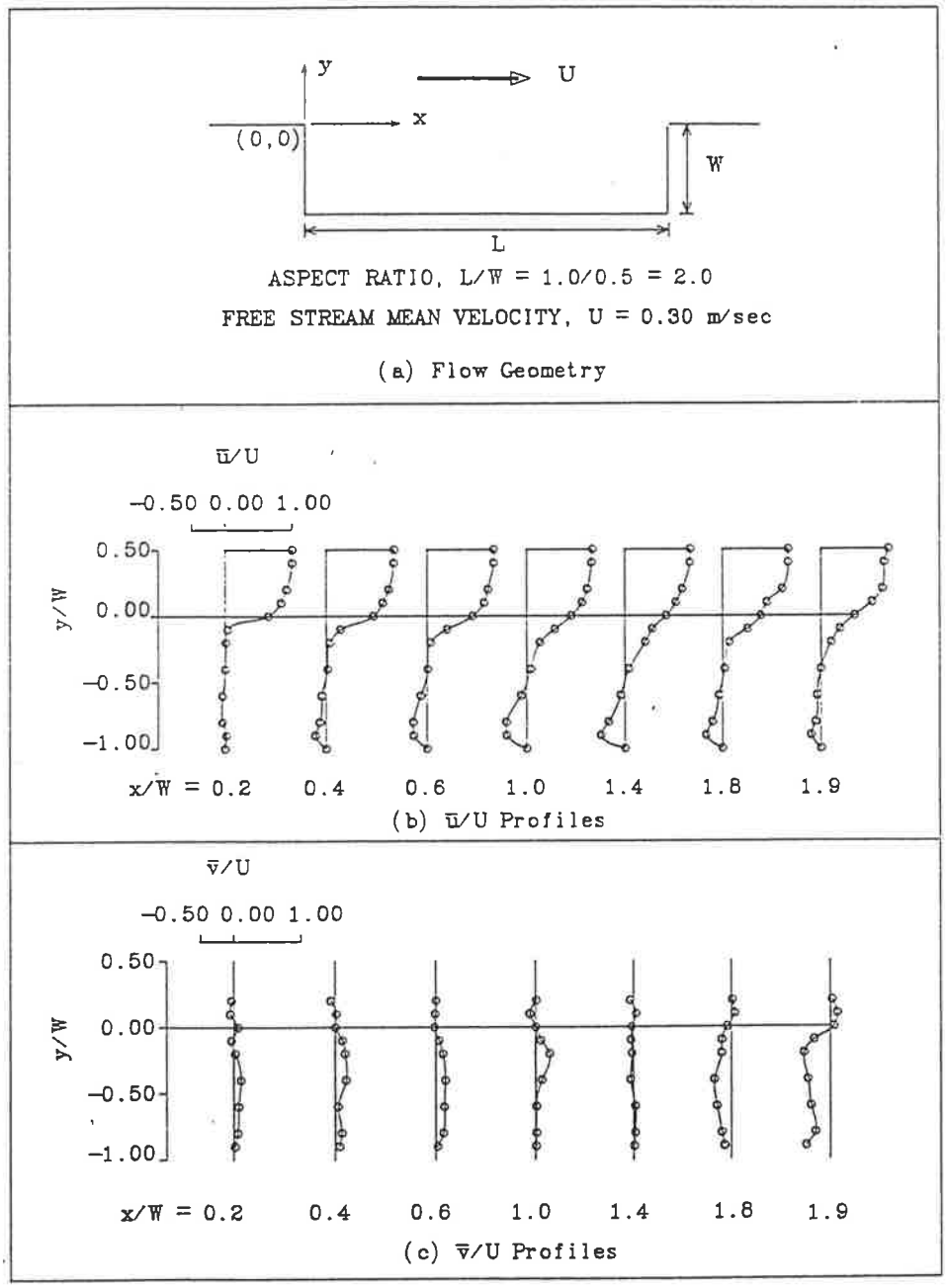


Figure 6.1: Streamwise and transverse mean velocity profiles;
aspect ratio = 2.0; U = 0.30 m/sec.

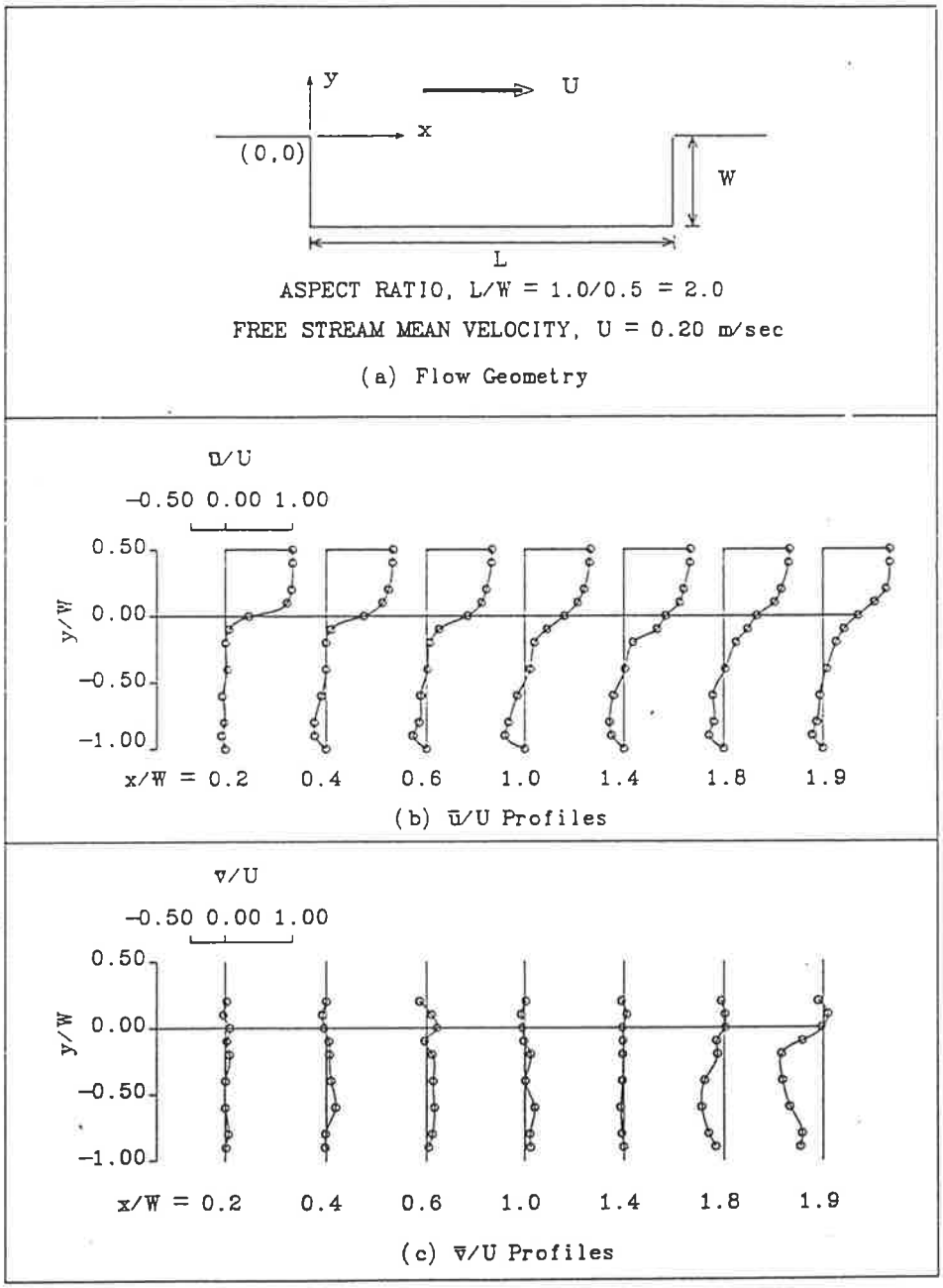


Figure 6.2: Streamwise and transverse mean velocity profiles;
aspect ratio = 2.0; U = 0.20 m/sec.

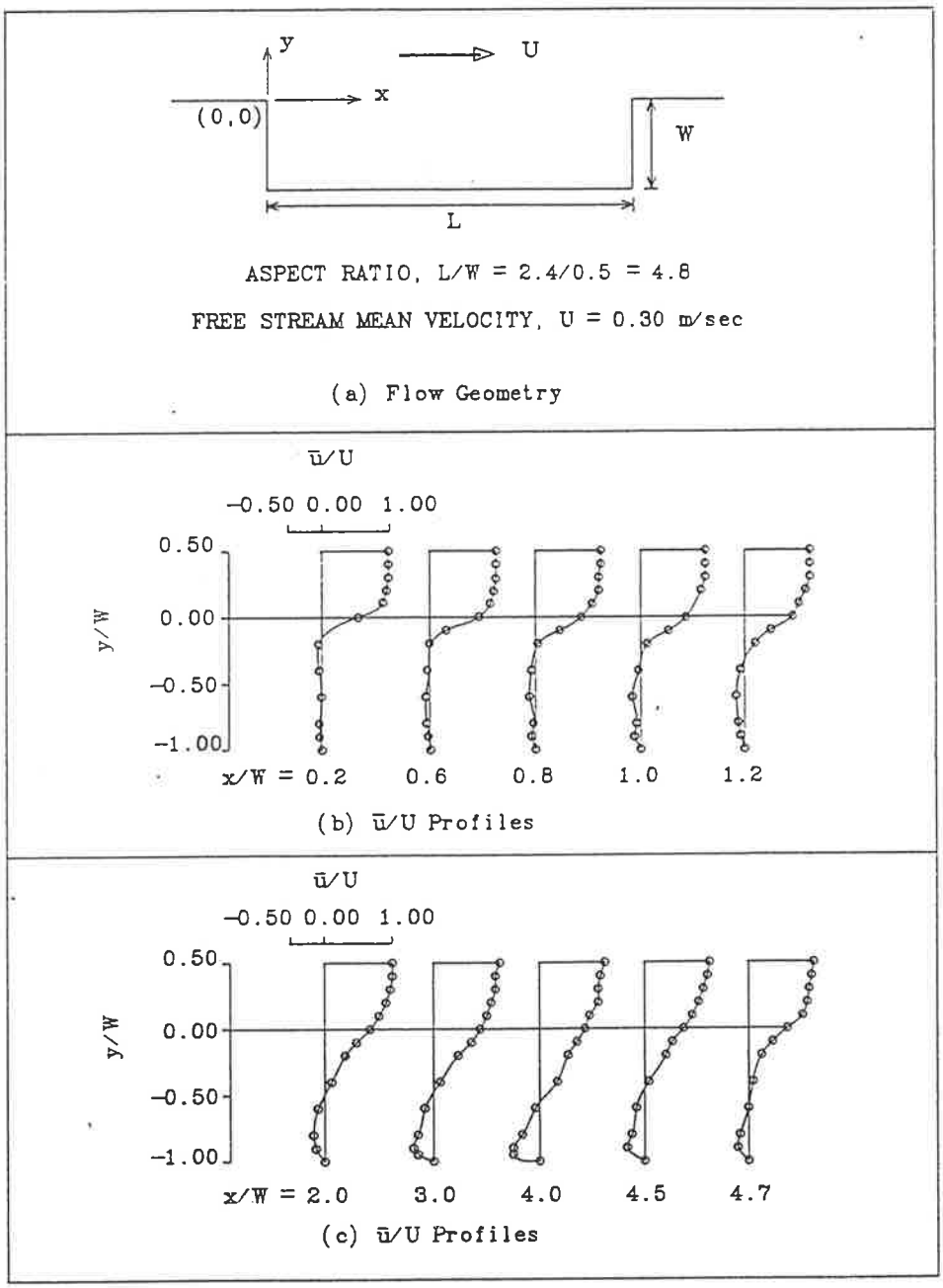


Figure 6.3: Streamwise mean velocity profiles; aspect ratio = 4.8; U = 0.30 m/sec.

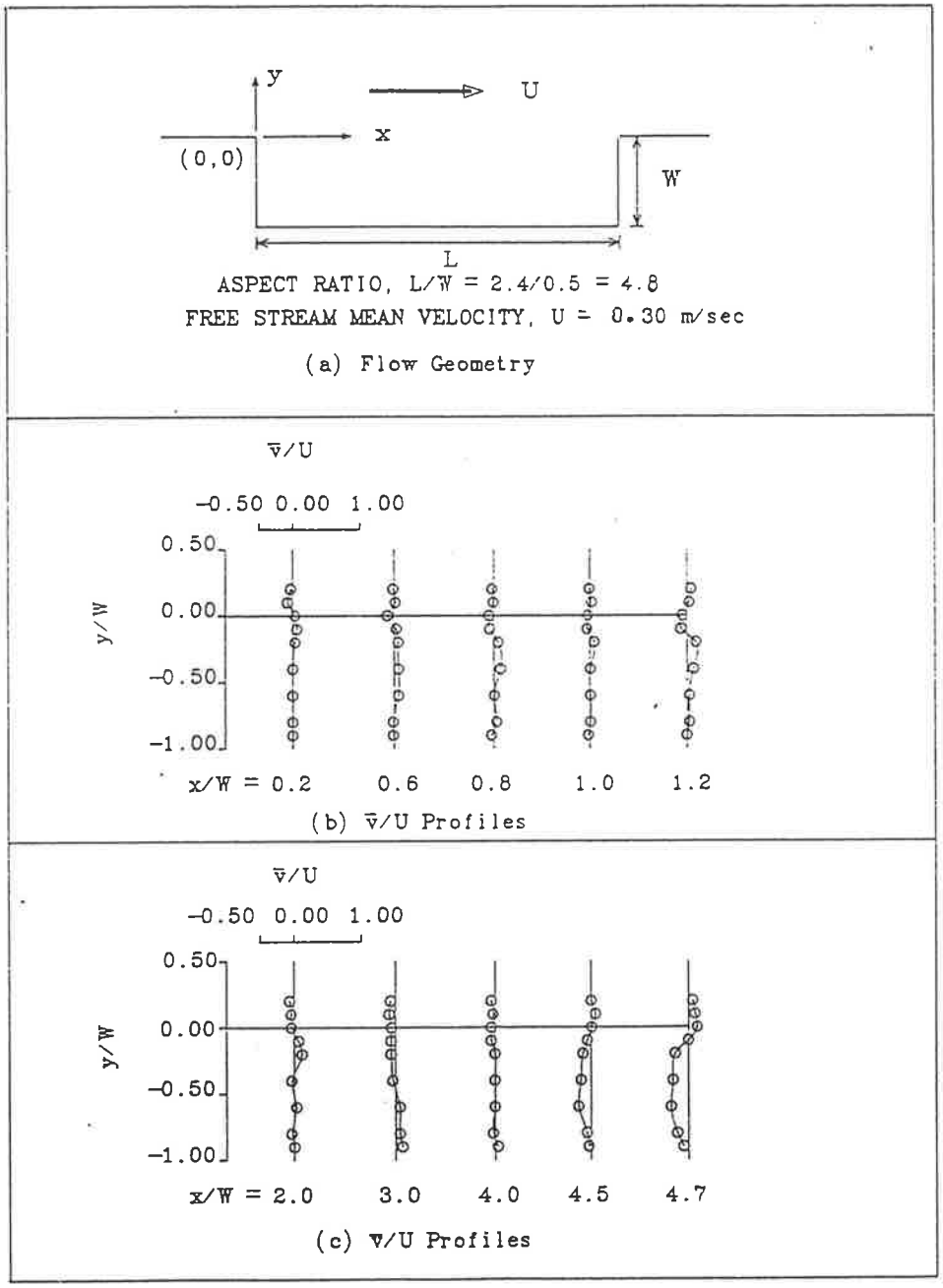


Figure 6.4: Transverse mean velocity profiles; aspect ratio = 4.8;
U = 0.30 m/sec.

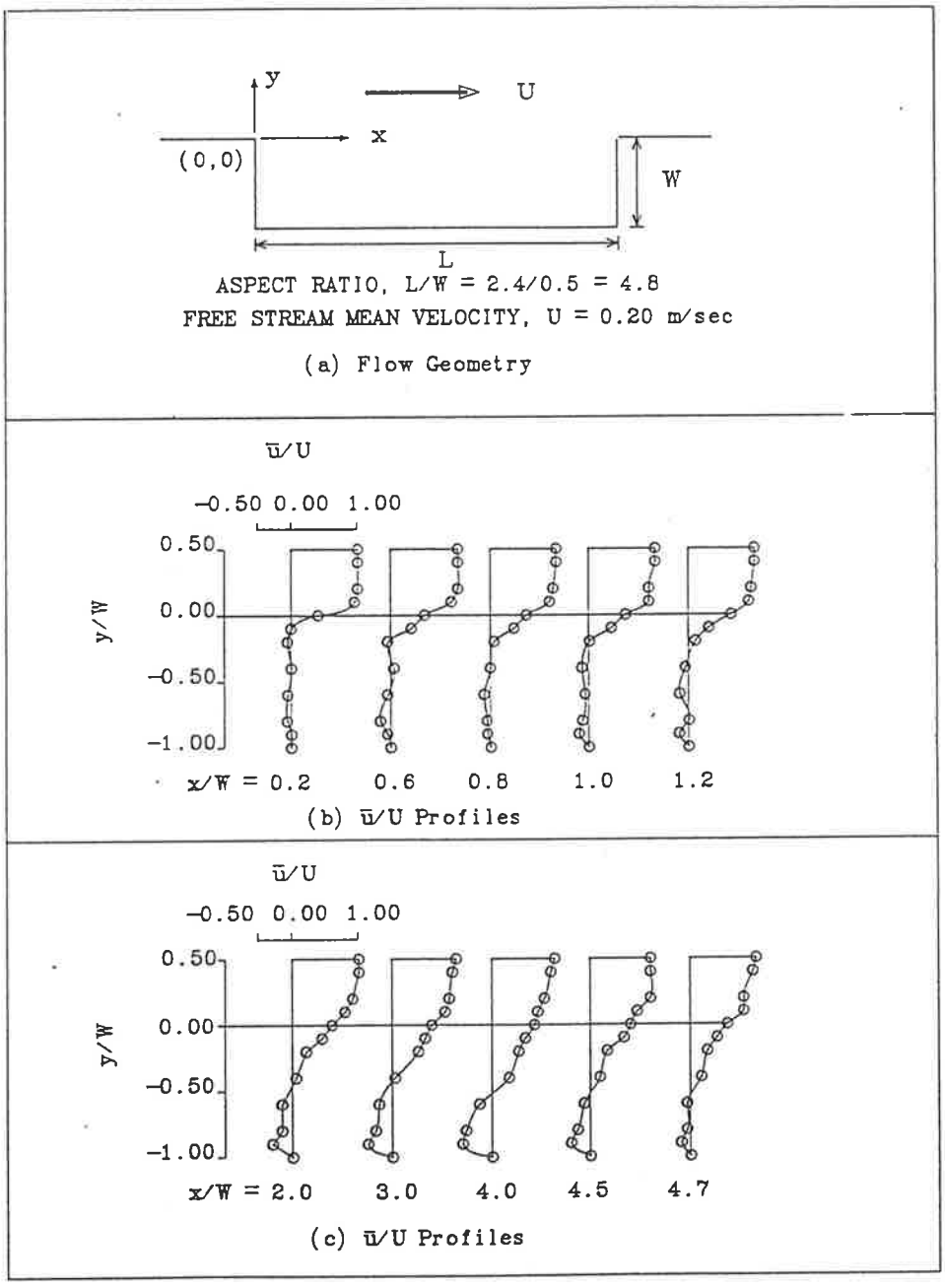


Figure 6.5: Streamwise mean velocity profiles; aspect ratio = 4.8;
U = 0.20 m/sec.

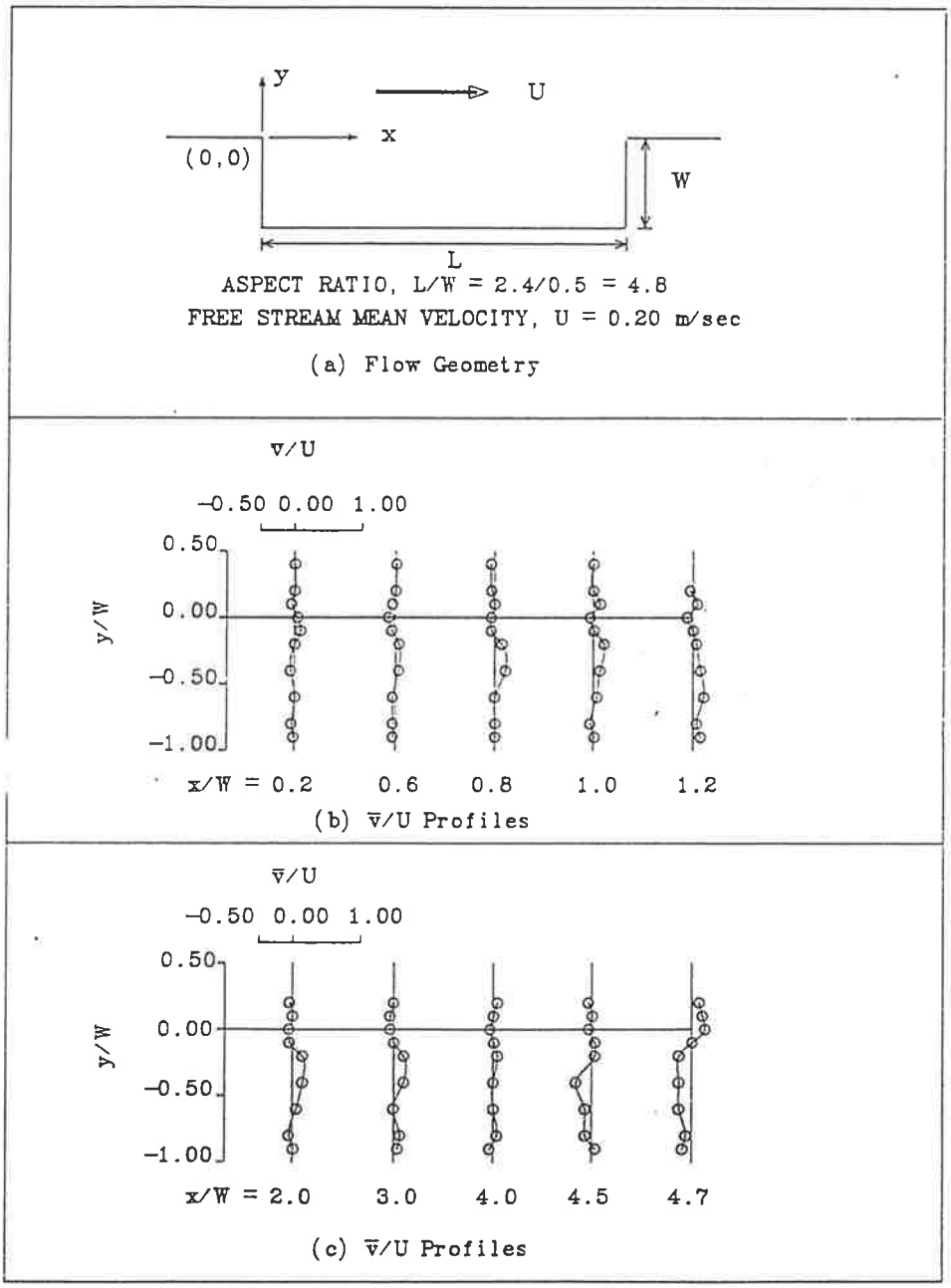


Figure 6.6: Transverse mean velocity profiles; aspect ratio = 4.8;
U = 0.20 m/sec.

eddy jet is formed near the wall, propagating along the walls of the separated region. The negative peaks in the streamwise mean velocity profiles indicate the existence of a such wall boundary layer jet in each case of geometrical and flow conditions considered. For the aspect ratio of 2.0, this boundary jet appears to reach up to x/W = 0.4, whereas for the aspect ratio of 4.8, it can be traced near x/W = 0.6. This is consistent with what has been observed in the earlier visual experiments. However, the variations due to different flow conditions and even in one flow condition are not clear from the mean velocity profiles.

In all cases, the almost zero streamwise mean velocity at x/W = 0.2, within the separated region, indicates a stagnant region, although there are visual indications of relatively weaker secondary recirculating eddies in these profiles. The maximum mean velocity within the separated recirculating region appears to be in the boundary wall jet region. For the aspect ratio of 4.8 and the free stream mean velocity of 0.20 m/sec, the maximum streamwise mean velocity within the separated region is upto 45% of the free stream mean velocity (at x/W = 4.0, y/W = - 0.9 of Figure 6.5c). For aspect ratio of 2.0 and U = 0.30 m/sec, this maximum reaches upto 37.7% of the free stream mean velocity (at x/W = 1.4, y/W = - 0.9 of Figure 6.1b). These values are larger than the values reported earlier in similar separated flows. For example, Roshko (1955) measured a maximum of about 34% of the free stream mean velocity at a similar region of a square cavity flow with air as the fluid medium. The absolute maximum of his measurements however, was at the rear wall of the cavity flow which was close to about 45% of the free stream mean velocity. Also, Eaton and Johnston (1981) reported maximum velocity in the separated region of the backward facing step flows of over 20% of the free stream mean velocity.

### 6.2.2 Transverse mean velocity

The transverse mean velocity profiles at corresponding downstream locations are shown in Figures 6.1c, 6.2c, 6.4 and 6.6. For the aspect ratio of 2.0, the negative values of $\bar{v}/U$ at x/W = 1.8 and 1.9 and the positive values between x/W = 0.2 and 1.0 in Figures 6.1c and 6.2c indicate the flow of the recirculating eddy jet. Apart from the large negative $\bar{v}/U$ values near the rear wall region which indicate deflection of the shear layer into the separated region, the relatively stronger (about 14 to 20% of U) positive $\bar{v}/U$ values at about x/W = 0.4 to 1.0 suggest possible interaction of the recirculating eddy jet with the shear layer around that region. At about x/W = 0.2 and 1.4, negligible transverse velocity component indicate a relatively stagnant area.

For the aspect ratio of 4.8, the positive $\bar{v}/U$ values are larger between x/W = 0.6 and 2.0 again indicating a relatively stronger recirculating eddy front flowing towards the free shear layer. The $\bar{v}/U$ values for aspect the ratio of 4.8 are however, smaller compared to those for the aspect ratio of 2.0, as are expected. This can be clearly seen by comparing the profiles at x/W = 4.5 and 4.7 (in Figures 6.4c and 6.6c) for the aspect ratio of 4.8 with those at x/W = 1.8 and 1.9 (in Figures 6.1c and 6.2c) for the aspect of 2.0. In the latter case however, the values are larger for the smaller free stream velocity (U = 0.20 m/sec).

## 6.3 Growth of the Separated Shear Layer

The rate of growth of the separated shear layer is determined by relating the development of a local characteristic width of the layer with the downstream distance. The local width is defined as the transverse distance between the location at which the velocity is equal to 95% of the free stream velocity and

the location at which it is equal to 10% of the free stream mean velocity, i.e.,

$$\delta = (y_{0.95} - y_{0.10})$$

Figure 6.7 shows the measured rate of growth of the separated shear layer for two different flow and geometrical conditions. Several interesting features can be noticed from these plots of shear layer width vs. streamwise distance.

In Figure 6.7a, the growth rate increases almost linearly for both flow conditions up to a certain downstream distance and then decreases abruptly near the reattachment region. This abrupt decrease in growth rate can be attributed to the impact of the impingement of the shear layer on the reattaching surface which prohibits growth near that region. This can also be noticed in Figure 6.7b for the aspect ratio of 4.8. In this case however, a non-linear growth in the initial region of the shear layer can be seen for both flow conditions which indicates that the flow is not fully developed in that region.

Another interesting point to be noted from these plots of growth rate is that in the linear growth region, the rate of growth is faster when the free stream mean velocity is slower, i.e., when the velocity was 0.20 m/sec than when it was 0.30 m/sec. This faster growth rate for the slower free stream velocity can also be seen in Figure 6.7b for the aspect ratio of 4.8.

This result is of fundamental importance and is consistent with the previous results of Browand and Latigo (1979) in two stream plane mixing layer flow. They observed that the mixing layer grows more rapidly from an initially laminar boundary layer than from an initially turbulent boundary layer, although they did not give an adequate explanation of it. Browand and Latigo (1979) also confirmed that this difference in growth rate was not the result of the initially thicker turbulent boundary layer as this was eliminated by normalization. Hussain and Zedan (1978) observed two stages of linear

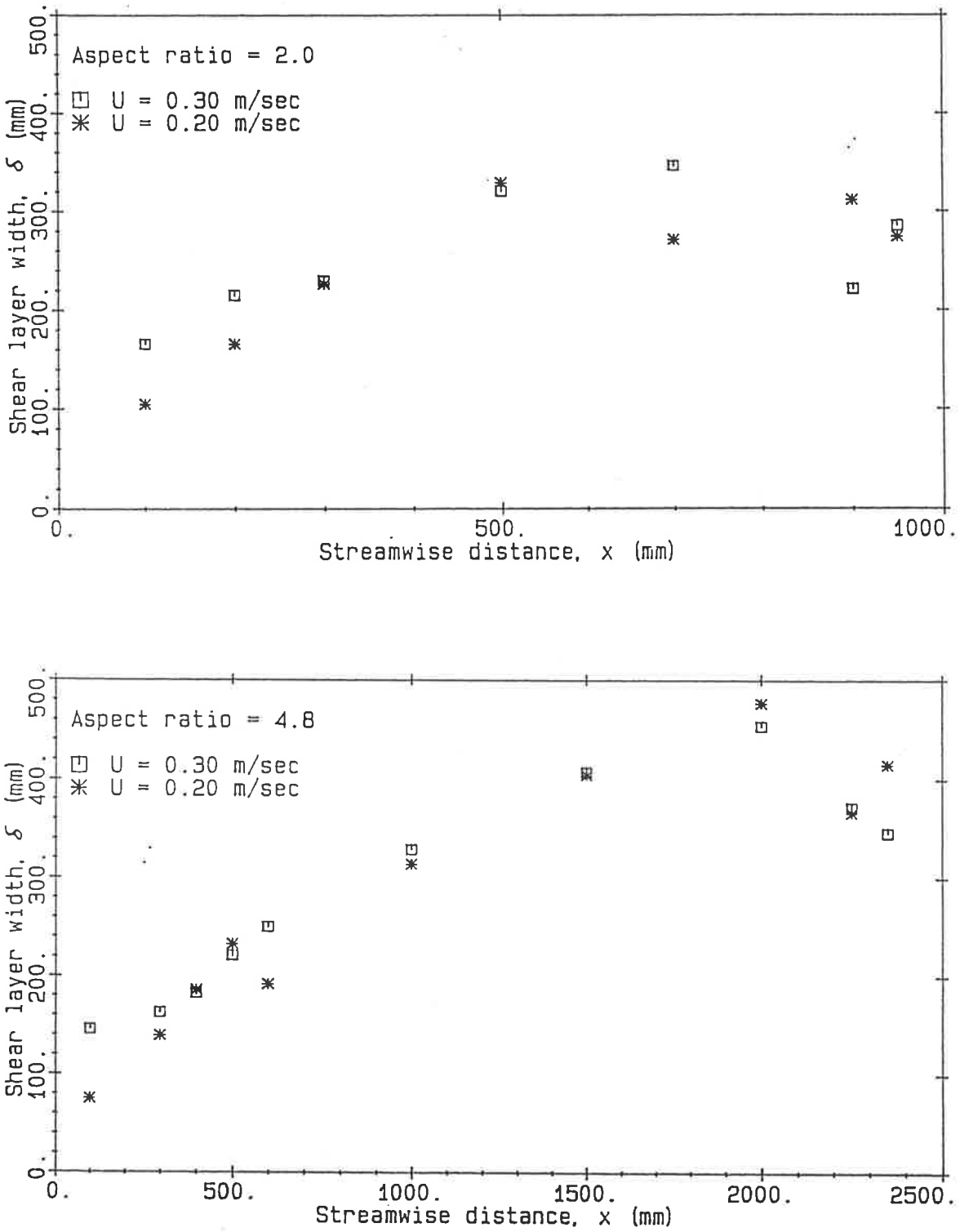


Figure 6.7: The separated shear layer growth for various flow and geometrical conditions.

growth for an initially turbulent boundary layer condition, the growth rate being slower in the first stage. They speculated that such two stage growth is controlled by the coherent large structure dynamics.

The present results do not show this two stage growth (most probably due to the reattachment effect). The difference in growth rates due to different flow conditions (faster growth for slower free stream flow and vice versa) is however, clearly established in the results.

A more meaningful and widely used parameter for representing the shear layer growth is the downstream development of local momentum thickness, defined as

$$\theta = \int_{-\infty}^{\infty} \frac{\bar{u}}{U}(1 - \frac{\bar{u}}{U})dy$$

This integral thickness is determined by integration of the mean velocity profiles between points $y_{0.1}$ and $y_{0.95}$ at various downstream locations. It should be noted here that truncation of integration at these points will slightly underestimate the actual momentum thickness. However, as pointed out by Hussain and Zaman (1985) that the error in measuring $\bar{u}$ due to high turbulence and flow reversal would overestimate $\theta$ and thus have a cancelling effect.

The results shown in Figure 6.8, again demonstrate regions of initial non-linear growth, intermediate linear growth and a sharp decrease in growth near reattachment. The slower growth rate for faster free stream mean velocity is also evident from the figure. (In Figure 6.8b the value of momentum thickness at x = 700 mm, is unusually low for U = 0.20 m/sec compared to the value for U = 0.30 m/sec which is suspect and is attributed to experimental error.)

It therefore, appears that the growth rate of the separated shear layer is almost similar to that of a plane mixing layer except in the reattachment region where the rate decreases sharply.

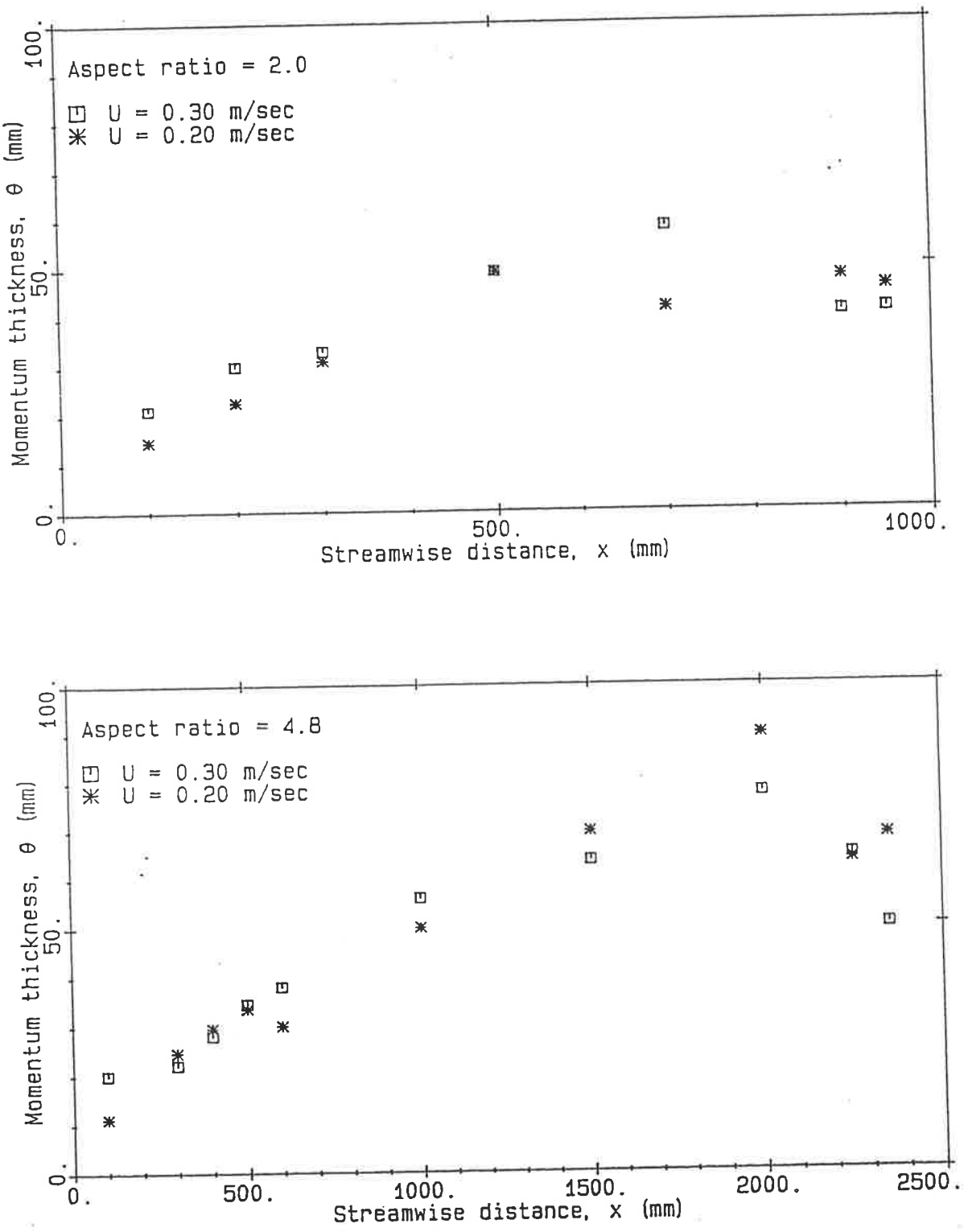


Figure 6.8: Growth of the local momentum thickness for various flow and geometrical conditions.

## 6.4 Similarity in Mean Motion

Because of the departure of the separated shear layer growth rate from the plane mixing layer growth rate, in the reattachment region, it is instructive to look at the similarity behaviour of the separated shear layer. Self-similarity, as indicated in Chapter 2, is an important theoretical expectation of free shear flows. The implication is that the various processes involved in the flow can be considered to be in dynamic equilibrium, each changing downstream at a constant rate.

In order to demonstrate the self-similar behaviour of the separated shear layer for the present experimental case, the similarity profiles for the streamwise mean velocity are presented in Figures 6.9 and 6.10.

The transverse distances are normalized by the characteristic length scale, the momentum thickness, $\theta$, and the velocity scale chosen here is the free stream mean velocity, U. From the profiles of both the figures the self-similar behaviour of the separated free shear layer is established although a considerable scatter is present in the low speed side which can be attributed to the complex interaction between the shear layer and the recirculating flow in the separated region. In Figure 6.9a, the profiles of the initial region (x = 100 mm) and the reattachment region (x = 900 and 950 mm) show scatter as might be expected. The scatter in the initial region indicates the stage of flow development and the scatter (to a lesser extent) in the reattachment region can be expected due to decreased growth rate in that region. In Figure 6.9b however, scatter is seen only in the intial region, up to x = 200 mm, indicating longer flow developing region. The reason that there is no scatter in the reattachment region in this case is most probably due to the lesser impact of reattachment on the shear layer growth with slower free stream flow. This can also be noted from Figures 6.7 and 6.8; that is, the decrease in growth

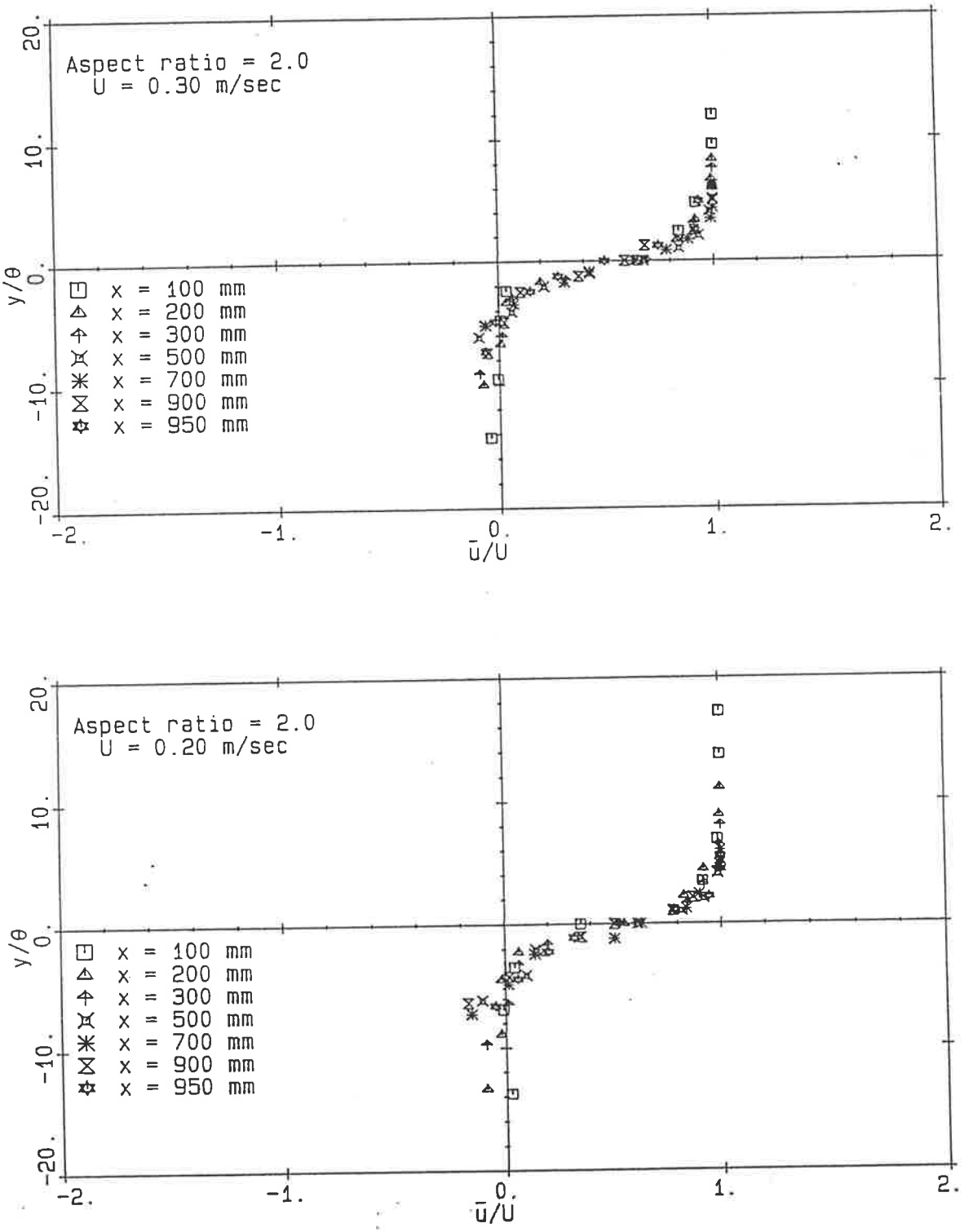


Figure 6.9: Similarity profiles for streamwise mean velocity; A.R. = 2.0; (a) U = 0.30 m/sec; and (b) U = 0.20 m/sec.

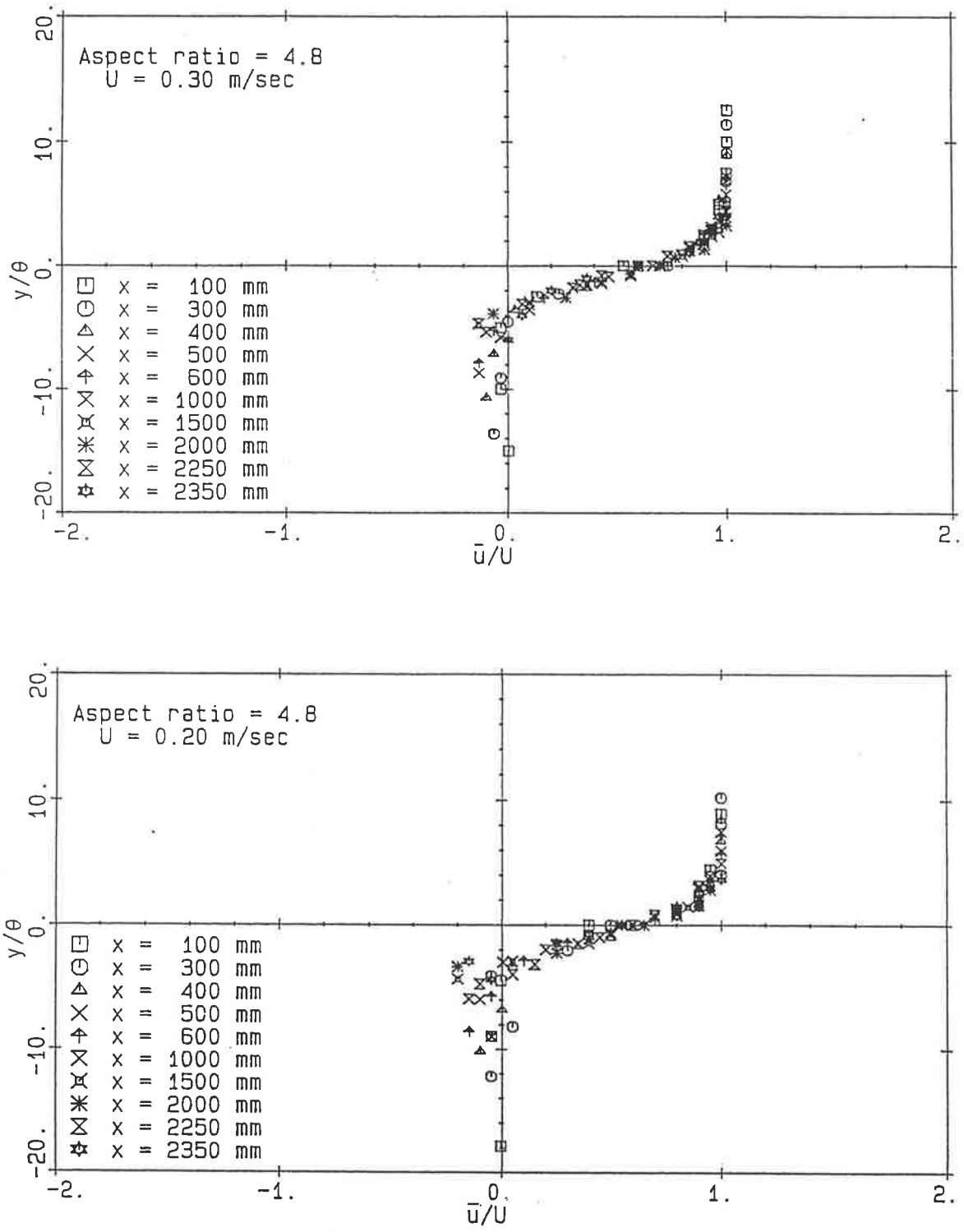


Figure 6.10: Similarity profiles for streamwise mean velocity; A.R. = 4.8; (a) U = 0.30 m/sec; and (b) U = 0.20 m/sec.

near reattachment is relatively moderate when the free stream velocity is 0.20 m/sec.

Similar features can also be noticed from the profiles for the aspect ratio 4.8 shown in Figure 6.10. Scatter in the profiles of the reattachment region in this case is even less apparent. However, scatter in the intial region (x = 100 mm in Figure 6.10a; and x = 100 and 300 mm in Figure 6.10b) can be identified. In general, when the free stream mean velocity is lower the similarity profiles show more scatter than when the free stream flow is faster.

From the similarity analysis it can be inferred that the behaviour of the separated free shear layer and the plane mixing layer are quite similar. This was also indicated by Eaton and Johnston (1980) when comparing the reattaching shear layer of the backward facing step flow, with plane mixing layer flow. The implication is that the effects of many parameters such as free stream turbulence, and upstream boundary layer state could be predicted using plane mixing layer data. However, the low frequency motion in the separated shear layer which arises because of the complex interaction of the pulsatile motion in the recirculating eddy jet with the large coherent eddy structures of the shear layer, is not apparent from the analysis of the mean motion.

## 6.5 Turbulence Intensity Profiles

The measured profiles of the streamwise and the transverse turbulence intensities, defined as $\sqrt{\overline{u'^2}}/U$ and $\sqrt{\overline{v'^2}}/U$ respectively, are presented in Figures 6.11 to 6.16 inclusive. The root-mean-square (r.m.s) value of a fluctuating quantity, as pointed out by Bradshaw (1971), is not a very appropriate term for random functions and it is the mean-square-fluctuation (m.s.f) which appear in equations with physical meaning. The r.m.s values are however,

mostly used for the analysis of sinusoidal signals and a useful property of them is that the r.m.s of the sum of two fluctuating quantities is the sum of the r.m.s of each quantity.

This simple relation does not always hold for random functions and the statistical description is made in terms of mean squares and mean product. This is particularly important for the analysis of second or higher order correlations. In the present study however, with the one component laser Doppler velocimeter system, analysis of higher order correlations was not intended and the r.m.s analysis of the streamwise and the transverse turbulence quantities, measured separately, were considered satisfactory. Previous measurements in separated flows (e.g., Etheridge and Kemp, 1978; Smyth, 1979; and Stevenson et al, 1984) were also presented as r.m.s intensities for longitudinal and transverse turbulence quantities.

### 6.5.1 Streamwise Turbulence

The profiles of the streamwise turbulence intensity for various flow and geometrical conditions are presented in Figures 6.11b, 6.12b, 6.13 and 6.15. The profiles show a consistent pattern in all cases. Peak turbulence intensities can be noticed in almost all the profiles along the dividing line $y/W = 0.0$. These peak values however, do not monotonically increase with downstream distance as are reported in earlier measurements of separated flows such as in step flows (Ehteridge and Kemp, 1978), flows in sudden expansions (Smyth, 1979; Minh and Chassaing, 1977; Mehta, 1979 and 1981) and in rectangular cavity flows (Tani et al 1969). In Figures 6.11b and 6.12b, these peak values are larger between $x/W = 0.2$ and 1.0 (maximum being at about $x/W = 0.4$) and from there upto reattachment ($x/W = 1.9$) the peaks are lowered and have almost constant values.

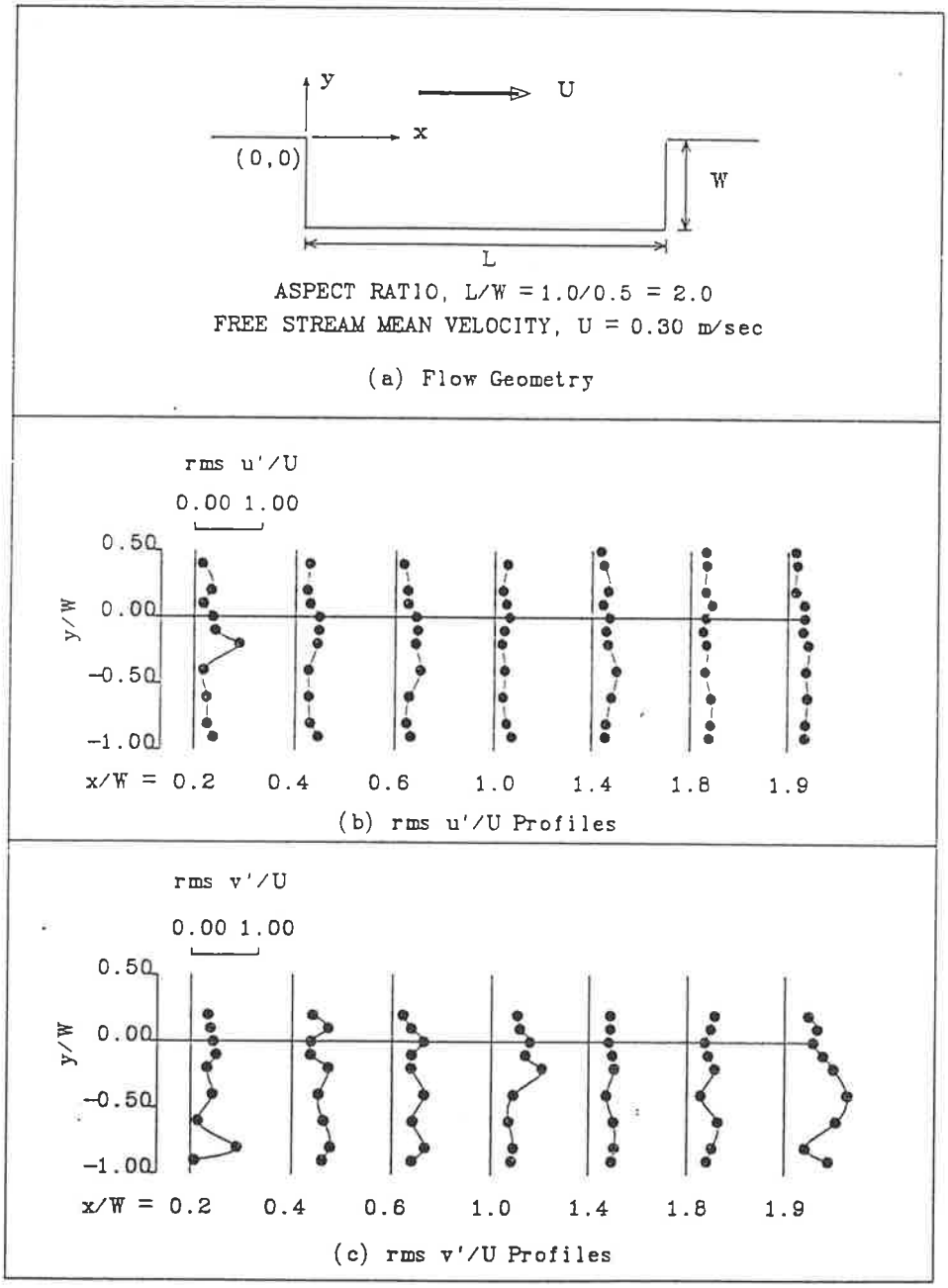


Figure 6.11: Profiles of the streamwise and transverse turbulence intensities; aspect ratio = 2.0; U = 0.30 m/sec.

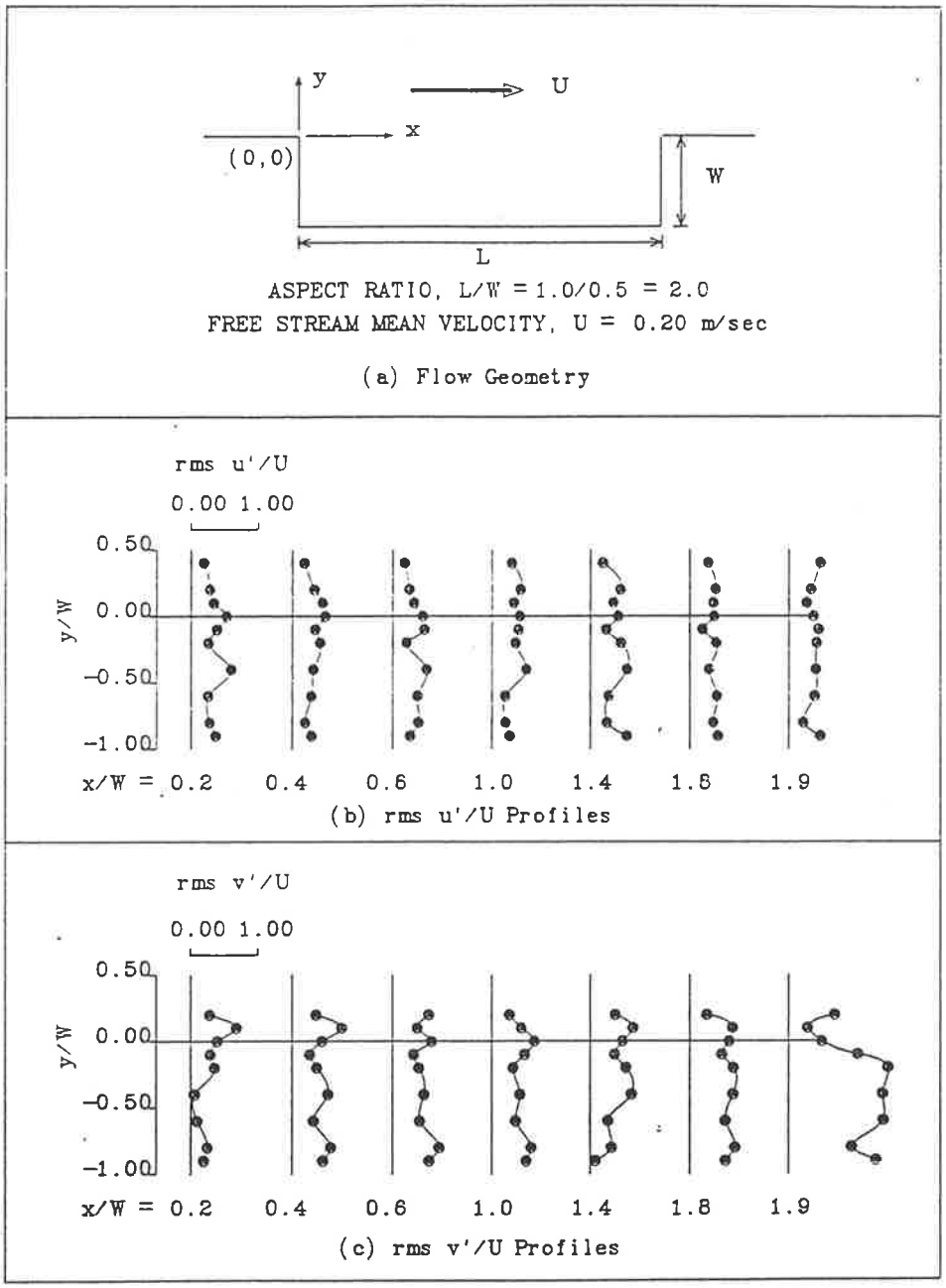


Figure 6.12: Profiles of the streamwise and transverse turbulence intensities; aspect ratio = 2.0; U = 0.20 m/sec.

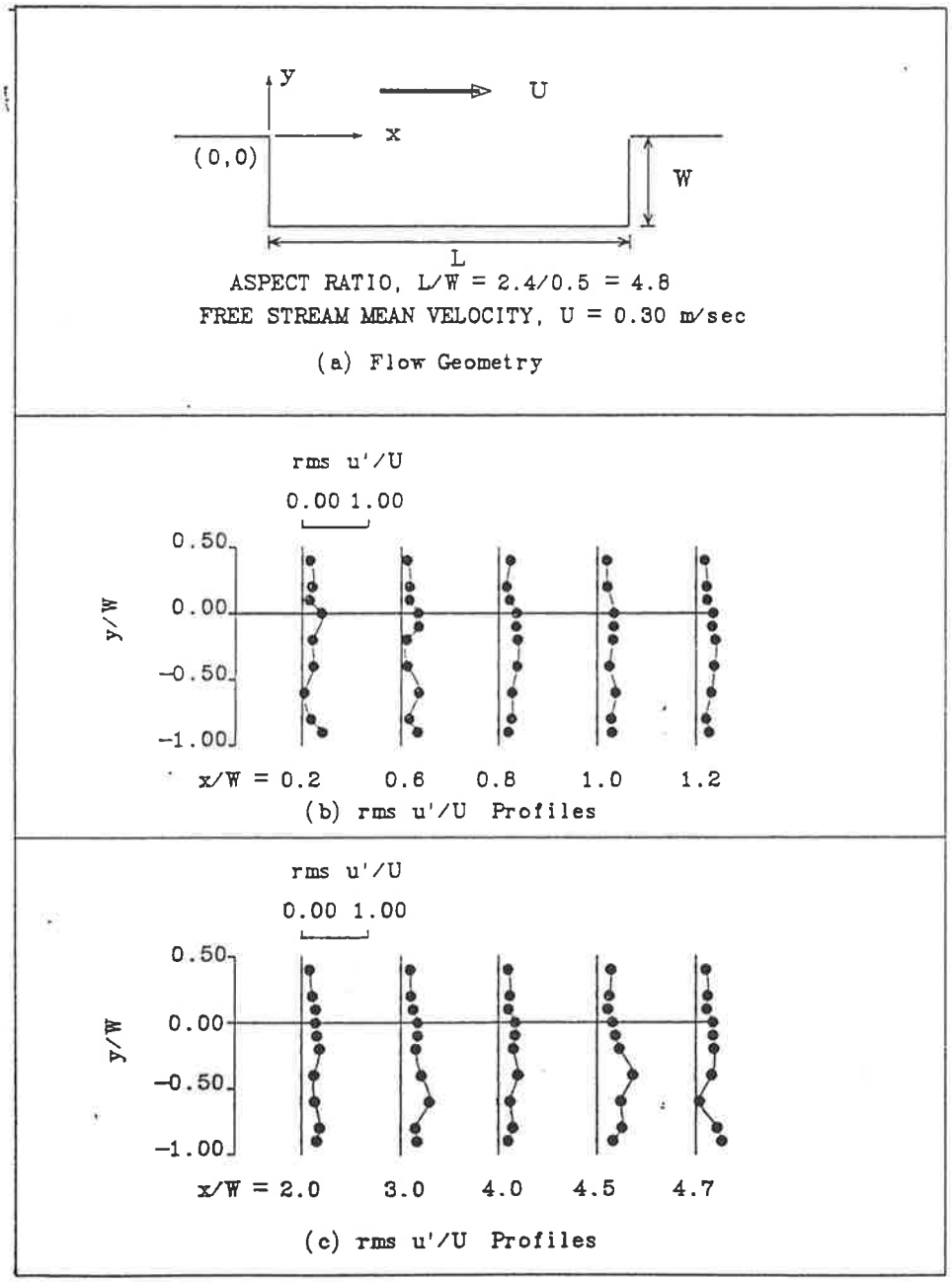


Figure 6.13: Profiles of the streamwise turbulence intensities; aspect ratio = 4.8; U = 0.30 m/sec.

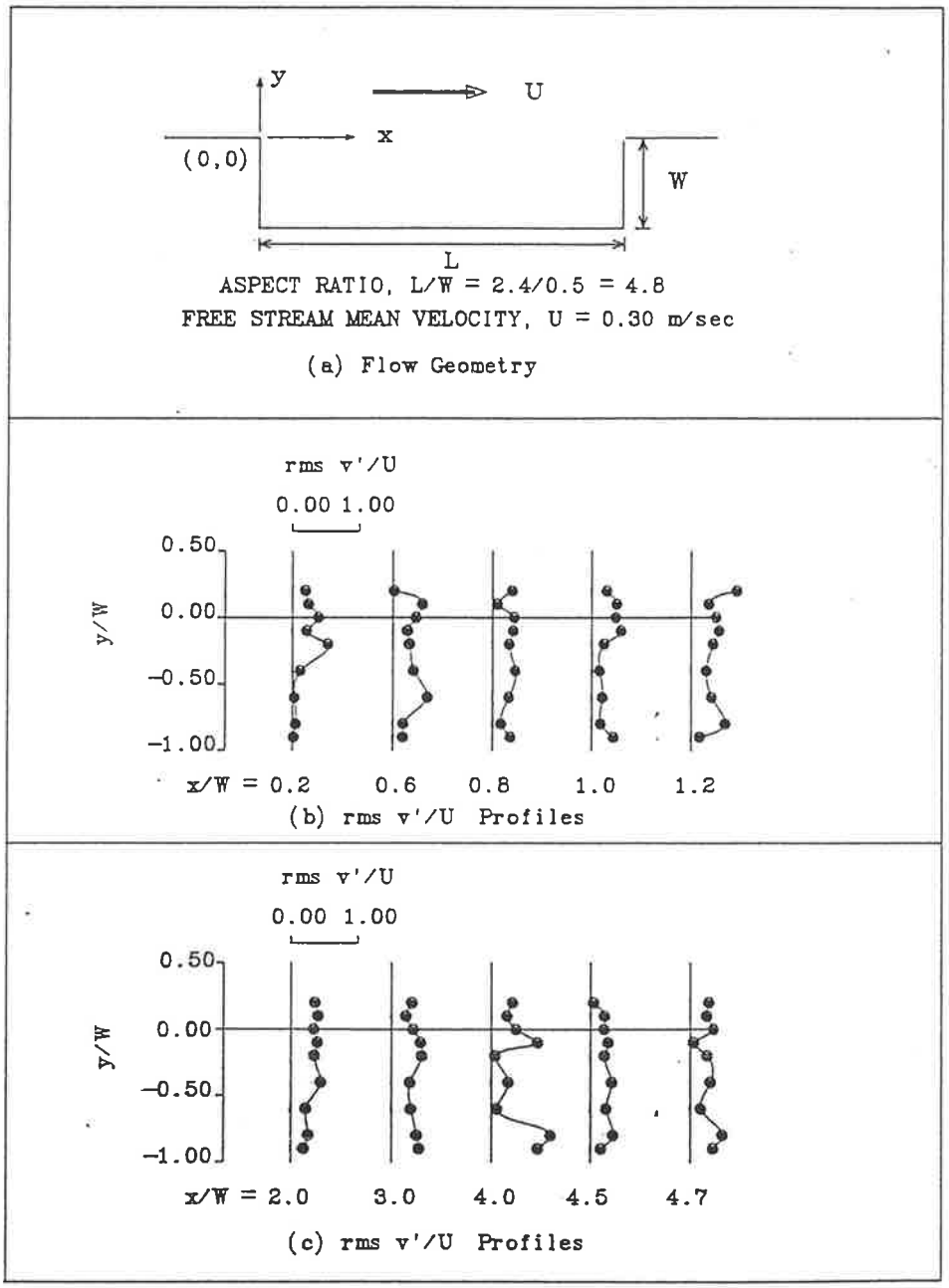


Figure 6.14: Profiles of the transverse turbulence intensities; aspect ratio = 4.8; U = 0.30 m/sec.

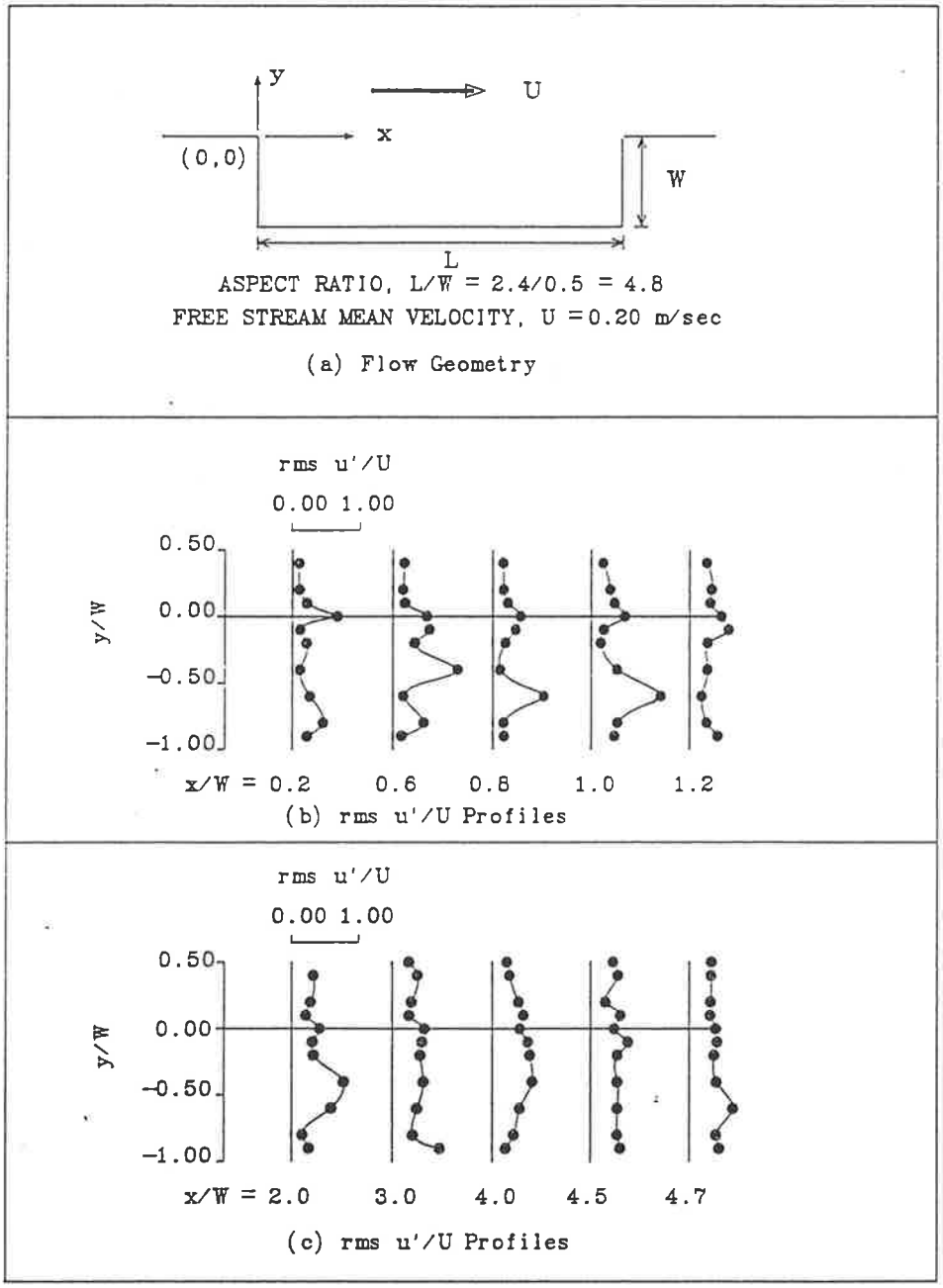


Figure 6.15: Profiles of the streamwise turbulence intensities;
aspect ratio = 4.8; U = 0.20 m/sec.

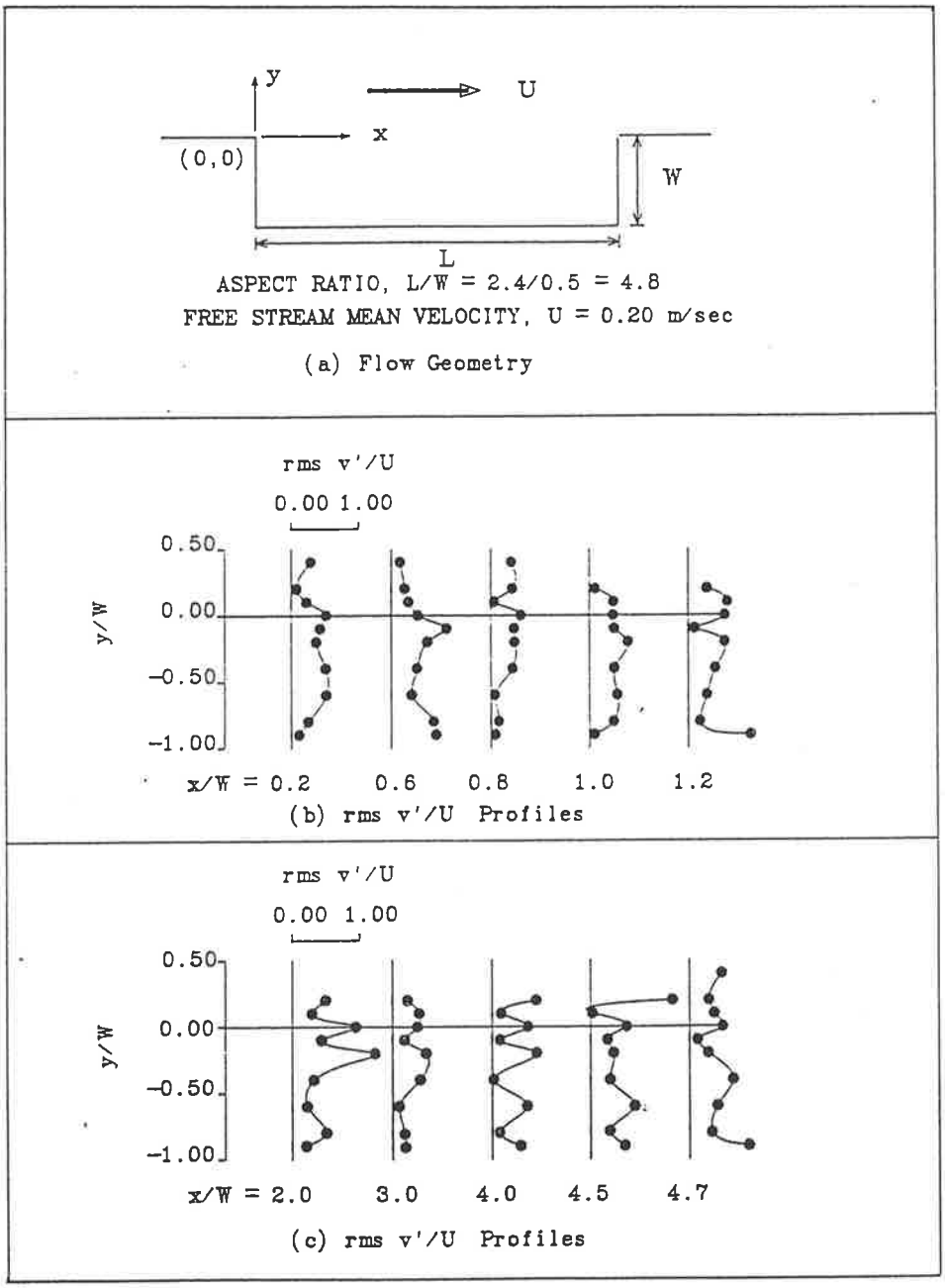


Figure 6.16: Profiles of the transverse turbulence intensities;
aspect ratio = 4.8; U = 0.20 m/sec.

Similarly, for the aspect ratio 4.8, the peaks have larger values upto about x/W = 1.2 (maximum being at about x/W = 0.6) and after that have nearly constant smaller values up to reattachment. This is an indication of the complex intense interaction between the recirculating eddy front and the large coherent eddy structures in the separated shear layer. Surprisingly, for both aspect ratios, the peak values of streamwise turbulence intensity are larger when the free stream mean velocity was smaller (0.20 m/sec). The reason could be similar to that of the faster shear layer growth with slower free stream flow which is not clearly understood.

Another remarkable feature is the existence of a second peak in most of the profiles within the separated region. These peaks are even stronger, for both aspect ratios, particularly when the free stream velocity is smaller. The reason for the development of such strong peaks in the streamwise turbulence intensity profiles is most probably due to the induced motion by the large coherent eddy structures in the separated free shear layer as they rotate and advect downstream periodically. The values of streamwise turbulence in the free stream side (above the line y/W = 0.0) are very much similar in all cases indicating a nearly homogeneous turbulence field in that region.

### 6.5.2 Transverse Turbulence

Figures 6.11c, 6.12c, 6.14 and 6.16 show the transverse turbulence intensity profiles at different locations of the separated flow for various flow and geometrical conditions. Apart from a few measurement points such as at x/W = 4.0 of Figure 6.14c and at x/W = 2.0, 4.0 and 4.5 of Figure 6.16c, the profiles show a consistent pattern over the entire flow field. The dubious values in the above mentioned figures are perhaps due to a very low yet non-zero velocity component tending to infinite turbulence intensity without significant physical meaning.

The relatively large values of transverse turbulence intensities in the reattaching region (at x/W = 1.9 of Figure 6.11c and 6.12c; and at x/W = 4.7 of Figures 6.14 and 6.16) indicate large fluctuations in the transverse velocity which is indicative of the pulsating motion through the recirculating eddy jet arising due to the lateral movement of the shear layer as noticed in the visual observations. The large peaks in the other upstream profiles within the separated region, at about y/W = - 0.5, (at x/W = 0.4, 0.6 and 1.0 of Figures 6.11c and 6.12c; and at x/W = 0.6 to 1.2 of Figures 6.14 and 6.16) also indicate large lateral velocity fluctuations again indicative of pulsating motion in the recirculating eddy front at that region. The relatively smaller peaks along the dividing line (y/W = 0.0) in all cases, indicate fluctuations due to the lateral movement of the large structures within the shear layer.

The large value of transverse intensity at x/W = 0.2 in all cases, shows considerable fluctuations although the mean velocity profiles indicate almost zero velocity there. It is believed to be due to the oscillatory motion in the initial vorticity layer region near separation which causes such large fluctuations particularly in the transverse direction.

## 6.6 Energy Spectra of Fluctuating velocity

In an effort to provide further evidence of the presence of the pulsating motion in the recirculating eddy jet within the separated region which causes the interaction between the large eddy structures in the shear layer and the recirculating eddy front, frequency spectra were measured for both u and v fluctuations at several important locations in the flow field.

Figure 6.17 shows two separate time records of instantaneous streamwise velocity at the same location downstream of the separation point, at x = 50 mm and y = 0.0, and Figure 6.18 shows the respective spectral density

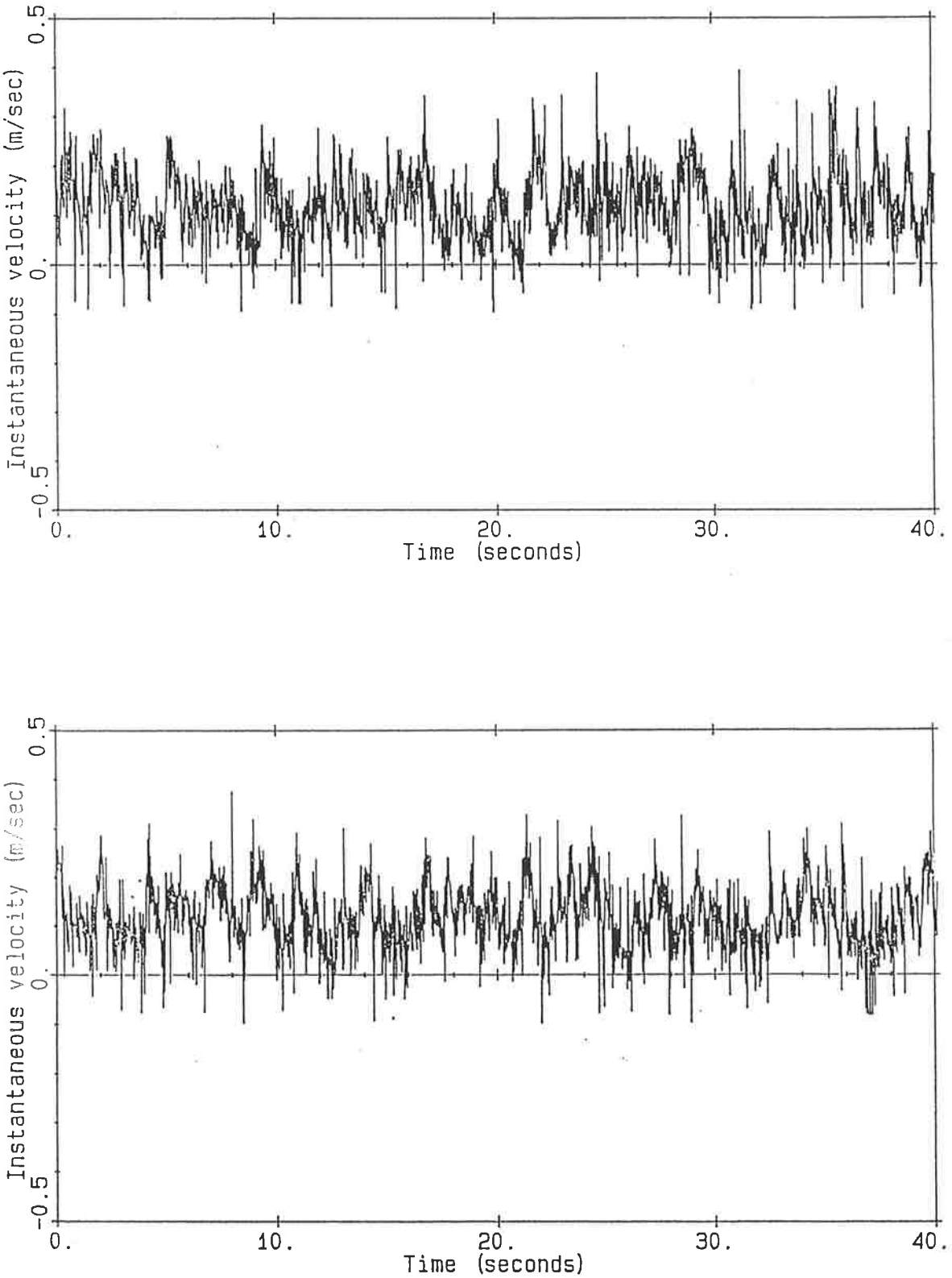


Figure 6.17: Time records of instantaneous velocity; x = 50 mm, y = 0.0; A.R. = 2.0; U = 0.30 m/sec.

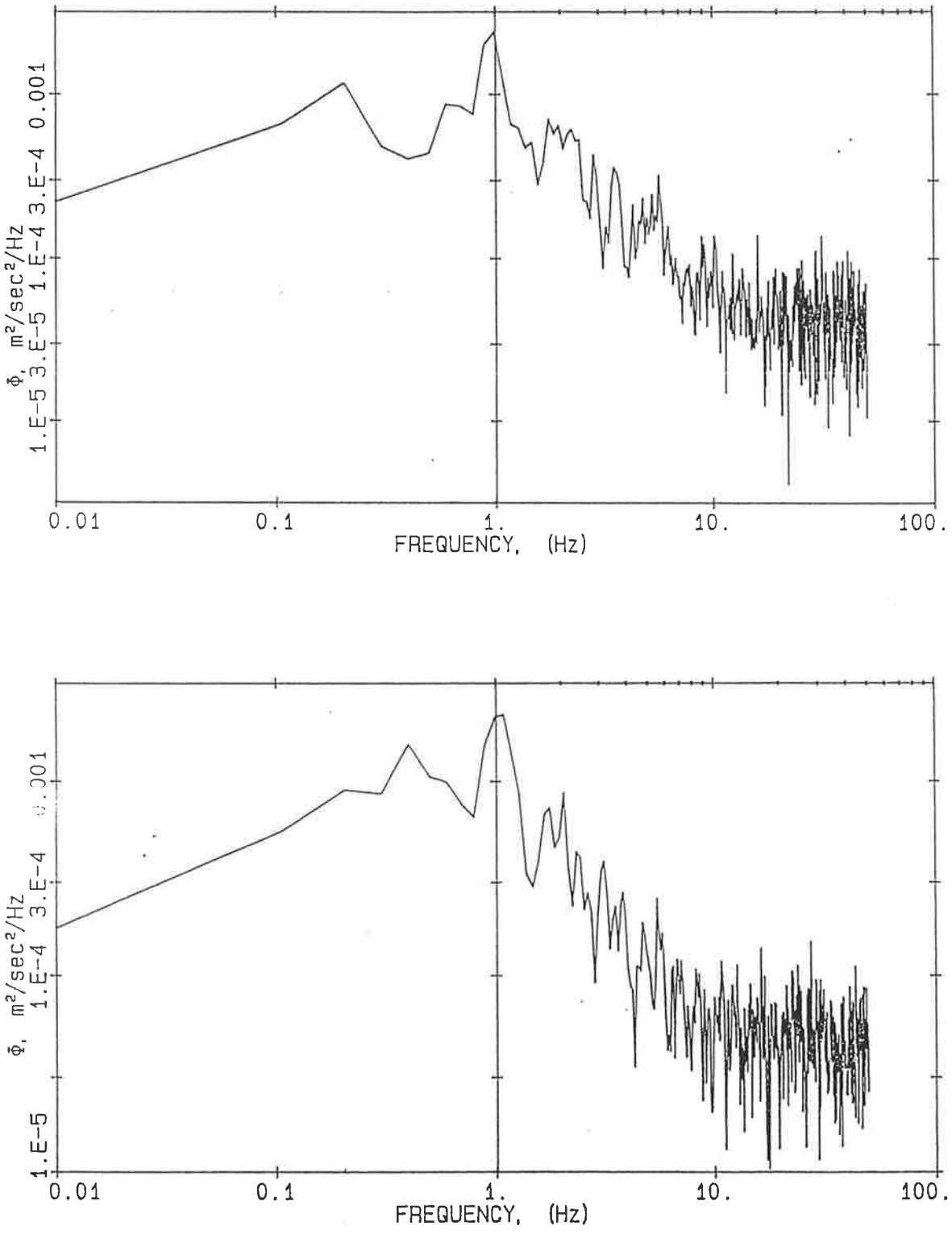


Figure 6.18: Power spectra for u fluctuations of the time series in Fig. 6.17

function plots. Two separate records were measured at the same location in order to see the repeatability of the frequency characteristics in the spectra which is quite good as can be seen from Figure 6.18. Two distinct peaks at about 0.2 Hz and 1.0 Hz can be noticed in both the spectra. The peaks at 1.0 Hz in both the spectra indicate the passage of large coherent eddy structures. The visual observation also revealed the passage of large structures at that point of time scale of the order of one second. The peaks at about 0.2 Hz are due to the low frequency oscillatory motion which was also observed in the initial vorticity layer after separation. The time records of the instantaneous streamwise velocity in Figure 6.17 also indicate both the periodicities at about every 1.0 and 5.0 seconds.

Figure 6.19 shows power spectra of $u'$ for three streamwise locations (at x = 200, 500 and 900 mm respectively) of the shear layer measured at y = 0.0 in each case. In all the three spectra the peaks at about 0.04 to 0.06 Hz indicate the low frequency motion in the shear layer. The peaks at about 0.3 Hz in the first spectra and at about 0.2 Hz in the second are the indication of large structure passage. The third spectra (x = 900 mm) does not distinctly show any peak for large structure passage probably due to the reattachment effect.

Spectra of $v'$ for three different locations within the separated region are shown in Figure 6.20. These locations are at 200, 400 and 900 mm downstream of the separation point each measured at y = - 200 mm which is about the middle of the recirculating region. These locations are chosen because the recirculating eddy jet, as observed from the flow visualization experiments, passes through these points after being deflected at the reattachment surface. The intention has been to check the presence of the pulsating motion in the recirculating eddy jet. Figure 6.20 clearly shows the low frequency hump in each of the spectra (frequency level of 0.03 to 0.08 Hz) which is an indication of the presence of the pulsating motion through the recirculating jet. It can

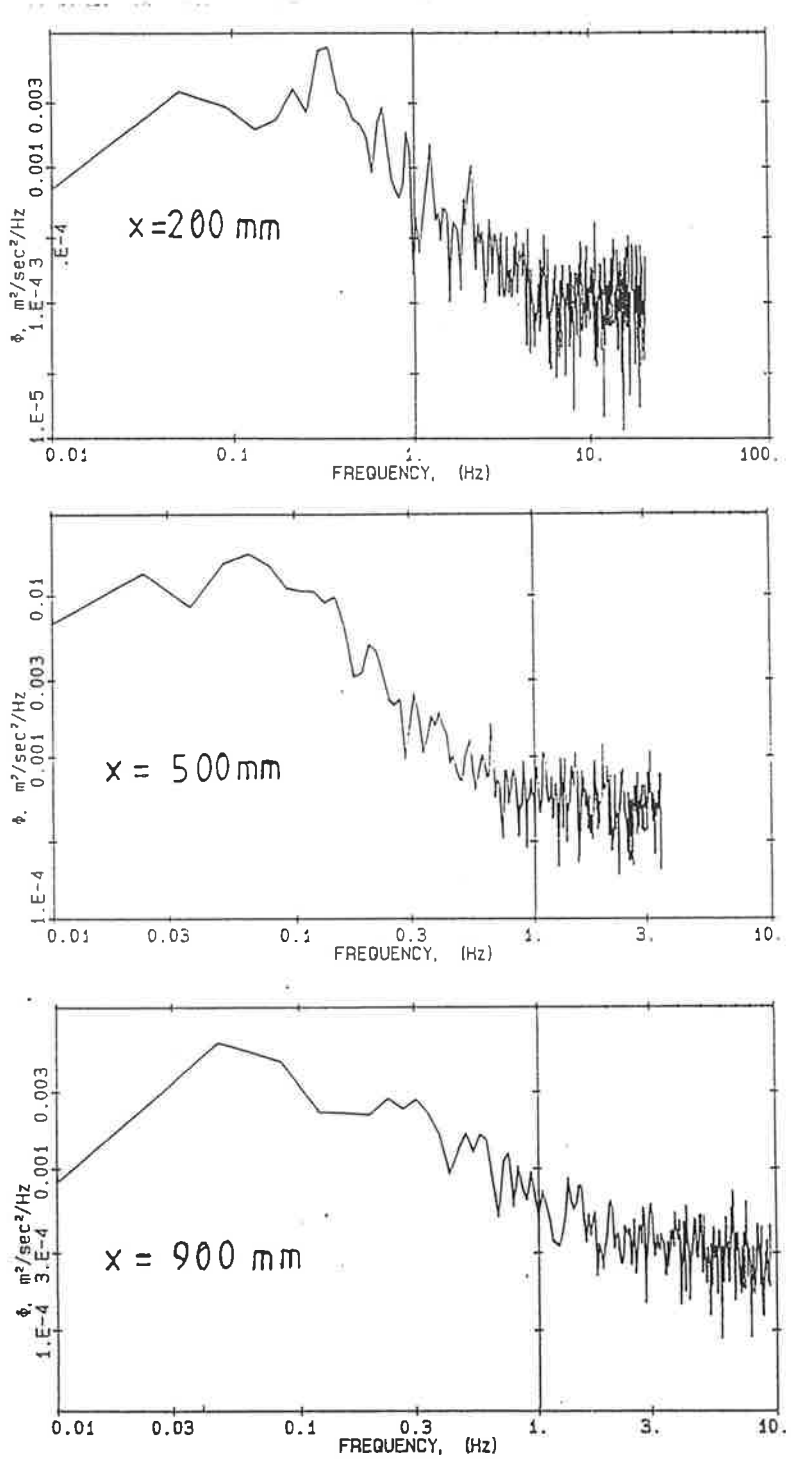


Figure 6.19: Power spectra of $u'$ at three downstream locations;
A.R. = 2.0; U = 0.30 m/sec.

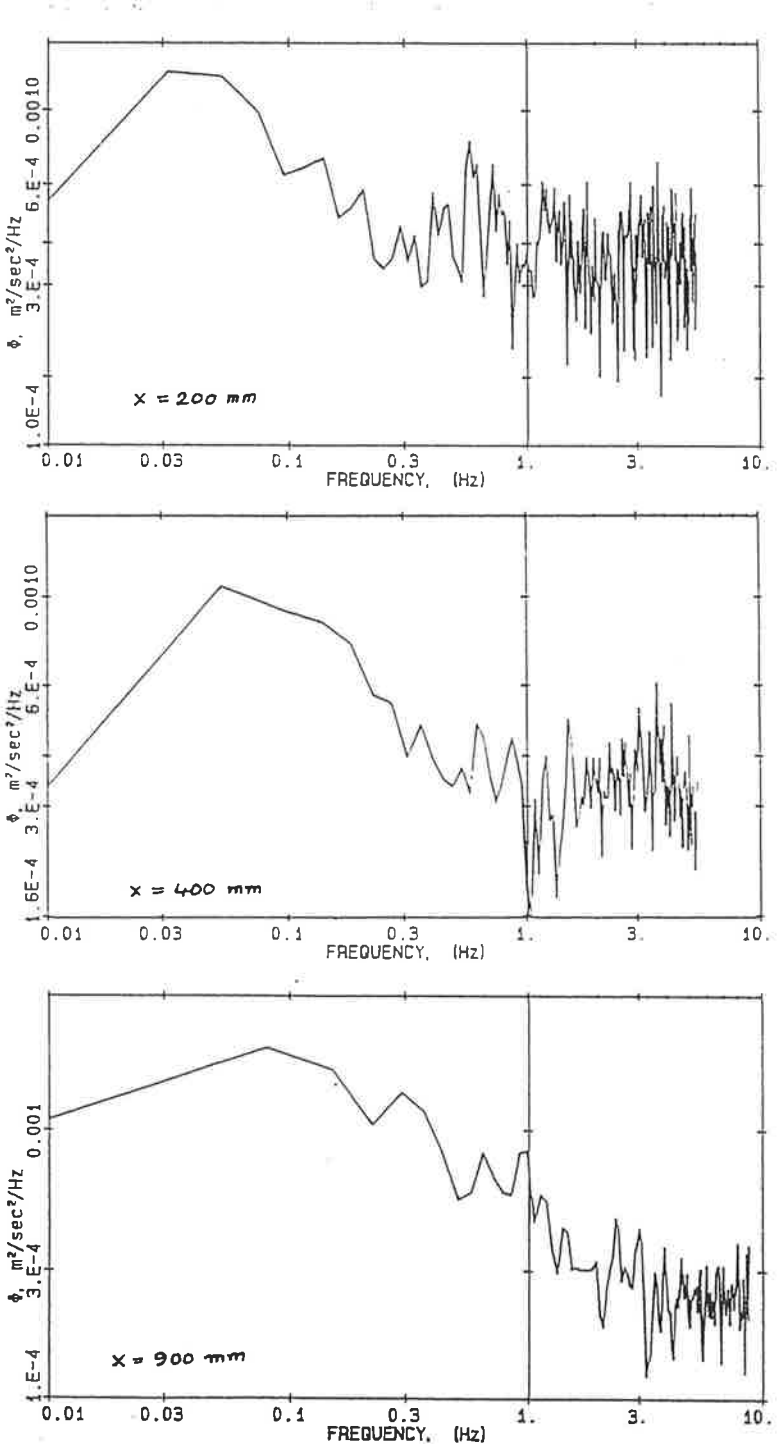


Figure 6.20: Power spectra of $v'$ at three locations within the separated flow region; A.R. = 2.0; U = 0.30 m/sec.

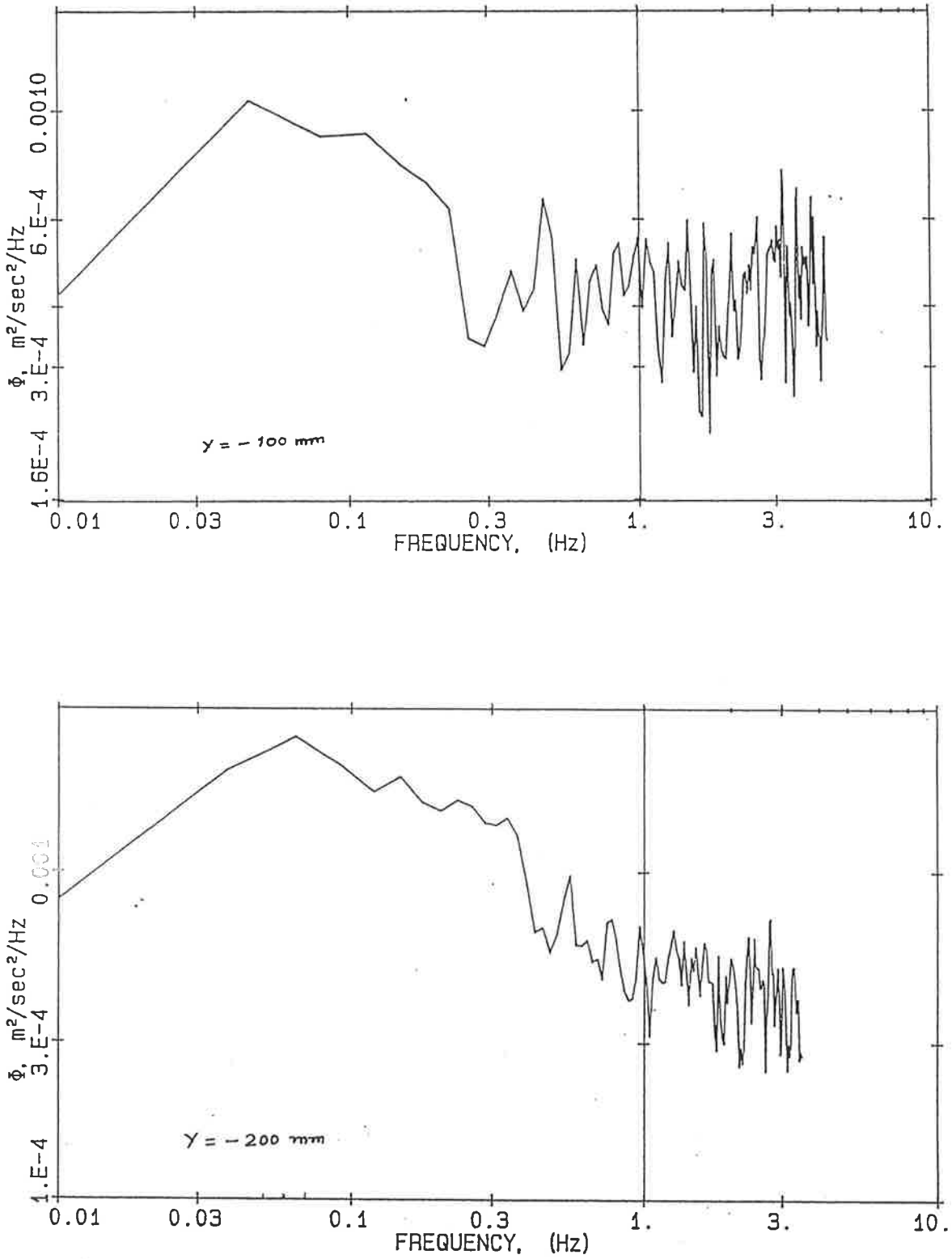


Figure 6.21: Spectra of $v'$ at x = 500 mm; and y = - 100 and - 200 mm; A.R. = 2.0; U = 0.30 m/sec.

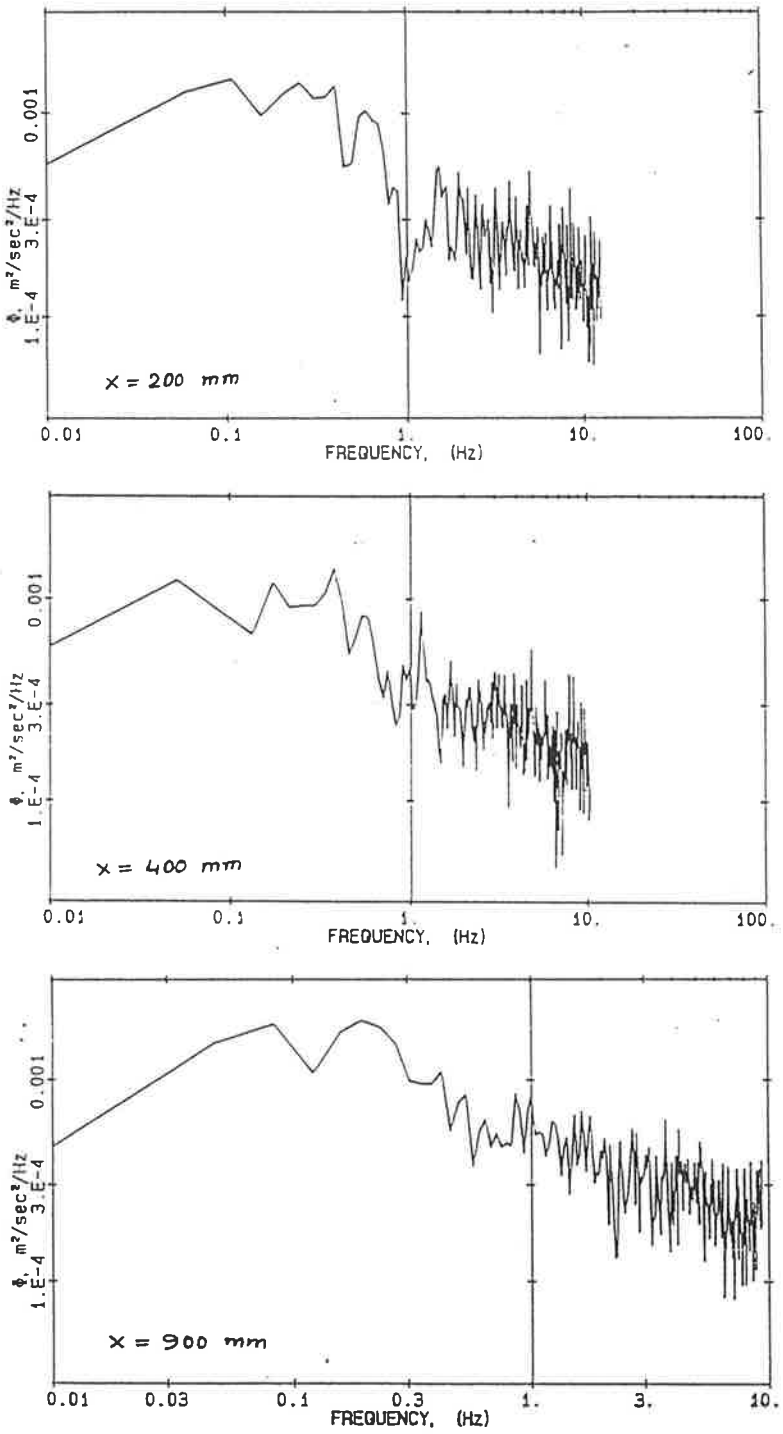


Figure 6.22: Spectra of $u'$ at several downstream distances;
A.R. = 2.0; U = 0.20 m/sec.

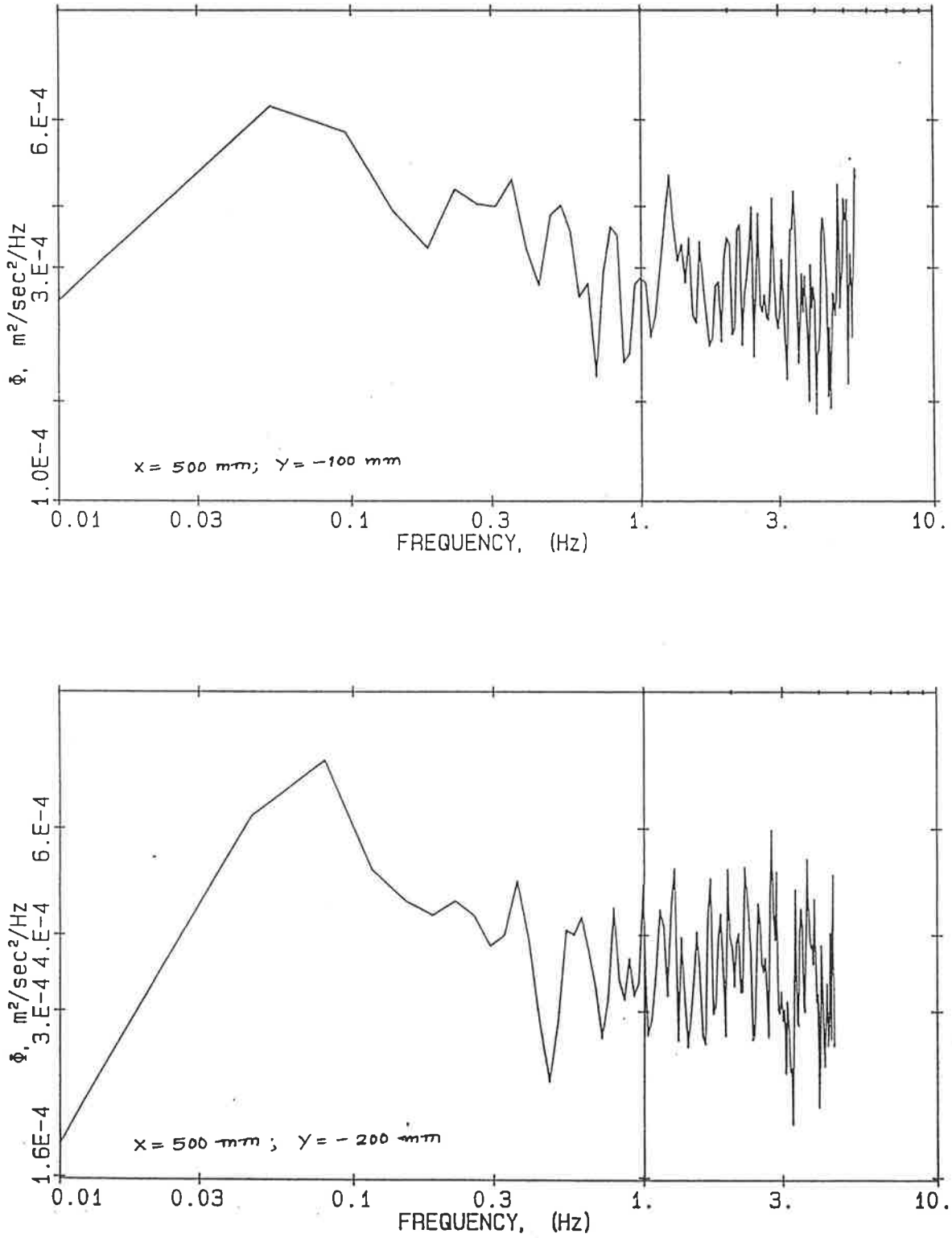


Figure 6.23: Spectra of $v'$ at locations within the separated region;
A.R. = 2.0; U = 0.20 m/sec.

also be noted from these spectra that the hump frequency decreases as the jet travels upstream (towards x = 200 mm) from the reattachment region (x = 900 mm).

Spectra of $v'$ measured at two lateral positions y = - 100 and - 200 mm both at x = 500 mm are shown in Figure 6.21. Both spectra contain humps at a frequency range similar to those in Figure 6.20 thus confirming the presence of pulsatile motion in the recirculating eddy front. Figures 6.22 and 6.23 shows power spectra of $u'$ and $v'$ respectively for the other flow condition (U = 0.20 m/sec) of the same aspect ratio, also indicating large structure passage in the separated shear layer and low frequency pulsating motion in the recirculating eddy which is responsible for the lateral movement of the shear layer.

## 6.7 Entrainment of Ambient Fluid

As mentioned in Chapter 2, there are controversies regarding the basic processes of entrainment of ambient fluid into the turbulent region. Two basic lines of approaches were discussed in section 2.5.4. The results of flow visualization experiments of the present study suggest that the second line of approach, i.e., entrainment by the engulfing action of the large coherent structures in the turbulent shear layer is the primary process. In this section however, without referring to the details of the basic entrainment processes, a simple analysis was performed following Albertson et al's (1950) analysis of volume flux, $Q/Q_o$ as a function of downstream distance, $x/B_o$.

Figures 6.24 and 6.25 show this analysis for different flow and geometrical conditions. The analysis of Albertson et al (1950) is given by the expression,

$$\frac{Q}{Q_o} = 1 + 0.080\frac{x}{B_o}$$

where,

$Q_o$ = the volume flux in the main stream flow at separation;
$Q$ = the local cumulative volume flux downstream of separation; and
$B_o$ = the width of the main stream channel.

The above expression was used by Albertson et al (1950) for the initial mixing layer region which they called the zone of flow establishment. The present calculations were made using the measured entrainment velocity at different downstream locations. It is however, to be noted that Albertson et al's analysis was performed on submerged jets with ambient fluid extended to infinity whereas in the present case the extent of ambient fluid has a finite boundary, i.e., limited in the separated recirculating region. The difference is immediately apparent in both Figures 6.24 and 6.25 which show that the volume flux ratio sharply decreases near reattachment region indicating re-entrainment of turbulent fluid into the separated region.

It can be seen from Figure 6.24, for the aspect ratio of 2.0, that in the initial region of the separated free shear layer (up to about $x/B_o = 0.5$) the volume flux rate of the present measurement agrees quite well with Albertson et al's analysis. After that the present measurement shows the entrainment to be in excess of what is predicted by the analysis (up to about $x/B_o = 1.85$). This excess entrainment can be attributed to the effects of the large coherent eddy structures in the shear layer and to the higher entrainment velocity due to recirculation in the separated region.

For the aspect ratio of 4.8, in Figure 6.25, the volume flux ratio for two different flow conditions differs quite substantially. Although the entrainment during the slower flow condition (U = 0.20 m/sec) is higher than the predicted amount, the faster flow condition (U = 0.30 m/sec) shows considerably lower values of the volume flux ratio with the downstream distance. The pattern of

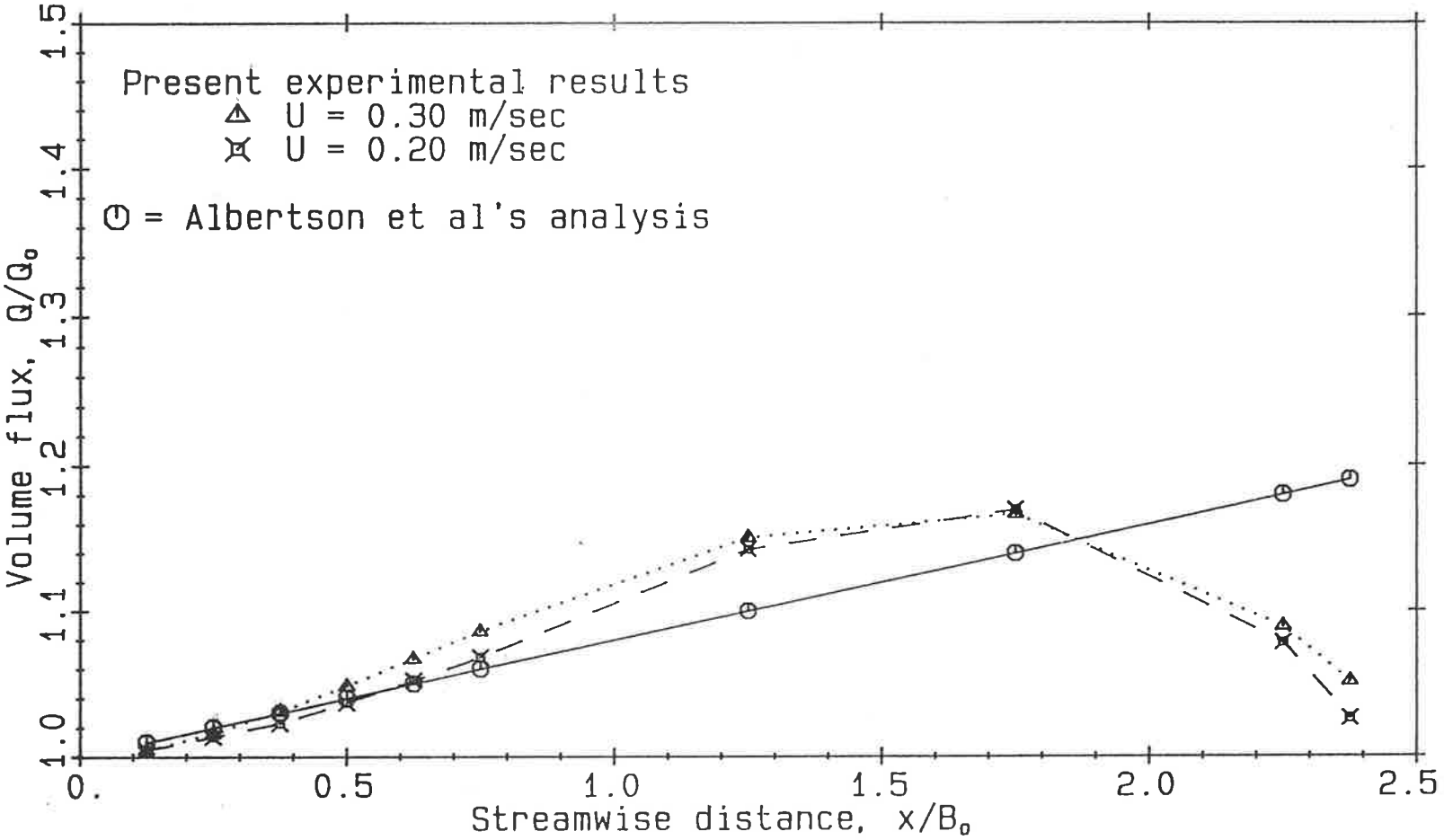


Figure 6.24: Volume flux ratio as a function of downstream distance for the aspect ratio of 2.0.

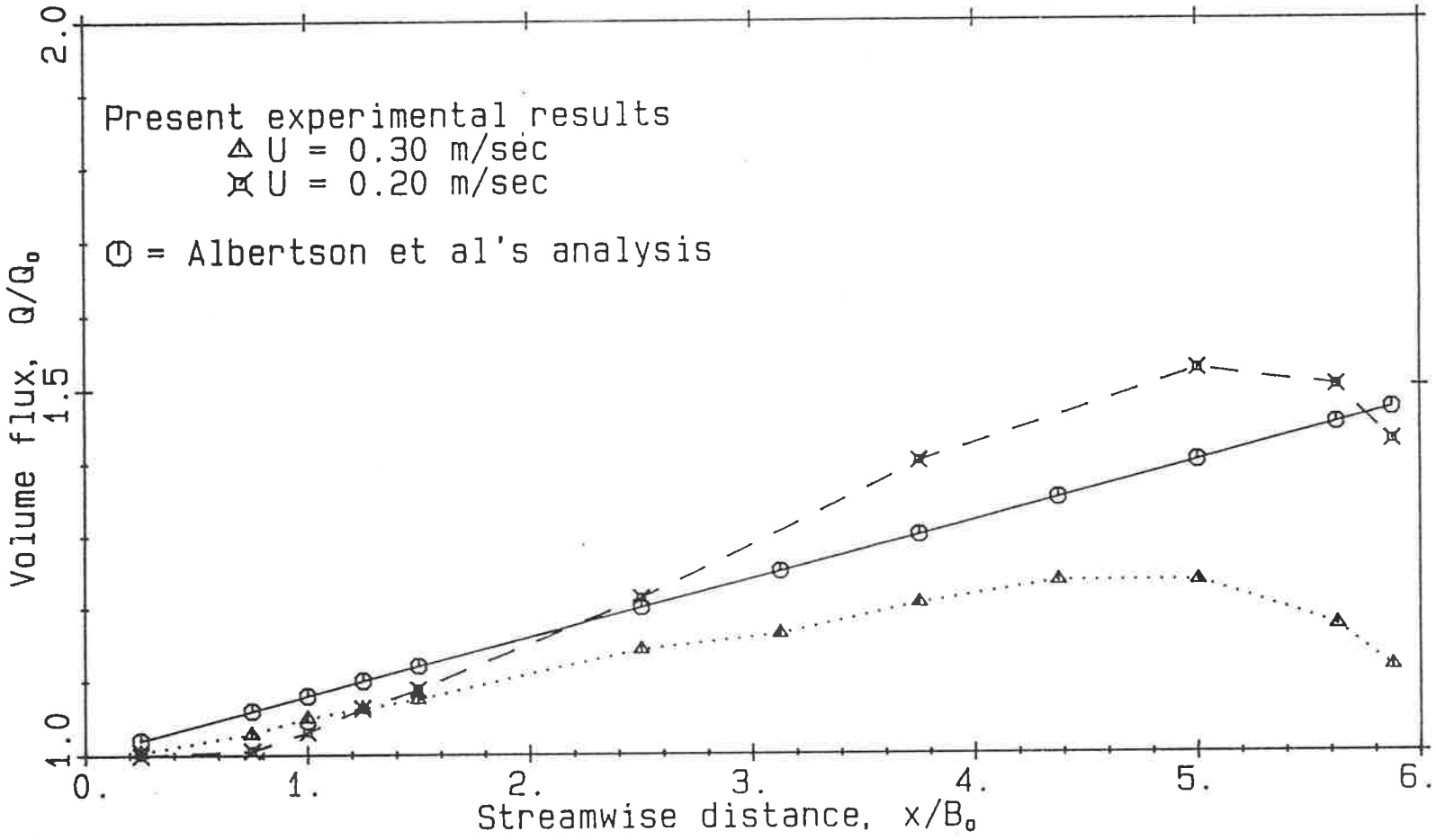


Figure 6.25: Volume flux ratio as a function of downstream distance for the aspect ratio of 4.8.

the curves for both cases however, is similar. The reason of such ambiguous difference is not clear. One possible explanation could be the 'spatial jitter' in the large eddy structures which was more in case of the faster free stream flow, particularly in the downstream region. Because of this spatial jitter, the large structures were relatively less coherent and hence the volume of entrainment was lower.

## 6.8 Discussion and Concluding Remarks

Measurements of the mean and the turbulence quantities in both streamwise and transverse directions revealed various complex but fundamentally important phenomena of the separated shear flow considered in this present investigation. The streamwise and transverse mean velocity profiles provided information about the separated shear layer growth and also the pattern of the recirculating eddy flow.

The differences in growth rates due to different free stream flow conditions raises an interesting point regarding the role of large coherent eddy structures in the separated shear layer. When the free stream velocity was lower, the large structures near the separation region were observed to be much more coherent and the initial pairing of structures were more organised hence a higher growth rate resulted than when the free stream velocity was higher. Also the large structures in the shear layer, for faster free stream flow, are subject to more intense interaction with the recirculating eddy front in the initial region and hence more spatial jitter leading to a much lower growth rate.

Browand and Troutt (1985) gave similar physical reasoning for the differences in growth rate but concluded that initial turbulence must interfere with pairing thus lowering the growth rate for initially turbulent boundary

layer condition. Troutt et al (1984) also attributed to the interference in vortex pairing by residual small scale boundary layer turbulence.

The development of fluctuating motions within the separated recirculating region also appears to be caused by the dynamics of the large coherent eddy structures present in the separated shear layer. The large peaks in the streamwise turbulence intensity profiles are a consequence of the induced motion of the large structures as they rotate and advect downstream. The transverse intensity profiles also exhibit strong peaks within the separated region particularly near reattachment and at upstream regions where the recirculating eddy front approaches the shear layer. These fluctuations are developed due to the presence of pulsatile motion in the recirculating eddy jet which is caused by the by the intermittent deflection of structures fluid mass into the separated region. Such deflection again causes the lateral movement of the shear layer contributing to the uneven entrainment of fluid into the region.

These peak intensities were also noticed by Mehta (1979) in his measurements of flow field in a sudden expansion and the probable reason was speculated to be due to a complex interaction of return flow in the eddy pocket with the turbulent boundary layer inside the eddy, and with the shear layer.

The pulsating motion present in the recirculating eddy jet is confirmed from the low frequency peak exhibition in the power spectra of $v'$ measured within the separated region. This pulsating motion is responsible for the interaction between the recirculating eddy flow and the shear layer structures and due this interaction periodic lateral movement of the shear layer occurs. Such periodic low frequency motion is also apparent in the power spectra of $u'$ in the low frequency region.

Finally, the results of this phase of experiments provide useful information regarding the behaviour of the mean flow pattern and the turbulent characteristics for the separated shear flow considered. These results complement

and support the findings of the flow visualization experiments.

# Chapter 7

# Presentation and Discussion of Results - Phase III

## 7.1 Introduction

This chapter comprises the results of tracer concentration measurements in the separated flow field which were performed in the third phase of the experimental programme. The objectives of the measurements, as mentioned earlier in Chapter 1 and 4, were to obtain an insight into the processes of mixing and mass transfer in a separated shear flow considered in the present investigation.

First the temporal variations of the instantaneous tracer concentrations at different locations of the flow field are presented through iso-concentration contours. The short time mean concentration and the power spectra of con-

centration fluctuations at various important locations are also presented. Mass transfer analysis was then performed based on the short time mean concentration and applying the conventional gradient transfer hypothesis. Finally, an effort is made to demonstrate the effects of large coherent eddy structures found in the separated shear layer on the mixing and mass transfer processes. The results are discussed wherever appropriate according to the objectives outlined earlier in Chapter 4.

## 7.2 The Concentration Field

### 7.2.1 Iso-Concentration Contours

The iso-concentration contours of Figures 7.1, 7.2, 7.3 and 7.4 show the distribution of tracer concentration on lateral planes in the separated flow field for different flow and geometrical conditions. Each contour map illustrates the change of instantaneous concentration with time at a particular transverse section of the flow field. The concentration contours were obtained from the instantaneous values of tracer concentration at different points of the transverse section every 10 seconds interval from a continuous experimental run of approximately 90 seconds long. The tracer was released from the back end of the separated region (position 3) in all cases and the release was continued until the tracer spread over the entire separated region. The release was then stopped and the measurements commenced after allowing some time to minimize the effects of any disturbance which may have caused by the release. The instantaneous concentration values were normalized by the maximum concentration value in the entire separated region for a particular experimental run. The contours are plotted as a function of the transverse distance (non-dimensionalized by the width of the separated region) and the time.

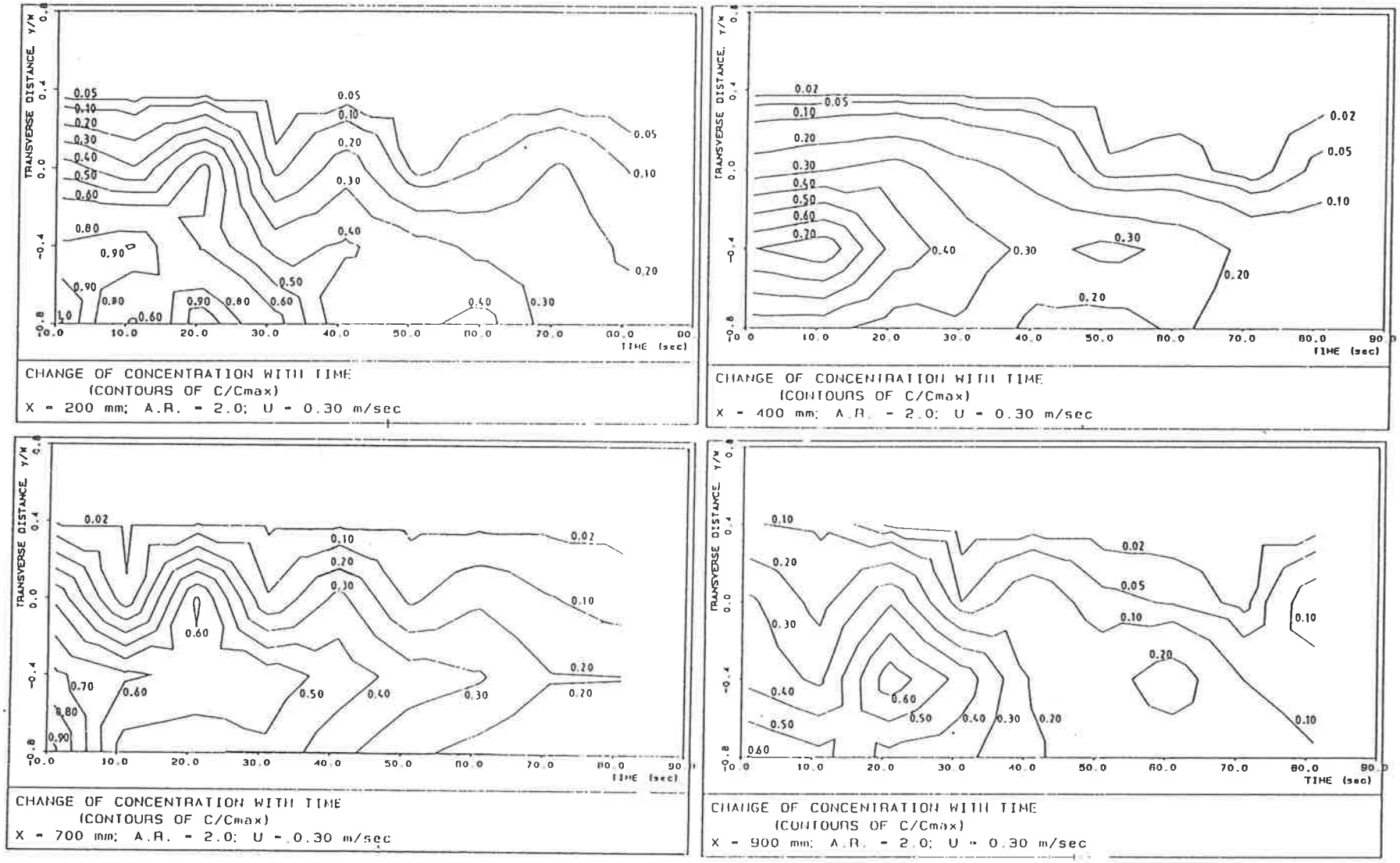


Figure 7.1: Contours of $C/C_{max}$ at different downstream locations; values of successive contours are indicated; A.R. = 2.0; U = 0.30 m/sec.

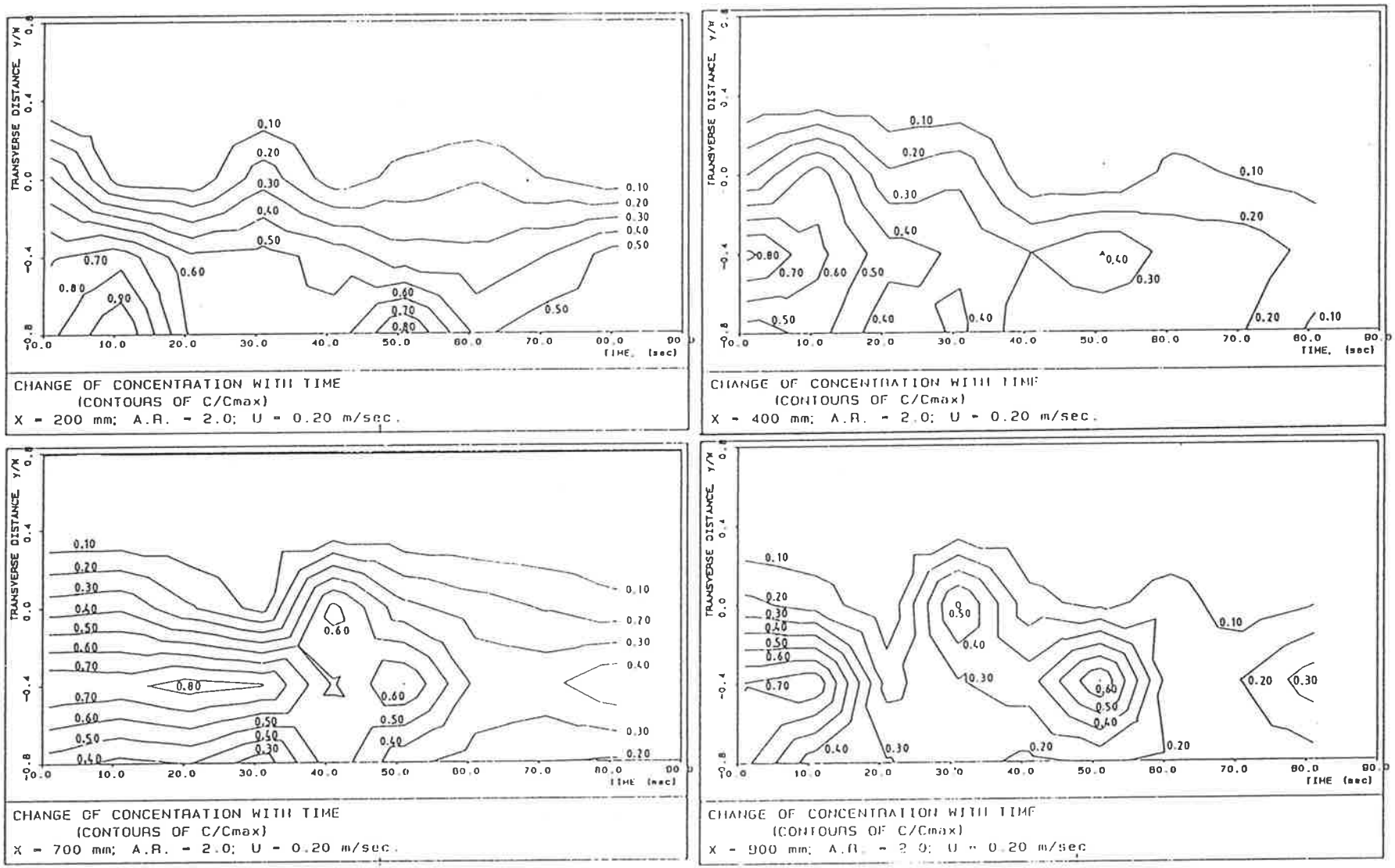


Figure 7.2: Contours of $C/C_{max}$ at different downstream locations; values of successive contours are indicated; A.R. = 2.0; U = 0.20 m/sec.

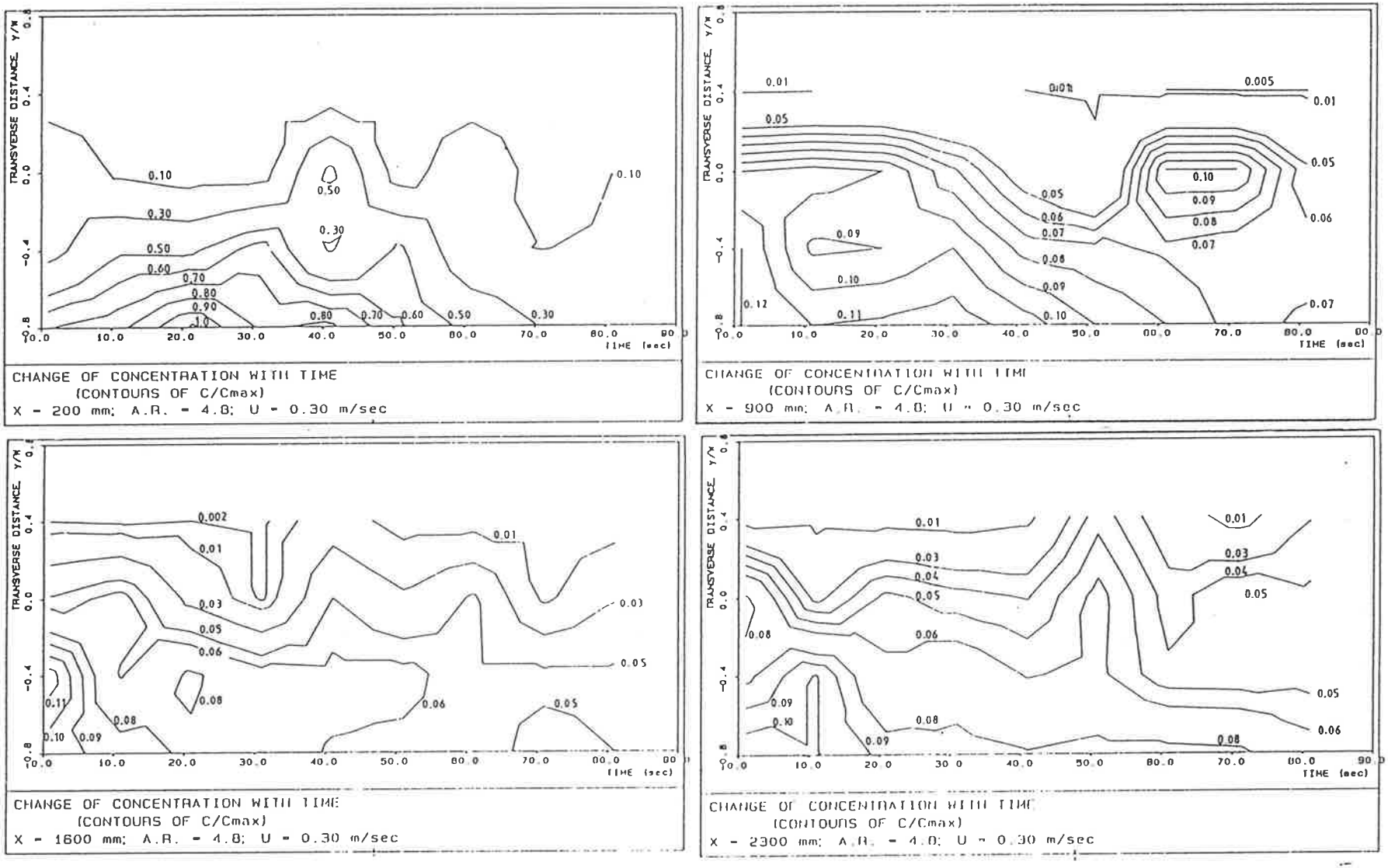


Figure 7.3: Contours of $C/C_{max}$ at different downstream locations; values of successive contours are indicated; A.R. = 4.8; U = 0.30 m/sec.

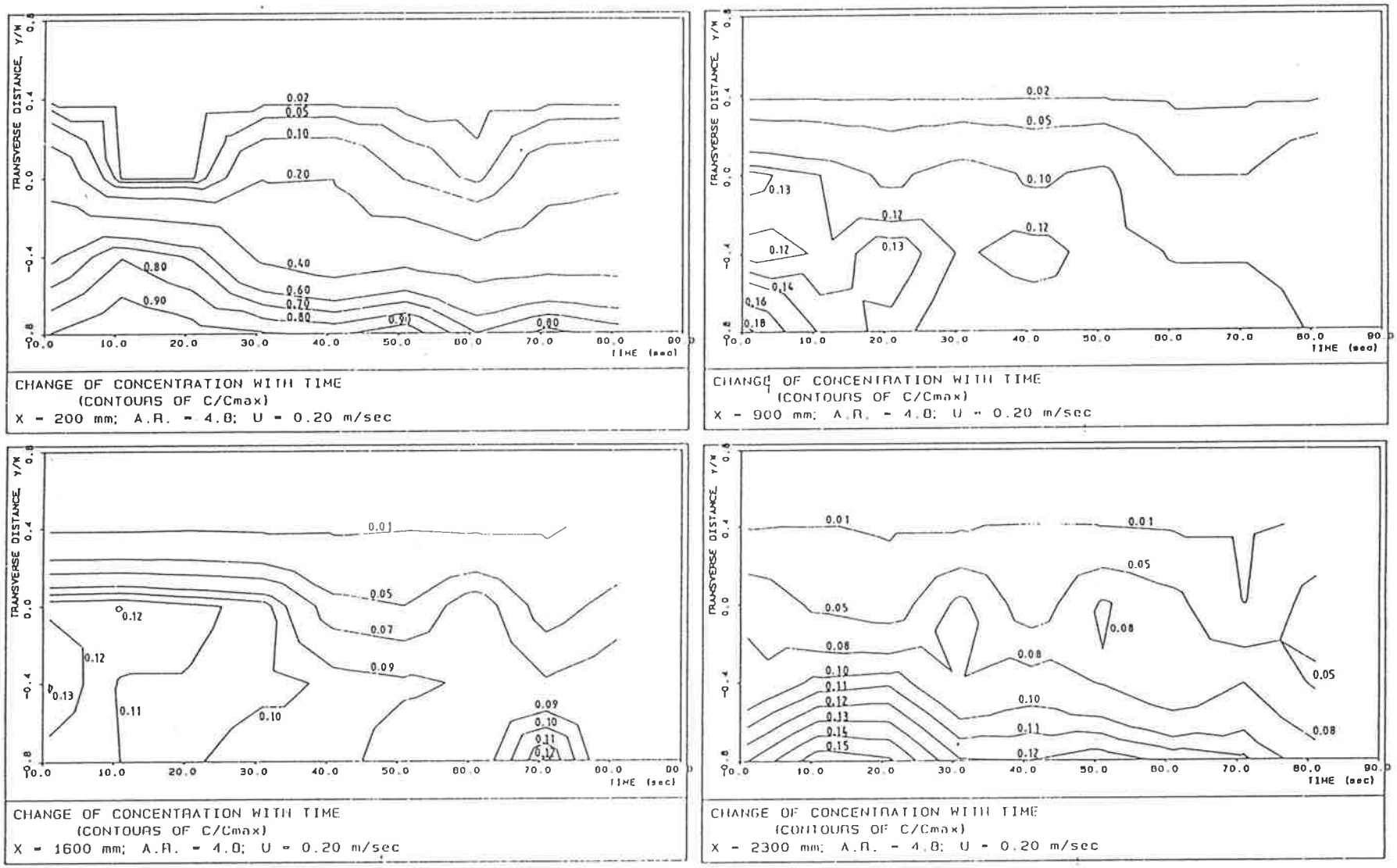


Figure 7.4: Contours of $C/C_{max}$ at different downstream locations; values of successive contours are indicated; A.R. = 4.8; U = 0.20 m/sec.

The concentration contours clearly demonstrate the spatial and temporal variation of the concentration field in the separated region. From Figures 7.1 and 7.2 it appears that x/W = 0.4 (between y/W = -0.4 and -0.8) is the region of maximum concentration. Also at x/W = 1.4, between y/W = -0.4 and -0.8 (y/W = -0.4 only in Fig.7.2c) high concentration values can be noticed. This is consistent with the observations of the flow visualization experiments which suggest that the region upstream of x/W = 0.4 and the region at x/W = 1.4 and y/W = -0.4 are the two relatively stagnant areas with lower diffusivity. This is also apparent in the mean velocity profiles presented in the previous chapter.

Another important feature of these contour plots is the decay of concentration with time. In Figure 7.1a, it can be noticed that at y/W = -0.8 the decay of concentration is not consistent. At first the concentration decreases with time up to about 10 seconds and then increases again at about the 20 second mark and then decreases again. At about the 60th second the concentration remains unchanged from its value near 40th second at $C/C_{max}$ = 0.40. This, in real terms, is an increase in concentration at that point in time. Therefore, the concentration at that point is not decaying consistently at certain rates rather it decreases and suddenly increases after some time and that the process appears to be quasi periodic. This can also be noticed in the similar location in Figure 7.2a. In Figures 7.1d and 7.2d this particular feature of concentration decay can be noticed in the region at y/W = -0.4 where the concentration alternately decreases and increases with time.

This result is not in agreement with that of Westrich (1976) who found, in a similar study, that the concentration decreases exponentially with time for steady flow conditions. This discrepancy between the result of Westrich (1976) and the present study is to be expected because Westrich's result is based on a single point measurement which was located in a relatively stagnant area which he considered as representative for the entire 'dead zone'

with an assumption that the half-life period of concentration would vary only within 10%.

The present unsteady nature of concentration decay at several locations is considered to be associated with the pulsatile motion in the recirculating eddy. This pulsatile motion in the recirculating eddy, caused by the intermittent passage of large coherent eddy structures in the separated shear layer, was also revealed in the visual observations of Phase 1 experiments as well as in the spectra of time records of velocity fluctuations measured in Phase 2 experiments.

A similar result can also be noticed in case of the larger geometry (A.R. = 4.8) shown in Figures 7.3 and 7.4. Such unsteady decay of concentration is less apparent in Figure 7.3 in which case the free stream flow was faster. The reason for this is that the tracer concentration in the recirculating eddy gets diluted very quickly due to higher turbulent diffusion. The contours of Figure 7.4 (at about y/W = -0.8 of Fig 7.4a; y/W = -0.4 of Fig 7.4b and y/W = -0.8 of Fig 7.4c), in which the free stream flow was slower, show such unsteady decay of concentration. However, it must be remembered that these contours are constructed by using the instantaneous concentration values at every 10 seconds interval and there remains an uncertainty of picking up a value which is unreasonably high or low due to non-uniform mixing. Also, inherent in the calculation of such contours is the assumption of linear variation of concentration over the period of 10 seconds. In the following subsection therefore, an attempt is made to present the time mean concentration decay at various points of the separated flow field in order to minimize the above uncertainty and to see whether the effects of pulsatile motion is reflected in the concentration decay curve.

### 7.2.2 Short Time Average Concentration Decay

Figures 7.5 to 7.10 show the decay of short time average concentration at different locations of the separated region for aspect ratio 2.0. Figures 7.5 to 7.7 show concentration decay for the faster free stream flow case whereas Figures 7.8 to 7.10 are for the slower free stream flow case. The purpose of short time averaging is to smooth out the small scale concentration fluctuations and yet retain the interesting features associated with the large scale coherent eddy structures in the separated shear layer and with the recirculating eddy in the separated region. Averaging over a period of one second i.e., an average over 100 values, was considered appropriate in the present case considering the average passage time of large eddy structures in the shear layer of the order of one second. The tracer release condition was similar as mentioned in the previous sub-section and the short time average (STA) concentration was normalized by the maximum average value of the entire region.

The plots of Figure 7.5 show the decay of STA concentration at four different downstream locations along the separation line (y = 0). The peaks in the decay curve certainly demonstrate the periodic passage of coherent eddy structures. However, it would be misleading if these peaks are considered as a measure of structures passage because the peaks can be developed between structures as well where the elongated 'braid' region contains substantial amount of tracer concentration which pass these locations. A more realistic measure of large structure passage frequency would be the peaks at the high speed edge of the shear layer as was suggested by Hussain and Zaman (1985). For instance, plot (d) of Figure 7.5 shows a decreased number of peaks as one would expect at a downstream location but plots (b) and (c) do not manifest a similar trend. Moreover the peaks do not show any decaying trend due to the continuous supply of tracer concentration from the separated region for entrainment by the large structures in the shear layer.

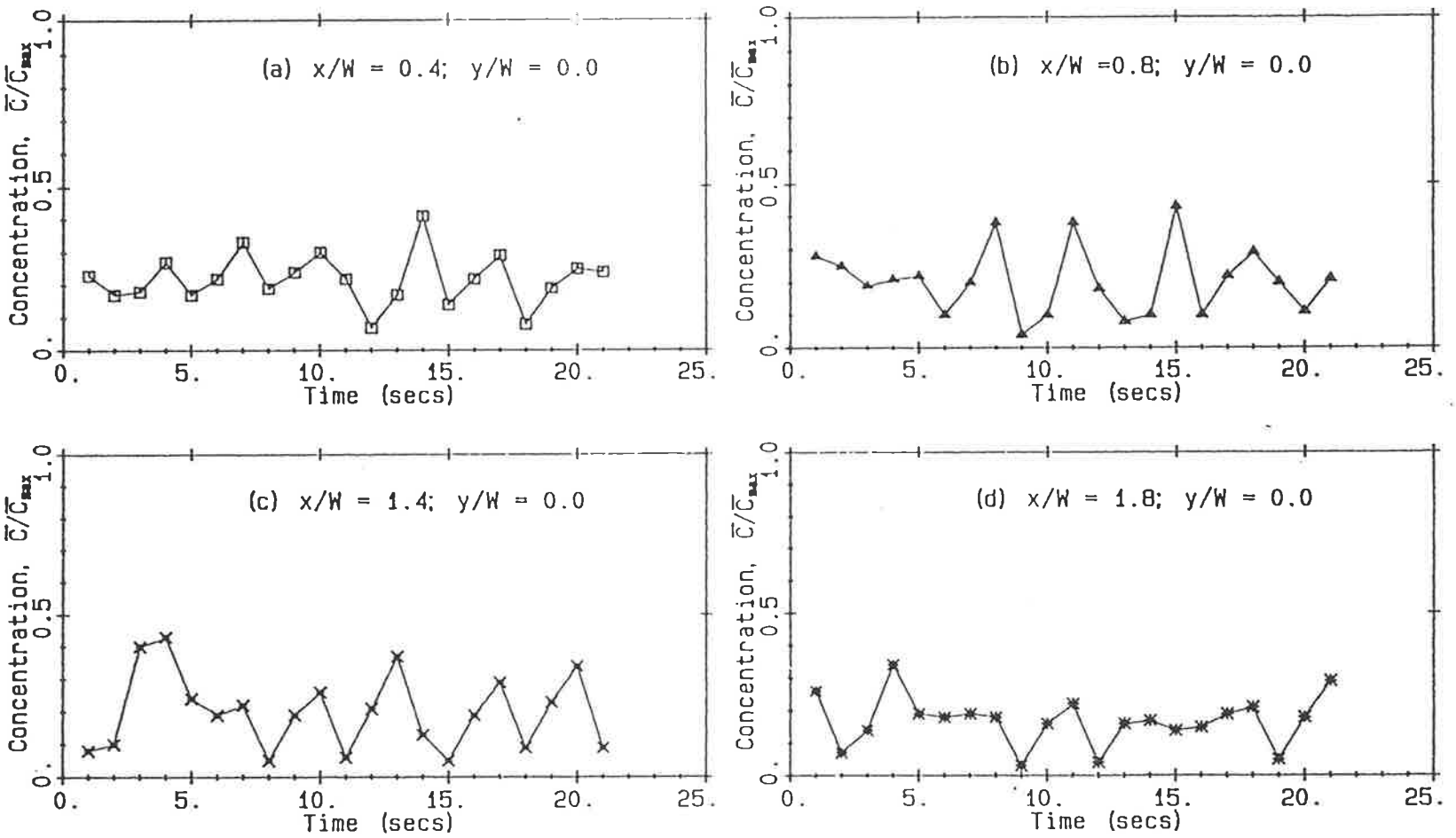


Figure 7.5: Plots of short time average concentration at different downstream locations; y/W = 0.0; A.R. = 2.0; U = 0.30 m/sec.

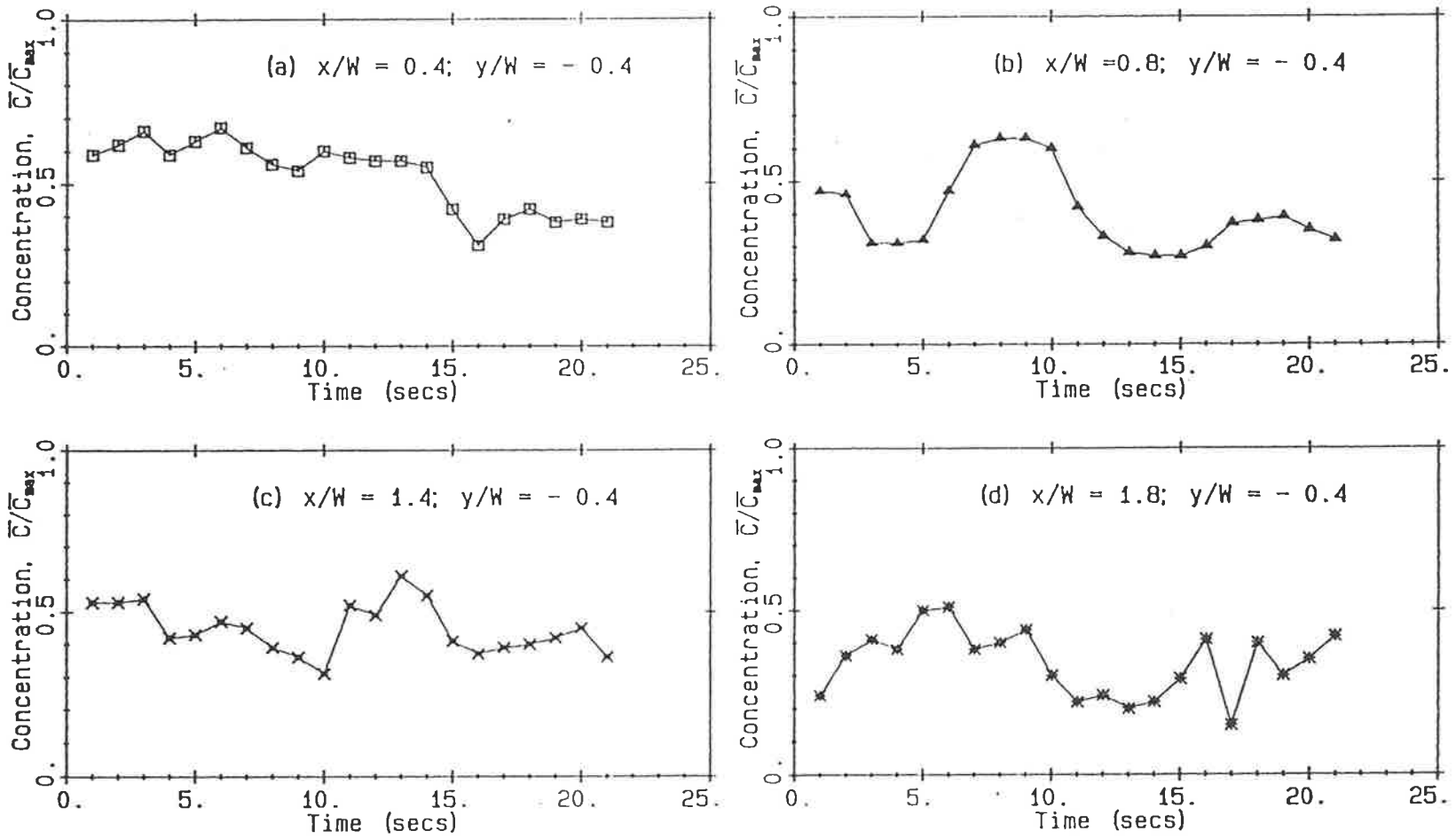


Figure 7.6: Plots of short time average concentration at different downstream locations; y/W = - 0.4; A.R. = 2.0; U = 0.30 m/sec.

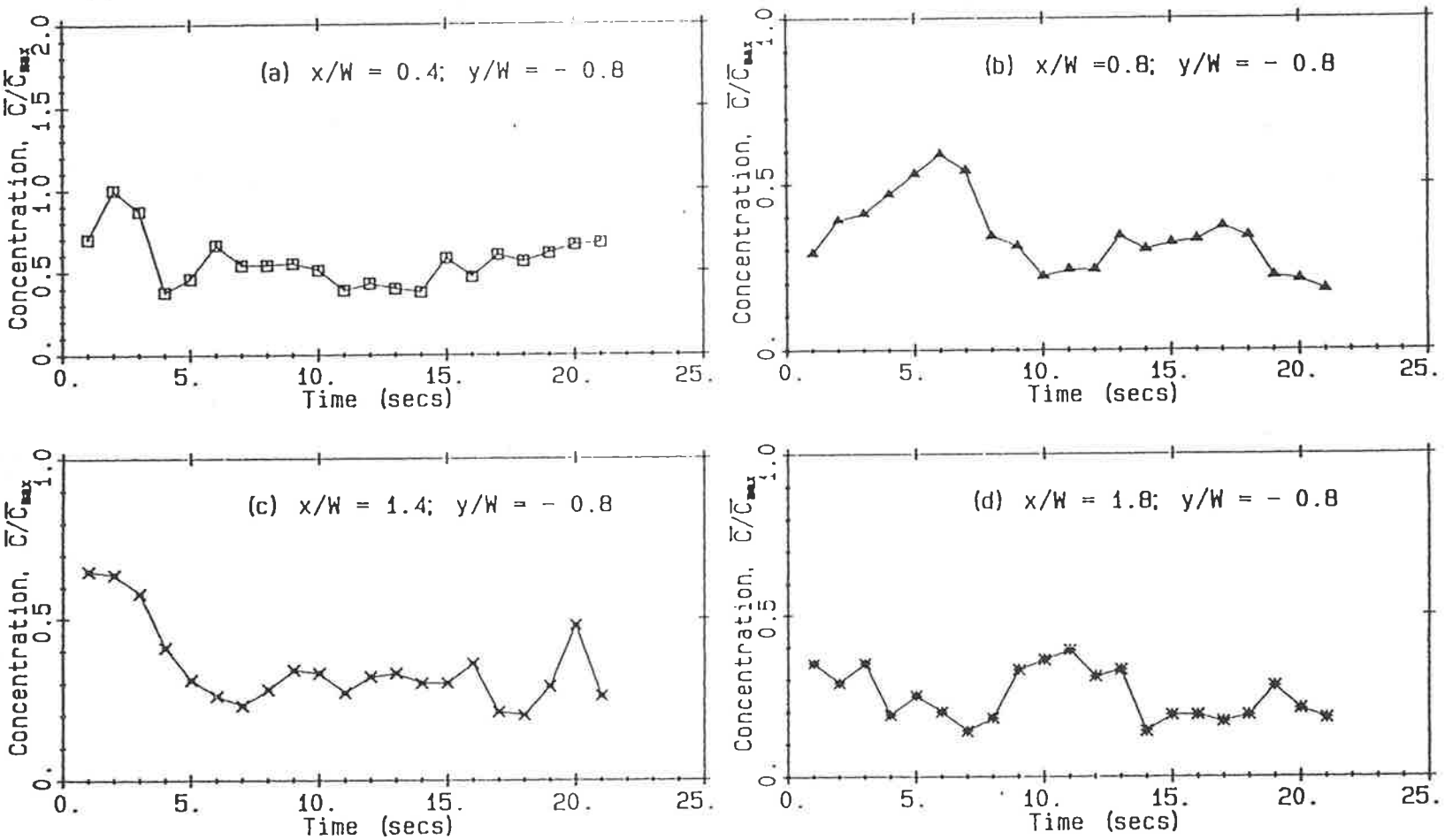


Figure 7.7: Plots of short time average concentration at different downstream locations; y/W = - 0.8; A.R. = 2.0; U = 0.30 m/sec.

Figure 7.6 shows some interesting plots at similar downstream locations almost at the middle of the separated region (y = - 200 mm). Plot (a) shows the decay of concentration at an approximately uniform decreasing rate indicating the region to be relatively stagnant. The shape of the curve of plot (b) is of particular interest in which the STA concentration decreases in an unsteady manner producing several peaks within the period considered. The location of the measuring probe for this plot was approximately in the middle of the recirculating eddy front approaching the shear layer. As was observed in the visual experiments, the undulating shape of the decay curve is most likely to be associated with the quasi periodic pulsatile motion which was found to exist in the recirculating eddy.

Part of the highly concentrated large eddy structures in the shear layer, as they impinge on the reattaching surface, is deflected back in the separated region and thus the recirculating eddy intermittently carries a blob of tracer cloud of relatively high concentration giving rise to a higher value of average concentration. The concentration decay curves for which the probes were located on the travel path of the recirculating eddy exhibit more or less similar behaviour. For instance, plots (b) and (d) of Figure 7.6 and the plots (b), (c) and (d) of Figure 7.7 indicate this process. However, it should be pointed out here that the concentrated tracer blob torn from the large structure at reattachment is being diffused as it travel along the recirculating eddy due to small scale fluctuating motion thus producing varying peak levels on the decay curves at different locations. Also there is diffusive transfer of tracer concentration from the relatively stagnant regions (e.g., at x/W = 0.4, y/W = - 0.4 and - 0.8; and at x/W = 1.4, y/W = - 0.4) into the recirculating eddy, although at a lower rate, changes the average concentration level.

Plots (a) and (c) of Figure 7.6 and plot (a) of Figure 7.7 are for the relatively stagnant regions. Plot 7.7a is for the most stagnant part of the separated region showing very high concentration at that point (note change of vertical

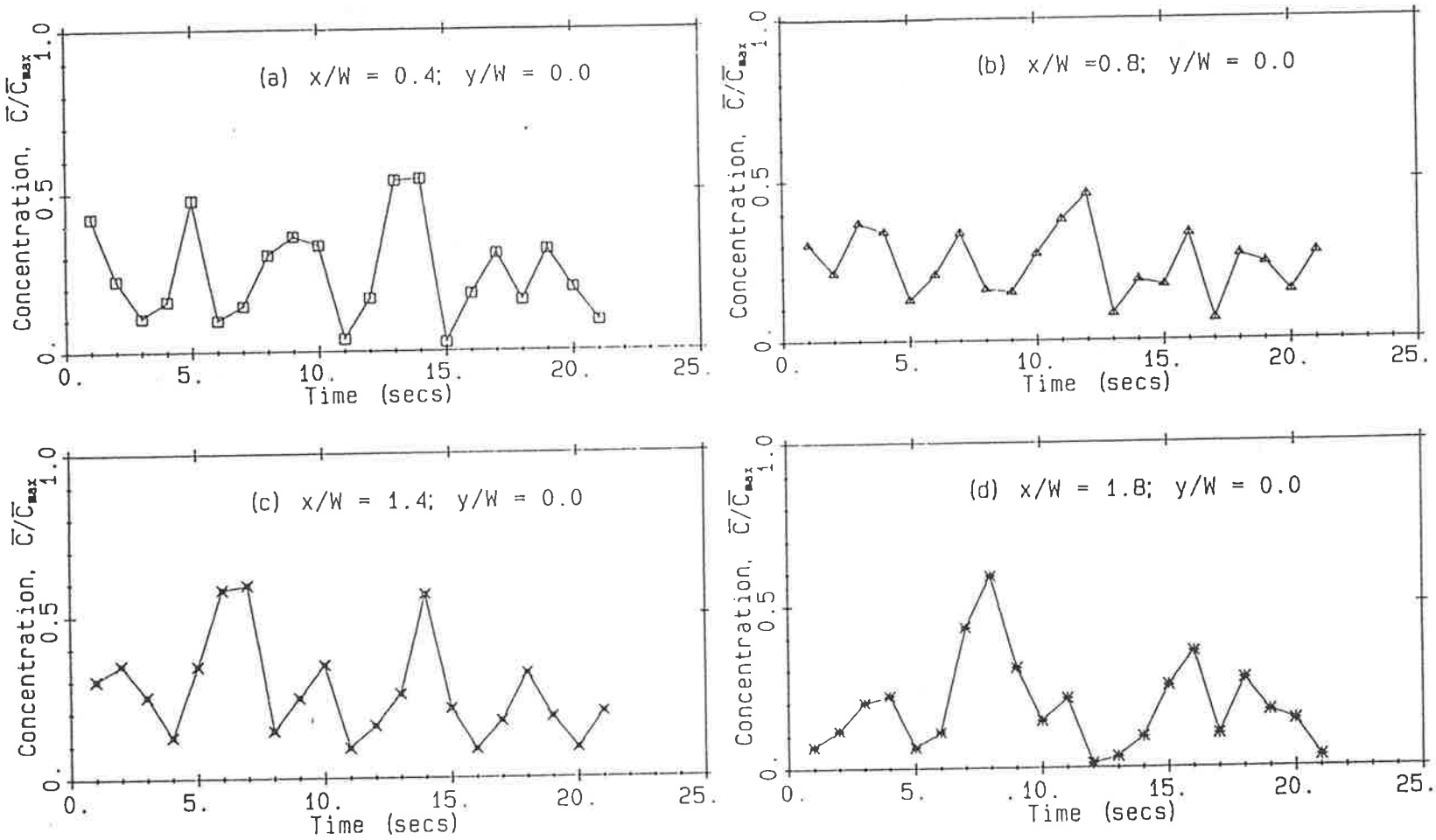


Figure 7.8: Plots of short time average concentration at different downstream locations; y/W = 0.0; A.R. = 2.0; U = 0.20 m/sec.

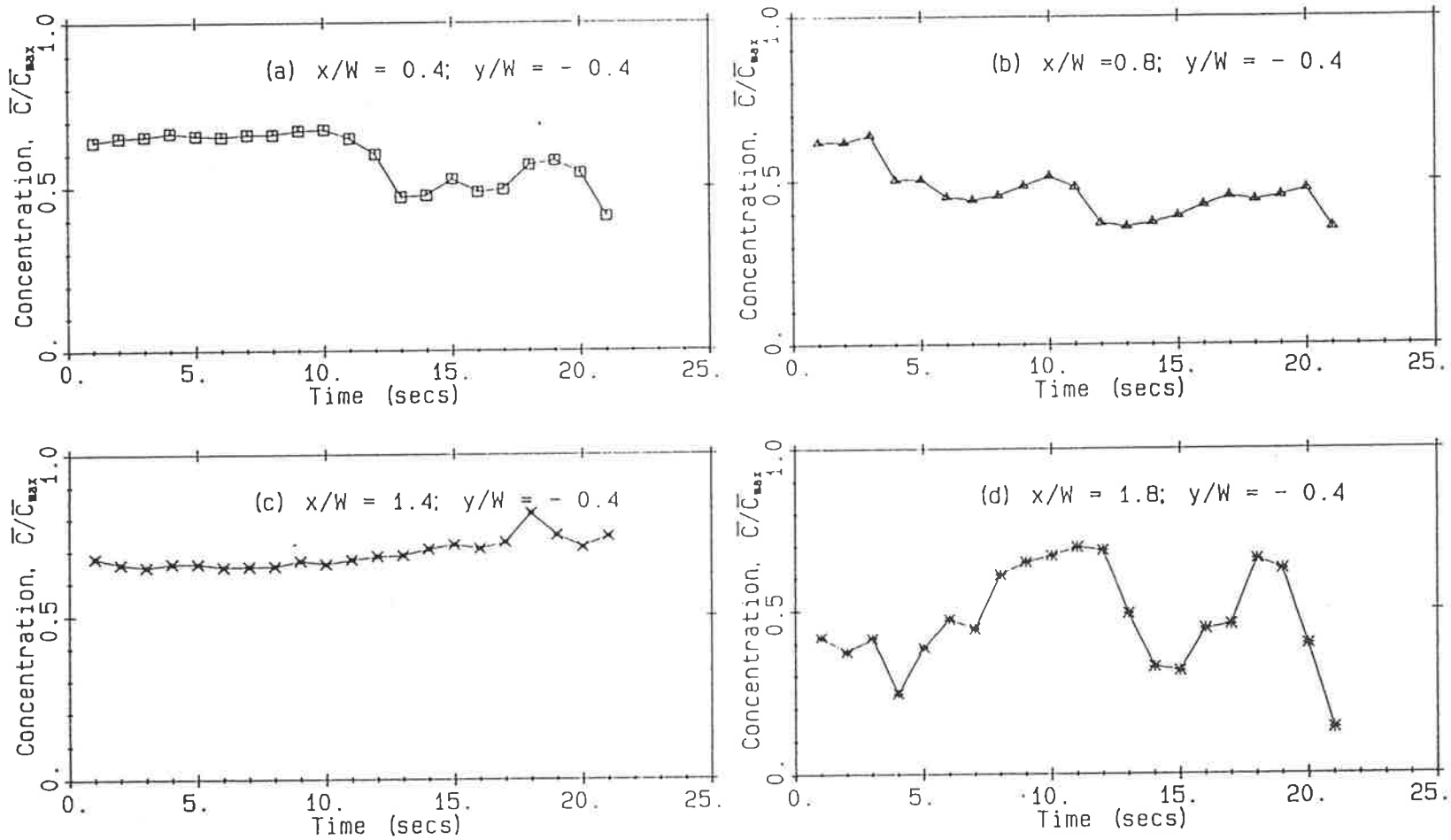


Figure 7.9: Plots of short time average concentration at different downstream locations; y/W = - 0.4; A.R. = 2.0; U = 0.20 m/sec.

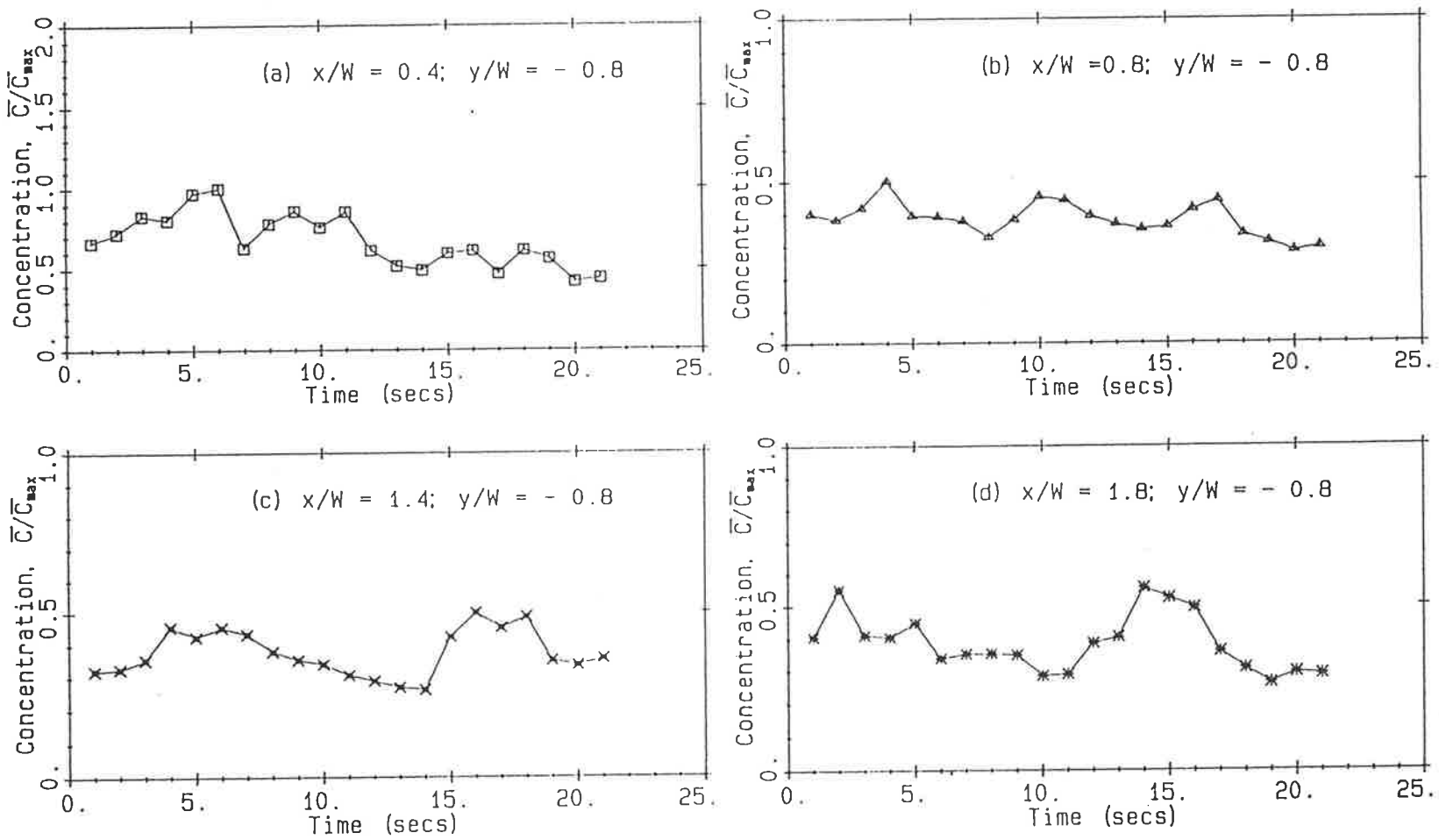


Figure 7.10: Plots of short time average concentration at different downstream locations; y/W = - 0.4; A.R. = 2.0; U = 0.20 m/sec.

scale in this plot). As can be seen from the curve the decay is very slow due to very low diffusivity in the region. The plot at x/W = 1.4 and y/W = - 0.4 of Figure 7.6 appears to be rather unusual. Located almost at the centre of the recirculating eddy, although from visual observations the region was considered to be essentially stagnant, the unsteady nature of the concentration decay curve indicates the development of fluctuating motion in the region. This was also observed in the turbulence intensity profiles in both transverse and longitudinal directions presented in the previous chapter. As indicated earlier, the passage of the large eddy structures in the shear layer above that region induces the development of fluctuating motion. As the large structure rotates and advects downstream through that region, some tracer mass from the stagnant region are being entrained by the engulfing action of the large structure thus introducing a turbulent motion in the region.

Another associated process which occurs in this region and also in the other relatively stagnant region is the tracer accumulation from the surrounding recirculating eddy. The diffusive transfer of tracer mass by the surrounding recirculating eddy accumulates into these areas and because the transfer rate from these regions is low due to lower diffusivity, the average concentration level occasionally becomes high. The major transfer of tracer mass from these regions is through entrainment by the large eddy structures of the shear layer. Thus if the entrainment rate is low for some reason (for instance, at the downstream end of the separated shear layer where eddy pairing is often prohibited due to lack of appropriate phase relationship between the fundamental and the sub-harmonic), the tracer accumulation rate becomes higher than the transfer rate within the stagnant regions. Therefore, the average concentration decay curve sometimes shows an increasing trend. This is particularly manifested in the case when the free stream mean velocity was lower (see for instance plot (c) of Figure 7.9).

Figures 7.8, 7.9 and 7.10 show the plots of STA concentration decay curves

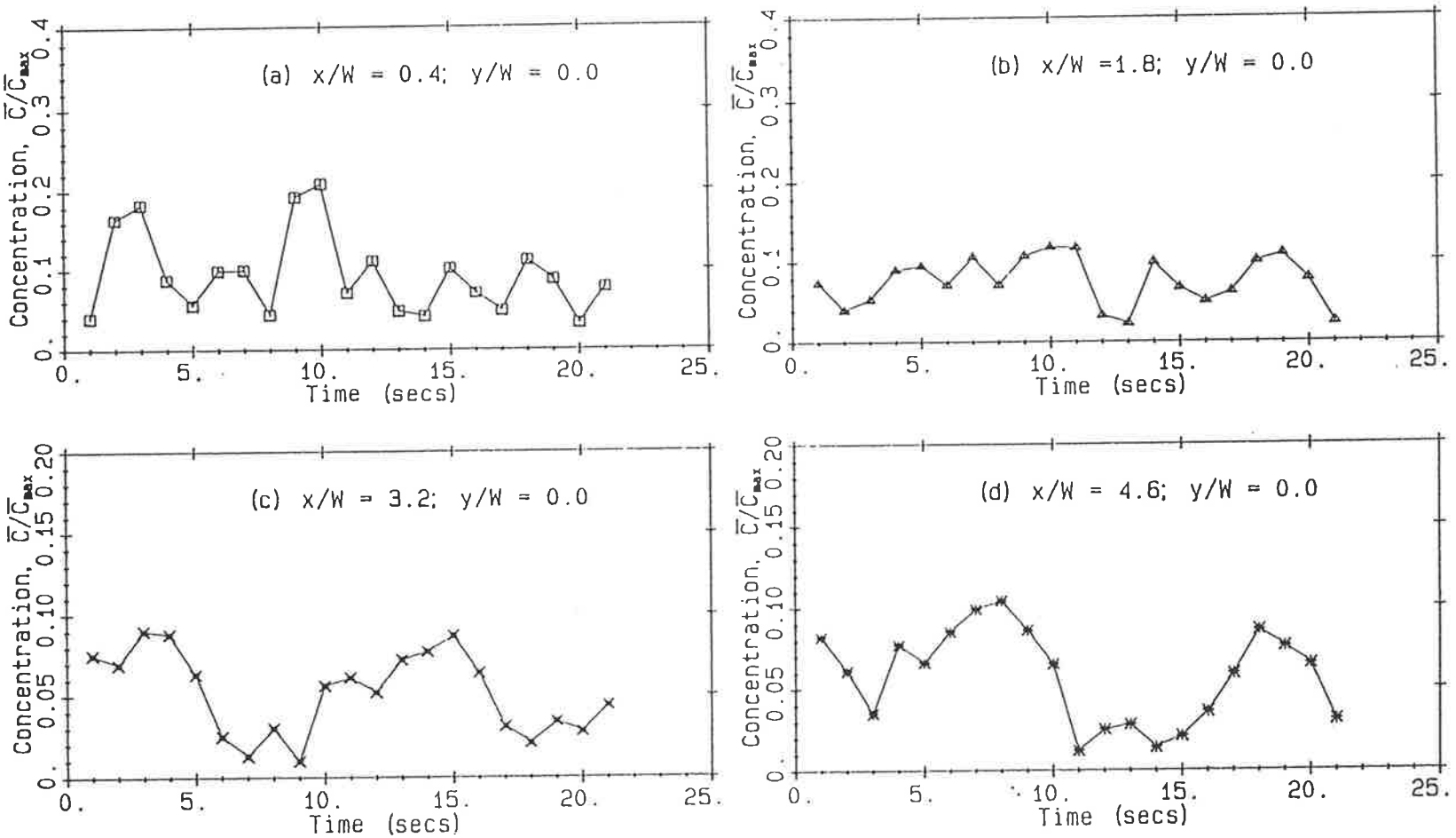


Figure 7.11: Plots of short time average concentration at different downstream locations; y/W = 0.0; A.R. = 4.8; U = 0.30 m/sec.

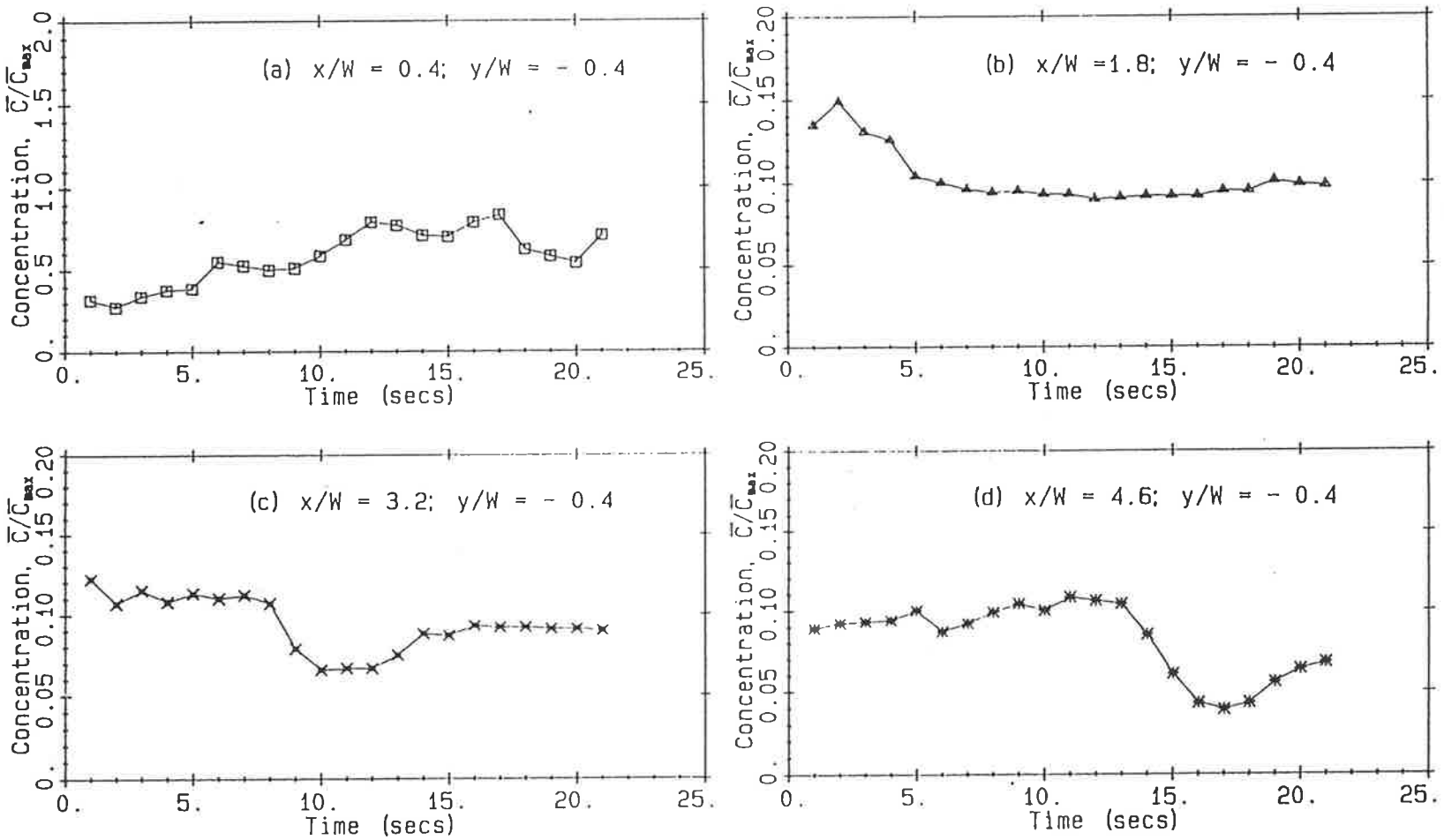


Figure 7.12: Plots of short time average concentration at different downstream locations; y/W = - 0.4; A.R. = 4.8; U = 0.30 m/sec.

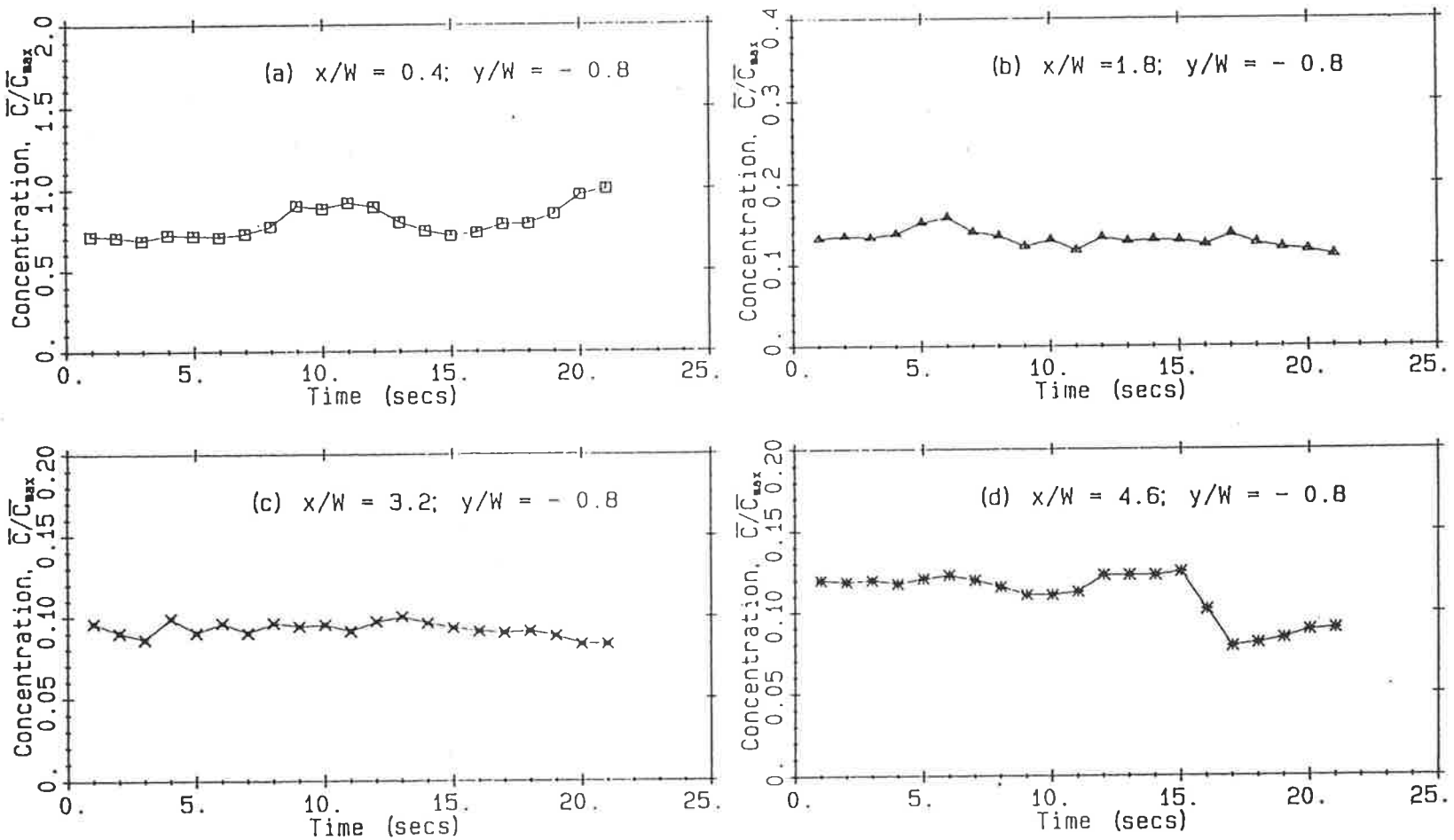


Figure 7.13: Plots of short time average concentration at different downstream locations; y/W = - 0.8; A.R. = 4.8; U = 0.30 m/sec.

at different locations in the separated region for the aspect ratio 2.0 when the free stream mean velocity was lower, i.e., U = 0.20 m/sec. As can be seen from the figures, there is no significant difference in the concentration decay curves from those explained earlier for the faster free stream flow case, except that the concentration level is slightly higher. The locations which are within the travel path of the recirculating eddy exhibit a similar undulating shape in the concentration decay curve, again indicating the pulsatile motion in the recirculating eddy.

Figures 7.11, 7.12 and 7.13 show the concentration time plots for the free stream mean velocity of 0.30 m/sec for the larger geometry of the separated region (A.R. = 4.8) while Figures 7.14, 7.15 and 7.16 show similar plots for the free stream mean velocity of 0.20 m/sec for the same geometrical condition. It is to be noted here that although the lateral positions of measurement are the same as for the aspect ratio 2.0, the longitudinal stations are far more sparsely located (up to x/W = 4.6, i.e., upto x = 2.3 metres) because of the limited number of conductivity probes which was again limited by the management of buffer space in the software used for data collection at the desired faster sampling rate. Also the maximum tracer concentration was limited by the 12 bit resolution A/D converter thus limiting the use of highly concentrated salt solution in this case. The result is very low concentration level at some downstream parts of the region. Consequently, the vertical scale of the concentration - time plots were changed in most cases for clarity.

The regions at x/W = 0.4 and y/W = - 0.4 and - 0.8 are the most stagnant part of the separated region as can be seen from the concentration - time plots of Figures 7.12a, 7.13a, 7.15a and 7.16a where the high level of concentration remains almost constant or in some cases increases with time due to very low diffusivity in these regions. Complete wash out of tracer concentration from these regions takes a much longer period compared with other parts of the separated region. Figures 7.11 and 7.14 indicate, as before, passage

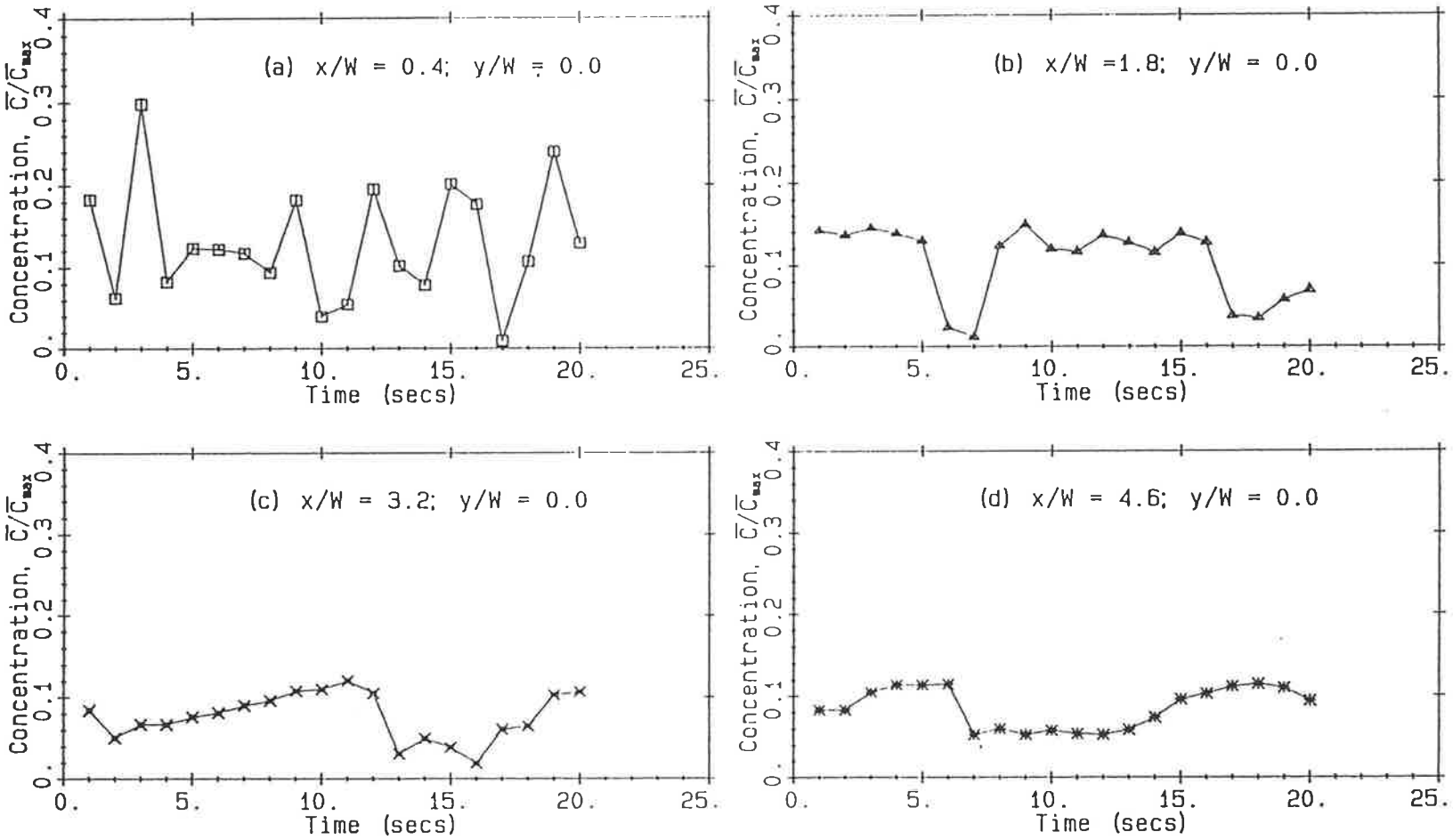


Figure 7.14: Plots of short time average concentration at different downstream locations; y/W = 0.0; A.R. = 4.8; U = 0.20 m/sec.

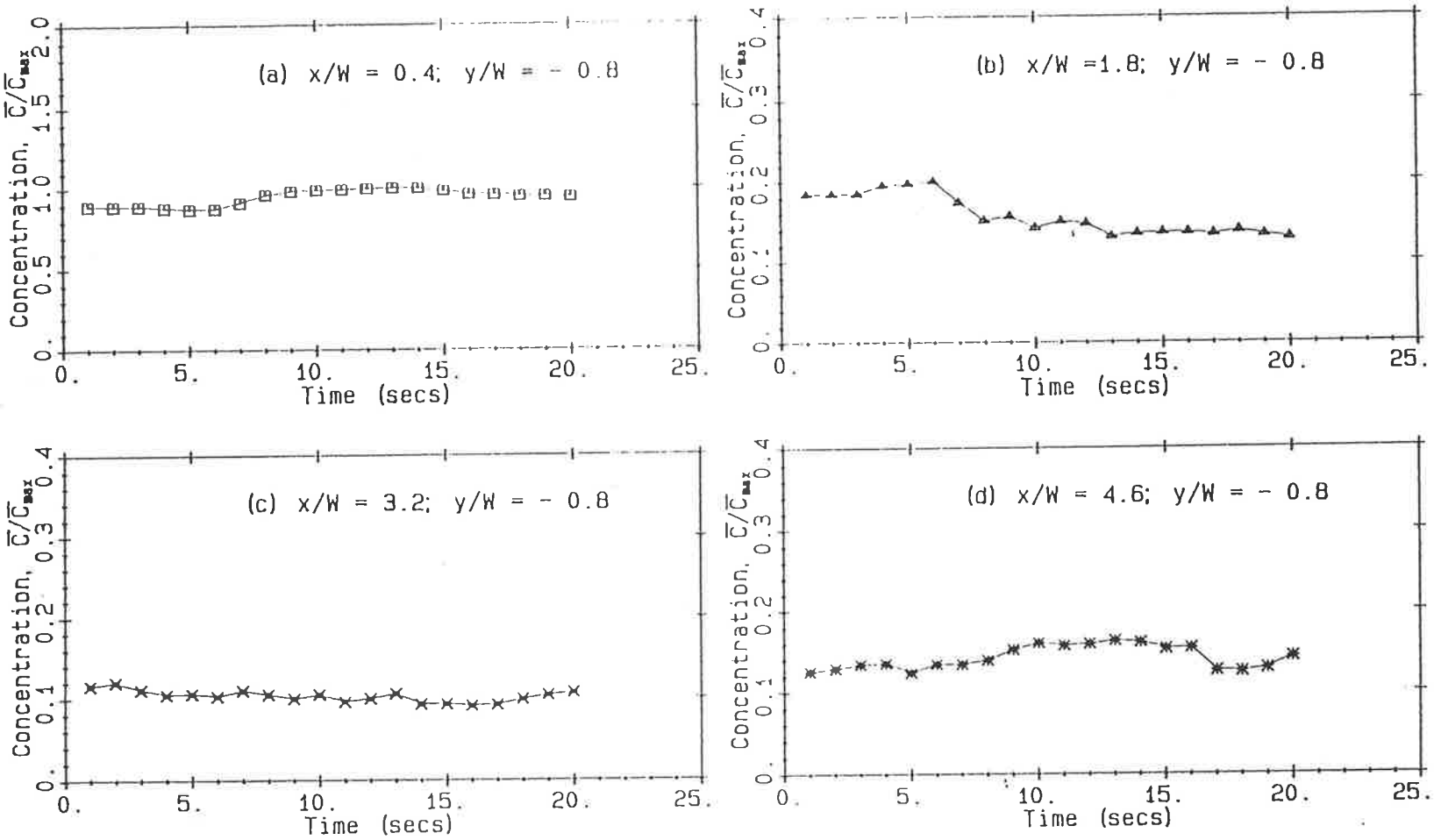


Figure 7.16: Plots of short time average concentration at different downstream locations; y/W = - 0.8; A.R. = 4.8; U = 0.20 m/sec.

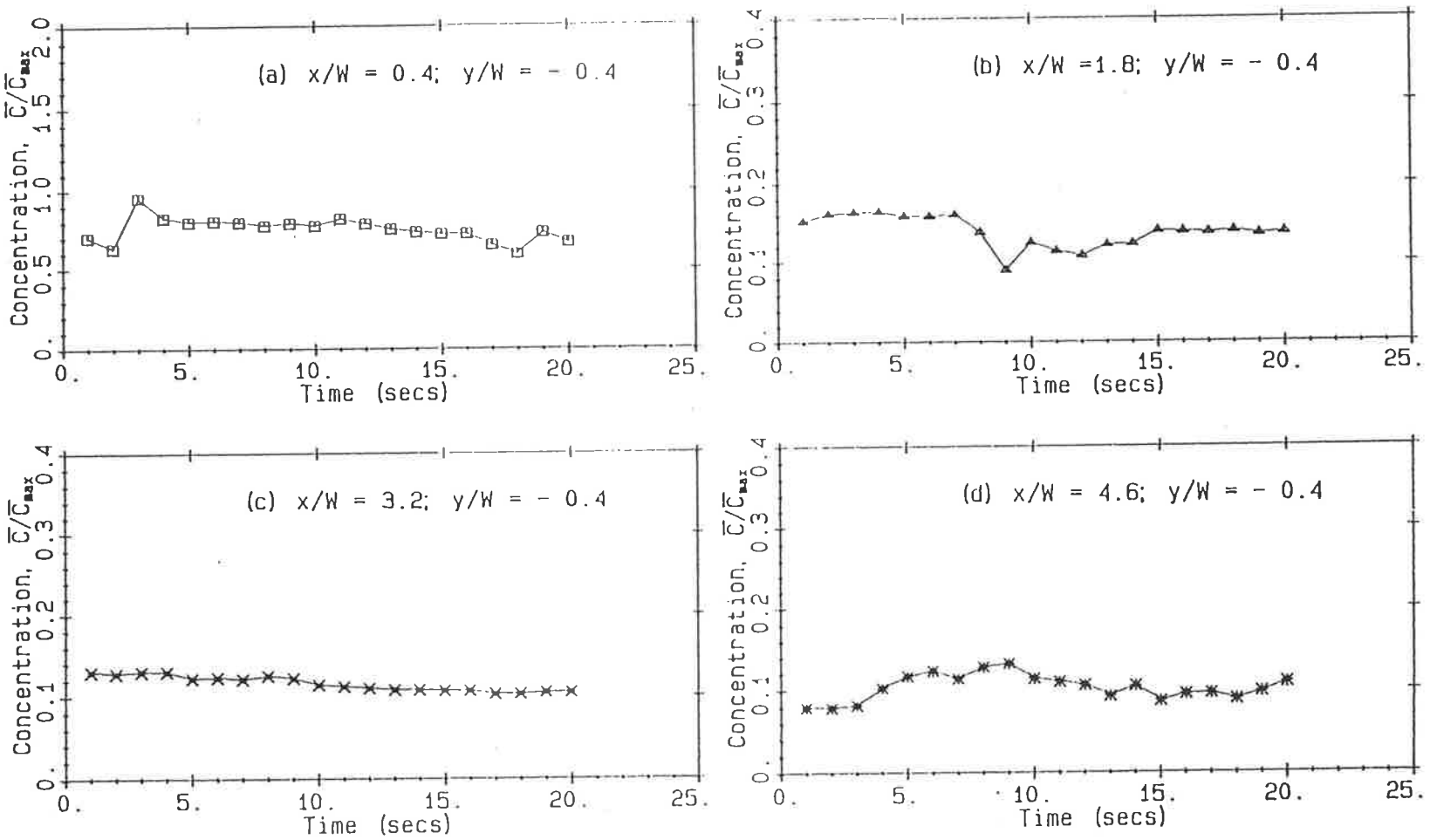


Figure 7.15: Plots of short time average concentration at different downstream locations; y/W = - 0.4; A.R. = 4.8; U = 0.20 m/sec.

of periodic large coherent structures through the shear layer. The plots of Figures 7.12b and 7.12c are not located in the travel path of the recirculating eddy and hence do not show any peak in the decay curve rather they show the trend of steady decrease in concentration.

Figures 7.13b and 7.13c show the plots for which the probes were located on the travel path of the recirculating eddy. The peaks are not clearly established in these plots, however, a slight trend can be noticed. This is to be expected in such a large separated region where the tracer cloud contained in the torn structure at reattachment has to travel a long distance through the recirculating eddy path, long enough to get diluted back close to the level of concentration of the surrounding regions. The concentration level of large coherent structures near reattachment is already very low due to dilution (see Figures 7.11d and 7.14d) compared to the maximum value at the upstream stagnant areas.

However, the plot of Figure 7.12d for which the probe location was close to reattachment and still on the recirculating eddy path does show the unsteady character of concentration decay due to pulsatile motion. Figure 7.13d for which the probe was located further inside the separated region (y/W = -0.8) but still at the same x station shows a similar, delayed undulation in the decay curve. Similar is the case in Figures 7.15d and 7.16d (note change of scale in these figures) for the slower free stream flow.

The nature of the concentration - time decay curves at various locations of the separated region, particularly along the travel path of the recirculating eddy, prompted an examination of the spectra of concentration fluctuations at various points. These spectra at several points on the recirculating eddy travel path are presented in the following subsection in search of further evidence of such pulsatile motion in the recirculating eddy.

### 7.2.3 Spectra of Concentration Fluctuations

Figures 7.17 and 7.18 show the power spectra of concentration fluctuations at four different locations along the recirculating eddy. The tracer release condition was the same as mentioned in the previous subsection, i.e., released until it was spread over the entire region and then stopped when measurements commenced during the washout period. The difficulty in measuring power spectra of concentration fluctuations due to quick dilution of tracer is therefore, recognized. The spectra of Figures 7.17 and 7.18 are taken from the measurements of concentration in the smaller separated region. The spectra of Figure 7.17a correspond to the measurement location of x/W = 1.8; y/W = - 0.4, on the recirculating eddy which was close to the reattachment point yet outside the reattaching shear layer. As can be seen from the figure a clear hump is exhibited in the spectrum in the frequency range of 0.4 to 0.6 Hz which is indicative of the high concentration pulses through the region.

Such behavior in the power spectra indicates that the pulsatile motion in the recirculating eddy dominates the mass transfer through that region. The flatness of the peak is most likely due to the diffusive property of the tracer concentration pulse which passes randomly through the region. Such randomness occur due to the random passage of coherent structures in the separated shear layer. Another reason for this randomness is due to the lateral movement of the shear layer, as observed in the flow visualization experiments, which is again caused by the pulsatile motion in the recirculating eddy. When the shear layer is deflected into the main stream flow, only a small portion of the torn structure of lower tracer concentration constitute the concentration pulse through the measuring point region and vice versa.

A similar hump can also be noticed in the spectra of Figure 7.17b which corresponds to the concentration measurement location of x/W = 1.8; y/W = - 0.8. The hump in this case is, however, fairly broad over the frequency

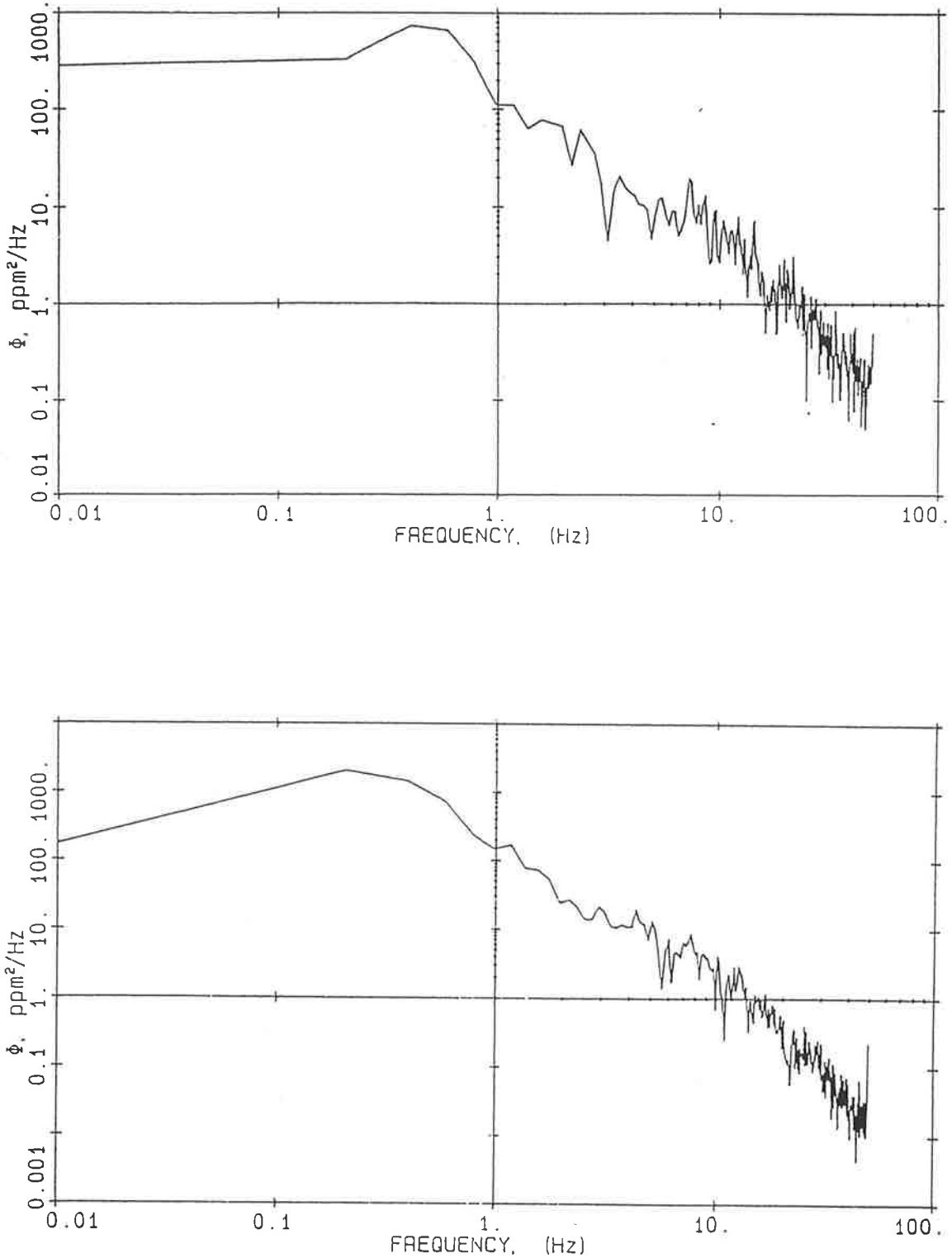


Figure 7.17: Spectra of concentration fluctuations; U = 0.30 m/sec;
(a) x/W = 1.8, y/W = - 0.4; (b) x/W = 1.8, y/W = - 0.8

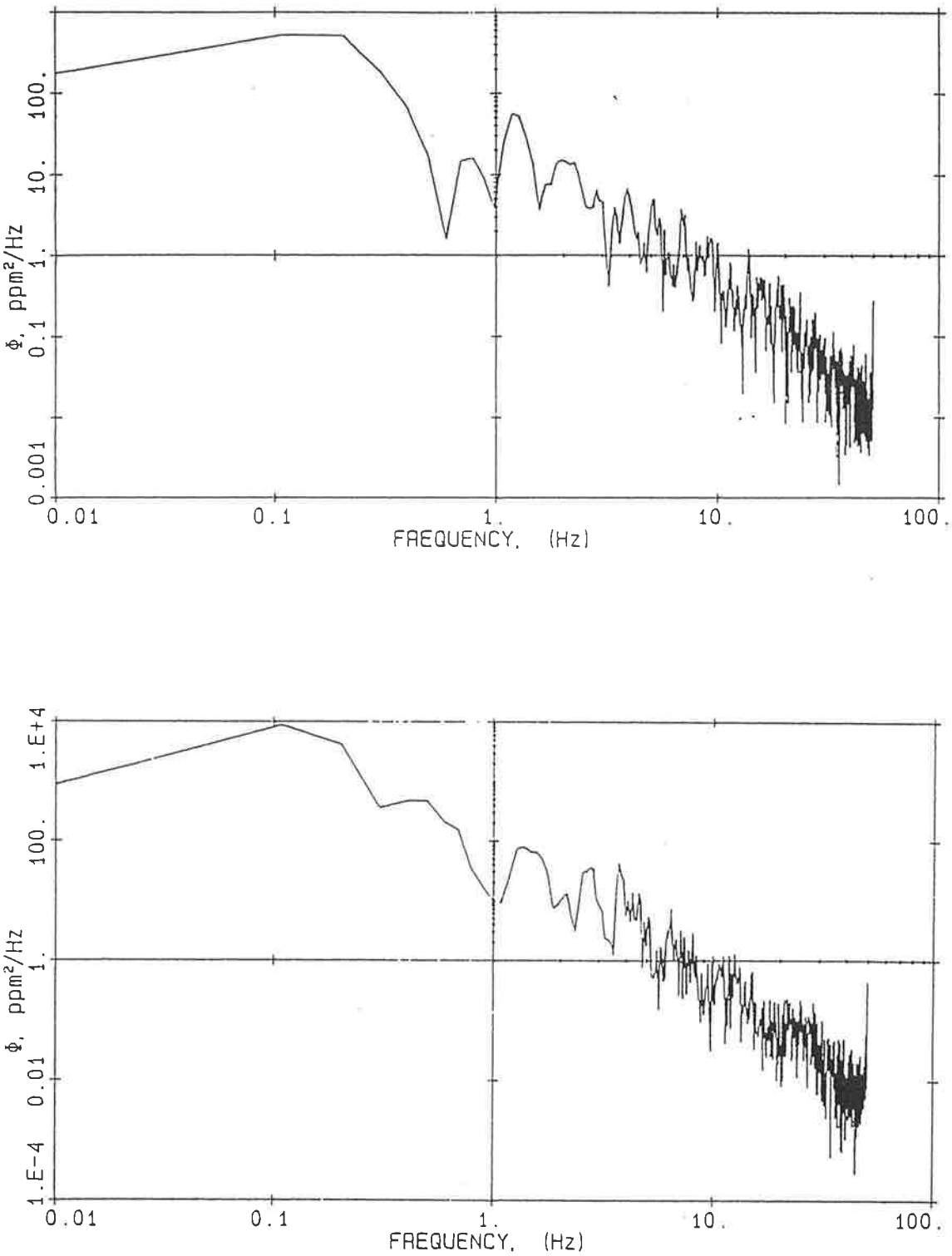


Figure 7.18: Spectra of concentration fluctuations; U = 0.30 m/sec;
(a) x/W = 1.4, y/W = - 0.8; (b) x/W = 0.8, y/W = - 0.4

range of 0.2 to 0.7 Hz. Again the diffusive transfer of tracer concentration from and to the surrounding region can be held responsible. The spectra of Figure 7.18 which correspond to the locations of x/W = 1.4, y/W = - 0.8; and x/W = 0.8, y/W = - 0.4 also exhibit similar broad peaks in the low frequency region indicating quasi periodic pulsatile component in the recirculating eddy motion.

### 7.2.4 Spatial Average Concentration Decay

In this subsection an attempt is made to demonstrate the decay of spatial average concentration with time in the separated flow region. Spatial averaging was done by taking the concentration values from different locations of the separated flow so that the average is truly representative of the entire region. It should be noted here that the concentration values from different locations were already averaged over a period of one second (i.e., over 100 values) in order to minimize the small scale fluctuations due to non-uniform mixing, yet not long enough to cause considerable transfer of tracer concentration.

Figures 7.19 and 7.20 show the spatial average concentration decay with time for aspect ratios of 2.0 and 4.8 respectively. The top three plots in each figure are for the faster free stream flow case (U = 0.30 m/sec) whereas the bottom three of each figure correspond to the slower free stream flow case (U = 0.20 m/sec). Although the three plots in each row of each figure show different run numbers, they were measured from a single continuous experimental run. Continuous recording of concentration measurements for a longer period of time at a desired faster rate and simultaneously at various suitable locations was hampered by some limitations in the data collection software as discussed earlier. Consequently, several sets of data, each 20 seconds long, were recorded with an interval of 10 seconds between the sets from a single experimental run as can be seen from the plots. It can be

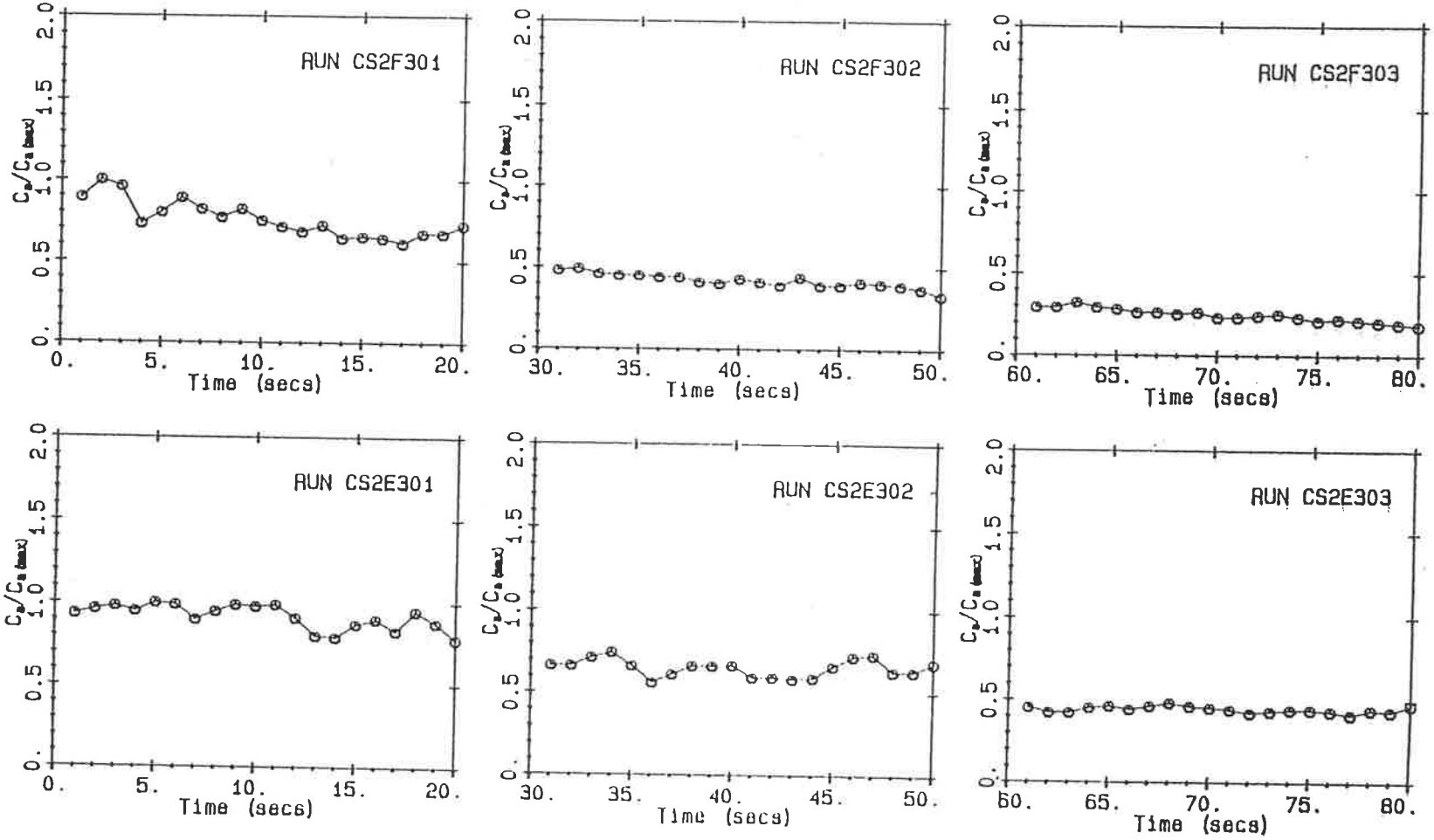


Figure 7.19: Decay of Spatial Average Concentration with Time in the Separated Region; A.R. = 2.0.

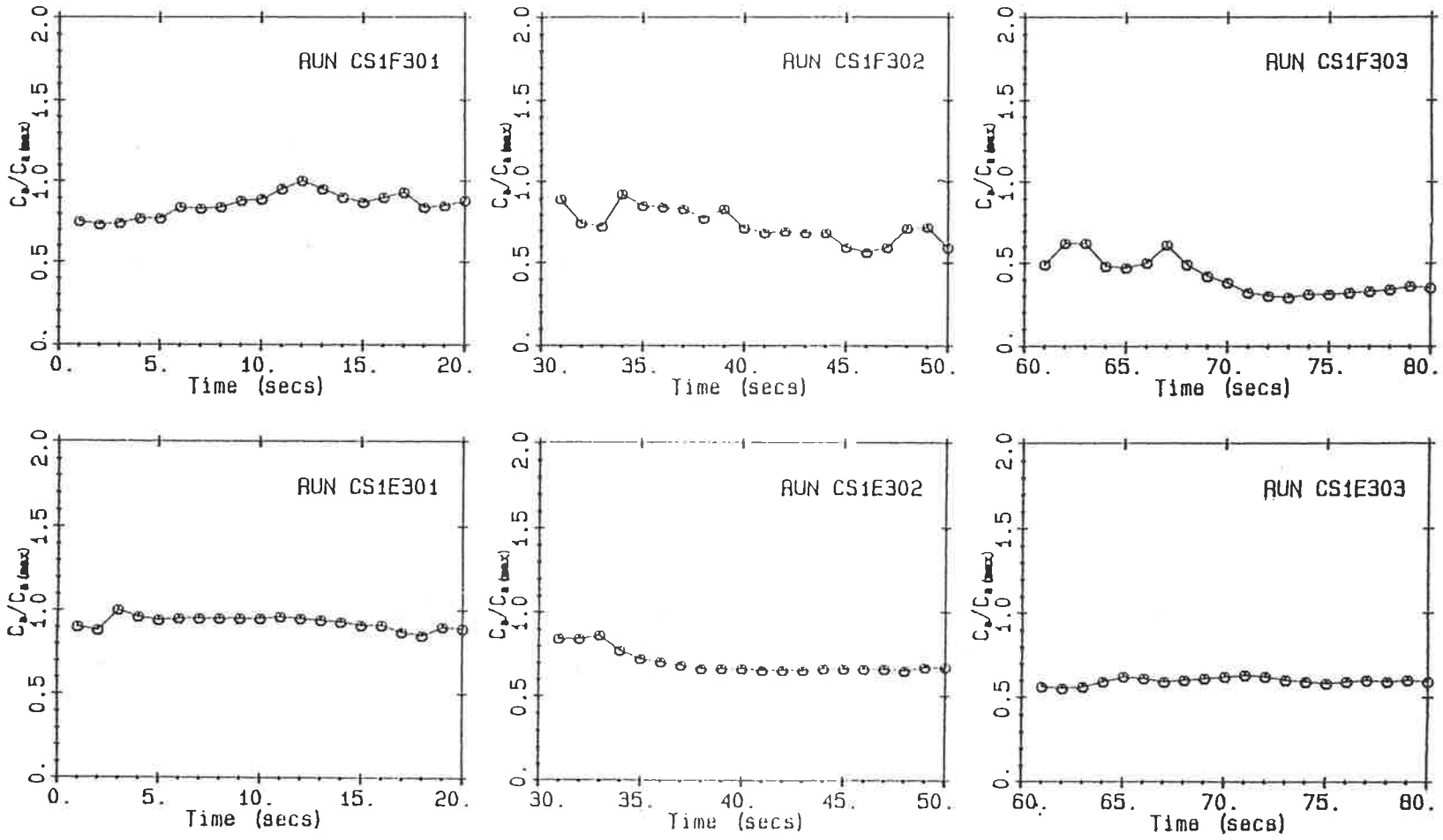


Figure 7.20: Decay of Spatial Average Concentration with Time in the Separated Region; A.R. = 4.8.

mentioned here that each 20 seconds long data record contained 32000 values from sixteen different locations at a rate of 100 samples per second for each probe location.

These spatially averaged concentration decay curves provide several important pieces of information regarding the transport of tracer material within the separated region and transfer into the mainstream channel. The overall pattern shows decay with time in all cases, the decay being faster when the free stream flow velocity was higher. There are several reasons for this.

Firstly, as discussed previously, the large coherent eddy structures in the separated shear layer give rise to the development of turbulent motion in the separated region. In the case of the faster free stream flow, this turbulence is relatively homogeneous compared to the slower free stream flow case. Thus the tracer mass is more uniformly mixed in this case and hence more readily available for entrainment by the large structures of the shear layer.

Secondly, for the faster flow case, the interactions among the coherent structures in the initial region of the separated shear layer are more frequent leading to an increased rate of entrainment in that region. It can be mentioned here, as observed in the visual experiments, that entrainment is a spatially localized process and occurs through interactions among structures. Hussain (1984) also expressed a similar view regarding entrainment from his extensive study of the axisymmetric mixing layer. He also mentioned that the entrainment via vortex interactions is locally far in excess of that which can be accounted for through turbulent diffusion. The entrainment analysis presented in the previous chapter (in section 6.7) also supports this view.

Finally, for the faster free stream flow case the recirculating eddy is shifted further upstream than for the slower free stream flow case, thus reducing the area of relative stagnation of lower diffusivity. Hence the transfer of the tracer material in this case is quicker, as can be seen in the decay curves.

Although the overall pattern of the decay curves shows decrease in concentration with time, the decrease does not appear to be uniform, particularly during the initial period. For instance, the plot for RUN CS1F301 in Figure 7.20 shows an increase in concentration with time and then decrease in the following runs. The reason for this non-uniform decay is that the tracer concentration is not uniformly distributed throughout the entire separated region and since the spatial averaging was done by taking values from different parts of the region it appears to have had an effect on the decay curve as expalined below.

There are two particular areas which contain most of the tracer concentration for a longer period of time with very low diffusive transport. These are, as pointed out in Chapter 5 and 6, the upstream part (near separation) of the separated region and the central core region surrounded by the recirculating eddy. The size of these two relatively stagnant regions varies with the free stream flow condition and the geometry of the separated region.

During the early period of decay, although most of the tracer is concentrated in these two areas, tracer material is also spread over other parts of the region and is being continuously transported by the recirculating eddy. Moreover, part of the torn shear layer structure with some tracer concentration in it intermittently deflects back into the recirculating eddy. These advective and diffusive transport of tracer mass by the recirculating eddy jet cause transfer of tracer mass into the two relatively stagnant areas and increases the concentration there. The major transfer route from these areas is through entrainment by the large coherent eddy structures in the shear layer. Since the passage and interactions of the large structures are not regular, entrainment from these areas is also not a regular process. Thus the level of tracer concentration in these areas sometimes becomes relatively high leading to a higher average value.

At some later stage however, when there is not much tracer concentration left in the other parts except in the two relatively stagnant areas, the tracer mass from these stagnant areas is transported back into the turbulent recirculating eddy jet in addition to the transfer through entrainment by the large structures. At this stage the spatial average concentration decay is approximately uniform as can be seen from the decay curves in Figures 7.19 and 7.20.

Another important reason for the non-uniform decay of average concentration is due to the lateral movement of the shear layer which is a quasi-periodic process caused by the pulsatile motion in the recirculating eddy. This was clearly observed in the present visualization study. As the shear layer is deflected outward into the mainstream channel more tracer material is transferred into the main stream compared with the situation when the shear layer is deflected into the separated region, thus causing a non-uniform transfer of tracer mass. This aspect can also be envisaged from the analysis of mass transfer rate across the shear layer which follows.

## 7.3 Mass Transfer Across the Shear Layer

An important objective of this study has been to evaluate the mass transfer rate across the shear layer of the separated flow field. The best approach would be to measure directly the turbulent mass flux, $-\overline{v'c'}$ across the shear layer. In the present study however, due to some limitations beyond control, direct measurement of the turbulent flux quantities was not possible. An indirect approach of calculating the transverse diffusivity, $\epsilon_y$, which expresses the rate of cross-wise transfer, was therefore taken.

In calculating the diffusivity coefficient, Prandtl's mixing length model was used. Although the model lacks a rigorous physical basis, as discussed in

Chapter 3, it has nonetheless proved to be quite successful in both boundary layer and free shear layer flow calculations. The model is based on the assumption that the turbulent shear stress is produced by the momentum transfer normal to the mean flow direction. The mixing length, $l$ is then defined (in rough analogy to the mean free path of a molecule) to be the average distance over which a fluid element transfers momentum. As mentioned in Chapter 3, a similar concept can also be directly applied to mass transfer analysis. Thus from eqn (3.16) for transverse mass transfer rate, the eddy diffusivity can be expressed, similarly to eddy viscosity, as

$$\epsilon_y \equiv l^2 \mid \frac{\partial \bar{u}}{\partial y} \mid$$

The length scales used in the present calculation are

$$l_v = \sqrt{\overline{v'^2}} / \frac{\partial \bar{u}}{\partial y}$$

and

$$l_c = \sqrt{\overline{c'^2}} / \frac{\partial \bar{c}}{\partial y}$$

Thus the expression for eddy diffusivity becomes

$$\epsilon_y = l_v l_c \mid \frac{\partial \bar{u}}{\partial y} \mid$$

This allows use of both the concentration and the lateral velocity fluctuation scales.

Figures 7.21 to 7.24 show the plots of transverse diffusivity, $\epsilon_y$, as a function of streamwise distance (x/W) for different flow and geometrical conditions. The strikingly notable result is the high diffusivity in regions at x/W = 0.8 for aspect ratio 2.0 and at x/W = 1.9 for aspect ratio 4.8. Interestingly, these locations are in the region of the shear layer where the interaction between the shear layer and the recirculating eddy takes place as was observed in the visual experiments. It was also inferred from visual observations that periodic violent mixing takes place around this location associated with the pulsatile motion in the recirculating eddy. This perhaps leads to a concentration

fluctuation scale considerably larger resulting in a much higher value of the diffusivity coefficient than would be expected for infinite boundary.

The three plots in Figure 7.21 are from three different runs at three different instants of time without varying any experimental parameter. The plots exhibit a high degree of similarity confirming higher diffusivity at x/W = 0.8 for aspect ratio 2.0. The plots of Figure 7.22 are for the same aspect ratio but for slower free stream flow case. These also exhibit a similar trend with diffusivity lower than the faster flow case. Higher diffusivity can also be noticed at x/W = 1.8, i.e., near reattachment in both cases.

Figures 7.23 and 7.24 show the diffusivity for the aspect ratio 4.8 for the faster and slower free stream flow cases respectively, at four different downstream locations namely, x/W = 0.4, 1.8, 3.2 and 4.6. With the exception of plot (c) in Figure 7.23, all other plots show a similar behaviour as for the aspect ratio of 2.0. The high value at x/W = 0.4 of Figure 7.23c could be attributed to experimental uncertainty. For the aspect ratio 4.8 however, the faster flow case exhibits a lower diffusivity value than the slower flow case. Whether there is any physical basis for such lower diffusivity value in case of the faster free stream flow for larger geometry, is not clear. This anomaly was also noticed in the entrainment analysis in the previous chapter where the volume flux rate was lower for faster flow case for aspect ratio 4.8.

No value of the transverse diffusivity coefficient which has been calculated locally in a separated shear layer flow has been found in the literature and hence a direct comparison was not possible. The values of non-dimensional mass transfer coefficient reported by Valentine and Wood (1977) and Weiss and Kuo (1982) in similar type of separated flow considered only the overall change in concentration between the so-called 'dead zone' and the main-stream channel. If the values of the diffusivity coefficient of the present study are non-dimensionalized by the the width of the separated region and

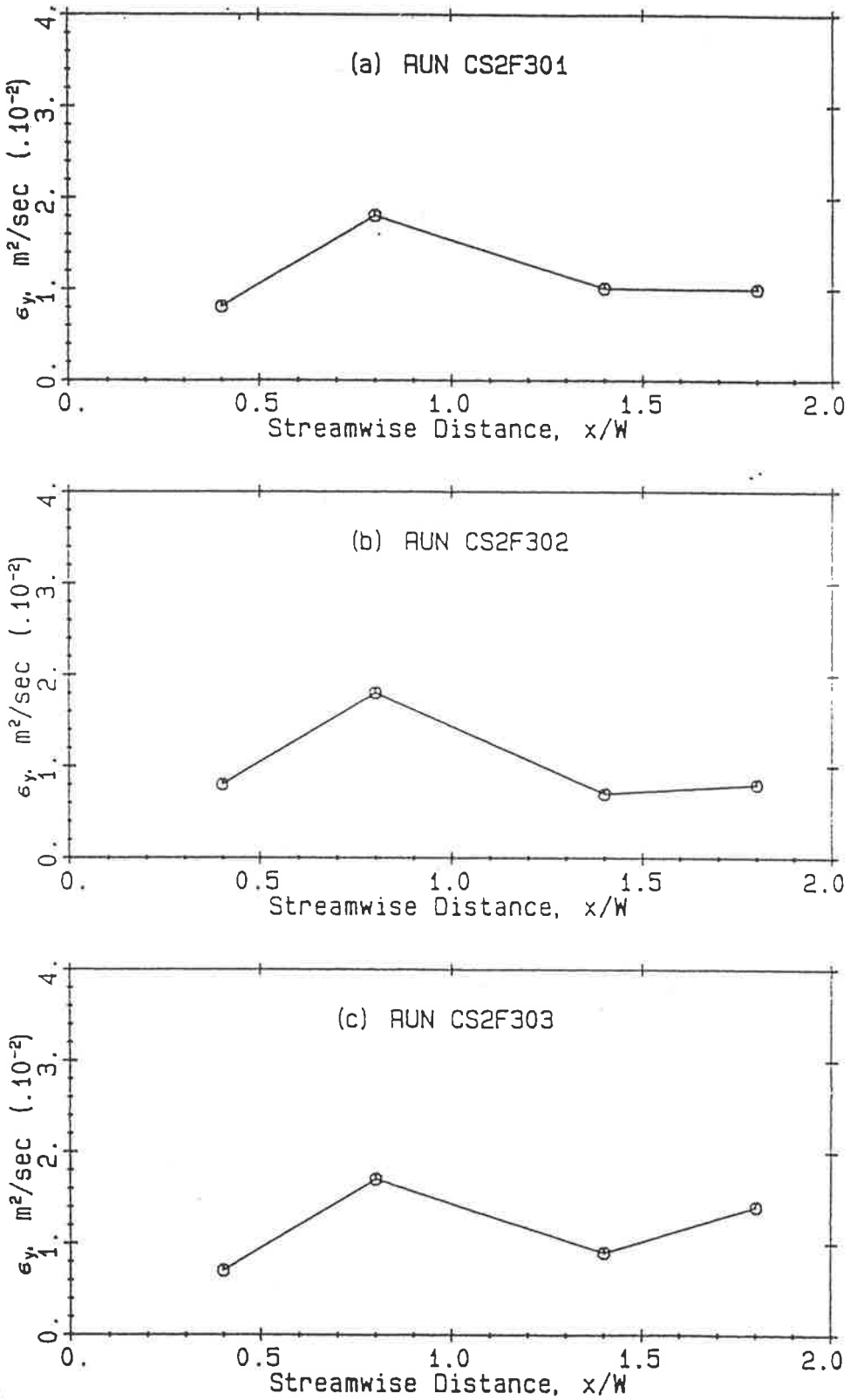


Figure 7.21: Diffusivity coefficient at various streamwise locations;
A.R. = 2.0; U = 0.30 m/sec.

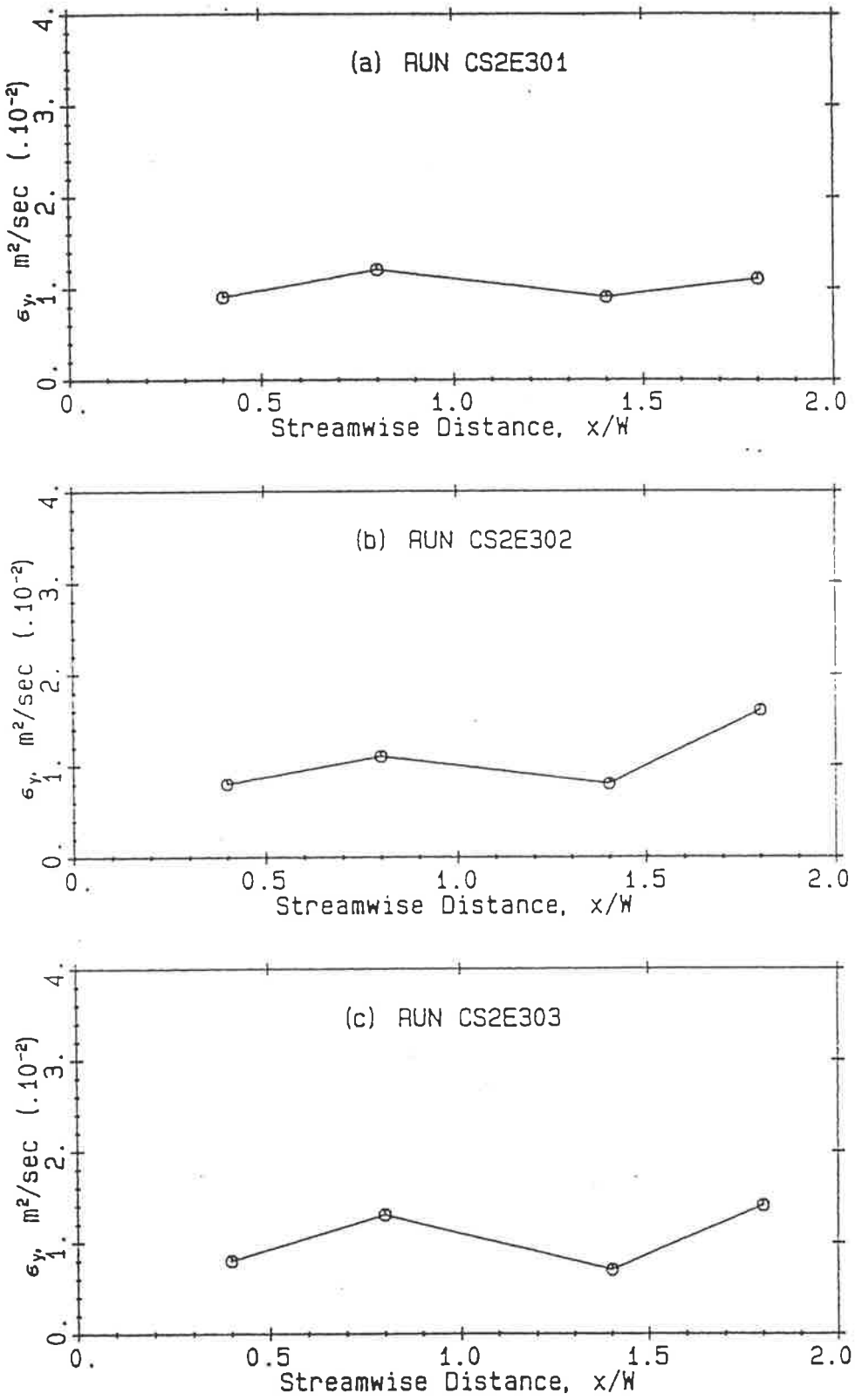


Figure 7.22: Diffusivity coefficient at various streamwise locations;
A.R. = 2.0; U = 0.20 m/sec.

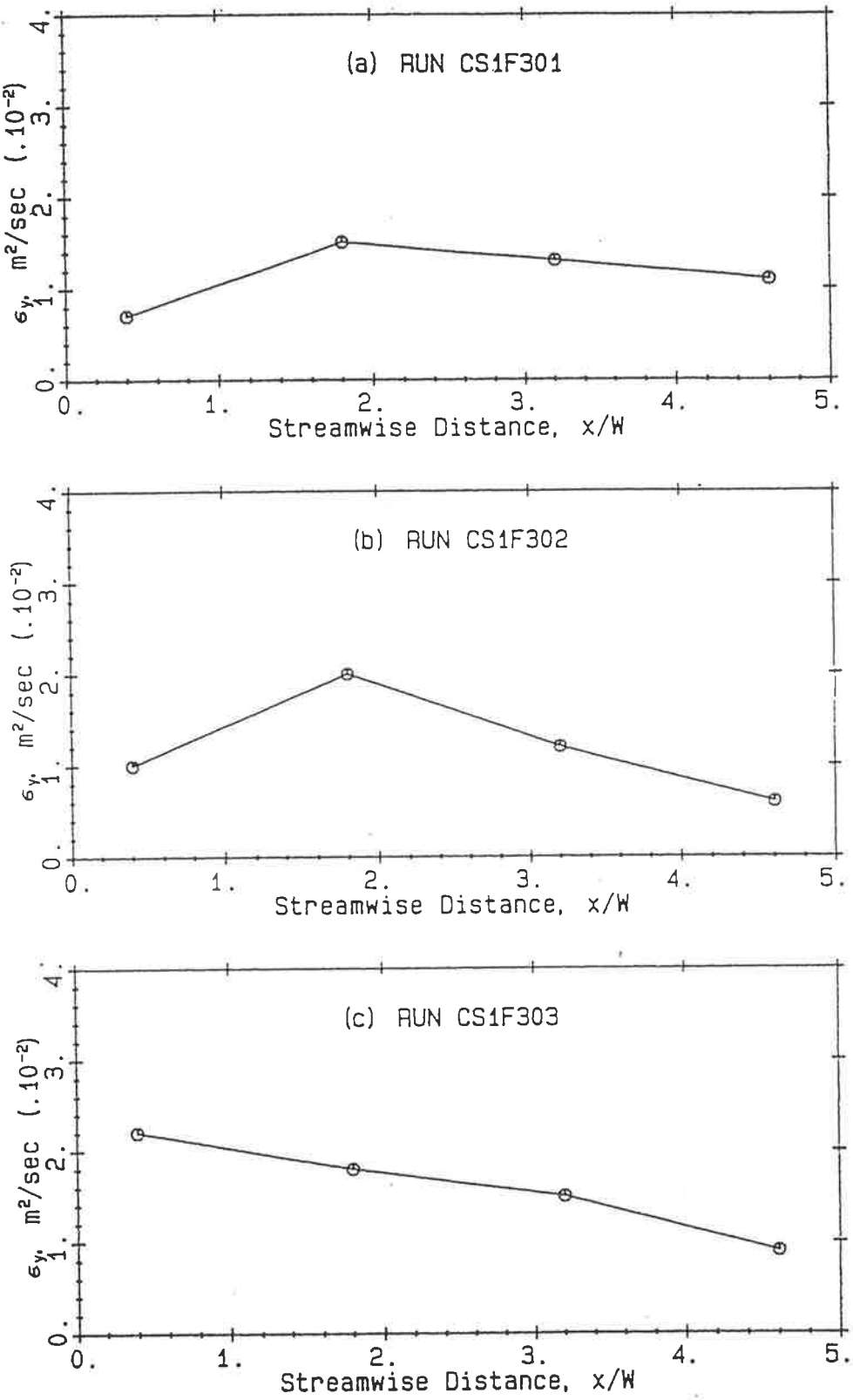


Figure 7.23: Diffusivity coefficient at various streamwise locations;
A.R. = 4.8; U = 0.30 m/sec.

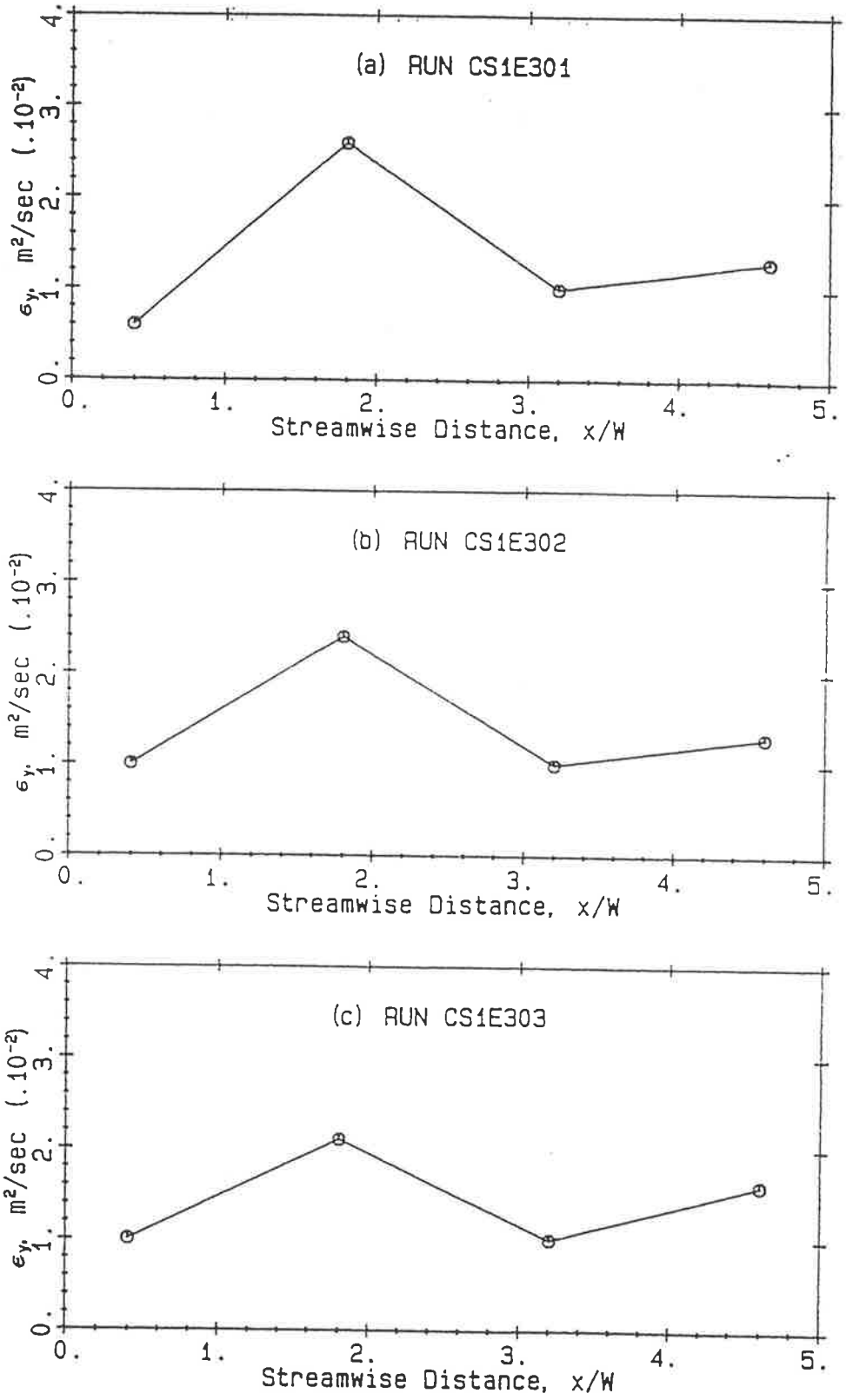


Figure 7.24: Diffusivity coefficient at various streamwise locations; A.R. = 4.8; U = 0.20 m/sec.

the free stream mean velocity, the values are still much higher than the values reported by them. However, the value range of non-dimensional transfer coefficient (ranged from approximately 0.02 to 0.50) as reported by Weiss and Kuo (1982) based on the second-order kinetics assumption are close to the present values.

The values of the transverse diffusivity coefficient in the separated shear layer of the present study are of the order of 100 times greater than the typical values published for open channel flow. Okoye (1970) reported a typical value of 3.26 $m^2/sec(.10^{-4})$ for similar flow condition in open channel flow. His calculation of depth-averaged transverse mixing coefficient was however, based on the growth of depth-averaged variance with streamwise distance.

## 7.4 Effects of Coherent Structures

Visual observations of phase 1 experiments and the spectral analysis of fluctuating velocity measurements in phase 2 experiments clearly indicated that the separated shear layer flow is largely dominated by the presence of coherent eddy structures. As discussed in previous two chapters, these large eddy structures are primarily responsible for several interesting phenomena occurring in the separated flow region. For instance, the process of entrainment being dominated by the engulfing action of these structures rather than by vorticity diffusion; development of fluctuating motion in the separated region due to the passage of these structures along the shear layer; and the most stimulating result of the existence of a quasi-periodic pulsatile motion in the recirculating eddy of the separated region. This pulsatile motion is again responsible for the periodic lateral movement of the shear layer.

In this section the results of concentration measurements pertaining to the presence of coherent eddy structures in the separated shear layer are pre-

sented. The purpose is to demonstrate the effects of these structures on concentration measurements across the shear layer at various downstream locations in order to provide further insight into the mixing and mass transfer processes in the separated flow. The short time average concentration decay with time and the power spectra of concentration fluctuation at several points in the separated region discussed in the previous section of this chapter, have already indicated the existence of a pulsatile motion in the recirculating eddy. The time records of concentration variation at various locations in the shear layer are presented first, and then the variations of the lateral concentration distribution with time are analyzed and discussed.

### 7.4.1 Time Records of Concentration

Figure 7.25 shows the time-records of concentration fluctuation at three different downstream locations along the separated shear layer at transverse position y/W = 0.0. Figures 7.26 and 7.27 show similar time-records for lateral positions of y/W = - 0.1 and 0.1 respectively at similar downstream locations. All these plots were taken from a typical run for aspect ratio 4.8 and for faster free stream flow condition. Tracer was released continuously from the separation point region.

Passage of coherent eddy structures can be easily seen from these plots. Number of eddy passage becomes lower in the downstream locations as can be seen in plots (b) and (c) of Figure 7.25. This is to be expected. The eddy structures as they advect downstream interact with neighbouring structures and form new structures of larger dimension as was observed visually.

The other important feature of these plots is the rapid change in concentration between x/W = 0.6 and 1.2. This supports the visual observation of a rapid mixing region around these locations where the recirculating eddy

front interacts with the shear layer.

The time-records of Figure 7.26 show concentration fluctuations at the same downstream locations but the transverse location is now on the low-speed side of the shear layer (y/W = - 0.1). The features are similar to those exhibited in the records of Figure 7.25. The only significant difference which can be noticed is that the concentration fluctuation is now more uniform. This is an indication that most mixing takes place on the low-speed side of the layer. This again supports another visual observation regarding the collapse of structures on the low-speed side. It was clearly observed that as a structure moves into the low-speed side of the layer, it stagnates for a while and breaks, most probably due to an interaction process with the recirculating flow. However, it does not lose its coherence completely. Rather it becomes elongated and is entrained by the engulfing action of one or more high-speed side structures as they advect downstream and rotate across the layer.

Figure 7.27 shows the time-records for the transverse position of y/W = 0.1, i.e., on the high-speed side of the separated shear layer. As can be seen from plot (a), not all the structures pass through this point. Only four pulses of concentration are recorded which is an indication of the lateral movement of the structures across the shear layer width. In the downstream plots of (b) and (c) however, since the structure dimensions become larger, most of the structure passages are recorded. The high concentration pulse at about 10 second mark of Figure 7.27b is of interest. This could be due to the large deflection of the shear layer into the main stream channel associated with the periodic violent interaction with the pulsating motion in the recirculating eddy of the separated region. This could be more clearly established when the analysis of lateral concentration distribution across the shear layer for the same concentration records are considered in the following subsection.

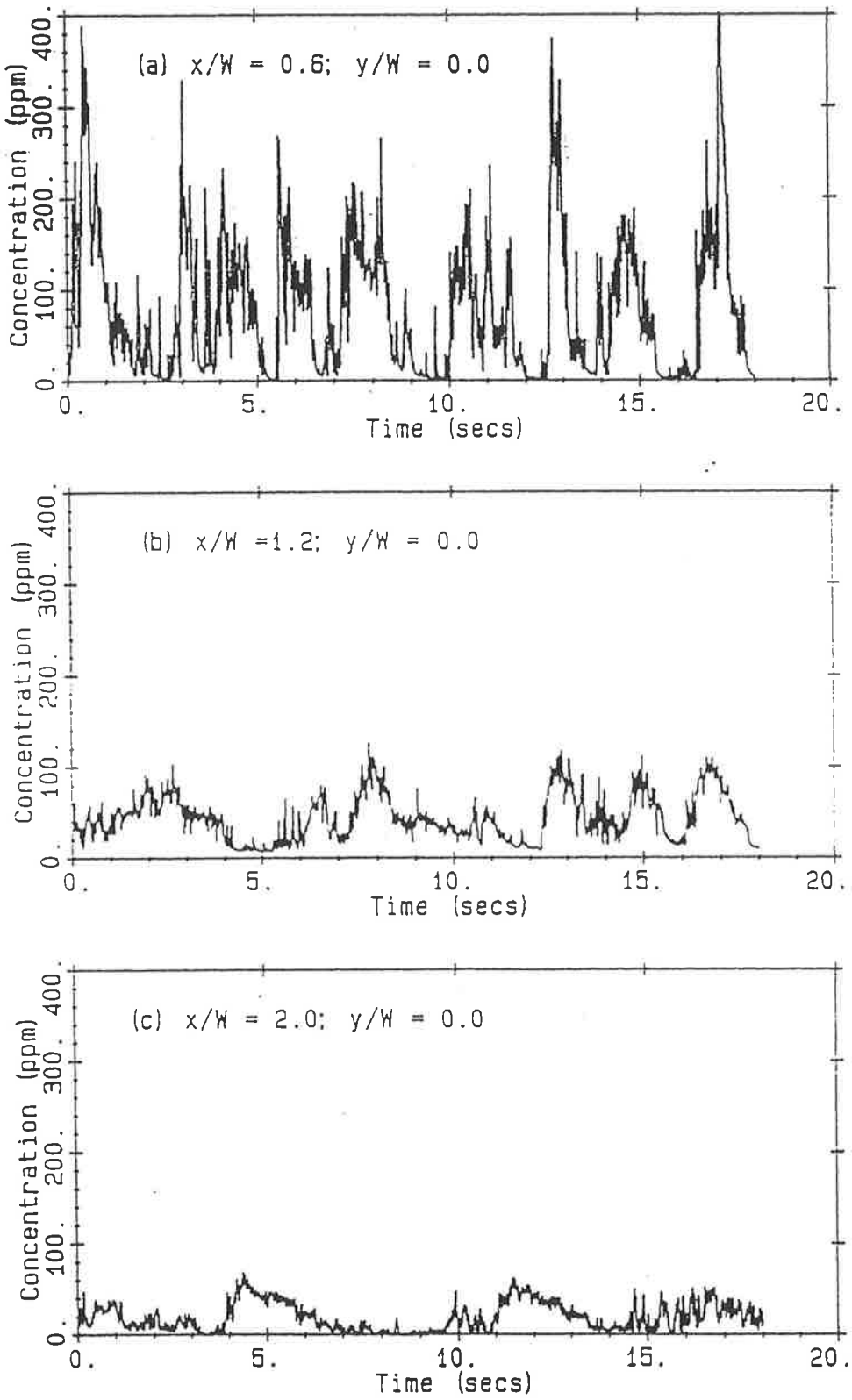


Figure 7.25: Time records of concentration fluctuation in the shear layer at y/W = 0.0; (a) x/W = 0.6; (b) x/W = 1.2; and (c) x/W = 2.0

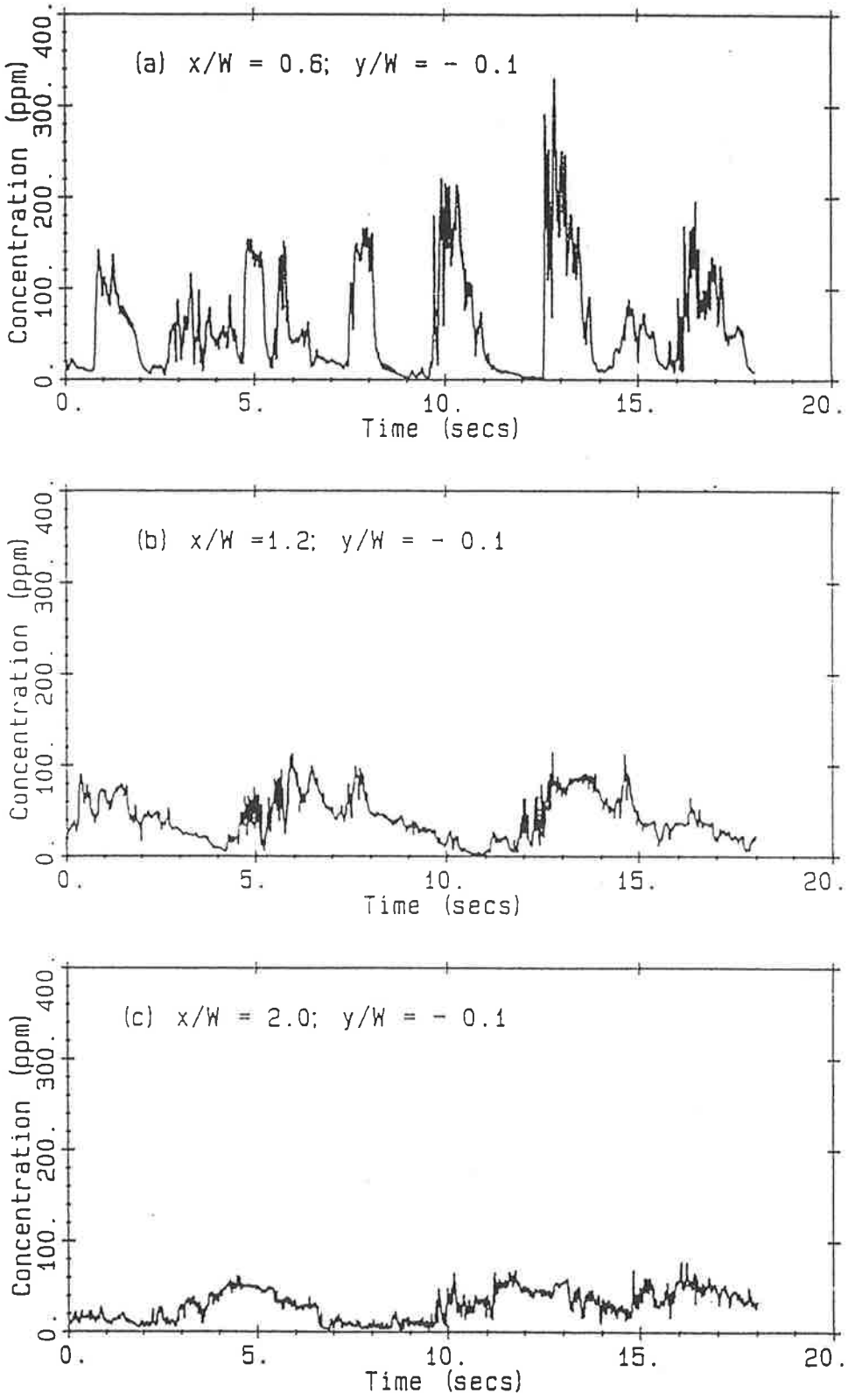


Figure 7.26: Time records of concentration fluctuation in the shear layer at y/W = - 0.1; (a) x/W = 0.6; (b) x/W = 1.2; and (c) x/W = 2.0

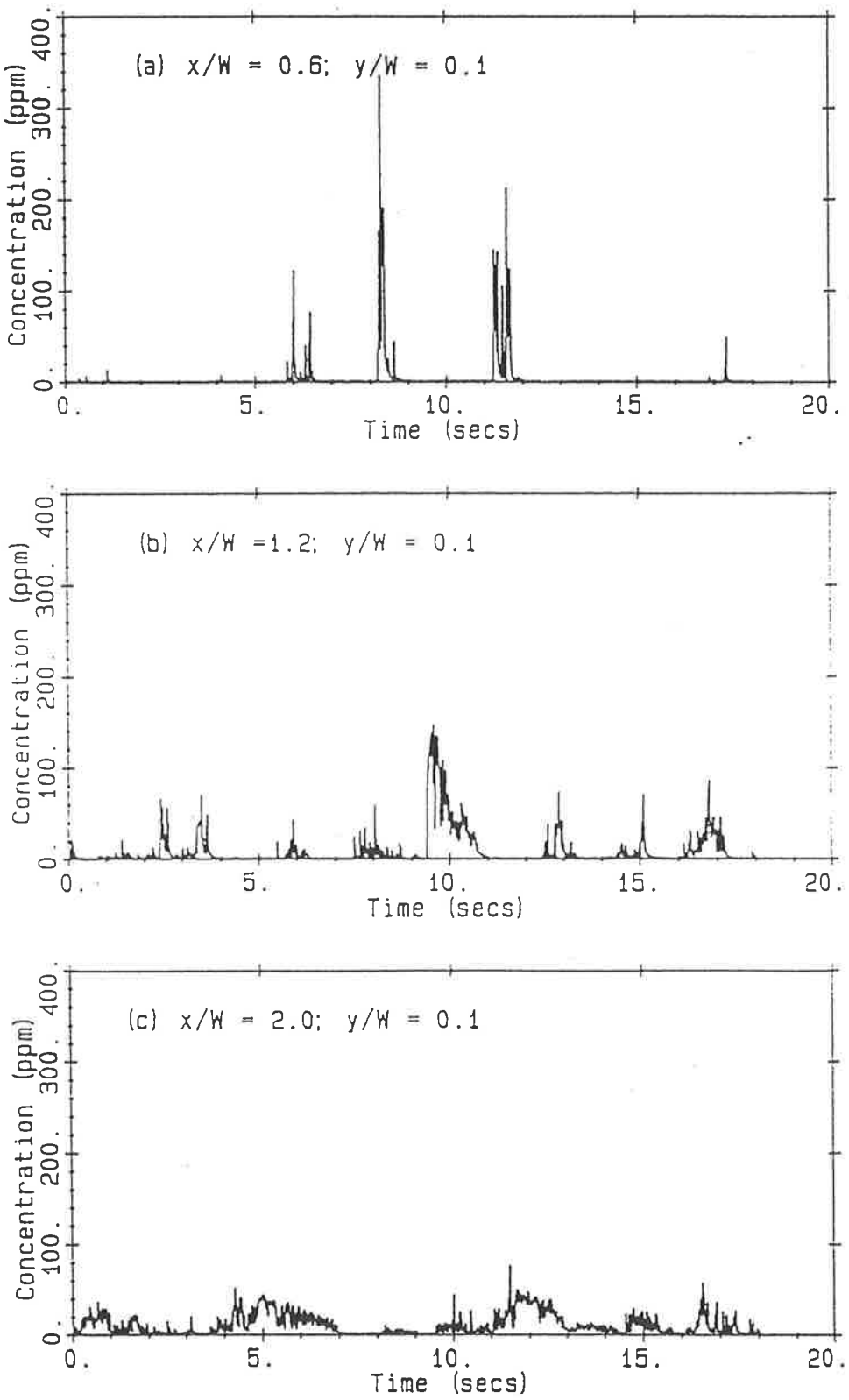


Figure 7.27: Time records of concentration fluctuation in the shear layer at y/W = 0.1; (a) x/W = 0.6; (b) x/W = 1.2; and (c) x/W = 2.0

### 7.4.2 Lateral Concentration Distribution

In an effort to obtain more information about the role of large eddy structures in the separated shear layer, analysis was performed on the lateral concentration distribution across the shear layer. A computer programme was written to calculate the centroid of lateral concentration distribution at every instant of time at various downstream locations. The movement of the large structures and their interactions were obtained from the high speed cine film photographed synchronously during concentration measurements.

Figures 7.28 and 7.29 show the locations of the centroid of lateral concentration distribution as a function of time at two downstream stations, namely $x/W = 1.2$ and 2.0 respectively. Concentration was measured at several lateral positions across the layer at these stations. The marks 'S' and 'B' on the figures stand for passage of structure and braid respectively.

From Figure 7.28 it can be seen that every structure passage is followed by a braid passage. During periods S2 and S3 however, there were interactions between structures. The large deflection in the centroid location into the high-speed side of the shear layer at the end of period S2 (at about the 10 second mark) corresponds to the high concentration pulse shown in Figure 7.27b at the same period of time. This confirms the periodic strong interaction by the pulsatile motion in the recirculating eddy with the shear layer structures.

A general pattern can be noticed from these plots. During the passage of structures the centroid locations move from the low-speed side to the high-speed side of the layer whereas during the passage of braid the movement is in the opposite direction. However, during interactions between two or more structures the pattern is slightly different. For instance, structure passage period S2 between 9 and 17 seconds in Figure 7.29 shows several peaks and

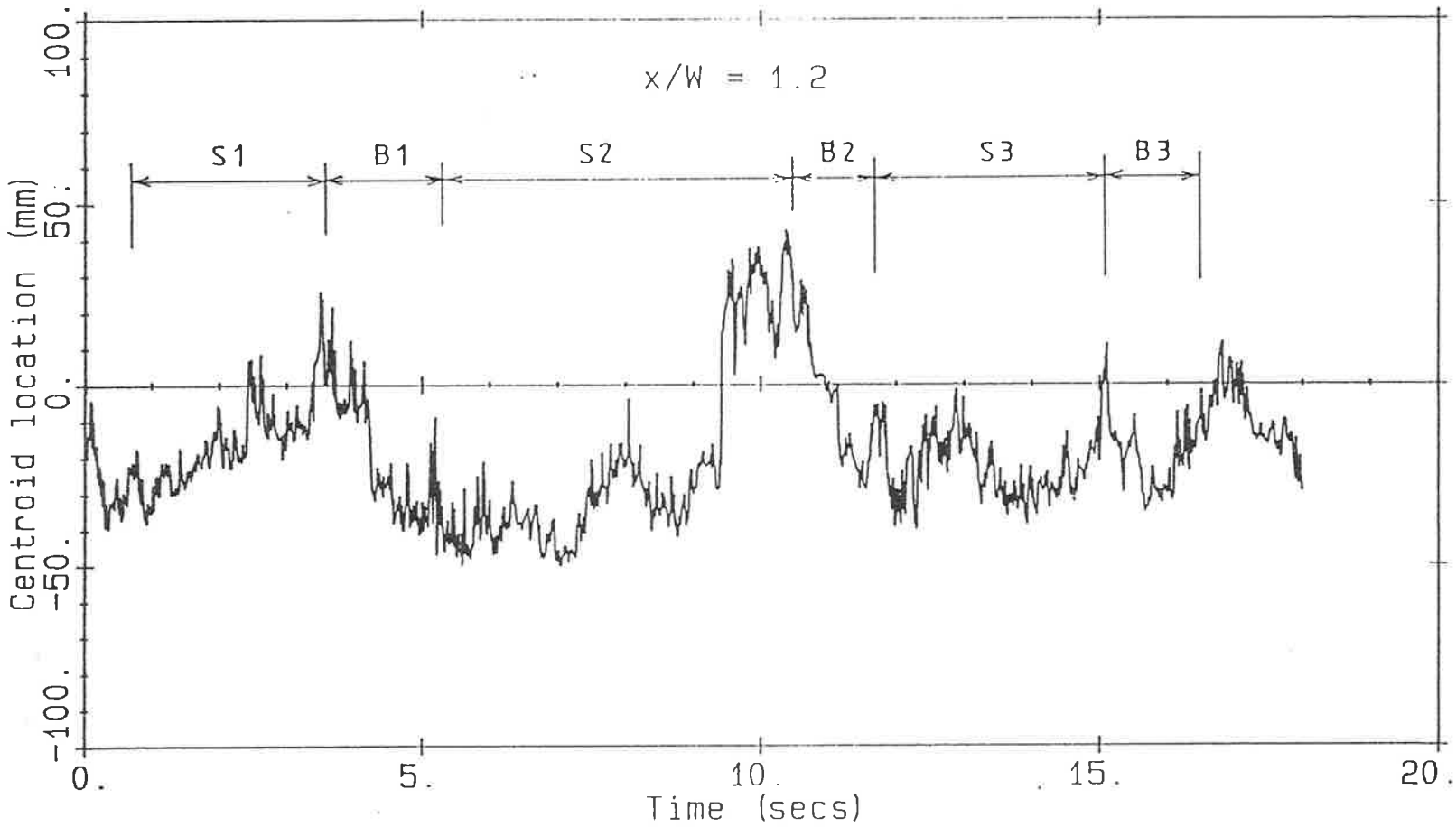


Figure 7.28: Centroid of lateral concentration distribution at x/W = 1.2; A.R. = 4.8; U = 0.30 m/sec.

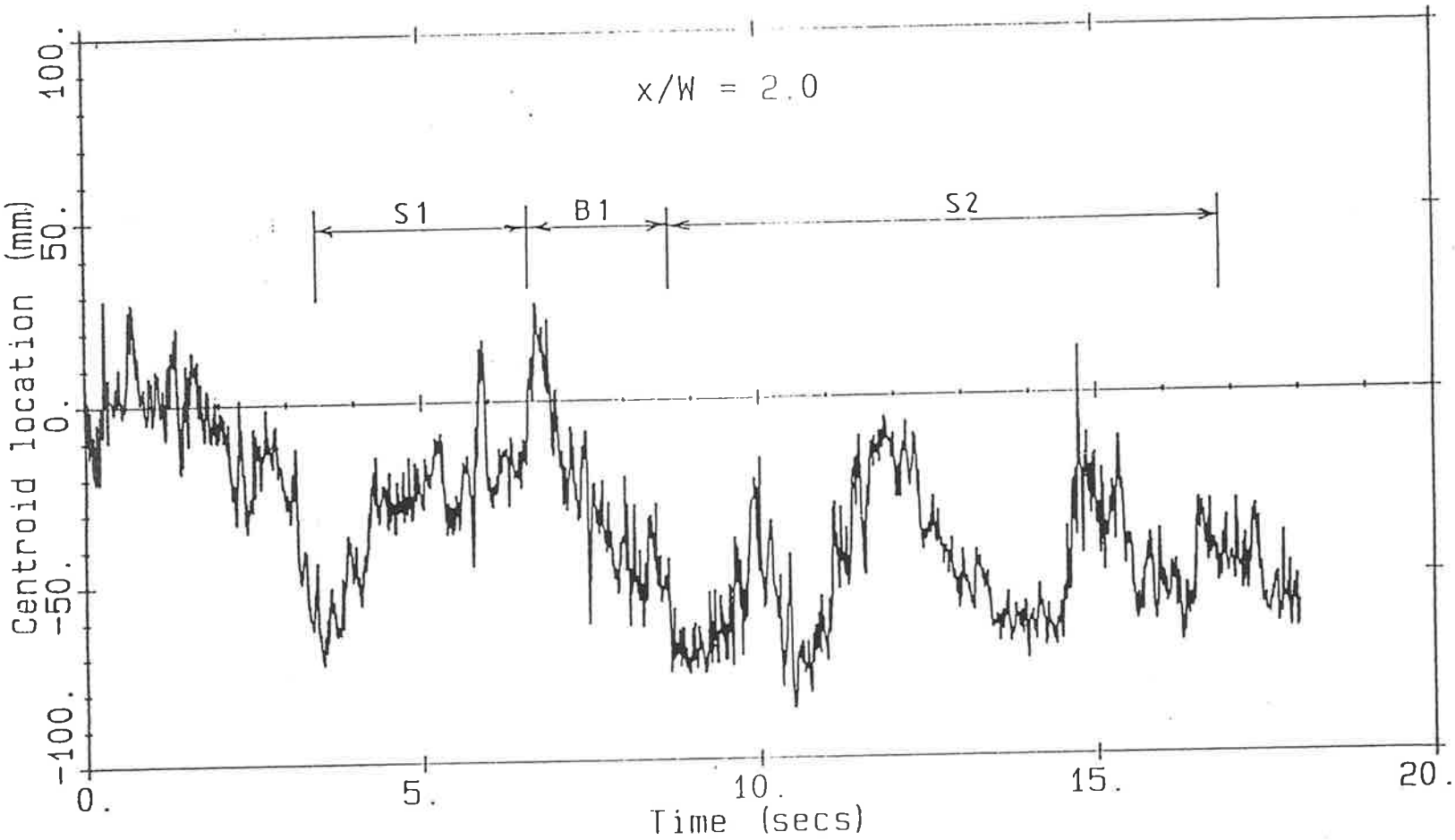


Figure 7.29: Centroid of lateral concentration distribution at x/W = 2.0;
A.R. = 4.8; U = 0.30 m/sec.

valleys in the movement of the centroid of lateral concentration distribution. It was observed from the film that these peaks and valleys do not correspond to the alternate passage of structures and braids. In fact no distinct braid passage could be seen during this period. Rather a complex interaction among several structures (four structures in this case) caused such movement of the centroid location. This is however, is not a regular feature since, as mentioned earlier, the interaction between structures is a random process. Generally, at a particular point in space, large structures passage is followed by a braid passage and occasionally followed by such complex interaction process among several structures.

It therefore, appears from the above analysis that the existence of these large eddy structures in the separated shear layer and their random interaction process will have significant impact on the mass transfer process of the separated shear flow.

## 7.5 Concluding Remarks

Analysis and results of concentration measurements in various forms have been presented and discussed in this chapter. The iso-concentration contours and the spatial average concentration decay provided an insight into the temporal variation of concentration and the transport tracer mass in the separated flow region. The short-time average concentration decay plots at various locations of the separated region and the power spectral density analysis of concentration fluctuation confirmed the existence of a pulsatile motion in the recirculating eddy observed in the visual experiments as well as in fluctuating velocity measurements in the separated region.

Mass transfer analysis and the demonstration of large structure effects appear to indicate that the calculation of mass transfer rates applying conventional

gradient transfer theory would most probably lead to an improper estimate. Even direct measurement of the mass transfer rate such as $-\overline{v'c'}$ based on long time-averaging would tend to underestimate the rate.

To obtain a good estimate of the mass transfer rate it seems that one should consider the periodic passage of large structures and their interactions. Phase averaging concept as discussed in coherent structure analysis in Chapter 3, would perhaps provide much appropriate estimate of mass transfer rate. Measurement of the quantities such as coherent and incoherent transfer rates, i.e., $\langle \hat{v}\hat{c} \rangle$ and $\langle v'c' \rangle$ would provide further information regarding the importance of these structures on mass transfer processes.

However, as mentioned earlier, although it was possible to obtain conditional concentration measurements through synchronous photography, simultaneous conditional velocity measurement was not possible and hence the evaluation of the quantities $\langle \hat{v}\hat{c} \rangle$ and $\langle v'c' \rangle$ could not be performed within the scope of the present study.

# Chapter 8

# Summary and Conclusions

## 8.1 Summary

The objective of the present study was to provide a further insight into the physical processes involved in mixing and mass transfer across a separated shear flow under free surface condition. The role of such separated flows in transporting contaminants in natural streams could only be assessed if the physical characteristics of the separated flow were fully understood. Accordingly the study focussed on these complex and highly interactive flow processes.

A rectangular cavity type flow was considered in which the upstream boundary layer in the main channel was transformed, after separation, into a free shear layer dividing the main stream channel and the separated recirculating region. An experimental investigation was conducted in a laboratory scale

model seeking both qualitative and quantitative information regarding the flow phenomena.

The whole experimental programme was divided into three distinct phases which consisted of visualization experiments employing dye tracing and high speed photography in phase I; measurements of the velocity field employing a one dimensional laser-Doppler velocimeter in phase II; and measurements of the concentration field using electrical conductivity probes, with synchronous photography in some measurements, in phase III. The results obtained from these phases of the experiments are summarized below which might be regarded as the achievement of the present research from the view point of contributing new knowledge to field of study.

### 8.1.1 Phase I

- The separated free shear layer was dominated by the existence of large coherent eddy structures which developed downstream of the separation point, through the roll-up of an initially unstable vorticity layer into larger two-dimensional vortex like structures. For the faster free stream flow case this intial roll-up was observed to be closer to the separation point than for the slower free stream flow case. The initial development was found to be independent of the geometrical conditions of the separated flow.

- The induced upstream motion produced by a downstream large structure, as it advects downstream and rotates across the layer, provides the necessary subharmonic perturbation for interaction between the structures in the separated shear layer. The lateral oscillatory motion observed in the initial part of the shear layer was a result of this induced motion which causes the large structures to be ejected on the high speed and the low speed side of the shear layer in a random fash-

ion thus causing interactions among structures random in space and in time. This result implies that the subsequent growth of the large structures and hence the shear layer, through the interactions among structures, is not totally independent of the intial conditions which is in disagreement with the conventionally accepted self-similar behaviour of free shear flows.

- The interaction mechanism in the separated shear layer appears to be different from, what is widely known as, eddy pairing between two large coherent structures in the case of other free shear flows. In the present case, the large eddy structure, after the initial roll-up, collapses on the low-speed side of the layer travelling a distance of the order of its size and stagnates for a while. It is then elongated due to shearing action, when a following structure (or structures) captures the collapsed elongated structure, as it passes over, in a fashion similar to the engulfing action of large structures during rotation across the layer.

- It was observed that, due to an interaction between the recirculating eddy in the separated region and the shear layer structures, a rapid mixing takes place in the shear layer the location of which varies with different flow and geometrical conditions. This rapid mixing is speculated to be in addition to the rapid transitional mixing due to the development of secondary streamwise small structures through an internal depthwise instability.

- The basic entrainment process was observed to be due to the engulfing action of the large coherent eddy structures in the separated shear layer rather than due to the conventionally held concept of vorticity diffusion. Also, major entrainment was noticed to be in the initial part of the shear layer associated with more frequent structure interactions.

- The most definitive result of this phase of the experiments was the observation of the quasi-periodic lateral movement of the shear layer. The

process is again associated with the passage of large eddy structures in the separated shear layer. As the structures intermittently impinge on the reattaching surface, part of the structure is deflected back into the recirculating region giving rise to a pulsatile motion in the recirculating eddy which has not been previously reported. This interacts with the shear layer near the rapid mixing region and periodically pushes the shear layer bodily outward into the main stream flow. This lateral movement of the shear layer again causes uneven entrainment of fluid into the separated region thus also further contributing to the movement. The process is a continuous repetitive one and causes considerable differences in the mixing and mass transfer rates at different downstream locations of such separated flow.

### 8.1.2 Phase II

- Measurements of the streamwise and transverse mean velocity profiles across the entire separated flow provided information about the separated shear layer growth and the recirculating flow pattern. The growth rate of the separated shear layer calculated from the streamwise mean velocity profiles provided two interesting results. Firstly, the growth rate decreases abruptly near the reattachment region which is attributed to the impact of the impingement of the shear layer on the reattaching surface prohibiting large structure interactions and hence growth near that region.

  Secondly, in the upstream region (except in the initial developing region in the vicinity of the separation point), the growth rate of the separated shear layer was found to be higher when the free stream mean velocity was slower. This was attributed to the higher degree of coherence of the structures in the shear layer when the free stream mean velocity was lower.

- The similarity analyses of the mean motion however, do not clearly indicate the above interesting results apart from showing some scatter in the initial flow development region and in the downstream reattachment region.

- Both the streamwise and transverse turbulence profiles demonstrate the development of large scale fluctuating motion in the separated flow region. Passage of large coherent eddy structures along the separated shear layer and the pulsatile motion in the recirculating eddy (also caused by the deflection of large structures at reattachment) induces the development of such fluctuating motion in the separated flow.

- The study has clearly shown that the recirculating flow assumed steady in earlier studies is certainly not so. The present study demonstrates it is pulsatile and this motion modifies the shear flow downstream of the separation point. The pulsatile motion present in the recirculating eddy jet is confirmed from the low frequency peak exhibited in the power spectra of $v'$ measured within the separated region.

- The entrainment analysis attempted indicates considerable difference from the calculation of volume flux following Albertson et al's (1950) analysis of submerged jet flow which is clearly indicative of the important role of large structures in the entrainment process involved in this free surface flow separation study.

### 8.1.3 Phase III

- Measurements of concentration across the separated flow field demonstrated the temporal and spatial variation of concentration throughout the entire region. The decay of concentration in the separated region was analyzed by three methods. These methods provided an insight into the transport of tracer mass within the separated region.

1. The iso-concentration contours across the transverse plane at several streamwise station indicated a non-uniform decay of instantaneous concentration with time.

2. The short time average concentration decay at fixed points at various parts of the separated region demonstrated passage of large coherent eddy structures in the shear layer and confirmed yet again the pulsatile motion in the recirculating eddy through the exhibition of peaks in the decay curve at different points in time.

3. The spatial average concentration (averaged over the entire region of the separated flow excluding the shear layer) although demonstrating an overall decrease in concentration with time, the rate of decrease did not appear to be uniform, particularly during the initial period. Two particular areas were identified in the separated region which contained most of the tracer concentration for a longer period of time from which there was very low diffusive transport. These two relatively stagnant areas were the upstream part of the region (near separation) and the central core region surrounded by the recirculating eddy and contributed to the non-uniform decay of spatial average concentration. The size of these areas varied with free stream flow condition and the geometry of the separated region, the areas being larger for the slower free stream flow case and for the larger geometrical configuration.

- Spectra of concentration fluctuations at several locations along the recirculating eddy path provided further indication of this previously unknown pulsatile motion in the eddy jet.

- Without the scope for direct measurements of the transverse mass flux across the shear layer, the transverse diffusivity coefficient was evaluated, at several downstream locations in the separated shear layer, em-

ploying mixing length analysis. The results show considerably higher diffusivity at the location where the interaction between the recirculating eddy and the shear layer takes place. The diffusivity values are much higher than those reported in the literature for similar separated flows.

- Finally, the time records of concentration fluctuation and the analysis of centroids of the lateral concentration distribution across the separated shear layer provided a qualitative understanding of the effects of large structure dynamics on mixing and mass transfer across the separated shear layer.

## 8.2 Concluding Remarks

The prevalence of the dynamic events associated with the large coherent eddy structures in the separated shear layer largely dominates the mixing and mass transfer processes in the separated shear flow considered. The study showed the development of the fluctuating motion in the separated region due to these structures, particularly the pulsatile motion in the recirculating eddy. This pulsatile modification exerts significant influence on the mass transfer rates across such separated flows. Future calculation methods should therefore, incorporate the effects of these structures for more accurate predictions of the mass transfer rates.

However, further research is still necessary on similar and different flow and geometrical conditions in order to extend the present experimental results, and to provide additional information regarding the flow phenomena. Several important aspects such as the direct measurements of lateral mass flux considering phase-averaging technique and the effects of three dimensionality which could not be undertaken within the scope of the present study appears

to be profitable for future study in this field.

The present investigation has presented a clear qualitative understanding of a further component of the physical processes involved in the mixing and mass transfer across a separated shear flow, with a free surface. The experimental results have indicated that in many applications, for instance, in the dispersion of contaminants in natural streams, the complex characteristics of this separated flow will have significant influence which previously was believed to be of only secondary importance.

The study has shown that the separated region examined has virtually two major domains. An upstream one circulating slowly with a high concentration and a more active pulsatile recirculating zone of lower concentration which dominates the mixing with the free stream. The pulsatile recirculating flow provides the energy for both the domains.

While this investigation on the behaviour of separated flow phenomena is by no means comprehensive, the findings nevertheless have shown that additional large low frequency perturbations are present and interact with the large scale coherent structures and has laid the foundations for future extensive research into this field.

# Appendix A

# Laser Doppler Velocimetry

In this study, a single channel laser Doppler velocimeter (model 9100 - 3 of TSI Inc.) was used to measure the velocity field of the separated flow region. The dual beam method with back-scatter mode of light collection is employed in the measuring system. Only the essentials of laser-Doppler velocimetry related to the present study will be discussed in this appendix and it is not intended to describe in detail the operational techniques of the system which can be found in the literature, e.g., Durst et al, (1981) and Adrian (1983).

## A.1 Optical Arrangements

The schematic diagram of Figure A.1 shows the basic dual beam optical arrangement used in one dimensional laser Doppler velocimetry. The laser source was a Spectra - Physics model 124B, 35 mW, He-Ne laser. The intense, highly collimated light beam from the laser is passed through a beam splitter to produce two parallel beams of equal intensity. The parallel beams are

then passed through a focusing lens causing the beams to intersect at a point within the flow field. The spatial region from which measurements are obtained is essentially the intersection of these beams and is referred to as 'measurement volume'. A particle in the flowing fluid, as it passes through this intersection, scatters light from both illuminating beams to produce a heterodyne signal.

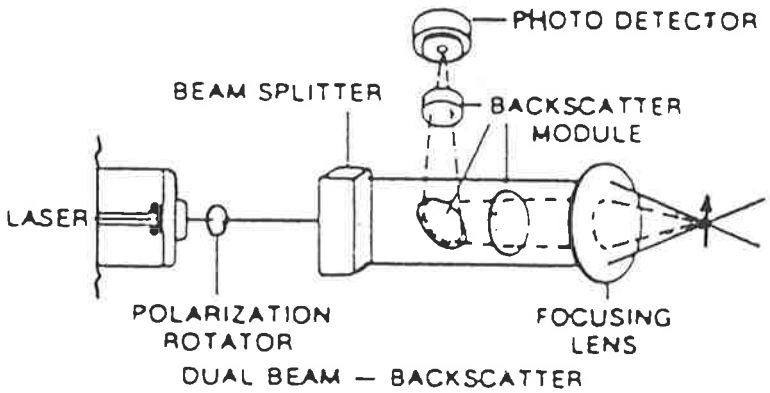


Figure A.1: Basic optical arrangements (after Adrian, 1983)

Scattered light is collected by a set of receiving lenses and focussed through a pinhole aperture onto a photomultiplier tube. The process of heterodyne detection (optical mixing) takes place on the active surface of the photodetector, where the two scattered light waves are mixed together. The photomultiplier signal is a series of short, random bursts of Doppler frequency sine waves caused by particles passing through the measurement volume. These frequencies of the Doppler bursts are measured in a counter type signal processor which converts them into a digital number proportional to the frequency.

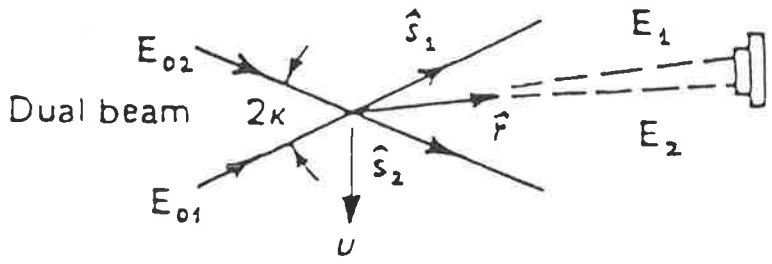


Figure A.2: Basic principle of a dual beam system (after Adrian, 1983)

## A.2 Basic Principle

The basic principle of the dual beam system (sometimes referred to as differential Doppler system) is to illuminate a scattering particle with two plane waves, $E_{01}$ and $E_{02}$ of frequencies $f_{01}$ and $f_{02}$ respectively propagating in two different directions, $\hat{s_1}$ and $\hat{s_2}$ respectively.

Referring to Figure A.2, the ith particle scatters two waves, $E_{1i}$ from $E_{01}$ and $E_{2i}$ from $E_{02}$, and the frequencies of these waves in the scattering direction $\hat{r}$ are, following Adrian (1983),

$$f_{1i} = f_{01} + \frac{v_i(\hat{r} - \hat{s_1})}{\lambda} \tag{A.1}$$

$$\text{and} f_{2i} = f_{02} + \frac{v_i(\hat{r} - \hat{s_2})}{\lambda} \tag{A.2}$$

where,

$v_i$ is the velocity of the ith particle; and

$\lambda$ is the wavelength of the laser light.

The frequency difference is,

$$f_{1i} - f_{2i} = f_s + f_D \tag{A.3}$$

where,

$f_s = f_{01} - f_{02}$, is a constant frequency difference determined by the illuminating beam frequencies, and

$f_D = \frac{v_i(\hat{s_2}-\hat{s_1})}{\lambda}$ is the difference between the Doppler shifts.

This difference is independent of the scattering direction $\hat{r}$ (Adrian, 1983), so the heterodyne frequency is the same at every point on the photodetector and independent of the detector's location.

Now following Edwards et al (1971), the difference between the Doppler shifts can be written in the form,

$$f_D = \frac{K.v_i}{2\pi}$$

where,

$$K = \frac{2\pi(\hat{s_2} - \hat{s_1})}{\lambda}$$

is a wave vector in the direction $\hat{s_2} - \hat{s_1}$.

Letting $u_i(t)$ be the component of $v_i$ in the $\hat{s_2} - \hat{s_1}$ direction, we have,

$$f_D = \frac{Ku_i(t)}{2\pi}$$

where, $\mid K \mid = \frac{4\pi \sin k}{\lambda}$ by simple geometry. Thus, $f_D$ depends only upon $k$, $\lambda$ and the velocity component $u_i$.

## A.3 Frequency Shifting

Usually the original laser light of frequency $f_0$ is splitted into two beams such that $f_{01} = f_{02} = f_0$. Then $f_{1i} - f_{2i} = f_D$, and the heterodyne frequency of the photodetector output is directly proportional to $u_i$. In this case, a sign change in $u_i$, and hence $f_D$, corresponds to $180^o$ phase change in the sinusoidal heterodyne signal which is difficult to detect electronically, particularly when the signal is contaminated by noise (Adrian, 1983). Consequently, whenever bipolar velocities are anticipated such as in case of reverse flow or high intensity turbulence, it is common practice to generate a frequency difference $f_s$ between the illuminating beams so that the fluctuations about zero velocity correspond to frequency fluctuations about the shift frequency, $f_s$. Frequency shifting is accomplished by splitting the original laser beam and shifting the frequency of one of the beams such that $f_{01} - f_{02} = f_s$.

The choice of a shift frequency to remove the directional ambiguity of a laser Doppler velocimeter has been examined by several authors (e.g., Buchhave, 1975; Durst et al, 1981), the general conclusion being that the shift frequency should be chosen such that the moving fringe velocity is twice the maximum flow velocity. That is, the required frequency shift should be twice the maximum local Doppler frequency in order to record all velocity fluctuations at a point in space. In many applications however, as pointed out by Tropea (1986), this result is not directly useful since the resulting shift frequency is too high. In such cases one is satisfied with a lower shift frequency and hence a lower minimum cycle requirement. Tropea (1986) also presented a concise computational guide for choosing the necessary shift frequency for such situations.

The frequency shift system used in this study consists of two separate components - the optics module and the electronics module the arrangement of which is shown in Figure A.3.

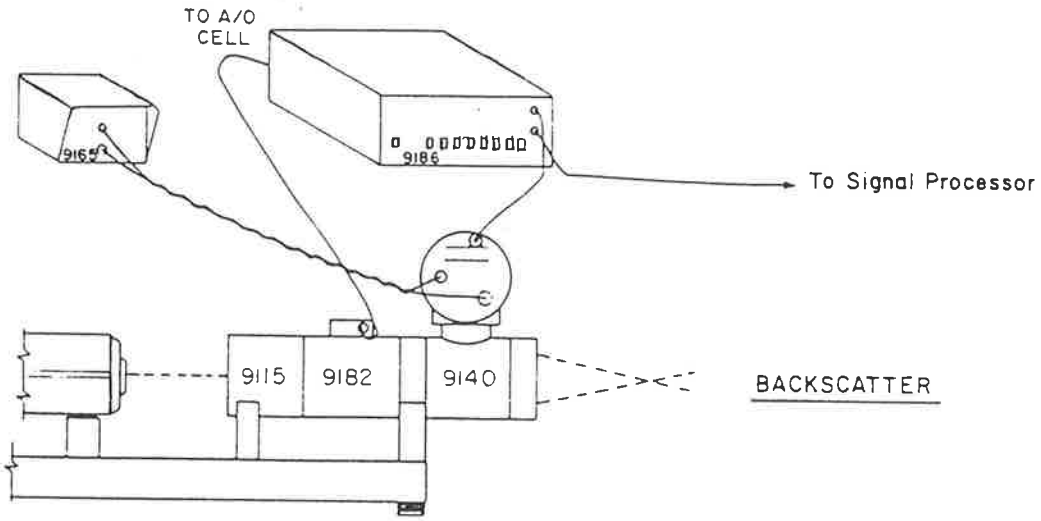


Figure A.3: Frequency shifting arrangements (after TSI Inc.)

The optics module contains an acuosto-optic cell, commonly referred to as Bragg cell, to shift the frequency by a fixed 40 MHz. The Bragg cell is installed in a cylindrical housing which is aligned with all other optics module as shown in the Figure A.3. A compensating wedge corrects for shifted beam deflection while a tilt adjustment shifts the light intensity to the deflected beam. The electronics module contains a downmix circuit which allows to decrease the effective frequency shift of the photodetector output to values from 10 MHz to 2 kHz, since a frequency shift of 40 MHz is too large. The maximum frequency from the downmix circuit to the signal processor is 25 MHz. In the present study it was found that a frequency shift of 0.5 MHz was satisfactory for the maximum anticipated velocity range of $\pm$ 0.5 m/sec.

## A.4 Fiberoptic Probe System

A single component Fiberoptic Probe system is used in conjunction with TSI's laser Doppler velocimeter system. The necessary fiberoptic components include the probe, the translator module, the coupling module and a photodetector base.

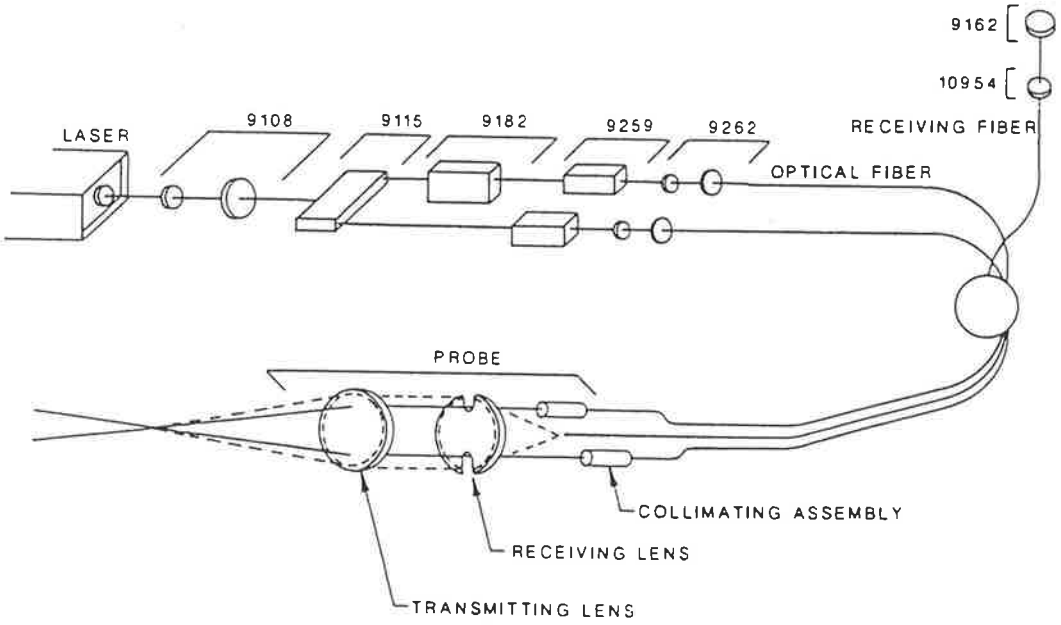


Figure A.4: Schematic employing fiberoptic probe system (after TSI Inc.)

Two laser beams generated by the optical system are launched into two single mode polarization - preserving fibers using the translator module and the double input coupler. In the probe head, lenses collimate the light from the fibers. The collimated laser beams are focussed and crossed with the transmitting lens. Scattered light is collected through the transmitting and receiving lenses and focussed onto a multimode optical fiber. The light from the receiving fiber is coupled into a photodetector using a photodetector base. Figure A.4 shows the entire optical system employing the fiberoptic probe system.

## A.5 Signal Processing

The primary output from a laser Doppler velocimeter is a current or voltage signal from the photodetector. This signal contains the frequency information relating to the velocity to be measured. The photocurrent also contains noise the primary source of which is the photodetection shot noise. This shot noise is inherent in the photodetection process, and it places a fundamental limit on the 'Signal-to-Noise Ratio' (SNR) (Adrien, 1983). The noise decreases as the signal power increases with the square of the photodetector current; on the other hand the noise increases in proportion to the photodetector current (TSI Inc. manual, 1987). Therefore, the parameter SNR is important, high SNR value being desirable for maximum amount of flow information from the signal.

An important aspect for the quality of the signal is the number of seeding particles present simultaneously in the measuring volume. This is expressed by the term 'burst-density'. A low burst-density signal has low probability of more than one particle residing in the measurement volume; conversely in a high burst-density signal this probability is high. Typical single and multi-particle Doppler burst signals are shown in Figure A.5.

Figure A.5(a) shows the raw detector signal for a single particle in the measurement volume. Figure A.5(b) shows the band-pass filtered signal which is in fact the input to the signal processor. The low frequency part which is removed from the signal by the high-pass filter is known as the 'Doppler pedestal'. The envelope of the Doppler modulated current reflects the Gaussian intensity distribution in the measuring volume. Figure A.5(c) shows a typical multi-particle signal. The detector current is the sum of the current bursts from each individual particle within the illuminated region. Since the particles are located randomly in space, the individual current contributions

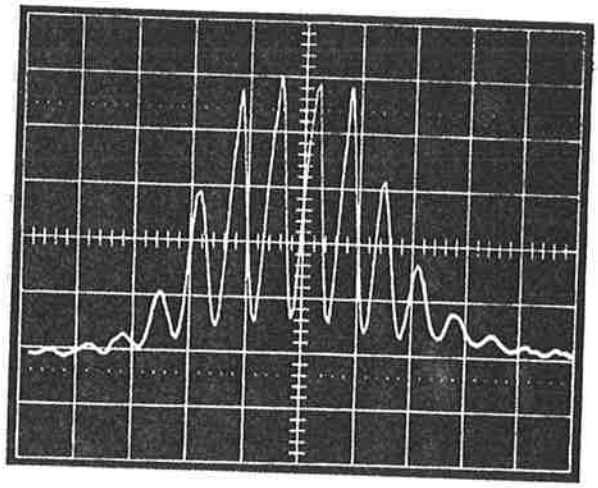

a.

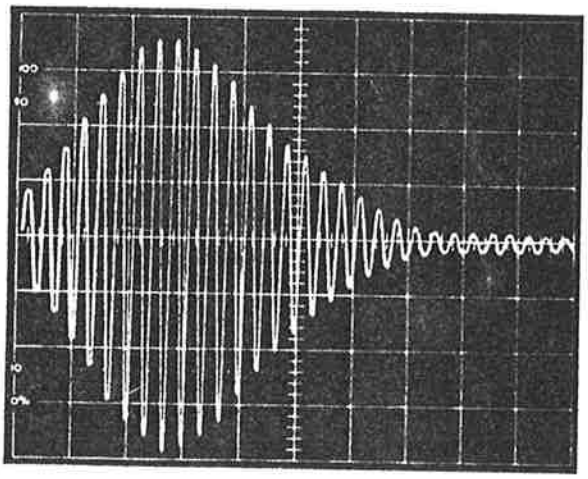

b.

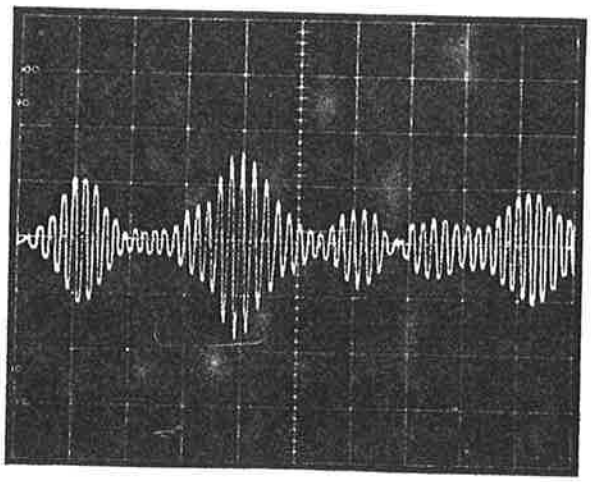

c.

Figure A.5: Typical Doppler burst signals (from 'DISA' LDA manual)

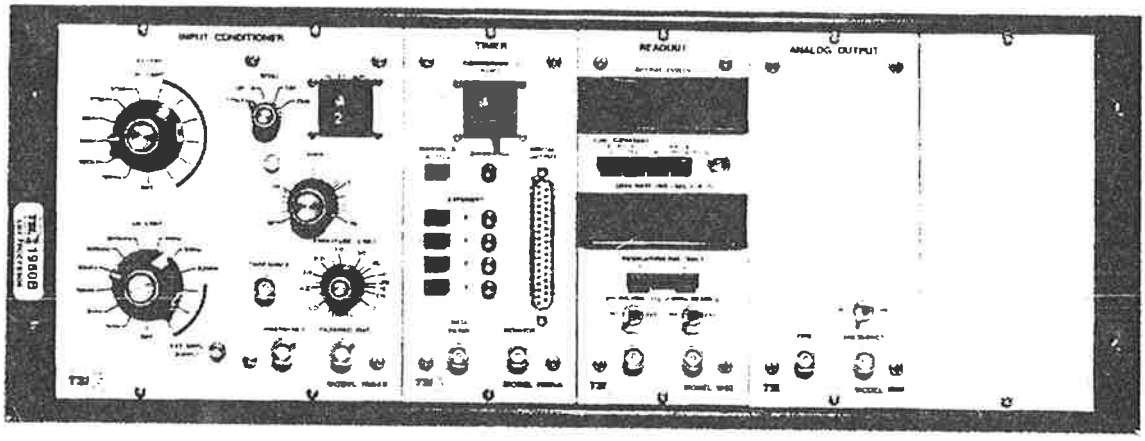


Figure A.6: Counter type signal processor (from TSI - manual)

are added with random phases, and the resulting Doppler signal envelope and phase will fluctuate. These fluctuations are often referred to as 'phase noise' associated with high burst-density signals.

The velocity information is present in the Doppler signal as a frequency modulation of the detector current. The signal processor functions essentially as a frequency demodulator which must be able to detect real-time frequency information containing high frequency components in the presence of wide bandwidth noise. In the present study a 'counter-type' signal processor (Model 1980B of TSI Inc.) was used for processing the signals.

The counter type signal processor (Figure A.6) measures the duration of a given number of cycles in a Doppler burst using a high resolution clock ($\pm$ 2 nanoseconds). This allows the calculation of frequency for discontinuous,

unrelated bursts and gives accurate, independent signal measurements. The model 1980B signal processor differs from a standard frequency counter in that it allows the measurement of the time for a preselected number of cycles. Once the signal processor converts the signal from a frequency to a voltage or a number which is proportional to velocity, the next step is to analyze the data for the desired information. In the present study, the signal processor was interfaced to a small personal computer for storing the voltage information which were then converted into velocity values for further subsequent analysis.

# Appendix B

# Computer Programs for Data Collection

---

The computer programs listed in this appendix were written for the collection of tracer concentration data in the third phase of the experimental programme. All the programs were written in FORTRAN IV compatible with the operating system, RSX - 11M of the PDP 11/34 computer.

The program 'REDAT' collects the raw data values, i.e., the voltage information from the electrical conductivity probes, using the subroutines available in the 'K- series' laboratory peripherials in conjunction with the PDP computer. A short definition of each of the callable subroutines used in the program is given below.

| | |
|---|---|
| ADINP | initiates single analog input |
| SETIBF | sets an array for buffered sweep |
| CLOCKA | sets clock rate |
| RLSBUF | releases data buffers |

| | |
|---|---|
| ADSWP | initiates synchronous A/D sweep |
| IWTBUF | waits for next buffer |
| STPSWP | stops sweep which was in progress |

The program 'REDAT' had the capacity of collecting data from sixteen conductivity probes simultaneously at a rate of 100 samples per second per probe.

Despite their inherent linear transfer characteristics, the conductivity probes required calibration in order to take into account the changes which might have been occurred due to different resistances, variations in materials and workmanship. The program 'CALPRB' was written for this purpose. The calibration data for each probe was subsequently used to convert the raw voltage values into actual concentration values.

The program 'CONCN' is the data processing program which reads the voltage values collected and stored onto a disc file by the program 'REDAT' and converts these voltage values into real concentration values by using the calibration records obtained by the program 'CALPRB'. These concentration values were the final data from the whole data collection programme which were saved and transferred to the main frame computer for subsequent analyses.

```
        PROGRAM REDAT
ccccccccccccccccccccccccccccccccccccccccccccccccccccccccccccccccc
c THIS PROGRAM COLLECTS AND STORES THE RAW DATA VALUES FROM c
c THE ELECTRICAL CONDUCTIVITY PROBES USING SUBROUTINES FROM c
c        THE K - SERIES LABORATORY PERIPHERIALS             c
ccccccccccccccccccccccccccccccccccccccccccccccccccccccccccccccccc
        DIMENSION IBUF(40),IBUF0(1700,6),IVUL(21)
        OPEN(UNIT=7,NAME='DL2:RAW.DAT',TYPE='NEW',
     *  ACCESS='DIRECT',RECORDSIZE=850)
C***
        J=1
1       CALL ADINP(0,32,IVAL)
        TYPE 21,IVAL
21      FORMAT(1X,I6)
        IF(IVAL.GT.2600) GOTO 5
        GOTO1
C***
5       CONTINUE
        TYPE 20
20      FORMAT(' START ')
        CALL SETIBF(IBUF,IND,0,IBUF0(1,1),IBUF0(1,2),
     *  IBUF0(1,3),IBUF0(1,4),IBUF0(1,5),IBUF0(1,6))
        CALL CLOCKA(5,-1,IND,0)
        CALL RLSBUF(IBUF,IND,0,1,2,3,4,5)
        CALL ADSWP(IBUF,1700,-1,0,1,30,0,32,17)
10      CALL IWTBUF(IBUF,30,IBUFNO)
        WRITE(7'J)(IBUF0(M,IBUFNO+1),M=1,1700)
C***
        DO 300 I=1,17
        IVUL(I)=IBUF0(I,IBUFNO+1)
300     CONTINUE
        TYPE 100,(IVUL(I),I=1,17),J
100     FORMAT(17I7,I4)
C***
        IVAL=IBUF0(1,IBUFNO+1)
        IF(IVAL.LT.2000) GOTO 11
        J=J+1
        CALL RLSBUF(IBUF,IND,IBUFNO)
        GOTO 10
11      CALL STPSWP(IBUF,+1,IND)
        CLOSE(UNIT=7)
        TYPE 25
25      FORMAT(' END ')
        RTIME=J/1.
        TYPE 27,RTIME
```

```
27      FORMAT(' DURATION WAS ',F5.0,' SECONDS ')
        END
C
ccccccccccccccEND OF THE RAW DATA COLLECTION PROGRAMcccccccccc


        PROGRAM CALPRB
ccccccccccccccccccccccccccccccccccccccccccccccccccccccccccccccc
c    THIS PROGRAM CALIBRATES THE CONDUCTIVITY PROBES USING  c
c          TRACER SOLUTIONS OF KNOWN CONCENTRATION          c
ccccccccccccccccccccccccccccccccccccccccccccccccccccccccccccccc
C
        DIMENSION ICVALS(17,16), IREAD(5)
C***
C       TYPE IN THE TOTAL NUMBER OF PROBES (NNUM)
C***
6       CONTINUE
        TYPE 106
106     FORMAT(/' TOTAL NUMBER OF PROBES..(2 DIGITS MAX) ')
        ACCEPT 107,NNUM
107     FORMAT(I3)
        IF(NNUM.GT.16) GOTO 6
C***
C       TYPE IN THE CALIBRATION SOLUTION IN PPM (ISOLN)
C***
        NSC=1          !SALT CONCENTRATION BATCH NUMBER
7       CONTINUE
        TYPE 102
102     FORMAT(/' SOLUTION SALT CONCENTRATION (PPM)....
      * (5 DIGITS MAX)')
        ACCEPT 103,ISOLN
103     FORMAT(I5)
C***
C       TYPE IN THE PROBE NUMBER (NPROB)
C***
3       CONTINUE
        TYPE 100
100     FORMAT(/'    PROBE NUMBER.....(2 DIGITS MAX) ')
        ACCEPT 101,IPROB
101     FORMAT(I3)
        IF(IPROB.GT.NNUM) GOTO 4
        NPROB=IPROB
        ICVALS(17,NSC)=ISOLN
C***
C       TAKES 5 READINGS FROM THE PROBE NUMBER SELECTED
```

```
C***
        DO 2 NAV=1,5
C***
C       WAIT FOR A SECOND BEFORE PROCEEDING
C***
        T1=SECNDS(0.0)
1       T2=SECNDS(T1)
        IF(T2.LT.1.0) GOTO 1
C
        CALL ADINP(0,NPROB+32,IREAD(NAV))
C       IREAD(NAV)=10+NPROB+NAV
2       CONTINUE
C***
C       GET THE AVERAGE OF 5 READINGS
C       AND PLACE IT IN AN ARRAY
C***
        ICVAL=IREAD(1)+IREAD(2)+IREAD(3)+IREAD(4)+IREAD(5)
        ICVAL=ICVAL/5
        ICVALS(NPROB,NSC)=ICVAL
C***
C       SEND VALUES TO SCREEN AND DO NEXT SOLUTION
C***
        TYPE 104,NSC,NPROB,ISOLN,ICVAL
104     FORMAT(/' READING..',I2,' CHANNEL NO..',I2,'
     *  SOLUTION..',I6,' VALUE..',I5//)
        GOTO 3
C***
C       PRINT THE CALIBRATION VALUES ON THE SCREEN
C***
4       CONTINUE
        DO 5 NA=1,NNUM
        TYPE 105,ISOLN,ICVALS(NA,NSC)
105     FORMAT(1X,2I7)
5       CONTINUE
C
        TYPE 108
108     FORMAT(/'  ANOTHER SOLUTION...(Y/N)? ')
        ACCEPT 109,NY
109     FORMAT(A1)
        IF(NY.EQ.'N') GOTO 8
        IF(NY.NE.'Y') GOTO 5
        NSC=NSC+1
        IF(NSC.LT.16) GOTO 7
        NSC=NSC-1
C
```

```
8       CONTINUE
C
        TYPE 110
110     FORMAT('  SEND VALUES TO DISC FILE...(Y/N)? ')
        ACCEPT 109,NY
        IF(NY.NE. 'Y') GOTO 9
C
        OPEN(UNIT=7,NAME='DL0:PROB.CAL',TYPE='NEW',
     *  ACCESS='DIRECT', RECORDSIZE=130)
        DO 9 J=1,NSC
        WRITE(7'J) (ICVALS(M,J),M=1,NNUM+1)
9       CONTINUE
C
        END
ccccccccccccccccccc END OF CALIBRATION PROGRAM ccccccccccc


        PROGRAM CONCN
ccccccccccccccccccccccccccccccccccccccccccccccccccccccccccc
c    THIS IS AN INTERACTION PROGRAM WHICH READS  THE        c
c    CALIBRATION VALUES FOR EACH PROBES AND CONVERTS        c
c  RAW DATA VALUES INTO REAL TRACER CONCENTRATION VALUES.   c
ccccccccccccccccccccccccccccccccccccccccccccccccccccccccccc
        DIMENSION ISOLN(15),ICVALS(20,15),IBUF(1700),
        DIMENSION IRCV(1700),IBV(16)
        OPEN(UNIT=7,NAME='DL0:PROB.CAL',TYPE='OLD',
     *  ACCESS='DIRECT', RECORDSIZE=130)
C***
C       READ IN THE CALIBRATION VALUES FOR ALL PROBES
C***
        NNUM=16          ! NUMBER OF PROBES
        IV=12            ! NUMBER OF CALIBRATION SOLUTIONS
        NFME=16          ! FRAME COUNT STARTS AT 16
        ITOG=2           ! TOGGLE FLAG FOR FRAME COUNT
C
        DO 1 J=1,IV
        READ(7'J,ERR=200) (ICVALS(I,J),I=1,NNUM),ISOLN(J)
        TYPE 4,J,ISOLN(J),(ICVALS(I,J),I=1,NNUM)
4       FORMAT(1X,(<NNUM+2>(1X,(I5))))
1       CONTINUE
200     CLOSE(UNIT=7)    ! CLOSE THE CALIBRATION VALUE FILE
C***
C       READ IN BACKGROUND CONCENTRATION VALUE
C                   FOR EACH PROBE
C***
```

```
        TYPE 47
47      FORMAT(1H//2X,'THESE ARE THE BACKGROUND VALUES',/)
C
        OPEN(UNIT=7,NAME='DL2:BG.CON',TYPE='OLD')
        READ(7,110) IZ,(IBV(M),M=1,NNUM)
110     FORMAT(1H 17I6)
        CLOSE(UNIT=7)
        TYPE 49,(IBV(M),M=1,NNUM)
49      FORMAT(1H 16I5//2X,'IS THIS OK (Y/N)')
        ACCEPT 50,IREP
50      FORMAT(A1)
        IF(IREP.NE.'Y') GOTO 310
C***
C       READ IN THE RAW DATA VALUES FOR ALL PROBES
C***
        OPEN(UNIT=7,NAME='DL2:RAW.DAT',TYPE='OLD',
     *  ACCESS='DIRECT',RECORDSIZE=850)
        OPEN(UNIT=8,NAME='DL2:REAL.CON')
C
        J=1
        HDVR=0.
        HCVR=0.
10      READ(7'J,ERR=300) (IBUF(I),I=1,1700)
        DO 11 K=1,1684,17
C***
C       UPDATE THE CAMERA FRAME COUNT.
C***
        IF(ITOG.GT.1) GOTO 40
        IF(IBUF(K).LT.3510) ITOG=2
        NFME=NFME+1                !INCREMENT FRAME COUNT
        GOTO 41
C
40      CONTINUE
        IF(IBUF(K).GT.3510) ITOG=0
41      CONTINUE
        IRCV(K)=NFME
C***
C       CONVERT THE RAW VOLTAGE VALUES INTO ACTUAL
C       CONCENTRATION VALUES USING THE CALIBRATION
C***
        DO 11 M=1,NNUM
        DVR=IBUF(K+M)        !DVR=RAW DATA VALUE (REAL).
        NCV=1                !NCV= NO. OF CALIBRATION VALUES.
13      CVR=ICVALS(M,NCV)    !CVR=CALIBRATION VALUE (REAL).
        IF(HDVR.LT.DVR) HDVR=DVR  !HDVR=HIGHEST DVR VALUE
```

```
        IF(HCVR.LT.CVR) HCVR=CVR  !HCVR=HIGHEST CVR VALUE
        IF(DVR.LT.CVR) GOTO 14
        NCV=NCV+1
        IF(NCV.GT.IV) GOTO 16
        GOTO 13
14      PCVR=ICVALS(M,NCV-1)      !PCVR=PREVIOUS CVR VALUE.
        SVR=ISOLN(NCV)            !SVR=SOLUTION VALUE (REAL).
        PSVR=ISOLN(NCV-1)         !PSVR=PREVIOUS SVR VALUE.
17      SLOPE=(CVR-PCVR)/(SVR-PSVR)
        RCV=((DVR-PCVR)/SLOPE)+PSVR
        IRCV(K+M)=RCV       !IRCV=REAL CONCENTRATION VALUE.
        IF(IRCV(K+M).LE.IBV(M))GOTO 31
        GOTO 20
31      IRCV(K+M)=IBV(M)
20      IRCV(K+M)=IRCV(K+M)-IBV(M)
11      CONTINUE
        TYPE 100,J,RCV,HDVR,HCVR,NFME
100     FORMAT(1X,I5,3F7.0,I7)
C***
C       WRITE ACTUAL CONCENTRATION VALUES IN
C       THE REAL.CON FILE
C***
        DO 18 K=1,1684,17
        WRITE(8,105) (IRCV(K+I),I=0,16)
105     FORMAT(1H 17I6)
18      CONTINUE
C***
C       UPDATE THE TIME BY ONE SECOND
C***
        J=J+1
        GOTO 10
C
16      PCVR=ICVALS(M,11)
        SVR=ISOLN(12)
        PSVR=ISOLN(11)
        GOTO 17
C
300     CLOSE(UNIT=7)
        CLOSE(UNIT=8)
310     CONTINUE
C
        END
ccccccccccccccccccc END OF PROGRAM CONCN ccccccccccccccccccc
```

# Appendix C

# Synchronous Data Collection

## C.1 Photo - synchronization System

The purpose of this system is to co-ordinate the tracer concentration values from a series of conductivity probes in the streamflow with the data recorded on the film using a cine camera. The block diagram of Figure C.1 explains the overall system employed for this synchronous data collection.

As the camera is switched on, the pulses from the camera shutter triggers the frame counter and the strobe flash light. The pulse from the frame counter also triggers the computer trigger circuit and once the control switch is set to start position data collection by the other sixteen conductivity probe channels commences. The same pulse from the frame counter could also be used to start the camera travel motor which would move the camera along the guide rails at a preselected speed corresponding to the flow structure.

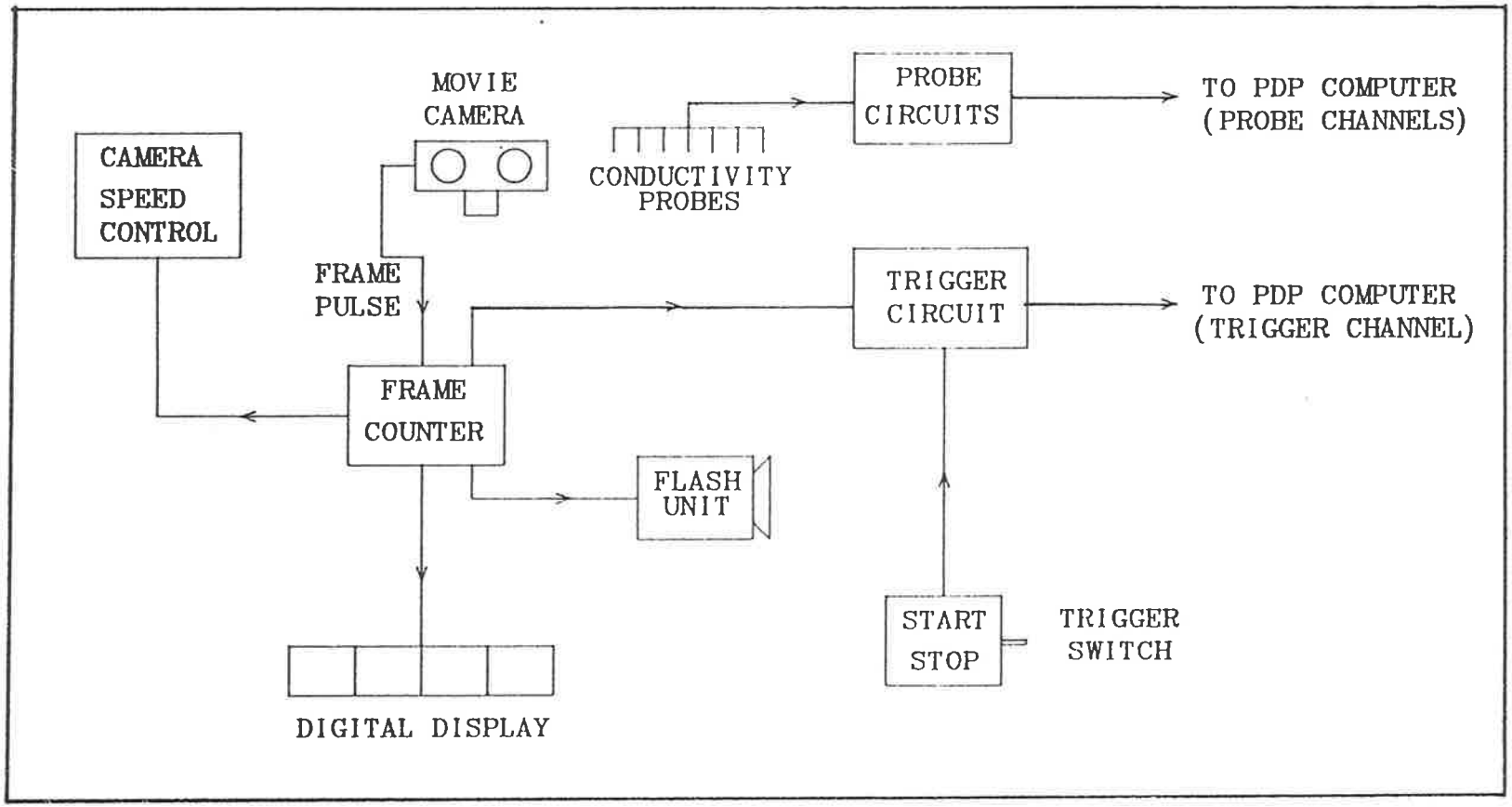


Figure C.1: Block diagram of the photo-synchronization system

The heart of the system is the generation of pulses synchronized to the shutter speed of the camera. A round slotted wheel is attached to the shutter control shaft of the camera (see Figure C.2). This wheel passes across the path of an infra red beam obtained from a small infra red light emitting diode. The beam is detected by a photo transistor which is mounted in line with the beam path. Normally the path of the beam is broken by the wheel, but the slots in the wheel allow the beam path to be completed and thus generating the required pulses. There are four slots in this trigger wheel spaced 90 degrees apart. These are lined up exactly at the point where the shutter of the camera is fully open. Hence the leading edge of this strobe pulse can be used to trigger the strobe flash light. The strobe pulse is however, squared up by Schmidt trigger devices in the camera frame counter circuit before going to the trigger input of the strobe light to give well defined triggering conditions.

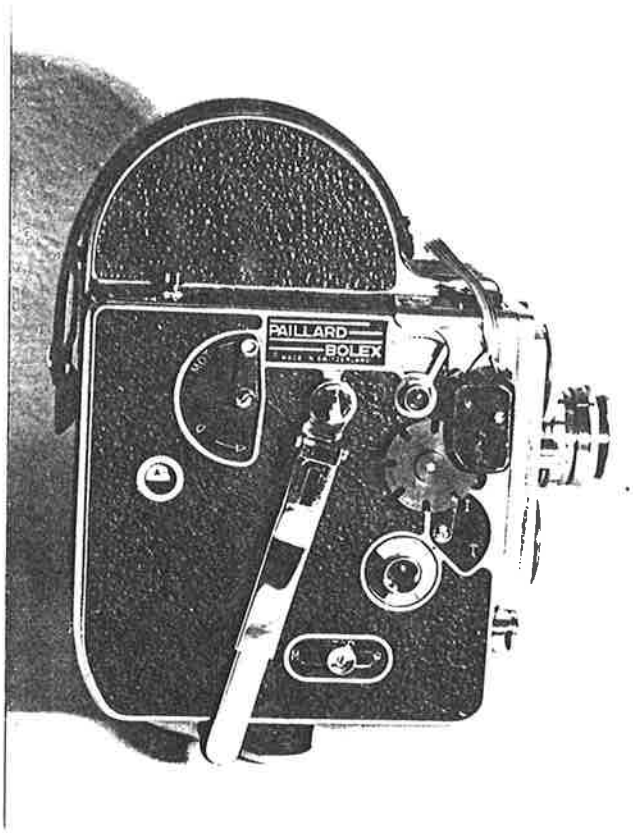


Figure C.2: Photograph of the movie camera with synchronization device

The PDP 11/34 computer was used to record the tracer concentration values through sixteen channels of the computer A/D converter from the sixteen conductivity probes. Another separate channel was used as a trigger channel. Voltage information from this trigger channel was also recorded by the computer along with the other sixteen conductivity channels. In this way, the trigger pulses from the cine camera became a part of the computer data record of the experiment and the frame count information from the film record could thus be lined up with the tracer concentration data in the computer. The computer trigger circuit diagram of Figure C.3 and the time line diagram of the pulses in Figure C.4 provide further understanding of the sequence of events which occurs during an experimental run.

## C.2 Procedure of Data Collection

The sequence of events associated with synchronous data collection during an experimental run can be listed as follows.

(1) The data collection programme 'REDAT' is run in the PDP 11/34. This monitors the trigger channel voltage and does nothing unless the voltage exceeds + 1 volt.

(2) The control box is switched on to 'START' position. This operation sets the control signal (line B of Figure C.4) to + 5 volts and enables the 74C193 down counter (see Figure C.3) ready to start counting the camera pulses.

(3) The cine camera is started and the pulses generated set the strobe light operating and also starts the camera transport motor if necessary. The same pulses are applied to the computer trigger circuit where they are superimposed in the form of + 0.5 volt pulses (line E of Figure C.4).

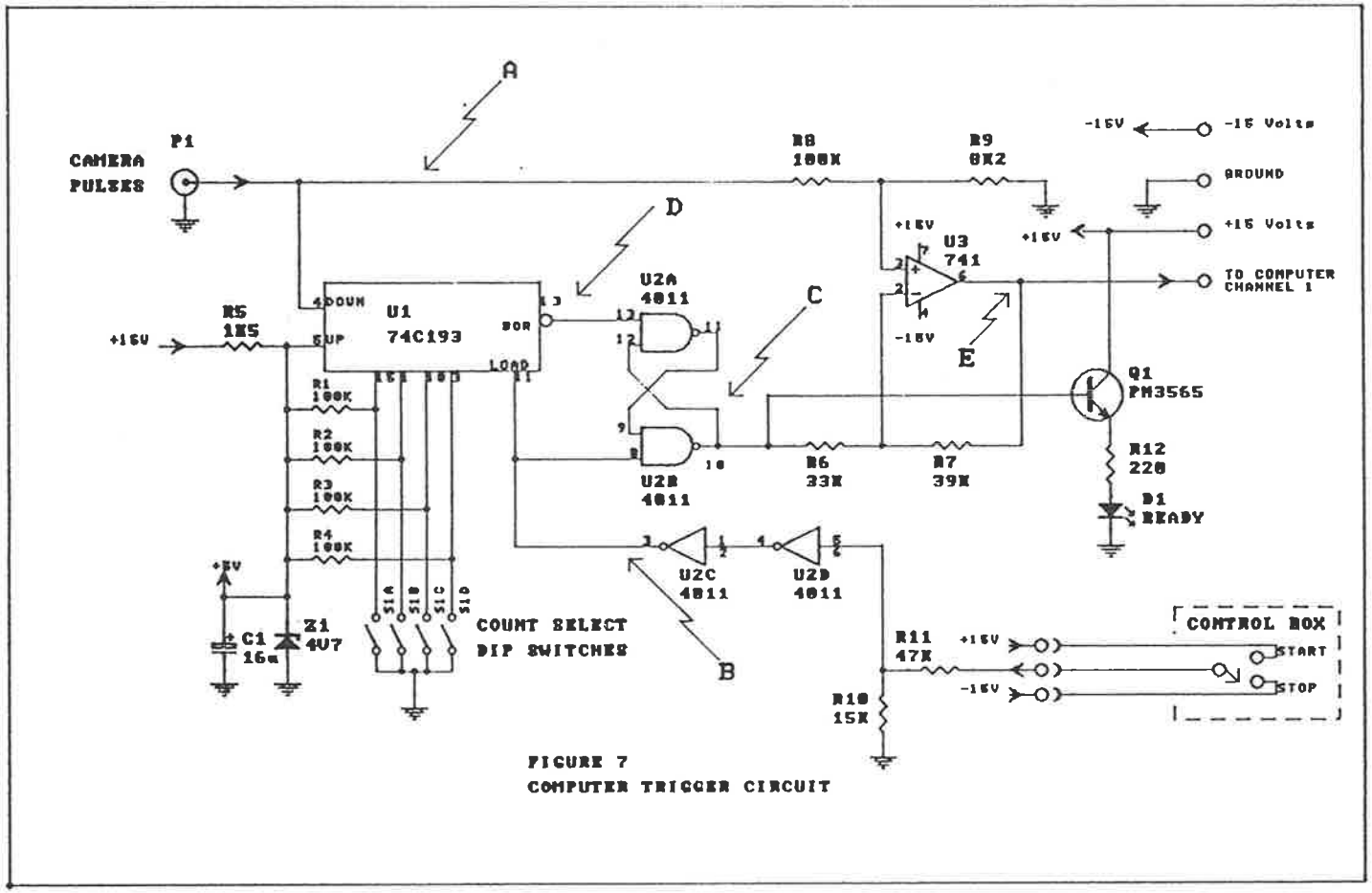


FIGURE 7
COMPUTER TRIGGER CIRCUIT

Figure C.3: Computer trigger circuit diagram

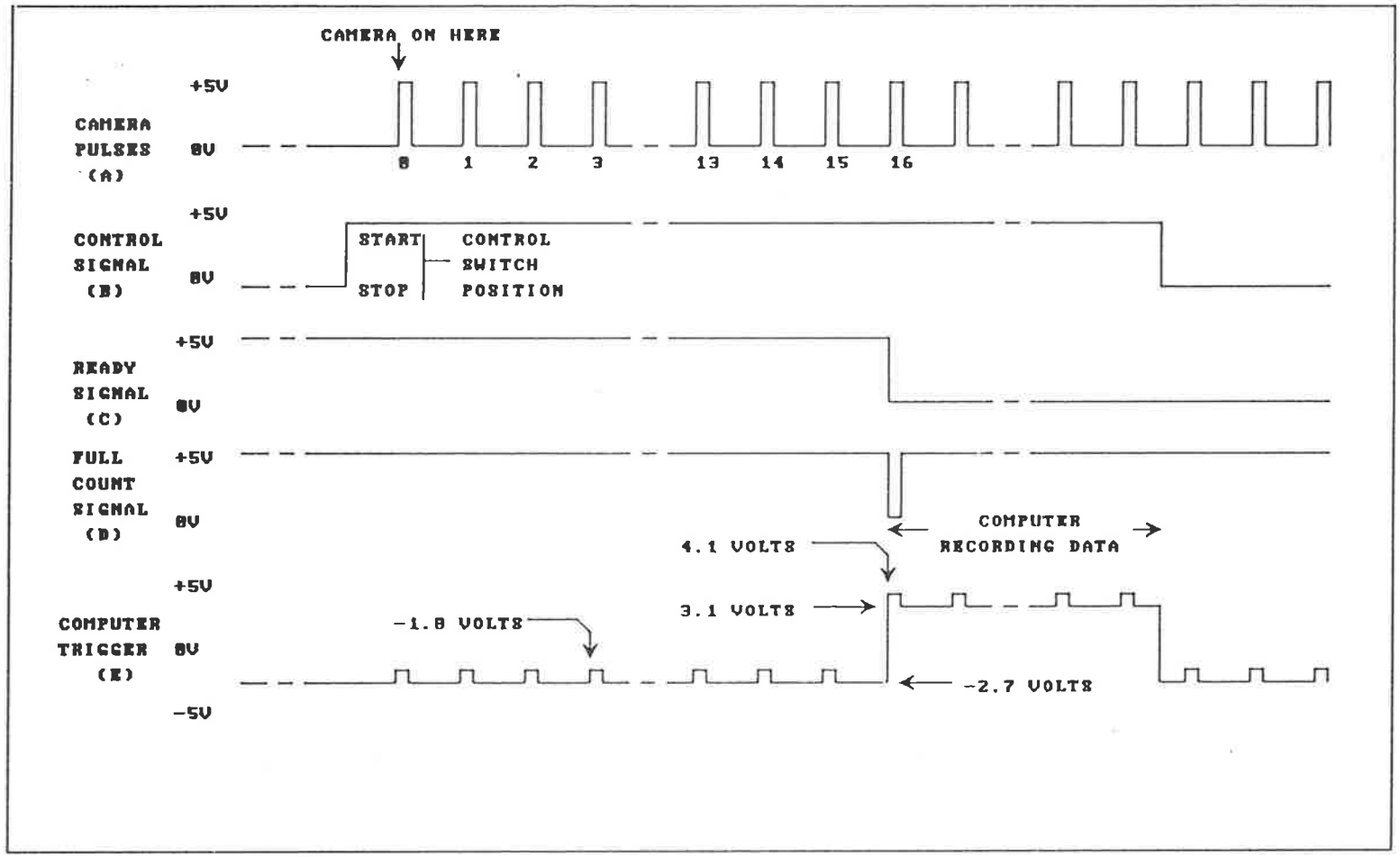


Figure C.4: The time-line diagram of the trigger circuit

However, the computer ignores them because they do not exceed + 1 volt.

(4) The camera pulses are now able to down count the value set by the count select switches (see Figure C.3) and trigger the ready signal (line C of Figure C.4) when full count is reached.

(5) When the ready signal goes from + 5 volts down to zero, the computer trigger signal (line E) rises from - 2.7 volts to + 4.1 volts. The computer now recognizes this as the signal for starting the collection of data, since the voltage exceeds + 1 volt and the data recording commences. This occurs when the camera is on the 16th frame of the film.

(6) The computer continues to collect data while the control box is in the 'START' position. However, immediately after the control signal falls to zero volt (i.e., to 'STOP' position), the computer trigger signal returns to - 2.7 volts and causes the data collection to cease. This operation also terminates the data collection program and the control box has no further effect, unless the program is restarted for another experimental run.

# Bibliography


[1] Abbot, D.E. and Kline, S.J. *(1962)* "Experimental Investigation of Subsonic Turbulent Flow Over Single and Double Backward Facing Steps", *Journal of Basic Engineering,* Transaction ASME, Series D, vol. 84, pp. 317-325.

[2] Abramovic, G.N. *(1963) The Theory of Turbulent Jets,* MIT Press, p. 671.

[3] Acton, E. *(1976)* "The modelling of large eddies in a two-dimensional shear layer", *Journal of Fluid Mechanics,* vol. 76, part 3, pp. 561-592.

[4] Adler, J.N., Robinson, M.C., Luttges, M.W. and Kennedy, D.A. *1985* "Visualizing unsteady separated flows", in *Flow Visualization III,* editor W.J. Yang, Hemisphere Publishing, pp. 342-347.

[5] Adrian, R.J. *(1983)* "Laser velocimetry", in *Fluid Mechanics Measurements,* editor R.J. Goldstein, Hemisphere publishing, pp. 155-244.

[6] Albertson, Jun., M.L., Dai, Y.B., Jensen, R.A. and Rouse, H. *(1950)* "Diffusion of Submerged Jets", *Transactions,* ASCE, vol. 115, pp. 639-697.

[7] Alonso, C.V. *(1970)* "Electrical conductivity probe for the measurement of concentration fluctuations", *Journal of Physics E: Scientific Instruments,* vol. 3, pp. 658-666.

[8] Antonia, R.A. *(1981)* "Conditional sampling in turbulence measurement", *Annual Review of Fluid Mechanics,* vol. 13, pp. 131-156.

[9] Aref, H. and Siggia, E.D. *(1980)* "Vortex dynamics of the two-dimensional shear layer", *Journal of Fluid Mechanics,* vol. 100, part 4, pp. 705-737.

[10] Arie, M. and Rouse, H. *(1956)* "Experiments on two-dimensional flow over a normal wall", *Journal of Fluid Mechanics,* vol. 1, pp. 129-141.

[11] Ashurst, W.T. *(1979)* "Numerical simulation of turbulent mixing layers via vortex dynamics", *First International Symposium on Turbulent Shear Flows,* in Turbulent Shear Flows 1, editors Durst et al., Springer-Verlag, pp. 402-413.

[12] Batt, R.G. *(1975)* "Some measurements on the effect of tripping the two-dimensional shear layer", *AIAA Journal,* vol. 13, no. 2, pp. 245-246.

[13] Beer, T. and Young, P.C. *(1983)* "Longitudinal Dispersion in Natural Streams", *Journal of the Environmental Eng. Division,* ASCE, Vol. 109, No. 5, pp. 1049-1067.

[14] Bernal, L.P. and Roshko, A. *(1986)* "Streamwise vortex structure in plane mixing layers", *Journal of Fluid mechanics,* vol. 170, pp. 499-525.

[15] Bernal, L.P., Breidenthal, R.E., Brown, G.L., Konrad, J.H. and Roshko, A. *(1979)* "On the development of three-dimensional small scales in turbulent mixing layers", *Second International Symposium on Turbulent Shear Flows,* in Turbulent Shear Flow 2, editors Bradbury et al., Springer - Verlag, 1980, pp. 305-313.

[16] Bevilaqua, P.M. and Lykoudis, P.S. *(1977)* "Some observations on the mechanism of entrainment", *AIAA Journal,* vol. 15, no. 8, pp. 1194-1196.

[17] Bevilaqua, P.M. and Lykoudis, P.S. *(1971)* "Mechanism of entrainment in turbulent wakes", *AIAA Journal,* vol. 9, no. 8, pp. 1657-1659.

[18] Birch, S.F. and Eggers, J.M. *(1973)* "A critical review of the experimental data for developed free turbulent shear layers", *Conference Proceedings, Free Turbulent Shear Flows,* vol. 1, NASA SP 321, pp. 11-40.

[19] Bogatyrev et al., *(1976)* "Experimental investigation of flow in a trench", *Journal of Applied Mechanics and Technical Physics,* vol. 17, no. 2, pp. 204-212, Translated from *Zhurnal Prikladnoi Mekhaniki i Tekhnicheskoi Fiziki,* no. 2, pp. 76-86.

[20] Bradshaw, P. *(1966)* "The Effect of Initial Conditions on the Development of a Free Shear Layer", *Journal of Fluid Mechanics,* vol. 26, pp. 225-236.

[21] Bradshaw, P. and Wong, F.Y.F. *(1972)* "The reattachment and relaxation of a turbulent shear layer", *Journal of Fluid Mechanics,* vol. 52, part 1, pp. 113-135.

[22] Breidenthal, R.E. *(1981)* "Structure in turbulent mixing layers and wakes using a chemical reaction", *Journal of Fluid Mechanics,* vol. 109, pp. 1-24.

[23] Breidenthal, R.E. *(1979)* "Chemically reacting, turbulent shear layer", *AIAA Journal,* vol. 17, pp. 310-311.

[24] Broadwell, J.E. and Breidenthal, R.E. *(1982)* "A simple model of mixing and chemical reaction in a turbulent shear layer", *Journal of Fluid Mechanics,* vol. 125, pp. 397-410.

[25] Browand, F.K. *(1966)* "An experimental investigation of the instability of an incompressible separated shear layer", *Journal of Fluid Mechanics,* vol. 26, pp. 281-307.

[26] Browand, F.K. and Latigo, B.O. *(1979)* "Growth of the two-dimensional mixing layer from a turbulent and nonturbulent boundary layer", *The Physics of Fluids,* vol. 22, part 6, pp. 1011-1019.

[27] Browand, F.K. and Laufer, J. *(1975)* "The role of large scale structures in the initial development of circular jets", *Proceedings of the Fourth Biennial Symposium on Turbulence in Liquids,* University of Missouri-Rolla, editors Zakin, J.L. and Patterson, G.K., Science Press, Princeton, New Jersey, pp. 333-344.

[28] Browand, F.K. and Troutt, T.R. *(1985)* "The Turbulent Mixing Layer : Geometry of Large Vortices", *Journal of Fluid Mechanics,* vol. 158, pp. 489-509.

[29] Browand, F.K. and Troutt, T.R. *(1980)* "A Note on Spanwise Structure in the Two-Dimensional Mixing Layer", *Journal of Fluid Mechanics,* vol. 97, part 4, pp. 771-781.

[30] Browand, F.K. and Weidman, P.D. *(1976)* "Large scales in the developing mixing layer", *Journal of Fluid Mechanics,* vol. 76, part 1, pp. 127-144.

[31] Brown, G.L. and Roshko, A. *(1974)* "On density effects and large structure in turbulent mixing layers", *Journal of Fluid Mechanics,* vol. 64, part 4, pp. 775-816.

[32] Brunn, H.H. *(1979)* "A time-domain evaluation of the large-scale flow structure in a turbulent jet", *Proceedings, Royal Society of London,* Series A, vol. 367, pp. 193-218.

[33] Brunn, H.H. *(1977)* "A time-domain analysis of the large-scale flow structure in a circular jet. Part 1. Moderate Reynolds number", *Journal of Fluid Mechanics,* vol. 83, pp. 641-671.

[34] Buchhave, P. *(1975)* "Biasing errors in individual particle measurements with the LDA-counter signal processor", *Proceedings of the LDA Symposium, Copenhagen,* in *The Accuracy of Flow Measurements by Laser Doppler Methods,* editors Buchhave et al., pp. 258-279.

[35] Cantwell, B.J. *(1981)* "Organized motion in turbulent flow", *Annual Review of Fluid Mechanics,* vol. 13, pp. 457-515.

[36] Castro, I.P. and Bradshaw, P. *(1976)* "The turbulence structure of a highly curved mixing layer", *Journal of Fluid Mechanics,* vol. 73, part 2, pp. 265-304.

[37] Chandrsuda, C. *(1976)* "A reattaching turbulent shear layer in incompressible flow", *Ph.D. Thesis,* Imperial College, London University.

[38] Chandrsuda, C. and Bradshaw, P. *(1981)* "Turbulence Structure of a Reattaching Mixing Layer", *Journal of Fluid Mechanics,* vol. 110, pp. 171-194.

[39] Chandrsuda, C., Mehta, R.D., Weir, A.D. and Bradshaw, P. *(1978)* "Effect of Free Stream Turbulence on Large Structure in Turbulent Mixing Layers", *Journal of Fluid Mechanics,* vol. 85, pp. 693-704.

[40] Chang, P.K. *(1970) Separation of Flow,* First edition, Pergamon Press, p. 777.

[41] Chatwin, P.C. *(1971)* "On the interpretation of some longitudinal dispersion experiments", *Journal of Fluid Mechanics,* vol. 48, part 4, pp. 689-702.

[42] Chatwin, P.C. *(1970)* "The approach to normality of the concentration distribution of a solute in a solvent flowing along a straight pipe", *Journal of Fluid Mechanics,* vol. 43, part 2, pp. 321- 352.

[43] Cherry, N.J., Hillier, R. and Latour, M.E.M.P. *(1984)* "Unsteady measurements in a separated and reattaching flow", *Journal of Fluid Mechanics,* vol. 144, pp. 13-46.

[44] Chevray, R. *(1984)* "Entrainment in turbulent flows: mechanisms and implications", in *Turbulence and Chaotic Phenomena in Fluids,* editor T. Tatsumi, Elsevier Science, pp. 365-369.

[45] Corcos, G.M. and Sherman, F.S. *(1984)* "The mixing layer: deterministic models of a turbulent flow. Part 1. Introduction and the two-dimensional flow", *Journal of Fluid Mechanics,* vol. 139, pp. 29-65.

[46] Corcos, G.M. and Lin, S.J. *(1984)* "The mixing layer: deterministic models of a turbulent flow. Part 2. The origin of the three-dimensional motion", *Journal of Fluid Mechanics,* vol. 139, pp. 67-95.

[47] Corrsin, S. and Kistler, A.L. *(1955)* "Free stream boundaries of turbulent flows", *NACA Technical Report No. 1244,* pp. 1033-1064.

[48] Cox, R.G. and Mason, S.G. *(1971)* "Suspended particles in fluid flow through tubes", *Annual Review of Fluid Mechanics,* vol. 3, pp. 291-318.

[49] Crow, S.C. and Champagne, F.H. *(1971)* "Orderly structure in jet turbulence", *Journal of Fluid Mechanics,* vol. 48, pp. 547-591.

[50] Csanady, G.T. *(1963)* "Turbulent diffusion in Lake Huron", *Journal of Fluid Mechanics,* vol. 17, pp. 360-384.

[51] Cunge, J.A., Holly, Jr., F.M. and Verwey, A. *(1980) Practical Aspects of Computational River Hydraulics,* Pitman Publishing, p. 420.

[52] Day, T.J. *(1975)* "Longitudinal Dispersion in Natural Channels", *Water Resources Research,* Vol. 11, pp. 909-918.

[53] Day, T.J. and Wood, I.R. *(1976)* "Similarity of the Mean Motion of Fluid Particles Dispersing in a Natural Channel", *Water Resources Research,* Vol. 12, pp. 655-666.

[54] Daniell, T.M. *(1974)* "The initial mixing zones of a dispersing pollutant in open channel flow", *M.Eng. Thesis,* The University of Adelaide, Australia.

[55] Dimotakis, P.E. *(1976)* "Single scattering particle laser Doppler measurements of turbulence", *AGARD-CP-193,* Paper 10.

[56] Dimotakis, P.E. and Brown, G.L. *(1976)* "The mixing layer at high Reynolds number: large-structure dynamics and entrainment", *Journal of Fluid Mechanics,* vol. 78, part 3, pp. 535-560.

[57] Durao, D.F.G., Laker, J. and Whitelaw, J.H. *(1980)* "Bias effects in laser-Doppler anemometry", *Journal of Physics E: Scientific Instruments,* vol. 13, pp. 442.

[58] Durst, F., Melling, A. and Whitelaw, J.H. *(1981) Principles and Practice of Laser-Doppler Anemometry,* Academic Press, 2nd edition, p. 437.

[59] Dürst, F. and Rastogi, A.K. *(1977)* "Theoretical and Experimental Investigations of Turbulent Flows with Separation", *First International Symposium on Turbulent Shear Flows,* in Turbulent Shear Flows 1, editors Durst et al., 1979, Springer-Verlag, pp. 208-219.

[60] Durst, F. and Ruck, B. *(1987)* "Effective particle size range in laser Doppler anemometry", *Experiments in Fluids,* vol. 5, no. 5, pp. 305-314.

[61] Dziomba, B. and Fiedler, H.E. *(1985)* "Effect of Initial Conditions on Two-dimensional Free Shear Layers", *Journal of Fluid Mechanics,* vol. 152, pp. 419-442.

[62] Eaton, J.K. and Johnston, J.P. *(1982)* "Low frequency unsteadiness of a reattaching turbulent shear layer", *Third International Symposium on Turbulent Shear Flows,* in Turbulent Shear Flows 3, editors Bradbury et al., Springer-Verlag, pp. 162-170.

[63] Eaton, J.K. and Johnston, J.P. *(1981)* "A Review of Research on Subsonic Turbulent Flow Reattachment", *AIAA Journal,* vol.19, no.9, pp.1093-1100.

[64] Edwards, R.V. et al., *(1971)* "Spectral analysis of the signal from the laser-Doppler flowmeter: time-independent systems", *Journal of Applied Physics,* vol. 42, pp. 837-850.

[65] Elder, J.W. *(1959)* "The dispersion of marked fluid in turbulent shear flow", *Journal of Fluid Mechanics,* vol. 5, pp. 544-560.

[66] Etheridge, D.W. and Kemp, P.H. *(1978)* "Measurements of Turbulent Flow Downstream of a Rearward-facing Step", *Journal of Fluid Mechanics,* vol. 86, part 3, pp. 545-566.

[67] Fackrell, J.E. and Robins, A.G. *(1982)* "Concentration fluctuations and fluxes in plumes from point sources in a turbulent boundary layer", *Journal of Fluid Mechanics,* vol. 117, pp. 1-26.

[68] Fiedler, H.E. *(1974)* "Transport of heat across a plane turbulent mixing layer", *Geophysics,* vol. 18A, pp. 93-109.

[69] Fiedler, H.E. and Thies, H.J. *(1978)* "Some observations in a large two-dimensional shear layer", *Lecture Notes in Physics,* vol. 75, pp. 108-117.

[70] Fiedler, H.E., Dziomba, B., Mensing, P. and Rosgen, T. *(1981)* "Initiation, evolution and global consequences of coherent structures in turbulent shear flows", *Lecture Notes in Physics,* vol. 136, pp. 219-251.

[71] Fischer, H.B. *(1966)* "Longitudinal dispersion in laboratory and natural streams", *W.M. Keck Laboratory of Hydraulics and Water Resources Report,* No. KH-R-12, Calif. Inst. of Tech., p. 250.

[72] Fischer, H.B. *(1967)* "The mechanics of dispersion in natural streams", *Journal of the Hydraulic Division,* ASCE, vol. 93, no. HY6, pp. 187-216.

[73] Fischer, H.B., List, E.J., Koh, R.C.Y., Imberger, J. and Brooks, N.H. *(1979), Mixing in Inland and Coastal Waters,* Academic Press, Inc., New York.

[74] Foss, J.F. *(1977)* "The effect of the laminar/turbulent boundary states on the development of a plane mixing layer", *Proceedings, First International Symposium on Turbulent Shear Flows,* pp. 11.33-42.

[75] Freymuth, P. *(1966)* "On transition in a separated laminar boundary layer", *Journal of Fluid Mechanics,* vol. 25, pp. 683-704.

[76] Gatski, T.B. and Liu, J.T.C. *(1980)* "On the interactions between large-scale structure and fine-grained turbulence in a free shear flow III - a numerical solution", *Philosophical Transactions of the Royal Society of London,* vol. 293, pp. 473-509.

[77] George, Jr., W.K. *(1975)* "Limitations to measuring accuracy inherent in the laser-Doppler signal", *Proceedings of the LDA Symposium, Copenhagen,* in *The Accuracy of Flow Measurements by Laser Doppler Methods,* editors Buchhave et al., pp. 20-63.

[78] Gibson, C.H. and Schwarz, W.H. *(1963)* "Detection of conductivity fluctuations in a turbulent field", *Journal of Fluid Mechanics,* vol. 16, pp. 357-364.

[79] Grass, A.J. *(1971)* "Structural features of turbulent flow over smooth and rough boundaries", *Journal of Fluid Mechanics,* vol. 50, pp. 233-

255.

[80] Haghgoogie, M., Kent, J.C. and Tabaczynski, R.J. *(1986)* "Verification of LDA and seed generator performance", *Experiments in Fluids,* vol. 4, no. 1, pp. 27-32.

[81] Ha Minh, H. and Chassaing, P. *(1979)* "Perturbations of Turbulent Pipe Flow", *First International Symposium on Turbulent Shear Flows,* in Turbulent Shear Flows 1, editors Durst et al., Springer-Verlag, pp. 178-197.

[82] Hanjalic, K. and Launder, B.E. *(1972)* "A Reynolds stress model of turbulence and its application to thin shear flows", *Journal of Fluid Mechanics,* vol. 52, pp. 609-638.

[83] Hays, J.R. *(1966)* "Mass transport mechanisms in open channel flow", *Ph.D. Thesis,* Vanderbilt University, Tennessee, U.S.A.

[84] Hernan, M.A. and Jimenez, J. *(1982)* "Computer analysis of a high speed film of the plane turbulent mixing layer", *Journal of Fluid Mechanics,* vol. 119, pp. 323-345.

[85] Ho, C.M. and Huang, L.S. *(1982)* "Subharmonics and vortex merging in mixing layers", *Journal of Fluid Mechanics,* vol. 119, pp. 443-473.

[86] Ho, C.M. and Huerre, P. *(1984)* "Perturbed free shear layers", *Annual Review of Fluid Mechanics,* vol. 16, pp. 365-424.

[87] Ho, C.M. and Nosseir, N.S. *(1981)* "Dynamics of an impinging jet, Part 1 - The feedback phenomenon", *Journal of Fluid Mechanics,* vol. 105, pp. 119-142.

[88] Ho, C.M. and Nosseir, N.S. *(1980)* "Large coherent structures in an impinging jet", *Second International Symposium on Turbulent Shear Flows* in Turbulent Shear Flows 2, editors Bradbury et al., pp. 297-304, Springer-Verlag.

[89] Holly, Jr., F.M. *(1985)* "Dispersion in rivers and coastal waters 1: physical principles and dispersion equations", in *Development in Hydraulic Engineering - 3,* editor P. Novak, pp. 1-37.

[90] Holly, Jr., F.M. *(1975)* "Two-dimensional mass dispersion in rivers", *Hydrology Paper No. 78,* Colorado State University, Fort Collins, Colorado, U.S.A.

[91] Holley, E.R. *(1971)* "Transverse mixing in rivers", *Report on Analytical, Laboratory and Field Studies for Non-buoyant Dissolved Substances, Part I and II,* Delft Hydraulics Laboratory, Delft, Netherlands.

[92] Holley, E.R. *(1969)* "Unified view of diffusion and dispersion", *Journal of the Hydraulics Division,* ASCE, vol. 95, no. HY2, pp. 621-631.

[93] Hosel, W. and Rodi, W. *(1975)* "Errors occurring in LDA measurements with counter signal processing", *Proceedings of the LDA Symposium, Copenhagen,* in The Accuracy of Flow Measurements by Laser Doppler Methods, editors Buchhave et al., pp. 251-257.

[94] Hussain, A.K.M.F. *(1984)* "Coherent structures and incoherent turbulence", in *Turbulence and Chaotic Phenomena in Fluids,* editor T. Tatsumi, Elsevier Science Publishers B.V. (North-Holland), pp. 453-460.

[95] Hussain, A.K.M.F. *(1983)* "Coherent Structures - Reality and Myth", *Physics of Fluids,* vol. 26, no. 10, pp. 2816-2850.

[96] Hussain, A.K.M.F. *(1981)* "Coherent structures and studies of perturbed and unperturbed jets", *Lecture notes in Physics,* Springer-Verlag, vol. 136, pp. 252-291.

[97] Hussain, A.K.M.F. *(1977)* "Mechanics of pulsatile flows of relevance to the cardiovascular system", in *Cardiovascular Flow Dynamics and*

*Measurements,* editors N.H.C. Hwang and N.A. Norman, University Park Press, Baltimore, pp. 541-632.

[98] Hussain, A.K.M.F. and Clark, A.R. *(1981)* "On the coherent structure of the axisymmetric mixing layer : a flow-visualization study", *Journal of Fluid Mechanics,* vol. 104, pp. 263-294.

[99] Hussain, A.K.M.F and Hayakawa, M. *(1987)* "Eduction of large-scale organized structures in a turbulent plane wake", *Journal of Fluid Mechanics,* vol. 180, pp. 193-229.

[100] Hussain, A.K.M.F. and Reynolds, W.C. *(1970)* "The mechanics of an organized wave in turbulent shear flow", *Journal of Fluid Mechanics,* vol. 41, pp. 241-258.

[101] Hussain, A.K.M.F. and Zaman, K.B.M.Q. *(1985)* "An Experimental Study of Organized Motions in the turbulent plane mixing layer", *Journal of Fluid Mechanics,* vol. 159, pp. 85-104.

[102] Hussain, A.K.M.F. and Zaman, K.B.M.Q. *(1981)* "The preferred mode of the axisymmetric jet", *Journal of Fluid Mechanics,* vol. 110, pp. 39-71.

[103] Hussain, A.K.M.F. and Zaman, K.B.M.Q. *(1980)* "Vortex pairing in a circular jet under controlled excitation, Part 2. Coherent structure dynamics", *Journal of Fluid Mechanics,* vol. 101, pp. 493-544.

[104] Hussain, A.K.M.F. and Zedan, M.F. *(1978)* "Effects of the initial condition on the axisymmetric free shear layer : Effects of the initial momentum thickness", *Physics of Fluids,* vol. 21, no. 7, pp. 1100-1112.

[105] Hussain, A.K.M.F. and Zedan, M.F. *(1978a)* "Effects of the initial condition on the axisymmetric free shear layer : Effect of the initial fluctuation level", *Physics of Fluids,* vol. 21, no. 9, pp. 1475-1481.

[106] Hussain, A.K.M.F., Kleis, S.J. and Sokolov, M. *(1980)* "A turbulent spot in an axisymmetric free shear layer. Part 2", *Journal of Fluid Mechanics,* vol. 98, pp. 97-135.

[107] Inoue, O. *(1985)* "Vortex simulation of a turbulent mixing layer", *AIAA Journal,* vol. 23, no. 3, pp. 367-373.

[108] Jimenez, J., Cogollos, M. and Bernal, L.P. *(1985)* "A perspective view of the plane mixing layer", *Journal of Fluid Mechanics,* vol. 152, pp. 125-143.

[109] Kelly, R.E. *(1967)* "On the stability of an inviscid shear layer which is periodic in space and time", *Journal of Fluid Mechanics,* vol. 27, pp. 657-689.

[110] Kim, J., Kline, S.J. and Johnston, J.P. *(1978)* "Investigation of separation and reattachment of a turbulent shear layer: flow over a backward-facing step", *Report No. MD-37,* Dept. of Mechanical Eng., Stanford University.

[111] Kim, H.T., Kline, S.J. and Reynolds, W.C. *(1971)* "The production of turbulence near a smooth wall in a turbulent boundary layer", *Journal of Fluid Mechanics,* vol. 50, pp. 133-160.

[112] Kistler, A.L. and Tan, F.C. *(1967)* "Some Properties of Turbulent Separated flows", *Physics of Fluids Supplement,* pp. S165-S173.

[113] Knight, D.D. *(1979)* "Numerical investigation of large scale structures in the turbulent mixing layer", *Proceedings of Sixth Biennial Symposium on Turbulence,* University of Missouri-Rolla, pp. 167-177.

[114] Knight, D.D. and Murray, B.T. *(1981)* "Theoretical investigation of interaction and coalescence of large scale structures in the turbulent mixing layer", *Lecture Notes in Physics,* vol. 136, pp. 62-92.

[115] Knisely, C. and Rockwell, D. *(1980)* "Vortex edge interaction mechanisms for generating low-frequency components", *Physics of Fluids,* vol. 23, pp. 239-240.

[116] Koochesfahani, M.M. and Dimotakis, P.E. *(1986)* "Mixing and chemical reactions in a turbulent liquid mixing layer", *Journal of Fluid Mechanics,* vol. 170, pp. 83-112.

[117] Koochesfahani, M.M. and Dimotakis, P.E. *(1985)* "Laser-Induced fluorescence measurements of mixed fluid concentration in a liquid plane shear layer", *AIAA Journal,* vol. 23, no. 11, pp. 1700-1707.

[118] Koochesfahani, M.M., Dimotakis, P.E. and Broadwell, J.E. *(1985)* "A 'flip' experiment in a chemically reacting turbulent mixing layer", *AIAA Journal,* vol. 23, no. 8, pp. 1191-1194.

[119] Kuehn, D.M. *(1980)* "Some effects of adverse pressure gradient on the incompressible reattaching flow over a rearward-facing step", *AIAA Journal,* vol. 18, pp. 343-344.

[120] Lau, J.C. *(1979)* "The vortex-street structure of turbulent jets. Part 2", *Proceedings, Royal Society of London,* Series A, vol. 368, pp. 547-571.

[121] Lau, J.C. and Fisher, M.J. *(1975)* "The vortex-street structure of 'turbulent' jets. Part 1", *Journal of Fluid Mechanics,* vol. 67, pp. 299-337.

[122] Laufer, J. *(1981)* "Instability and turbulence in Jets", in *Transition and Turbulence,* editor R.E. Meyer, pp. 63-76, Academic Press.

[123] Laufer, J. *(1975)* "New trends in experimental turbulence research", *Annual Review of Fluid Mechanics,* vol. 7, pp. 307-326.

[124] Launder, B. *(1976)* "Heat and mass transport", in *Topics in Applied Physics,* vol. 12, pp. 231-287.

[125] Liepmann, H.W. and Laufer, J. *(1947)* "Investigation of free turbulent mixing", *NACA Technical Note No. 1257.*

[126] Lin, S.J. and Corcos, G.M. *(1984)* "The mixing layer: deterministic models of a turbulent flow. Part 3. The effect of plane strain on the dynamics of streamwise vortices", *Journal of Fluid Mechanics,* vol. 141, pp. 139-178.

[127] Liu, J.T.C. *(1981)* "Interaction between large-scale coherent structures and fine-grained turbulence in free shear flows", in *Transition and Turbulence,* editor R.E. Meyer, pp. 167-214, Academic Press.

[128] Liu, J.T.C. and Merkine, L. *(1976)* "On the interactions between large-scale structure and fine-grained turbulence on a free shear flow 1: the development of temporal interactions in the mean", *Proceedings, Royal Society of London,* Series A, vol. 352, pp. 213-247.

[129] Logan, S.E. *(1972)* "A Laser Velocimeter for Reynolds Stress and Other Turbulence Measurements", *AIAA Journal,* vol. 10, no. 7, pp. 933-935.

[130] Lumley, J.L. *(1981)* "Coherent structures in turbulence", in *Transition and Turbulence,* editor R.E. Meyer, Academic Press, pp. 215-242.

[131] Mansour, N.N., Moin, P., Reynolds, W.C. and Ferziger, J.H. *(1979)* "Improved methods for large eddy simulations of turbulence", *First International Symposium on Turbulent Shear Flows,* in Turbulent Shear Flows 1, editors Durst et al., Springer-Verlag, pp. 386-401.

[132] Martin, J.M., Empey, R.W., McCroskey, W.J. and Cardonna, F.X. *1973* "Experimental analysis of dynamic stall on an oscillating airfoil", *Journal of the American Helicopter Society,* vol. 19, no. 1, pp. 26-32.

[133] Mathieu, J. and Charnay, G. *(1981)* "Experimental methods in turbulent structure Research", *Lecture Notes in Physics,* vol. 136, pp. 146-187.

[134] Maull, D.J. and East, L.F. *(1963)* "Three dimensional flow in cavities", *Journal of Fluid Mechanics,* vol. 16, Part 4, pp. 620-632.

[135] Maxworthy, T. *(1972)* "The structure and stability of vortex rings", *Journal of Fluid Mechanics,* vol. 51, pp. 15-32.

[136] Mehta, P.R. *(1981)* "Separated flow through large sudden expansions", *Journal of the Hydraulics Division, ASCE,* vol. 107, no. HY4, pp. 451-460.

[137] Mehta, P.R. *(1979)* "Flow characteristics in two-dimensional expansions", *Journal of the Hydraulics Divisions, ASCE,* vol. 105, no. HY5, pp. 501-516.

[138] Mehta, U.B. and Lavan, Z. *(1969)* "Flow in a two-dimensional channel with a rectangular cavity", *NASA Contractor Report - 1245*, p. 79.

[139] McGuinness, M. *(1978)* "Flow with a separation bubble - steady and unsteady aspects", *Ph.D. Dissertation,* Cambridge University.

[140] McGuirk, J.J. and Rodi, W. *(1979)* "Calculation of unsteady mass exchange between a main stream and a dead water zone", *Proceedings, 18th Congress, International Association for Hydraulic Research, Italy,* vol. 3, pp. 25-32.

[141] McGuirk, J.J. and Rodi, W. *(1978)* "A depth-averaged mathematical model for the near field of side discharges into open channel flow", *Journal of Fluid Mechanics,* vol. 86, Part 4, pp. 761-781.

[142] McLaughlin, D.K. and Tiederman, W.G. *(1973)* "Biasing correcting for individual realization of laser anemometer measurements in turbulent flows", *Physics of Fluids,* vol. 16, pp. 2082-2088.

[143] Melling, A. and Whitelaw, J.H. *(1975)* "Optical and flow aspects of particles", *Proceedings of the LDA Symposium, Copenhagen,* in The

Accuracy of Flow Measurements by Laser Doppler Methods, editors Buchhave et al., pp. 382-402.

[144] Merzkirch, W. *(1974) Flow Visualization,* Academic Press, p. 250.

[145] Mills, R.D. *(1965)* "On the closed motion of fluid in a square cavity", *Journal, Royal Aeronautical Society,* vol. 69, No. 650, pp. 116-118.

[146] Monkewitz, P.A. and Huerre, P. *(1982)* "Influence of the Velocity Ratio on the Spatial Instability of Mixing Layers", *Physics of Fluids,* vol. 25, no. 7, pp. 1137-1143.

[147] Monin, A.S. and Yaglom, A.M. *(1975) Statistical Fluid Mechanics,* vol. 2, editor J.L. Lumley, MIT Press.

[148] Monin, A.S. and Yaglom, A.M. *(1977) Statistical Fluid Mechanics,* vol. 1, editor J.L. Lumley, MIT Press.

[149] Moore, D.W. and Saffman, P.G. *(1975)* "The density of organized vortices in a turbulent mixing layer", *Journal of Fluid Mechanics,* vol. 69, pp. 465-473.

[150] Moss, W.D., Baker, S. and Bradbury, L.J.S. *(1977)* "Measurements of Mean Velocity and Reynolds Stresses in Some Regions of Recirculating Flow", *First International Symposium on Turbulent Shear Flows,* in Turbulent Shear Flows 1, editors Durst et al., 1979, Springer-Verlag, pp. 198-207.

[151] Nordin, Jr., C.F. and Sabol, G.V. *(1974)* "Empirical data on longitudinal dispersion in rivers", *U.S. Geological Survey,* Report no. USGS-WRD-74-035, p. 340.

[152] Nordin, Jr., C.F. and Troutman, B.M. *(1980)* "Longitudinal dispersion in rivers: the persistence of skewness in observed data", *Water Resources Research,* vol. 16, No. 1, pp. 123-128.

[153] Okoye, J.K. *(1970)* "Characteristics of transverse mixing in open channel flows", *Technical Report No. KH-R-23,* W.M. Keck Laboratory of Hydraulics and Water Resources, Calif. Inst. of Tech., CA, U.S.A.

[154] Pan, F. and Acrivos, A. *(1967)* "Steady flow in rectangular cavities", *Journal of Fluid Mechanics,* vol. 28, Part 4, pp. 643-655.

[155] Patel, R.P. *(1978)* "Effects of Stream Turbulence on Free Shear Flows", *Aeronautical Quarterly,* Royal Aeronautical Society of London, pp. 33-43.

[156] Patel, R.P. *(1973)* "An Experimental Study of a Plane Mixing Layer", *AIAA Journal,* vol. 11, no. 1, pp. 67-71.

[157] Patnaik, P.C., Sherman, F.S. and Corcos, G.M. *(1976)* "A numerical simulation of Kelvin-Helmholtz waves of finite amplitude", *Journal of Fluid Mechanics,* vol. 73, pp. 215-240.

[158] Pedersen, F.B. *(1977)* "Prediction of longitudinal dispersion in natural streams", *Series Paper No. 14,* Inst. of Hydrodynamics and Hydraulic Eng., Technical University of Denmark, Lyngby, Denmark.

[159] Phillips, O.M. *(1972)* "The entrainment interface", *Journal of Fluid Mechanics,* vol. 51, pp. 97-118.

[160] Pierrehumbert, R.T. and Widnall, S.E. *(1982)* "The two- and three-dimensional instabilities of a spatially periodic shear layer", *Journal of Fluid Mechanics,* vol. 114, pp. 59-82.

[161] Pierrehumbert, R.T. and Widnall, S.E. *(1981)* "The structure of organized vortices in a free shear layer", *Journal of Fluid Mechanics,* vol. 102, pp. 301-313.

[162] Prausnitz, J.M. and Wilhelm, R.H. *(1956)* "Turbulent concentration fluctuations through electrical conductivity measurements", *The Review of Scientific Instruments,* vol. 27, no. 11, pp. 941-943.

[163] Pui, N.K. and Gartshore, I.S. *(1979)* "Measurements of the growth rate and structure in plane turbulent mixing layers", *Journal of Fluid Mechanics,* vol. 91, pp. 111-130.

[164] Rajaratnam, N. *(1976) Turbulent Jets,* Elsevier Science, p. 304.

[165] Rastogi, A.K. and Rodi, W. *(1978)* "Predictions of heat and mass transfer in open channel flows", *Journal of the Hydraulics Division,* ASCE, vol. 104, No. HY3, pp. 397-420.

[166] Reynolds, W.C. and Hussain, A.K.M.F. *(1972)* "The mechanics of an organized wave in turbulent shear flow. Part 3. Theoretical models and comparisons with experiments", *Journal of Fluid Mechanics,* vol. 54, pp. 263-288.

[167] Rockwell, D. *(1983)* "Oscillations of impinging shear layers", *AIAA Journal,* vol. 21, no. 5, pp. 645-664.

[168] Rockwell, D.O. *(1972)* "External excitation of planar jets", *Journal of Applied Mechanics,* vol. 39, pp. 883-890.

[169] Rockwell, D. and Naudascher, E. *(1979)* "Self-sustained oscillations of impinging free shear layers", *Annual Review of Fluid Mechanics,* vol. 11, pp. 67-94.

[170] Rodi, W. *(1980)* "Turbulence models and their application in hydraulics", *State-of-the-Art Paper,* International Association for Hydraulic Research, Delft, The Netherlands, p. 104.

[171] Rodi, W. *(1975)* "A review of experimental data of uniform density free turbulent boundary layers", in *Studies in Convection,* editor B.E. Launder, Academic Press, pp. 79-165.

[172] Roos, F.W. and Willmarth, W.W. *(1969)* "Hydrogen bubble flow visualization at low Reynolds numbers", *AIAA Journal,* vol. 7, pp. 1635-1637.

[173] Roshko, A. *(1981)* "The plane mixing layer - Flow visualization results and three dimensional effects", *Lecture notes in Physics,* vol. 136, pp. 208-217.

[174] Roshko, A. *(1976)* "Structure of turbulent shear flows : A new look", *AIAA Journal,* vol. 14, no. 10, pp. 1349-1357.

[175] Roshko, A. *(1955)* "Some measurements of flow in a rectangular cut out", *Technical Note No. 3488,* NACA.

[176] Ruderich, R. and Fernholz, H.H. *(1986)* "An experimental investigation of a turbulent shear flow with separation, reverse flow and reattachment", *Journal of Fluid Mechanics,* vol. 163, pp. 283-322.

[177] Sabol, G.V. and Nordin, Jr., C.F. *(1978)* "Dispersion in rivers as related to storage zones", *Journal of the Hydraulics Division,* ASCE, vol. 104, No. HY5, pp. 695-708.

[178] Saffman, P.G. *(1977)* "Results of a two equation model for turbulent flows and development of a relaxation stress model for application to straining and rotating flows", *Project Squid Workshop on Turbulence in Internal Flows,* Hemisphere Publishing, pp. 191-231.

[179] Sayre, W.W. *(1973)* "Natural mixing processes in rivers", in *Environmental Impact on Rivers,* editor H.W. Shen, pp. 6.1-37.

[180] Sayre, W.W. *(1968)* "Dispersion of mass in open-channel flow", *Hydraulics Paper No. 3,* Colorado State University, Fort Collins, Colorado.

[181] Schlichting, H. *(1968) Boundary Layer Theory,* Pergamon Press.

[182] Schnelle, Jr., K.B., Thackston, E.L. and Krenkel, P.A. *(1967)* "Mathematical modeling of dispersion in rivers", *Proceedings, 12th Congress, International Association for Hydraulic Research,* vol. 3-4, pp. 33-41.

[183] Schraub, F.A. et al., *(1965)* "Use of Hydrogen bubbles for quantitative determination of time-dependent velocity fields in low-speed water flows", *Journal of Basic Eng.,* ASME, vol. 87, pp. 429-444.

[184] Smyth, R. *(1979)* "Turbulent flow over a plane symmetric sudden expansion", *Journal of Fluids Engineering,* Transactions of the ASME, vol. 101, pp. 348-353.

[185] Sokolov, M., Hussain, A.K.M.F., Kleis, S.J. and Husain, Z.D. *(1980)* "A turbulent spot in an axisymmetric free shear layer. Part 1", *Journal of Fluid Mechanics,* vol. 98, pp. 65-95.

[186] Squire, H.B. *(1956)* "Note on the motion inside a region of recirculation (cavity flow)", *Journal of the Royal Aeronautical Society,* vol. 60, pp. 203-205.

[187] Sreenivasan, K.R., Tavoularis, S. and Corrsin, S. *(1981)* "A test of gradient transport and its generalizations", *Third International Symposium on Turbulent Shear Flows,* in Turbulent Shear Flows 3, editors Bradbury et al., Springer-Verlag, pp. 96-112.

[188] Stanisic, M.M. *(1985) The Mathematical Theory of Turbulence,* Springer-Verlag, p. 429.

[189] Stevenson, W.H., Thompson, H.D. and Craig, R.R. *(1984)* "Laser Velocimeter Measurements in Highly Turbulent Recirculating Flows", *Journal of Fluids Engineering,* Transactions of the ASME, Series D, vol. 106, pp. 173-180.

[190] Subramanian, C.S., Rajagopalan, S., Antonia, R.A. and Chambers, A.J. *(1982)* "Comparison of conditional sampling and averaging techniques in a turbulent boundary layer", *Journal of Fluid Mechanics,* vol. 123, pp. 335-362.

[191] Sullivan, P.J. *(1971)* "Longitudinal dispersion within a two-dimensional turbulent shear flow", *Journal of Fluid Mechanics,* vol. 49, part 3, pp. 551-576.

[192] Sykes, R.I., Lewellen, W.S. and Parker, S.F. *(1984)* "A turbulent-transport model for concentration fluctuations and fluxes", *Journal of Fluid Mechanics,* vol. 139, pp. 193-218.

[193] Tani, I., Iuchi, M. and Komoda H. *(1961)* "Experimental investigation of flow separation associated with a step or a groove", in *Reports of the Aeronautical Research Institute,* Report No. 364, University of Tokyo, Japan.

[194] Taylor, G.I. *(1922)* "Diffusion by continuous movements", *Proceedings, London Mathematical Society,* Series 2, vol. 20, pp. 196-212.

[195] Taylor, G.I. *(1954)* "The dispersion of matter in turbulent flow through a pipe", *Proceedings, Royal Society of London,* Series A, vol. 223, pp. 446-468.

[196] Taylor, G.I. *(1953)* "Dispersion of soluble matter in solvent flowing slowly through a tube", *Proceedings, Royal Society of London,* Series A, vol. 219, pp. 186-203.

[197] Thackston, E.L. and Krenkel, P.A. *(1967)* "Longitudinal mixing in natural streams", *Journal of the Sanitary Engineering Division,* ASCE, vol. 93, No. SA5, pp. 67-90.

[198] Thackston, E.L. and Schnelle, Jr., K.B. *(1970)* "Predicting effects of dead zones on stream mixing", *Journal of the Sanitary Engineering Division,* ASCE, vol. 96, No. SA2, pp. 319-331.

[199] Townsend, A.A. *(1976) The Structure of Turbulent Shear Flow,* Cambridge University Press, 2nd edition, p. 429.

[200] Townsend, A.A. *(1956) The Structure of Turbulent Shear Flow,* Cambridge University Press, 1st edition, p. 315.

[201] Tropea, C. *(1986)* "Practical aid for choosing the shift frequency in LDA", *Experiments in Fluids,* vol. 4, no. 2, pp. 79-80.

[202] Troutt, T.R., Scheelke, B. and Norman, T.R. *(1984)* "Organized structures in a reattaching separated flow field", *Journal of Fluid Mechanics,* vol. 143, pp. 413-427.

[203] Valentine, E.M. and Wood, I.R. *(1979a)* "Dispersion in Rough Rectangular Channels", *Journal of the Hydraulics Division,* ASCE, Vol. 105, No. HY12, pp. 1537-1553.

[204] Valentine, E.M. and Wood, I.R. *(1979b)* "Experiments in Longitudinal Dispersion with Dead Zones", *Journal of the Hydraulics Division,* ASCE, Vol. 105, No. HY8, pp. 999-1016.

[205] Valentine, E.M. and Wood, I.R. *(1977)* "Longitudinal Dispersion with Dead Zones", *Journal of the Hydraulics Division,* ASCE, Vol. 103, No. HY9, pp. 975-990.

[206] Van Atta, C.W. *(1974)* "Sampling techniques in turbulence measurements", *Annual Review of Fluid Mechanics,* vol. 6, pp. 75-91.

[207] Weisbrot, I., Einav, S. and Wygnanski, I. *(1982)* "The nonunique rate of spread of the two-dimensional mixing layer", *The Physics of Fluids,* vol. 25, no. 10, pp. 1691-1693.

[208] Weiss, L.S. and Kuo, C.Y. *(1982)* "Mass Transfer Across a Dead Zone Boundary", *Proceedings of the Conference on 'Applying Research to Hydraulic Practice',* ASCE, pp. 216-223.

[209] Westrich, B. *(1976)* "Simulation of Mass Exchange in Dead Zones for Steady and Unsteady Flow Conditions", *Proceedings of Interna-*

*tional Symposium on Unsteady Flow in Open Channels,* Newcastle-upon-Tyne, England, Paper G3, pp. 23-34.

[210] Winant, C.D. and Browand, F.K. *(1974)* "Vortex pairing: the mechanism of turbulent mixing layer growth at moderate Reynolds number", *Journal of Fluid Mechanics,* vol. 63, part 2, pp. 237-255.

[211] Wygnanski, I. and Oster, D. *(1980)* "A forced, plane, turbulent mixing layer: a challenge for the predictor", *Second International Symposium on Turbulent Shear Flows,* in Turbulent Shear Flows 2, editors Bradbury et al., Springer-Verlag, pp. 314-326.

[212] Wygnanski, I., Oster, D., Fiedler, H. and Dziomba, B. *(1979)* "On the perseverance of a quasi-two-dimensional eddy-structure in a turbulent mixing layer", *Journal of Fluid Mechanics,* vol. 93, pp. 325-335.

[213] Wygnanski, I. and Fiedler, H.E. *(1970)* "The two-dimensional mixing region", *Journal of Fluid Mechanics,* vol. 41, part 2, pp. 327-361.

[214] Yang, W.J. *(1985)*, editor, "Flow Visualization III", *Proceedings of the Third International Symposium on Flow Visualization, Michigan,* Hemisphere Publishing.

[215] Yule, A.J. *(1981)* "Investigations of eddy coherence in jet flows", *Lecture Notes in Physics,* vol. 136, pp. 188-207.

[216] Yule, A.J. *(1980)* "Phase scrambling effects and turbulence data analysis", *Second International Symposium on Turbulent Shear Flows,* in Turbulent Shear Flows 2, editors Bradbury et al., Springer-Verlag, pp. 263-281.

[217] Yule, A.J. *(1978)* "Large-scale structure in the mixing layer of a round jet", *Journal of Fluid Mechanics,* vol. 89, part 3, pp. 413-432.

[218] Yule, A.J. *(1972)* "Spreading of turbulent mixing layers", *AIAA Journal,* vol. 10, no. 5, pp. 686-687.

[219] Zaman, K.B.M.Q. and Hussain, A.K.M.F. *(1984)* "Natural large-scale structures in the axisymmetric mixing layer", *Journal of Fluid Mechanics,* vol. 138, pp. 325-351.

[220] Zaman, K.B.M.Q. and Hussain, A.K.M.F. *(1981)* "Taylor hypothesis and large scale coherent structures", *Journal of Fluid Mechanics,* vol. 112, pp. 379-396.

[221] Zaman, K.B.M.Q. and Hussain, A.K.M.F. *(1980)* "Vortex pairing in a circular jet under controlled excitation, Part 1. General jet response", *Journal of Fluid Mechanics,* vol. 101, pp. 449-491.

[222] Zaman, K.B.M.Q. and Hussain, A.K.M.F. *(1979)* "The mechanics of vortex pairing in an axisymmetric mixing layer", *Second International Symposium on Turbulent Shear Flows,* in Turbulent Shear Flows 2, editors Bradbury et al., pp. 327-343.

[223] Zhak, V.D., Mukhin, V.A. and Nakoryakov, V.E. *(1981)* "Three dimensional vortex structures in cavities", *Journal of Applied Mechanics and Technical Physics,* vol. 22, no. 2, pp. 186-189, translated from *Zhurnal Prikladnoi Mekhaniki i Tekhnicheskoi Fiziki,* No. 2, pp. 54-59.